Towards Understanding the Magnetic Mineralogy of Archaeological Ceramics.

'Thesis submitted in accordance with the requirements of the University of Liverpool for the degree of Doctor in Philosophy by Derek Atkinson.'

September 1992

ABSTRACT

The magnetic properties of a collection of ancient ceramics have been investigated to elucidate the mineral type, the mass fraction and the domain states of the constituent magnetic particles. The sample set comprises a range of sherds from various locations including Europe, China, Peru and North America. These samples range widely in age from 3400 BC up to 1910 AD.

The magnetic mineralogy is dominated, in terms of the intensity of magnetisation, by magnetite-type minerals. Approximately 30% of the sherds investigated contain essentially pure magnetite while the remainder contain slightly titanium-substituted magnetite or cation deficient forms of magnetite or titanomagnetite. Haematite is present in about 53% of the sherds but commonly contributes less than 10% of the saturation isothermal remanence.

The saturation magnetisation was used to estimate the mass fraction of the ferrimagnetic content. This is found to be commonly less than 1% of the total sample mass.

The domain states were elucidated from a combination of high field magnetic hysteresis and low field magnetic susceptibility measurements. In general, the particle size distribution for the ferrimagnetic mineral was found to extend from below the superparamagnetic-stable single domain boundary in to the region of multidomain size particles. The particle size distribution is often skewed towards the smaller sizes, with sherds having a high superparamagnetic or stable single domain fraction.

The results of the magnetic mineralogy study are discussed with reference to comparisons between different groups of sherds, the implications for archaeomagnetic intensity determinations, and the effect of the mineralogy upon magnetic viscosity. It is shown that two of the groups of sherds studied can be distinguished on the basis of either their thermomagnetic parameters, or the distribution of coercivities, or, most suitably in this case, by the remanence ratio.

The magnetic mineralogy of ancient ceramics is often suited to archaeointensity determinations because of the high single domain fraction. However, the presence of multidomain material in about 30% of the sherds studied suggests that problems may arise from the non-linear NRM-TRM behaviour of such particles and from the cooling rate dependence of such particles which is opposite to that of single domain particles. In addition, archaeointensity determinations will be adversely affected by the occurrence of low temperature oxidation and by the irreversible nature of the thermomagnetic behaviour of many samples.

A review of magnetic viscosity is presented as part of an investigation of the feasibility of dating using this type of magnetisation.

The last chapter is a case study of the archaeomagnetism of a red sandstone kiln. The magnetic mineralogy of the kiln is greatly affected by firing which produces magnetite by the reduction of haematite. The characteristic remanence associated with firing was used as a dating tool, the date derived disagrees with the archaeological age, from which it is suggested that the kiln has suffered subsidence.

ACKNOWLEDGEMENTS

I am grateful for the help and support of a number of people during the course of this study. First, I would like to thank John Shaw for initiating this project, providing samples and for providing excellent research facilities. I would like thank Tim Rolph, Graham Sherwood and John Share of the Geomagnetism group and Dave Robertson and Derek France from the Geography department for technical assistance and advice about the equipment used in this study. I would like to thank the members of the Geomagnetism group for helpful discussions in particular Graham Sherwood, Tim Rolph, Yang Shanlin, Jennifer King and Neil Thomas. I would also like to thank Dave Robertson, Derek France, Bill O'Reilly, C. Radhakrishnamurty and Derek Walton for useful discussions and C. Radhakrishnamurty for his hospitality during a visit to the Tata Institute in Bombay.

I greatly appreciate the time and effort expended by both Tim Rolph and Jennifer King in their thorough review of this thesis.

I would like to thank all of the members of the Geomagnetism group for creating a friendly and interesting working environment. Also, I would like to thank my friends, in particular Nigel Willby, and my family for their continued interest and support during the course of this work.

Finally, I would like to thank my wife Jennifer, for her unstinting interest and support during the course of this study and for her efforts towards the completion of this thesis, for this, I dedicate this thesis to my wife.

"You could say that I'm a bitter man and I would agree I think this is true... and I will remain so until I know more than those that know more than I do."

The occasional flicker.
Kevin Rowland, Dexys
Midnight Runners

CONTENTS

1 Background

1.1 Introduction

Inorganic remains form the bulk of artefacts found at most archaeological sites. At pre-Neolithic sites (pre-3500 years BC in Britain, radiocarbon date; Megaw & Simpson, 1988), such remains consist primarily of implements made from stone such as flint. From the beginning of the Neolithic (literally the "new stone age") onwards, pottery fragments become common, while metallic objects appear regularly from the Early Bronze Age. The remains of larger features such as fireplaces, kilns, living accommodation, burial chambers and ceremonial structures have also been found at sites dating throughout prehistory.

The magnetic properties of many such materials have been investigated for both archaeological and geophysical purposes. The accurate dating of many fired artefacts, such as kilns and ceramics, has enabled their magnetic information to be used to establish curves which define the temporal variation of the Earth's magnetic field at several geographical regions. From these records, various aspects of the Earth's magnetic field have been investigated. The archaeological information which can be obtained from magnetic measurements includes dating, site surveying, the investigation of the manufacturing technology and the provenancing of artefacts.

1.2 The Earth's magnetic field

The recent geographic variation of the declination, inclination and the intensity of the Earth's magnetic field is shown in figure 1.1. The observed variations have been analysed in terms of dipole and non-dipole components which show that a single dipole component, inclined at approximately 11° to the axis of rotation of the Earth, accounts for about 90% of the energy of the surface magnetic field, with the remainder being contributed by various non-dipole features which bear no relationship to the surface topography (Roberts & Piper, 1989).

The dipole and non-dipole components that make up the geomagnetic field are not constant in time but vary over timescales from a few years up to many million years. The temporal changes which occur over short periods, less than 10^4 year, are termed secular variation. The most detailed secular variation information has been obtained from direct measurements of the magnetic field at land-based magnetic observatories and more recently from satellites. Direct measurements including early maritime records extending back to the early seventeenth century, have been used to study various aspects of the geomagnetic field. However, sufficient geographic coverage of data for detailed spherical-harmonic analysis, has only been available for the past fifty years (Roberts & Piper, 1989).

To study the Earth's magnetic field beyond the limits of direct measurements requires the use of indirect methods. The direction and intensity of the geomagnetic field have

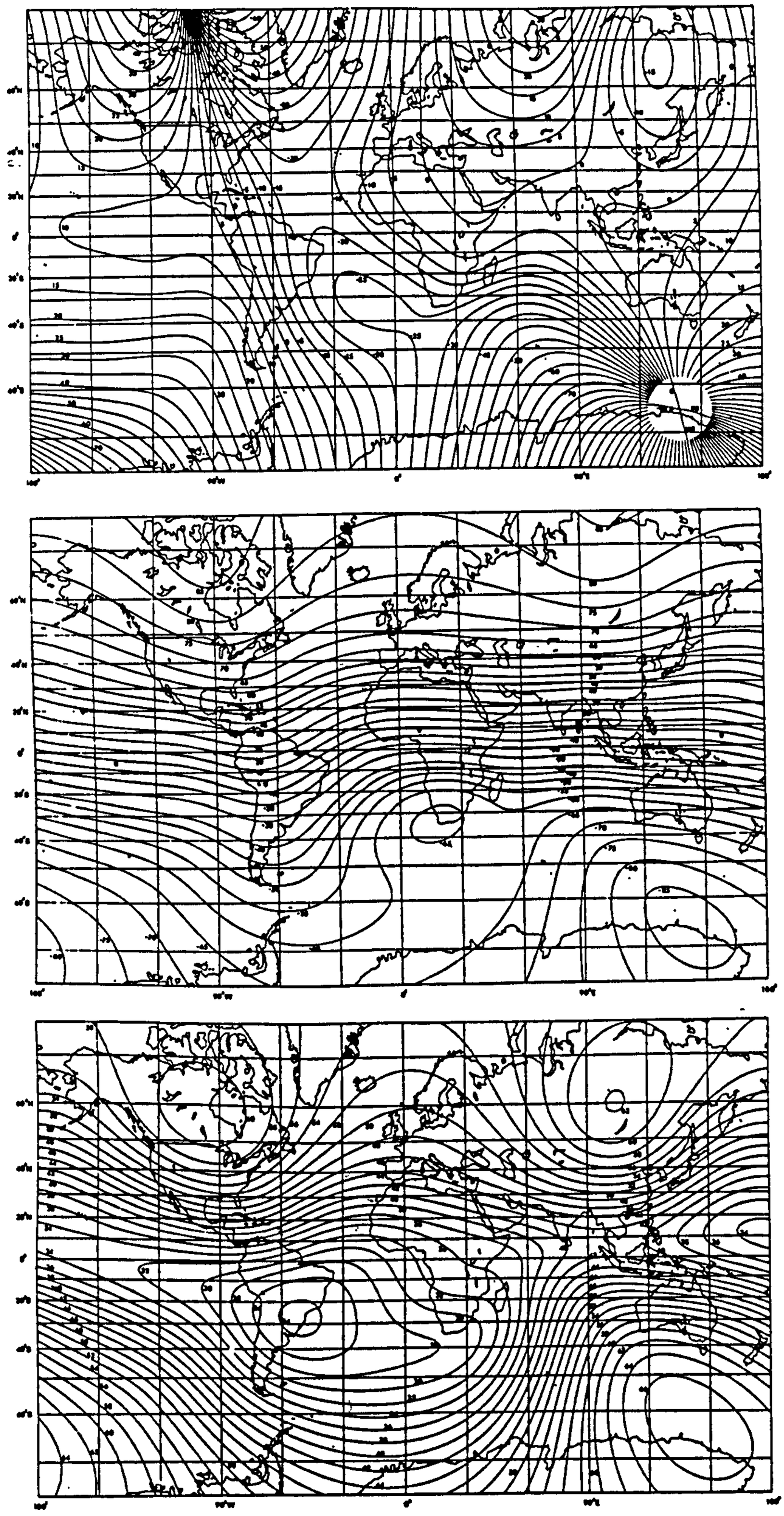

Figure 1.1. The global variation of (a) declination, (b) inclination and (c) total intensity (contours in 1000 nT) of the magnetic field at the Earth's surface in 1980. From Merrill & McElhinny (1983).

been principally obtained from the magnetic remanence of natural materials. These materials include fired archaeological artefacts (which can be particularly useful when they are precisely dated), volcanic rocks and both consolidated and unconsolidated sedimentary sequences.

The geographic coverage and dating of indirect field measurements has limited the information that can be derived about the Earth's magnetic field. However, one of the most important features of the geomagnetic field, the occurrence of periods of reversed polarity, was revealed by these indirect studies. More recently these records have provided insights into the nature of the magnetic field during such reversals of polarity. Indirect records spanning archaeological time have been used to extend the secular variation record beyond that of the historical records.

1.3 Geophysical information

The investigation of the magnetic properties of archaeological artefacts such as fireplaces, kilns and ceramics forms the basis of archaeomagnetism; the study of both the spatial and temporal variation of the Earth's magnetic field over archaeological time. An additional reason, and a reciprocal use for the development of such records is that they allow suitable artefacts of unknown age to be dated, this aspect is discussed in section 1.4.

Archaeological artefacts are often accurately dated and therefore their magnetic remanence may provide a spot

reading of the ambient magnetic field at the time of firing. The magnetic field information obtained depends on the nature of the artefact. Where artefacts have remained in the position in which they were fired, e.g. kilns and fireplaces, both the direction and the intensity of the ambient magnetic field can potentially be obtained. For smaller fired artefacts, e.g. bricks, tiles and pottery, only the intensity of the ambient magnetic field may be meaningfully determined since the position of these artefacts and hence the remanence direction, have been altered since the acquisition of remanence during firing. However, in certain situations the inclination of the ancient magnetic field may be deduced, provided that additional information or assumptions are made about the orientation during firing. For example, the orientation of an artefact to the vertical may be determined from the direction in which a glaze has flowed (Aitken, 1974), or it may be assumed in the case of tiles and bricks which are commonly fired in a horizontal position (Thellier, 1938 and Abrahamsen, 1973).

Reference curves of the direction and the intensity of the Earth's magnetic field have been compiled for several geographic regions including parts of Europe (e.g. Greece, Bulgaria and Britain), North and South America and China (see Aitken, 1990). These curves are biased in their geographical coverage as a result of the distribution of archaeological settlements and also the ease of access to the artefacts.

Archaeomagnetic records suffer primarily from lack of well dated sites, of which at least five are required per century to obtain a reliable curve (Aitken, 1990).

In addition to archaeomagnetic records, the recent secular variation of the geomagnetic field has been obtained as a near continuous sequence from various lacustrine sediments. The records obtained from unconsolidated lake sediments are subject to a variety of problems including inclination shallowing, bioturbation and smoothing of the geomagnetic record due to the nature of the remanence acquisition, as well as difficulties in determining the absolute orientation of long core samples.

Despite the difficulties of obtaining secular variation data from lacustrine sediments and archaeological artefacts, there are similarities in the form of the variation obtained from contemporary British records from these sources (Clark et al. 1988), see figure 1.2. These suggest a geomagnetic origin for the observed variations.

The curves of geomagnetic secular variation obtained from different regions show spatial and temporal similarities consistent with dipolar nature of the Earth's magnetic field and, when superimposed, show differences which reveal the presence of non-dipole features. Consequently these curves have been used to provide information pertinent to the geomagnetic field. For example, contemporaneous records from different regions have been compared in order to determine the direction and rate of motion of dipolar features. The rate of westward

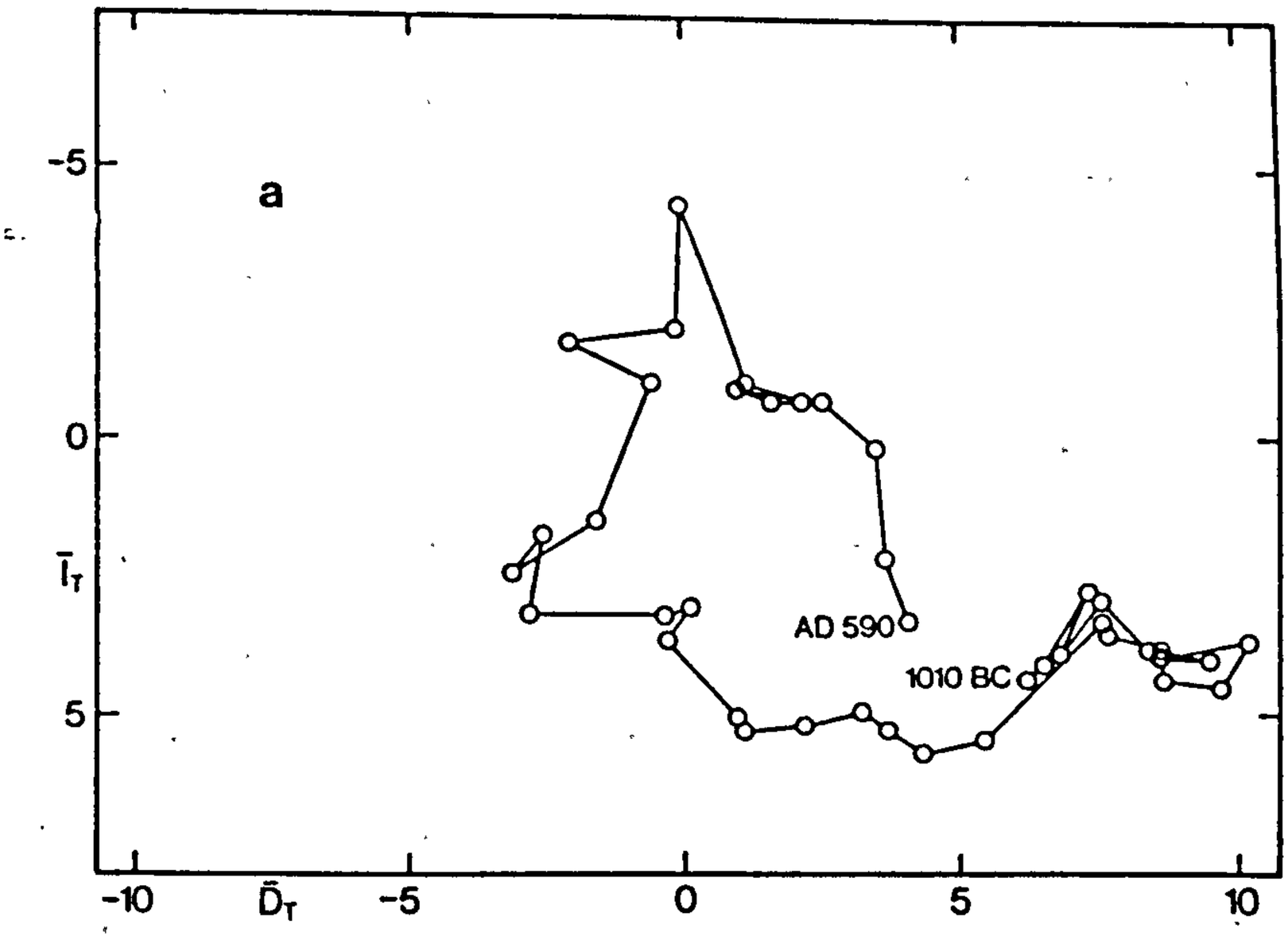

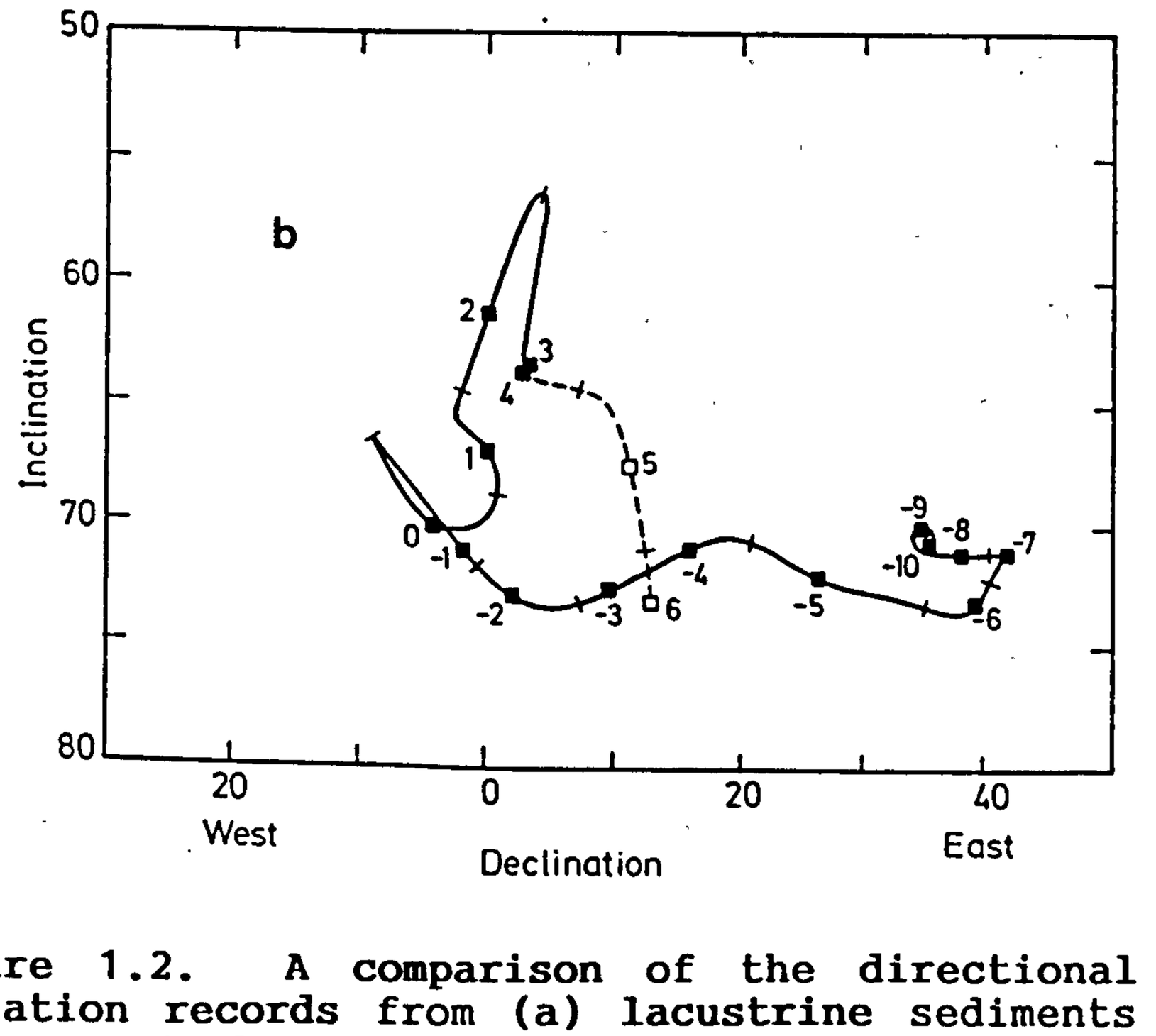

Figure 1.2. A comparison of the directional secular variation records from (a) lacustrine sediments and (b) archaeological artefacts in Britain between 1000 BC and 600 AD (the numbers in (b) indicate the age in hundreds of years, those with a minus sign indicate hundreds of years BC). After Clark et al. (1988) with data from Turner & Thompson (1979). Their is some agreement in the form of the variation although the amplitudes are different. This may be the result of the different recording processes (Clark et al. (1988).

drift has been estimated (e.g. Evans, 1987, Roberts & Piper, 1989), although both eastward and westward drift have been observed in some directional records (e.g. Kovacheva, 1982).

The potential of archaeomagnetic intensity records for detailed analysis of the geomagnetic field has been investigated by Gubbins & Roberts (1983). These workers used the frozen flux approximation (Roberts & Scott, 1965) to investigate the field gradients at the Earth's surface; as a result upper bounds could be placed on the Gauss coefficients, which are used to describe the Earth's magnetic field.

Gubbins & Roberts (1983) outline some of the problems associated with archaeomagnetic intensity records. The major problems are: the poor global coverage of the data, the difficulty of accurately establishing the contemporaneity of different sites due to imprecision of the dating, and the accuracy of the intensity data itself. The geographic distribution of archaeomagnetic data is dictated by the distribution of archaeological sites and the availability of material for research. The accurate determination of the contemporaneity of the records from different sites is important because large changes can occur within relatively short periods (less than 100 years e.g. Shaw, 1979). The accuracy of the geomagnetic field intensities obtained from archaeological artefacts has received considerable attention. Several factors which may affect the reliability and accuracy of archaeomagnetic

intensity estimates have been identified: variations of the ambient magnetic field during firing, magnetic refraction, magnetic fabric, the acquisition of only a partial thermoremanence, differences between experimental and original cooling rates and mineralogical changes subsequent to the initial firing or during experimental work. These factors are discussed in later sections.

1.4 Archaeological information

The derivation of archaeomagnetic records of geomagnetic secular variation was instigated by the requirements of both geophysics and archaeology. Much of the effort invested in determining geomagnetic secular variation has been prompted by the need to date archaeological artefacts and their associated sites.

Magnetic dating, effected by comparing the magnetic remanence direction obtained from an in-situ artefact with a previously established curve of geomagnetic secular variation, is a well established and widely used technique in regions in which geomagnetic secular variation is well documented (see Aitken, 1974, Clark et al., 1988 and Aitken, 1990).

The dating of artefacts by comparison of their record of the geomagnetic field intensity with references curves of the temporal variations of the intensity of the geomagnetic field are potentially more useful because smaller, unoriented artefacts such as potsherds and tile fragments are commonly recovered artefacts. However, the recovery of

a geomagnetic field intensity from an artefact is considerably more difficult than is the retrieval of the direction of remanence. Indeed, the rejection rate of intensity data often exceeds 50% (Aitken, 1990). Despite the difficulties, many geomagnetic intensity records have been compiled (see Creer et al., 1983) and have been used either alone or in conjunction with directional data to date archaeological sites.

Archaeomagnetic intensity measurements can also be used to test the authenticity of artefacts. A comparison of the field intensity obtained from an artefact with the present geomagnetic field intensity should yield a ratio which differs from unity if the artefact is genuine (Aitken, 1990). A similar study was undertaken to verify the authenticity of artefacts from the unique site of Glozel in France (Shaw, 1979). This involved a detailed study of the intensity of the geomagnetic field between 100 BC and 300 AD, which revealed a rapid, previously undetected (Barbetti, 1976), variation of the magnitude of the field between 0 and 200 AD.

An alternative method of magnetic dating based upon the time dependent nature of the magnetic remanence was devised and tested with reasonable success on some samples of igneous rock incorporated into Hadrian's Wall (Heller & Markert, 1973). The feasibility of magnetic viscosity dating is examined in detail in chapter 8.

The magnetic properties of a variety of artefacts have yielded other information pertinent to archaeology. The

natural remanent magnetisation of an artefact has been useful as an orientation tool and as a record of the thermal history of an artefact. For example, the direction of the magnetic remanence obtained from some Roman potsherds has been used to indicate the mode of stacking of the pottery during firing (Hedley & Wagner, 1990). In another study, the unblocking spectra of the magnetic remanence of remains from an early man site in Chesowanja, Kenya, were used to estimate the temperature to which the material was heated and thus deduce the use of fire (Gowlett et al., 1981). A similar study examined the vector composition of the natural remanence magnetisation obtained from some sixth century AD floor tiles. Three remanence components were identified which were considered to indicate the effects of cooking, a large scale fire and the original kiln firing (Evans & Mareschal, 1986).

The investigation of the magnetic properties of ancient coinage, in particular the acquisition of isothermal remanence, has shown that manufacturing technologies can be distinguished non-destructively, especially the difference between coins that are cast and those that are struck (Hoye, 1983). Measurement of the anisotropy of magnetic susceptibility has been used to determine the direction of rotation in which some Roman pottery was thrown (Hedley & Wagner (1990).

Characterisation of intrinsic magnetic properties such as magnetic hysteresis parameters may allow the provenance of an artefact to be assessed. By comparing the magnetic

parameters derived from a set of obsidian artefacts with several possible sources, McDougall & Tarling (1983) were able to identify the origin of the obsidian on the basis of the intensity of remanence, the low field susceptibility and the isothermal remanent acquisition. Coey et al. (1979) were able to separate a variety of Iranian pottery sherds on the basis of a comparison of their respective saturation magnetisations and coercivities. In addition to separating the sherds into various groups, Coey et al. (1979) demonstrated that the magnetic hysteresis parameters could be used to identify the firing conditions used in the production of the ceramics. See figure 1.3.

Apart from direct investigation of artefacts in the laboratory, the magnetic properties of many archaeological materials are utilised in the field. The magnetic remanence and susceptibility of many artefacts differ from those of the material in which they are buried because they contain different minerals or they have acquired their magnetic remanence by a different mechanism. This leads to anomalies in the local magnetic field which can be detected from the present surface level. Several methods of magnetic prospecting, in which either the total magnetic field or the vertical gradient of the magnetic field are measured at the surface are given by Aitken (1974). The differences between the magnetic minerals in archaeological materials and the surrounding soil have been used to identify new sites by studying the magnetic susceptibility measured at the surface (Taylor et al., 1990).

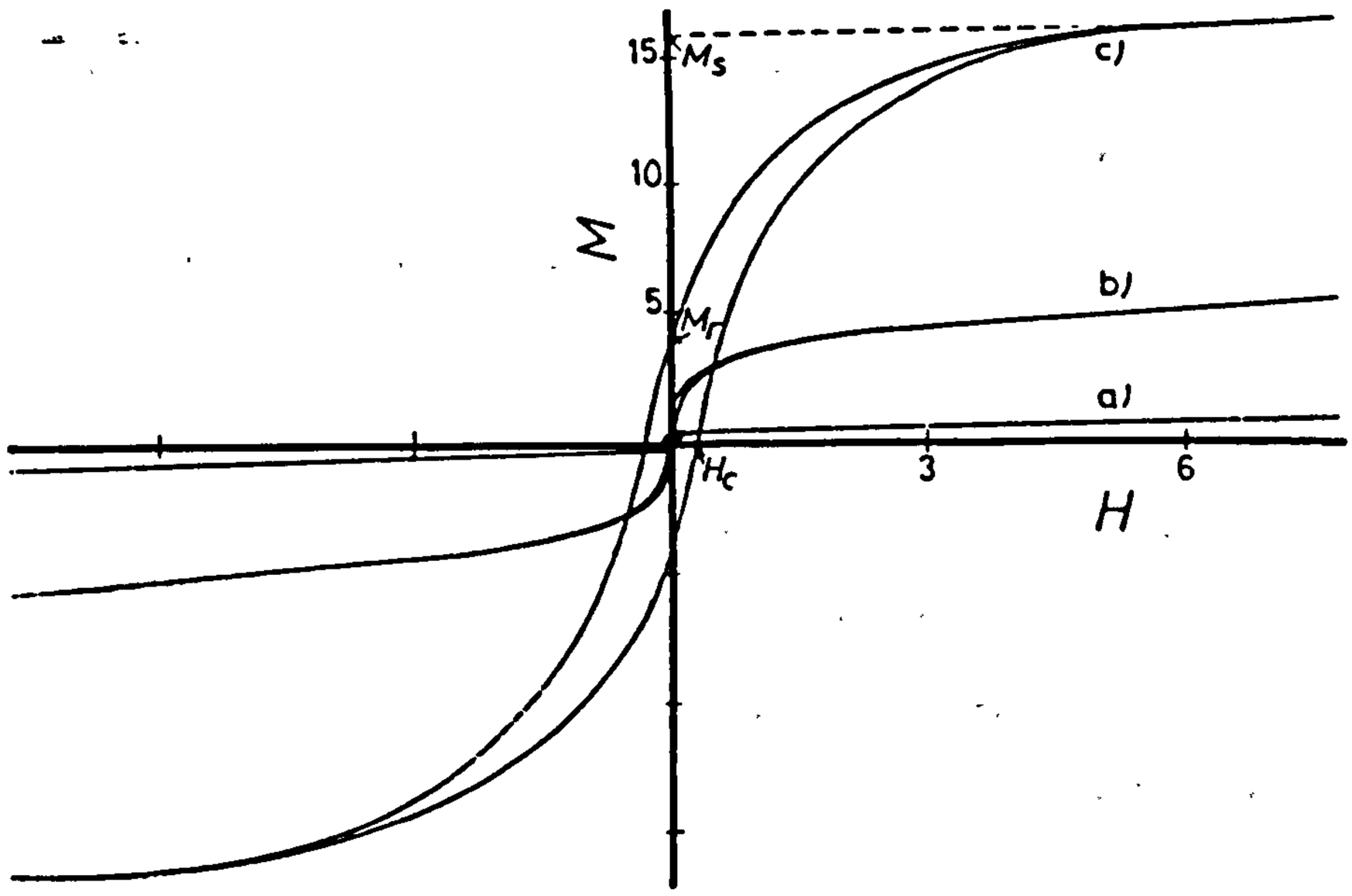

Figure 1.3. Magnetic hysteresis loops for (a) unfired soil, (b) a grey sherd and (c) a red sherd on the same M and H scales. The magnetisation and field are in arbitrary units. Adapted from Coey et al. (1979).

1.5 Archaeomagnetism

Many of the applications described in the previous sections have formed isolated studies and have not been developed. However, the use of the magnetic remanence of artefacts to determine the magnitude and direction of the geomagnetic field over archaeological time is an area of extensive study.

The determination of the direction of the ancient geomagnetic field requires access to artefacts which have retained a primary remanence and remained in-situ since the acquisition of this remanence. Samples from such artefacts

are orientated and then removed for laboratory analysis. This involves investigating the structure of the natural remanent magnetisation from which the direction of the primary remanence component can be determined. The direction of magnetisation of a specimen is obtained by measuring the intensity of the magnetisation in three orthogonal directions (in reality a more complex series of measurements is usually made to take account of any inhomogeneity of the magnetic minerals within a sample). The structure of the natural remanent magnetisation is then resolved by progressively erasing part of remanence by stepwise demagnetisation and remeasuring the remanent magnetisation remaining after each step. The primary remanence is then obtained from analysis of the demagnetisation data. The ancient field direction at the sampling site is obtained by transforming the primary remanence direction from the sample coordinate system to the geographic coordinate system. The precision of the data is improved by taking the vector mean of the field direction from several samples, which also allows the precision of the direction to be estimated. Apart from the random errors associated with the determination of geomagnetic directions from archaeological artefacts there are also some potential sources of systematic error. Systematic error can be introduced by misalignment of orientation equipment (Aitken, 1990) and distortion or subsidence of an artefact since firing (Clark et al., 1988). Other systematic errors can be introduced when the

ambient magnetic field during firing of an artefact is deviated by either the close proximity of large quantities of magnetic material, such as iron slag, or by magnetic refraction which occurs when the intrinsic magnetisation of the artefact is large (Aitken, 1990).

The principle of determining the magnitude of the geomagnetic field from samples which have a thermoremanent magnetisation, i.e. fired artefacts and igneous or baked rocks, is relatively simple and involves a comparison of the intensity of the magnetisation, M_{anc}, acquired in a field of unknown magnitude in antiquity, B_{anc}, with the intensity of the magnetisation, M_{lab}, acquired in a laboratory field, B_{lab}, of known intensity. The ancient field magnitude is then determined from the following equation:

$$B_{anc} = \frac{M_{anc}\ B_{lab}}{M_{lab}} \qquad (1.1)$$

(e.g. Aitken, 1983). The use of this equation presumes that a linear relationship between the magnetisation, M, and the field, B, exists over the range of fields investigated.

In practice, archaeomagnetic intensities are usually determined by comparing the magnetisations within equivalent parts of either the thermal unblocking spectrum (Thellier & Thellier, 1959) or the coercivity spectrum (Shaw, 1974) of a sample. The ancient field intensity is derived from the gradient of a plot of the ancient and

laboratory magnetisations held within each part of the spectrum, see figure 1.4. The advantage of this approach is that it gives an average value for the field intensity from different parts of the blocking/coercivity spectrum of a sample and it also reveals the presence of non-linearities between the ancient and laboratory magnetisations which indicate non-ideal behaviour.

Unfortunately, the lack of non-linear behaviour does not indicate the reliability of an archaeomagnetic intensity determination since, for example, linear thermal alteration may occur during laboratory heating (e.g. Walton, 1983). As a result of this uncertainty various methods have been developed in order to test the reliability of the data. The method of Shaw (1974) includes a test which checks for alteration of the coercivity spectrum of a sample as a result of the laboratory heating. This involves a comparison of the alternating field (AF) demagnetisation characteristics of anhysteretic remanent magnetisations (ARM) imparted before and after the laboratory heating. From this comparison, regions of the coercivity spectrum of a sample which are altered by heating, can be identified and used to reject data on the NRM-TRM plot.

The thermal method of Thellier & Thellier (1959) has been modified by Coe (1967) to include a test for alteration. This test involves repeat remagnetisations in temperature regions which have previously been activated, thus checking that the magnetisation acquired in these temperature regions remains unchanged and is not affected by

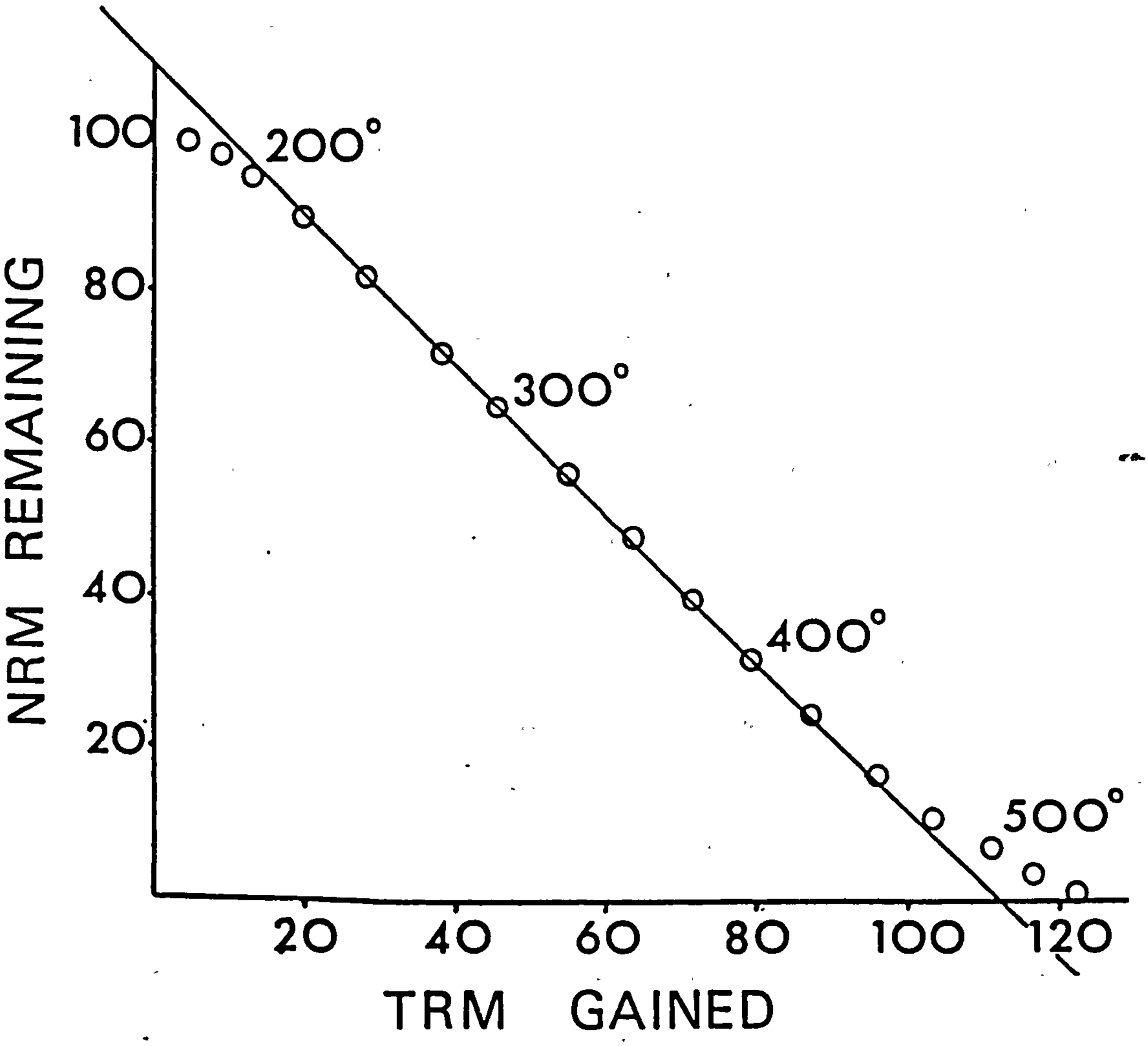

Figure 1.4. An Arai plot which compares the ancient magnetisation lost in a particular demagnetisation interval with the magnetisation gained in the same temperature interval by remagnetisation in the laboratory. The numbers indicate the temperatures steps used. The magnetisation is presented as a percentage of the natural remanent magnetisation value. From Aitken (1983).

alteration. Another test for the presence of thermal alteration involves monitoring the reversible magnetic susceptibility after each heat treatment (Walton, 1983a), although such tests may not reflect alteration of the magnetic particles which are responsible for the thermoremanence.

The identification of non-ideal behaviour and rejection of this data greatly increases the reliability of archaeomagnetic intensity determinations. Unfortunately this renders a considerable volume of data redundant. In consequence, several techniques have been developed to correct intensity data for non-ideal behaviour. The methods of correction for techniques based on AF demagnetisation have utilised the change of either the isothermal remanence (Carmichael, 1967) or anhysteretic remanence (Kono, 1978, Rigotti, 1978 and Rolph & Shaw, 1985) characteristics measured before and after heating. Thellier & Thellier type intensity experiments have been corrected by measuring the magnetisation acquired over different heating times; the correction involves extrapolating this data to zero time at which no alteration would have occurred (Tanguy, 1975, Walton, 1991).

1.6 The importance of the magnetic mineralogy of artefacts

For many of the applications described previously, such as magnetic surveying or archaeomagnetic direction determination, the precise nature of the magnetisation processes and the magnetic mineralogy of an artefact are

not of prime importance, suffice that the appropriate information can be obtained. In contrast, a thorough understanding of the magnetisation process and the magnetic mineralogy of an artefact is important for reliably obtaining the magnitude of the geomagnetic field in antiquity. A detailed knowledge of the magnetic mineralogy is also important for provenancing and comparing artefacts.

There are many magnetisation related factors which affect the reliability of archaeomagnetic intensity determinations. In the first instance the intensity obtained from an artefact may not be reliable because the ambient magnetic field during firing of the artefact in antiquity may have differed from the local geomagnetic field; such differences may be due to the presence of highly magnetic objects close to the site of firing. The original thermoremanent magnetisation of an artefact may also be affected by further heating during use in antiquity which leads to the acquisition of a partial thermoremanent magnetisation which replaces part of the original remanence and makes the natural remanent magnetisation more complex. The original remanence may also be altered by the thermal activation of certain of the magnetic particles at ambient temperature, which results in the acquisition of a viscous magnetisation. While the problem of the local magnetic field differing from the geomagnetic field is difficult to detect, the problems of partial thermoremanence and viscous remanence can often be identified and taken in to account (see Thomas, 1981). A further complication of the

magnetisation process is that the intensity of a thermoremanence depends on the cooling rate (Dodson & McClelland-Brown, 1980, Walton, 1980). It has been shown that when the cooling rate used during the induction of a laboratory thermoremanence differs significantly from the original cooling rate then the archaeomagnetic intensities determined from archaeological samples can vary systematically by up to a few percent from the true magnetic field value (Fox & Aitken, 1980).

The magnetisation of an artefact may be affected if there is a preferential alignment of the magnetic particles, i.e. a magnetic fabric. Such preferential alignment will bias the remanence direction acquired away from the local field direction towards the alignment axes. Rogers, Fox & Aitken (1979) suggested that such a fabric can be introduced during the manufacture of ceramics when the clay is pressed into a mould or turned on a wheel.

Several potential problems are associated with the type of magnetic mineral and the particle domain state. The magnetic remanence may be held by either stable single domain or multidomain particles. The thermal magnetisation process of single domain particles is relatively simple and it has been shown that there is close agreement between the magnetisation induced and the magnetisation removed within a particular temperature interval, in accordance with Thelliers' law of independence of partial thermoremanence (Levi, 1977). However, it has also been demonstrated that the thermal magnetisation and demagnetisation of

multidomain particles are dissimilar, resulting in non-linearity of NRM-TRM intensity plots (Levi, 1977). The domain state also affects the sense of the cooling rate dependence of the magnetisation. In the case of single domain assemblages, a decrease in the cooling rate leads to an increase in the intensity of magnetisation, while for multidomain assemblages the situation is reversed with slow cooling leading to a lower intensity of magnetisation (e.g. McClelland-Brown, 1984).

Problems also arise from single domain particles which are not thermally stable. Such particles may be described as superparamagnetic, or viscous, depending on their relaxation time at ambient temperatures. Viscous particles are problematic because their remanent magnetisation changes over time, thus erasing the part of the primary thermoremanent magnetisation which they acquired in antiquity and on which geomagnetic intensity determinations are based. The presence of superparamagnetic particles is less problematic since they carry no remanence, however, those with relaxation times of the order of an experimental measurement can lead to measurement errors since they can contribute a spurious component to the magnetisation over such times scales.

Apart from the physical problems associated with the domain structure of the magnetic minerals, the type, and more particularly chemical alteration, of the magnetic minerals may be important when considering the reliability of geomagnetic intensity determinations. The type of

magnetic mineral is important because it, in part, determines the intensity of remanence which thus affects the precision of a measurement. The mineral type is also important because it gives an indication of the chemical stability of the magnetic particles. For example, haematite is stable to oxidation but magnetite undergoes oxidation at low temperature to maghemite or at high temperature to haematite (see O'Reilly, 1984). Thus, the presence of maghemite in a sample probably indicates that chemical alteration has occurred.

As discussed, many of the problems associated with archaeomagnetic intensity determinations have been investigated. However, work on the magnetic mineralogy of archaeological artefacts has formed a part of only a few studies (Coey et al., 1979, Thomas, 1981 and Sternberg, 1989).

1.7 The objectives of this study

A general understanding of the magnetic mineralogy of archaeological artefacts has not been developed. Such an understanding would allow an assessment of the global similarities and differences between artefacts. This, in turn, would be useful for the assessment of the generic problems of using artefacts for archaeomagnetic intensity determinations, as well as for other applications such as the classification and sourcing of artefacts based on their magnetic mineralogy. Because pottery sherds are often the most abundant artefacts recovered at a site they form a

large part of the material used for archaeomagnetic work.

The principal objective of this study is to determine the mineralogy and domain states of the magnetic constituents of archaeological pottery. The definition of the magnetic mineralogy of this collection may allow an assessment of the similarities and variations intrinsic to fired clays. This knowledge may aid in assessing the reliability of archaeomagnetic intensity determinations and may be used to indicate the general applicability of magnetic measurements to the provenancing and manufacturing technology of such artefacts.

The magnetic mineralogy study will also be useful for assessing the feasibility of dating pottery on the basis of the magnitude of its viscous remanent magnetisation.

1.8 The sample set

In order to obtain a general understanding of the magnetic mineralogy of ancient ceramics, a collection of pottery sherds has been assembled which is geographically extensive, see figure 1.5, and which covers a range of ages. A description of the source of the sherds, their geographic location and ages (where available) are listed in appendix 1. The sherds are grouped in sets according only to their geographical origin. Thus the groups may be made up of samples from a single site covering a particular time scale or from several different sites within a region. A description of the groups follows.

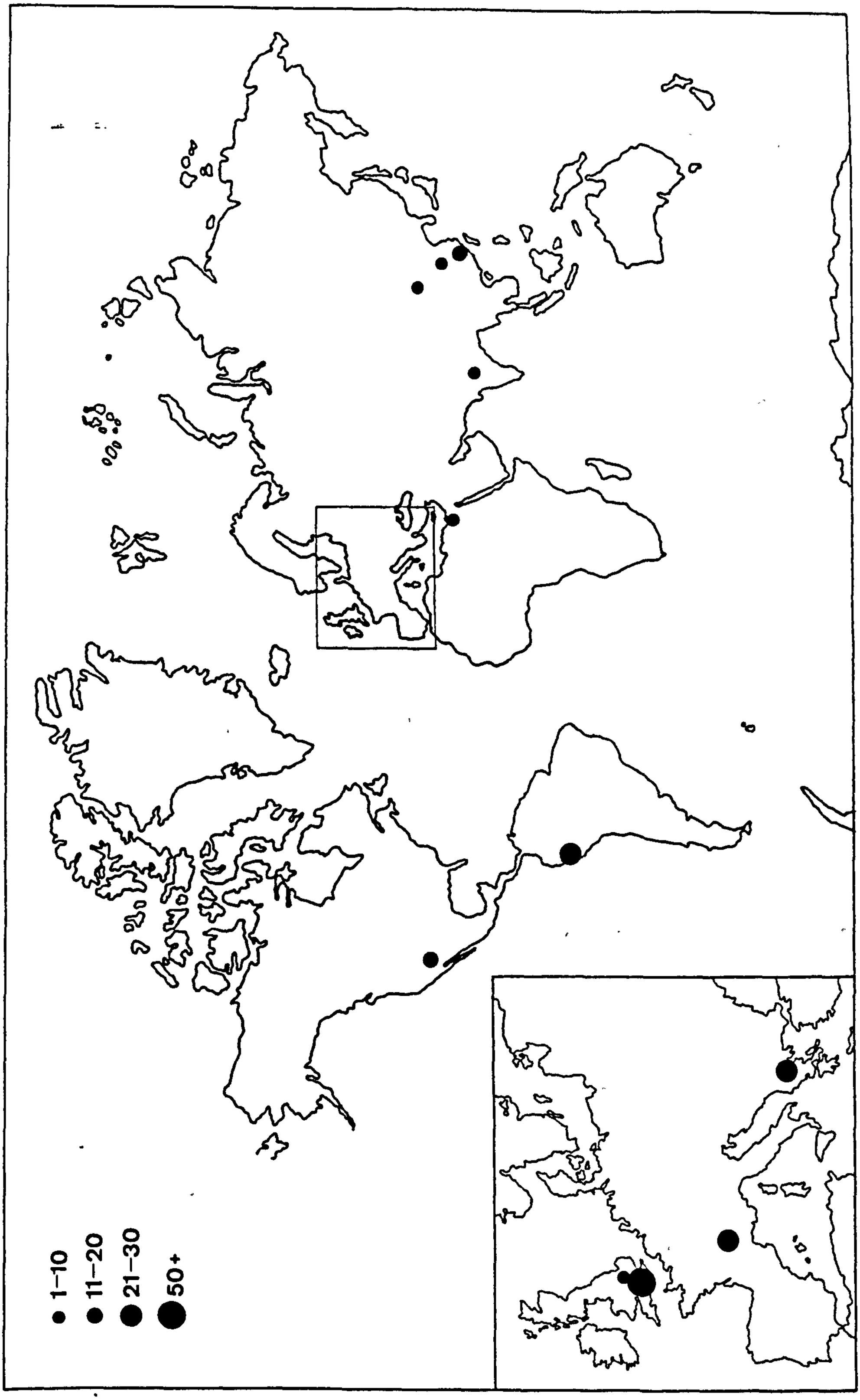

Figure 1.5. The geographical distribution of the sherds investigated in this study. The symbol size indicates the number of sherds.

French I

Set code: MC01

Apart from the country of origin no further information was available for these sherds. The set contained six coarse textured sherds.

British

Set code: MC02

This set consists of two sherds, both from Fengate, near Peterborough. One of the sherds is of Neolithic age and the other is from a collared urn of Early Bronze Age. Both sherds are poorly preserved.

Peruvian

These sherds are divided into five sets on the basis of the specific locations of the sherds. Each set is from a different site.

Set code: MC05

Five samples ranging from 300-700 BC to 300-700 AD were obtained from a single site. These sherds are of medium-fine ware.

Set code: MC06

Two sherds dating from about 1000 AD were obtained from a single site.

Set code: MC07

Five sherds of a medium-textured ware were obtained from a cave site. They are dated to about 1400 AD.

Set Code: MC08

Three coarse textured sherds were obtained from the same site as sherds of MC07.

Set code: MC09

Five sherds were obtained from a funerary or ceremonial context of a site. They range in age from 300-1000 BC to 300-800 AD.

Set code: MC10

Two very coarse, orange-coloured sherds were obtained from the same site, and are dated to 1700-1750 AD and 1600-1750 AD respectively. In addition to this a sherd of modern reproduction ceramic is included in this set.

French II

This comprises two sets of sherds which formed complimentary collections in the Geomagnetism Laboratory in Liverpool and the Research Laboratory for Archaeology and History of Art in Oxford.

Set code: MC11

Ten samples from various locations and varying in age from 0-50 BC up to 1500-1550 AD. Many of the sherds are from glazed fine ware.

Set code: MC13

Eleven sherds obtained from the Research Laboratory for Archaeology and History of Art, Oxford University form a similar and complimentary set to MC11 in both distribution and age. Indeed a sherd from the same pot occurs in both sets.

Egyptian

Set code: MC12

This set contains two sherds that were found embedded in adobe bricks. Consequently the ages are uncertain but

estimated at 2000-3000 BC.

Greek-Servian

Three sets from Servia in Northern Greece have been investigated. The samples have been obtained from three excavation trenches, with each set representing a separate trench.

Set code: MC14

This set contains three medium-ware sherds dated to Early-Bronze Age or Neolithic. These sherds have a relatively thick cross section.

Set code: MC15

Thirteen sherds were collected from the same trench. These are dated to the Late Early-Bronze Age. The sherds have been identified on the basis of their appearance, e.g. tooled ware and scored ware.

Set code: MC16

This set contains five sherds from the same site. They are dated to the Early-Bronze Age or Neolithic. These sherds are all geometrically painted coarse ware.

South-Western USA

Set code: MC17

This set contains thirteen sherds from various sites in the South-Western USA. The sherds vary in date from between 600-650 AD to 1875-1910 AD. Most of the sherds are medium to fine in texture.

Romano-British

A large collection of sherds was obtained from the major Romano-British manufacturing site of Alice Holt Forest in

Hampshire. The sherds are mostly a medium-fine grey ware which are a typical product of the reducing conditions used in the firing process. This group has been divided into eight sets on the basis of the original classification, which is based on age and location at this large site. The sherds range from 60-270 AD.

Set code: MC18 Nine sherds specific dates not available.

Set code: MC19 Nine sherds dated to 60-150 AD.

Set code: MC20 Twelve sherds specific dates not available.

Set code: MC21 Nine sherds dated to the latter part of 60-270 AD.

Set code: MC22 Nine sherds dated to 60-270 AD.

Set code: MC23 Six sherds dated to 60-270 AD.

Set code: MC24 Five sherds dated 60-150 AD.

Set code: MC25 Five sherds dated to 150-200 AD..

Chinese I

Set code: MC26

This set consists of eight medium-ware sherds from various locations in China, which range in age from 5400-5000 BP to 2300-2000 BP (thermoluminescence dates).

Chinese II

Set code: MC27

This set contains thirteen sherds of medium-ware and porcelain-type ware from various locations. The ages of these sherds ranges from 420-589 AD to 960-1279 AD, based on knowledge of the Dynastic system.

Indian

Set code: MC28

A single sherd represents this set. This sample is of black fine-medium ware from Northern India. No additional information is available.

1.9 Methodology

Magnetic mineralogy can be investigated in a variety of ways. Optical or scanning electron microscopy may be used to directly image the minerals. Indeed, the latter technique has made an important contribution to the study of the manufacturing technology of ceramics (see Tite, 1991). Unfortunately, the concentration of magnetic minerals in ancient pottery is commonly below one percent of the total mass, which makes finding particles difficult. In addition, the resolution of scanning electron microscopes (SEM) used for mineral analysis is often not much better than 0.1 μm (Robertson, 1990) which restricts the observation and mineralogical identification of potentially important magnetic constituents such as single domain magnetite particles. These difficulties most likely account for the fact that no magnetic minerals were identified during a preliminary SEM investigation of some samples used in this study.

Magnetic separation is potentially useful since it can increase the concentration of the magnetic minerals, which could then be identified using SEM (including energy dispersive X-ray analysis, EDX) or by X-ray diffraction. Magnetic separation was attempted as part of this study using a simple system in which crushed samples were

deposited in a water column, part of which passed through the pole pieces of a permanent magnet. Magnetic material was attracted to the edges of the pole pieces where the magnetic field gradient, and hence the force, was largest. The deposited material was examined in a SEM but only clay minerals were revealed, from which it was concluded that the ferri-magnetic minerals were swamped by the para-magnetic clay minerals to which they may have been adhered.

Mossbauer spectroscopy has been used by various workers to investigate the iron-containing minerals in pottery (e.g. Coey et al., 1979 and Hsia et al., 1988). Mossbauer spectroscopy probes the quantum energy state of the particular nuclei being excited, e.g. Fe^{57}, in the study of iron-containing minerals. The method can distinguish between the oxidation states of iron and also shows the presence of magnetic order and thus it can be used to identify magnetic minerals. Unfortunately, iron is a constituent of several clay minerals found in pottery and as a result the Mossbauer spectra are complex and assumptions must be made about the components present in order to interpret the spectra (Hsia et al., 1988). The clay minerals form a large fraction of pottery and contribute a large 'paramagnetic doublet' component which can dominate the Mossbauer spectrum of a sample. Figure 1.6 shows examples of the spectra obtained from two sherds investigated in this study.

The magnetic mineralogy may, of course, be investigated by measuring its magnetic properties. The primary

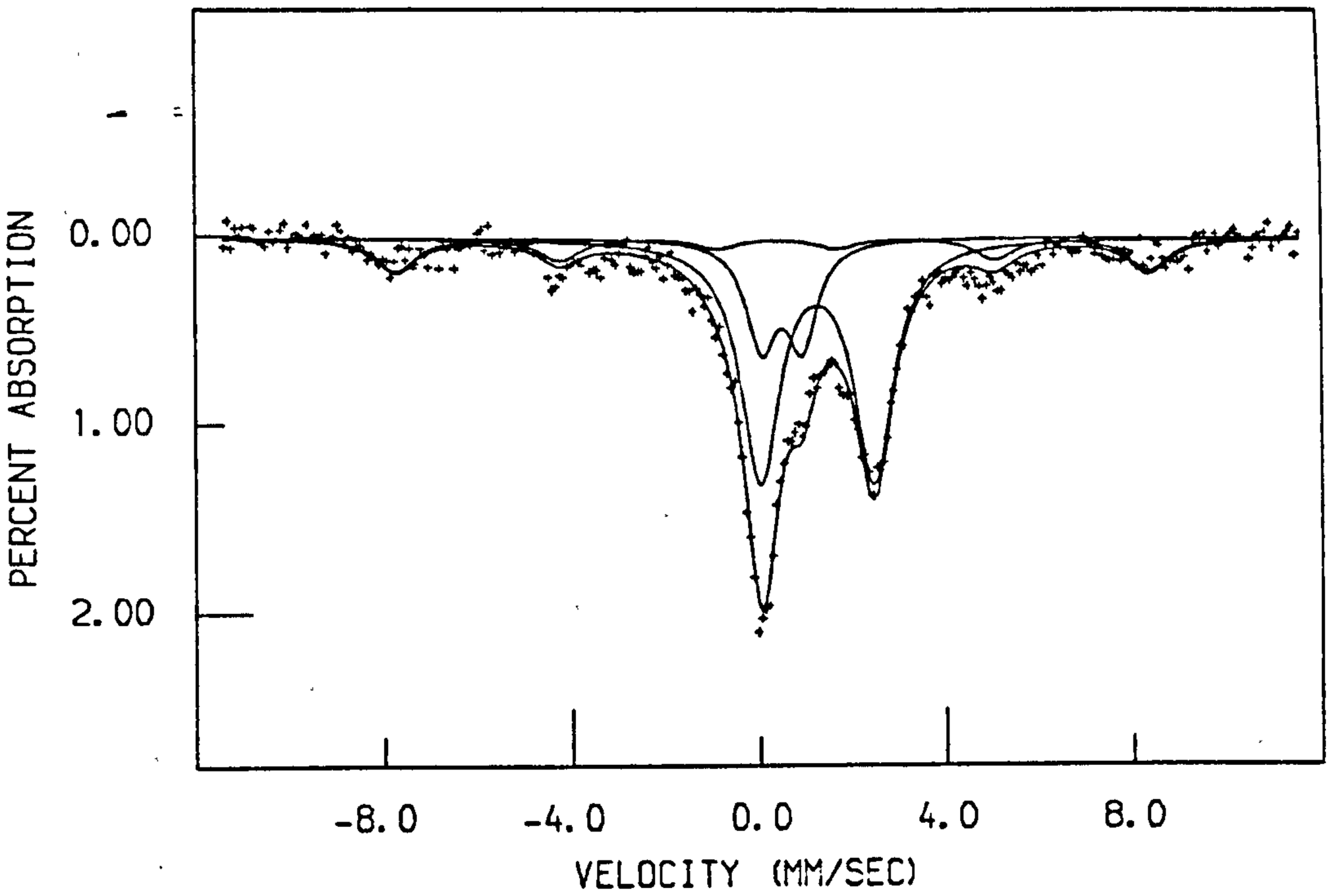

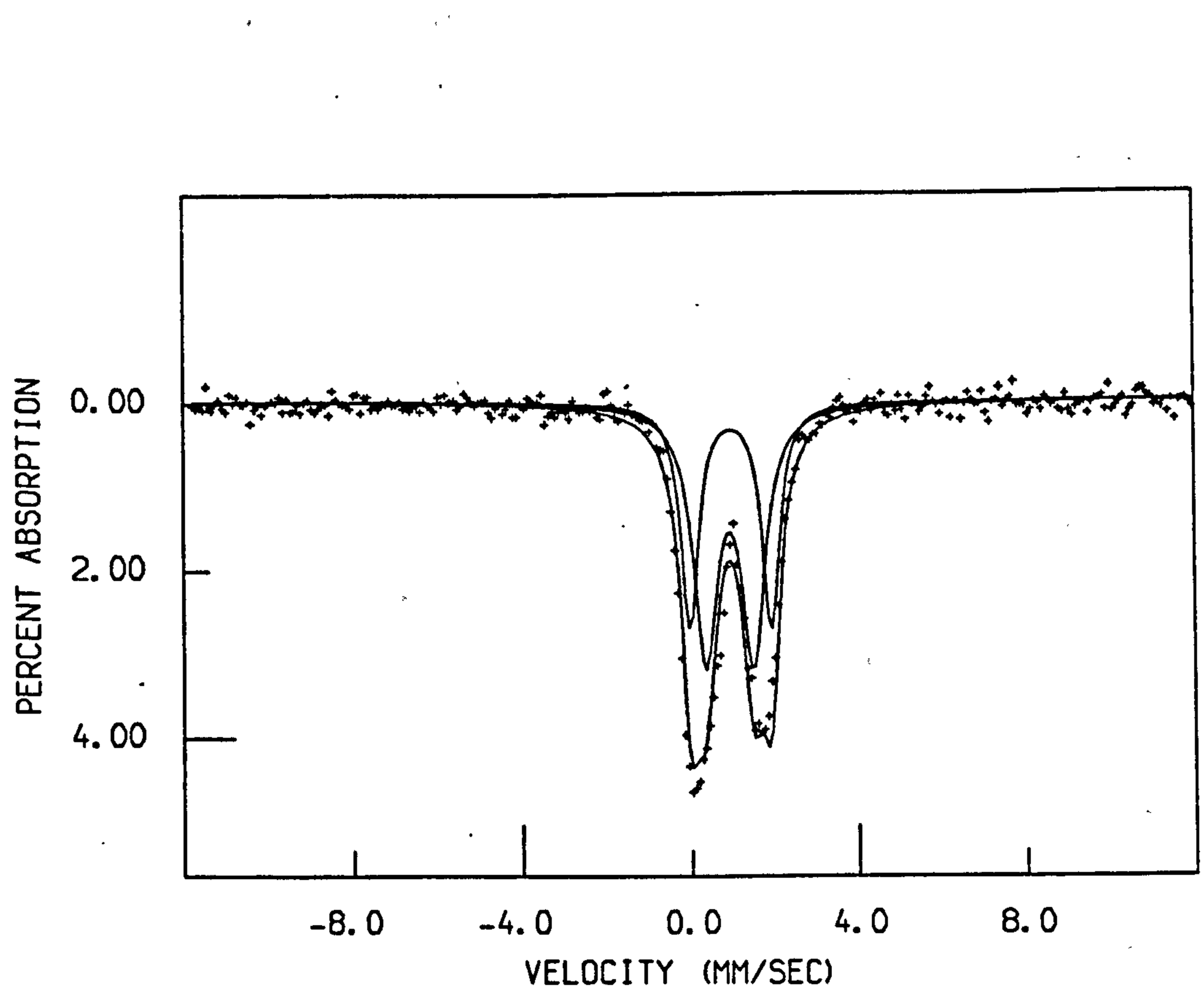

Figure 1.6. The Mossbauer spectra of two samples of Romano-British pottery measured in this study. The central doublet arises from paramagnetic Fe ions.

disadvantage is that the magnetic response of a system can become complex when it contains more than one magnetic mineral component. This problem can be improved by using several techniques which probe different aspects of the magnetisation.

Magnetic measurements have been used in this study to elucidate the composition, concentration and domain structure of the magnetic constituents of the collection of potsherds described above.

The composition of the magnetic minerals in the samples has been investigated principally by measuring the high field thermomagnetic behaviour of the samples with additional information obtained from the acquisition of isothermal remanence and from the variation of low field susceptibility with temperature from -196°C up to room temperature.

The concentration, i.e. the mass fraction of the ferrimagnetic minerals, has been determined using the value of the saturation magnetisation, obtained from magnetic hysteresis measurements, and using the mass specific saturation magnetisation of the appropriate mineral.

The domain states of the ferromagnetic minerals present in a sample have been investigated using magnetic hysteresis measurements, by measurement of the low field susceptibility at room temperature and by measuring the variation of susceptibility from -196°C up to room temperature. A detailed description of the methods and analysis are presented in the relevant chapters.

2 Physical Basis of Magnetism

2.1 Introduction

An understanding of the physical basis of magnetism is a prerequisite for the interpretation of macroscopic magnetic measurements. The following section discusses the atomic basis of magnetism, the mechanisms which give rise to the phenomena of diamagnetism, paramagnetism and ferromagnetism (including antiferro- and ferrimagnetism) and simple magnetic domain theory.

2.2 Atomic magnetism

The atomic basis of magnetism is restricted here to the simple systems of atoms and ions which have a partially filled inner shell; these systems are applicable to the minerals investigated in this work.

2.2.1 Diamagnetism

The macroscopic observation of diamagnetism is of a weak induced magnetisation which is proportional to, and directed in opposition to, an applied field. This phenomenon can be understood simply on the basis of Lenz's Law (Kittel, 1966) where a change in the magnetic field applied to a system induces a current which acts to oppose the applied field. The induced current in the atomic context arises from the precession of the electron distribution about the nucleus. The associated magnetic moment is opposite to the applied field. The magnitude of the diamagnetic moment can be determined from the product

of the current and the mean square radius of the electron orbits. This in turn allows the formulation of the diamagnetic susceptibility per unit volume (X) as:

$$X=\frac{Nu}{H}=-\frac{Ze^2N}{6mc^2}\overline{r^2} \qquad (2.1)$$

(Kittel, 1966), where N is the number of atoms per unit volume, Z is the number of electrons per atom, r^2 is the mean square radius of their orbits, e is the charge on an electron and μ is the magnetic moment.

All materials exhibit diamagnetism. Diamagnetic susceptibilities are small compared to other forms.

2.2.2 Paramagnetism

Paramagnetism is observed as an induced magnetisation which is directed parallel to the applied magnetic field. The induced moment increases linearly in applied fields up to a few Tesla and varies linearly with the reciprocal of temperature. Paramagnetic behaviour can be explained by considering that the atomic magnetic moments, which are associated with electron spin (spin ½ has a magnetic moment defined as one Bohr magneton), are pulled into alignment by an applied field and disturbed from this alignment by their thermal energy. More specifically, the application of a magnetic field alters the energy levels of the electron. In the case of an electron with no orbital moment, the spin ½ levels are split into one of higher and one of lower energy on application of a magnetic field; the lower energy level having the spin moment parallel to the applied field. The net paramagnetic moment for a material

containing N atoms is therefore the difference between the populations of the two spin states and depends on the field strength and temperature. See figure 2.1. The magnetic susceptibility, X, for paramagnetic materials at room temperature and fields less than a few Tesla is described in the form of the Curie Law:

$$X=\frac{C}{T}=\frac{N\mu^2}{3kT} \qquad (2.2)$$

(Crangle, 1977), where C is the Curie constant.

2.2.3 Spontaneous magnetism

Ferro- and ferri-magnets are characterised by the presence of spontaneous (remanent) magnetisation and high susceptibilities. The spontaneous magnetisations of both are strongly temperature dependent and break down at the Curie Point. Antiferromagnetism is closely allied to ferro- and ferri-magnetism but is characterised by the absence of spontaneous magnetisation.

The magnetic structures of ferro-, antiferro- and ferri-magnetic materials are similar in that the atomic dipole moments (arising essentially from the electron spin) are ordered over large distances (compared to atomic dimensions). This ordering arises from a quantum mechanical interaction termed the exchange interaction. In simple ferromagnets the electron spins are coupled parallel and directly, giving rise to regions with spontaneous magnetisation. In antiferromagnets the adjacent spins are coupled antiparallel, resulting in long range order with no net spontaneous magnetisation. Ferrimagnetic materials

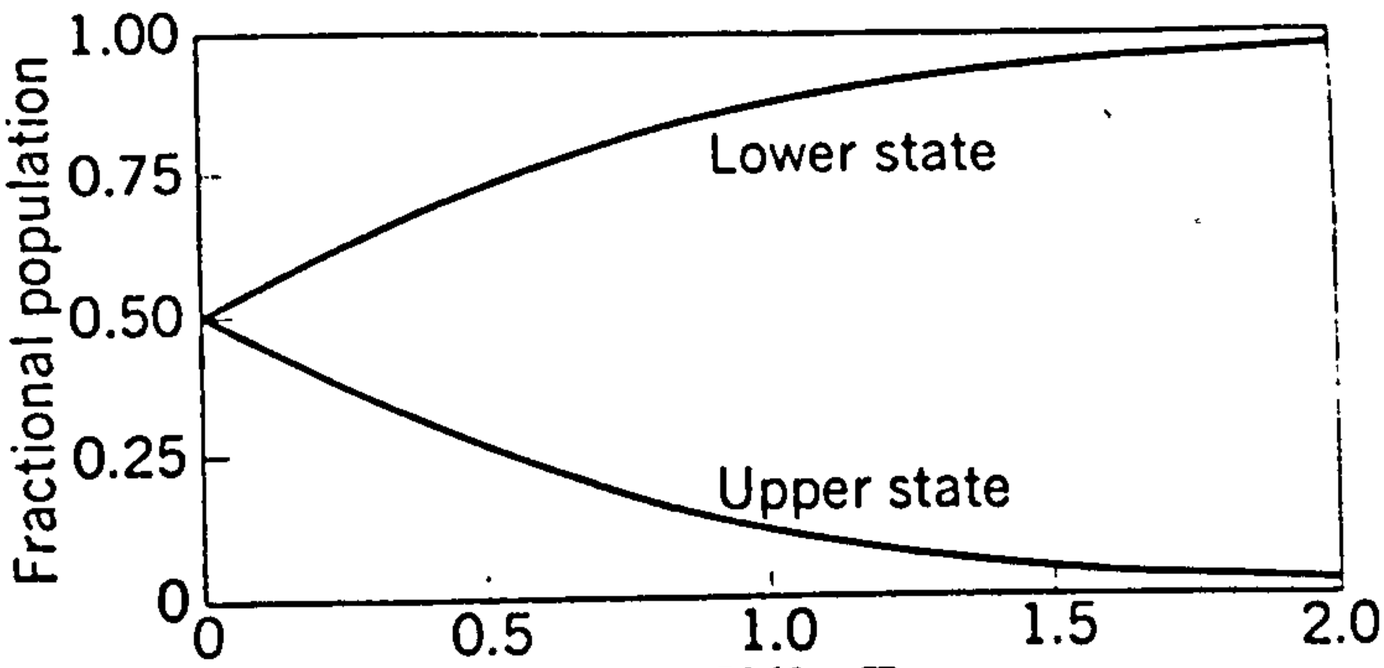

Figure 2.1. The fractional population of the two spin levels in a paramagnetic system in equilibrium at a temperature, T, and magnetic field, H. The magnetic moment of the system is proportional to the vector sum of the spins. It can be seen that increasing the magnetic field or decreasing the temperature increases the net magnetic moment.

have a coupling structure similar to antiferromagnets but the opposing atomic moments are of unequal magnitude, leaving a net magnetisation. The atomic coupling relationships that lead to ferro-, ferri-, and antiferromagnetism can be understood in terms of a model invoking two opposing sublattices. The net magnetisation M of such a system can be described by:

$$M=yM_1-(1-y)M_2 \qquad (2.3)$$

(Crangle, 1977), where M_1 and M_2 are the magnetic moments on the first and second sublattices respectively and y is a fraction between 0 and 1.

For a ferromagnet y=1 (or y=0) indicating that the magnetisation arises from a single lattice configuration.

For a simple antiferromagnet y=0.5 which produces two equal but oppositely magnetised sublattices resulting in zero net moment. For the ferrimagnetic case 0<y<0.5 (or 0.5<y<1) giving two opposing but unequal sublattice moments which partially cancel to leave a net magnetisation.

2.3 Magnetic iron oxides

The discussion of spontaneous magnetisation has so far been general. However, in natural samples the spontaneous magnetisation is most often attributable to iron oxide minerals. An extended discussion of the geometrical and magnetic structures of some of the relevant iron oxides is, therefore, pertinent to the present work.

In the preceding section an explanation of the coupling which gives rise to long range magnetic order was briefly mentioned; in the case of iron oxides the coupling mechanism is similar but more complex. For direct coupling, the outer electron distributions of adjacent cations must overlap. Since the Pauli exclusion principle operates in the region of overlap, no two electrons can occupy the same energy state and consequently if an electron occupies a subshell already containing another electron their respective spins must be antiparallel. Conversely, if an electron enters an unfilled subshell its spin moment will be parallel to others in the same shell. The spins in both cases are coherently coupled. This is termed direct exchange.

The separation of adjacent cations in iron oxides

suggests that positive (parallel) exchange interaction is possible. However, it has been observed that the strongest interaction between cations is negative (antiparallel) (Gorter, 1954). The proposed mechanism involves the oxygen ion between two cations, which acts as an electron bridge. This indirect coupling is termed superexchange. Both exchange and superexchange are short-range forces.

2.3.1 Ferrimagnetic iron oxides

The ferrimagnetic iron oxides have the general formula $Fe_{3-x}M_xO_4$, where M represents one or more substituted cations. These oxides have the inverse spinel structure. A unit cell of the spinel structure contains eight formula units. The oxygen anions, of which there are thirty-two in the unit cell, form a close-packed face-centred cubic structure, with the cations ordered between them on sites having either four (tetrahedral (A) sites) or six (octahedral (B) sites) nearest neighbours (O'Reilly, 1984). The unit cell contains eight cations on the tetrahedral sites and sixteen on the octahedral sites (Crangle, 1977). See figure. 2.2.

The spontaneous magnetisation of the spinel structure is explained simply in terms of the two-sublattice model discussed earlier in section 2.2.3. The tetrahedral and octahedral configurations constitute the two sublattices in the spinel structure. The net magnetisation is dependent upon the number and type of cations occupying the respective sites. In the case of magnetite (Fe_3O_4), Fe^{3+} ions occupy the eight tetrahedral sites of the unit cell,

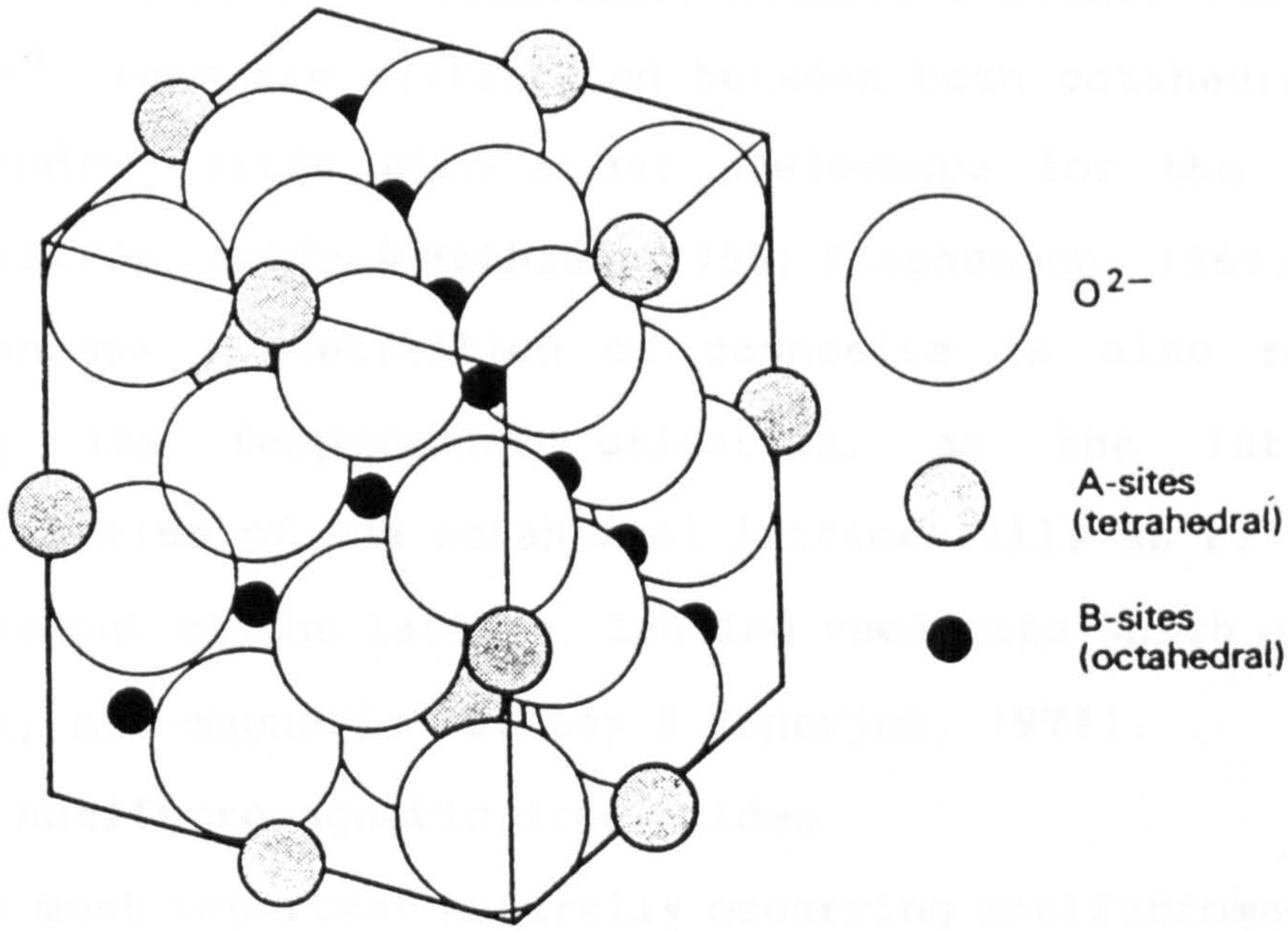

Figure 2.2. A schematic illustration of the structure of a ferri-magnetic spinel iron oxide. After Crangle (1977).

giving a total magnetisation of five Bohr magnetons, which oppose the combined magnetisation of eight Fe^{3+} (also five Bohr magnetons) and eight Fe^{2+} ions (four Bohr magnetons) which occupy the octahedral positions. This opposition produces a resultant magnetisation of four ((4+5)-5) Bohr magnetons per unit cell (Gorter, 1954). The effect of substituted cation species on the spontaneous magnetisation is dependent upon their lattice site preference and the distribution of Fe^{3+} and Fe^{2+} in the presence of these cations. When iron is partially replaced by titanium the spontaneous magnetisation is reduced. In

this case, the non-magnetic Ti^{4+} ions preferentially occupy the octahedral sites (Ishikawa, Akimoto & Syono, 1964) and the Fe^{3+} ions are distributed between both octahedral and tetrahedral sites with a net preference for the latter (Chevallier, Bolfa & Mathieu, 1955; Stephenson, 1969). The spontaneous magnetisation of magnetite is also reduced during low temperature oxidation, as the intrinsic magnetisation of the octahedral lattice falls as Fe^{2+} ions diffuse out of the lattice, leaving vacancies which are, of course, non-magnetic (Stacey & Banerjee, 1974).

2.3.2 Antiferromagnetic iron oxides

The most important naturally occurring antiferromagnetic mineral is haematite, α-Fe_2O_3. Haematite has a trigonal structure (Deer, Howie & Zussman, 1966), where the oxygen anions form a hexagonal close packed lattice. The cations, which occupy two thirds of the octahedral interstices, are ordered hexagonally in layers (O'Reilly, 1984). See figure 2.3. The hexagonal unit cell comprises twelve Fe^{3+} ions and eighteen oxygen ions. The antiferromagnetic order arises from the opposition of the intrinsic moments on alternating cation layers (the layers are equivalent to the opposing sublattices of the model described earlier).

Despite antiparallel exchange coupling between adjacent cation layers, haematite has a small spontaneous magnetisation. This has been explained in terms of a 'spin canting' effect (Dzyalozinski, 1958) where the moments of all layers are displaced from the plane of the layer by a small angle. The resulting magnetisation is perpendicular

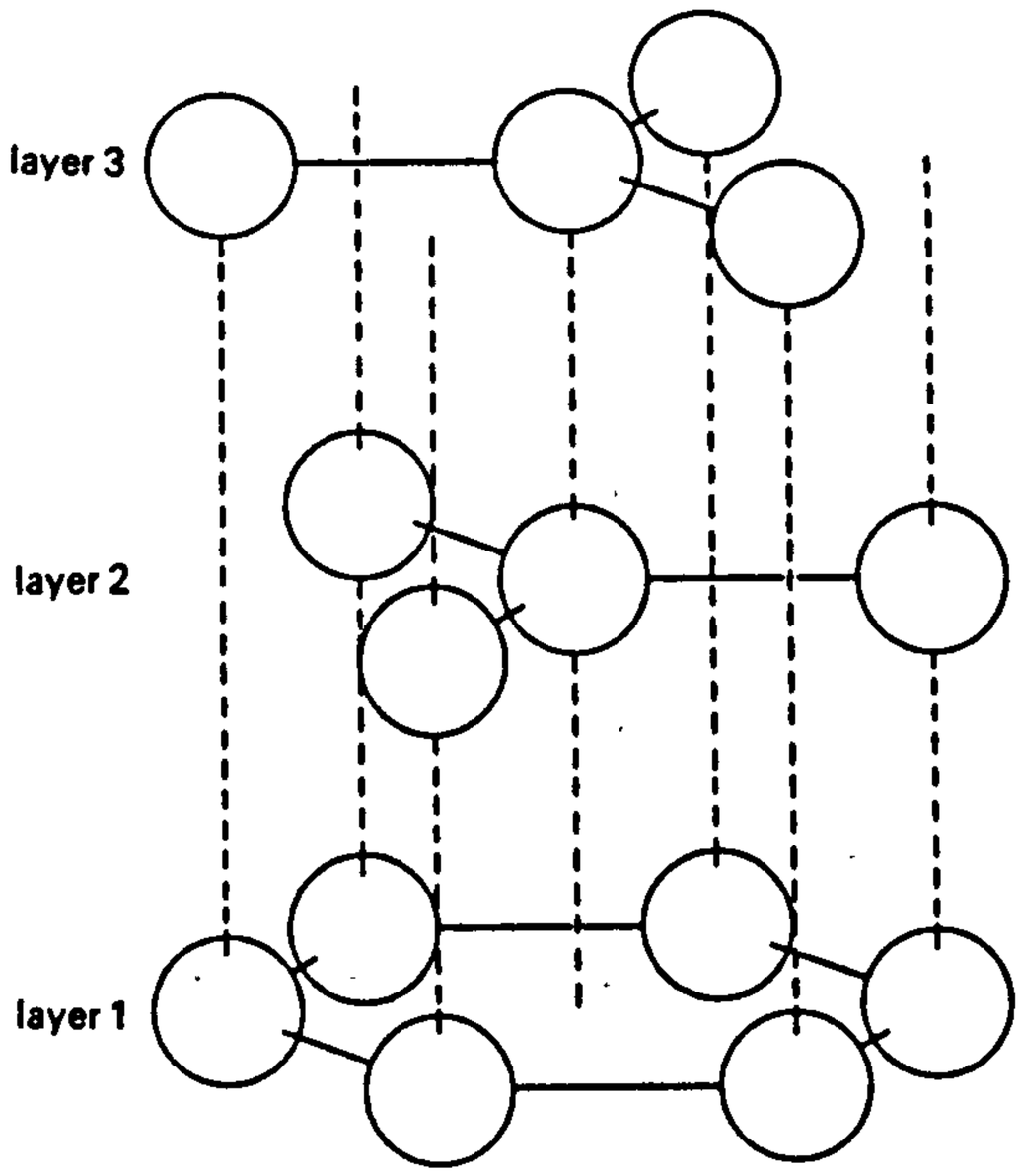

Figure 2.3. A schematic illustration of the cation arrangement of haematite. After O Reilly (1984).

to the cation planes. In addition to this mechanism a defect moment has been noted by various workers (see Dunlop, 1971). The origin of this moment is not well understood but may arise from either intergrowths of epitaxial Fe_3O_4 or ferrimagnetic forms of Fe_2O_3, or alternatively from impurities such as maghemite or magnetite (Dunlop, 1971).

Another antiferromagnetic mineral of importance in nature is the iron hydroxide, goethite, α-FeOOH. Goethite has an orthorhombic structure, with four formula units per unit cell (Deer et al., 1966). The structure is similar to that of haematite with the oxygen ions arranged in a close-packed hexagonal lattice with the cations positioned at

octahedral interstices. The coupling between adjacent cation layers is antiparallel, with the spontaneous magnetisation being ascribed to the presence of Al^{3+} impurities which preferentially occupy particular sites thus reducing the magnetisation of some layers to leave an unbalanced magnetic moment (Hedley, 1971). An alternative explanation for the spontaneous magnetisation suggests that the presence of vacancies in the oxygen ion sites causes breaking of some of the iron-oxygen-iron chains leaving unopposed spins (Stacey & Banerjee, 1974).

2.4 Domain magnetism

2.4.1 Anisotropy

The previous sections have dealt with the atomic phenomena which produce spontaneous magnetism. However, the phenomena described would produce magnetisations that were not fixed in any particular configuration but would follow the ambient magnetic field. Stable remanent magnetisation occurs as a result of magnetic anisotropy, which constrains the magnetisation to a set of preferred orientations within a material. Magnetic anisotropy arises from various sources.

2.4.2 Shape anisotropy

Shape anisotropy can be explained by considering a magnetic particle which is uniformly magnetised. The magnetisation of the particle gives rise to surface poles which produce an external field and an equal and opposite internal field, see figure 2.4; the internal field is

termed the demagnetising field, as it is directed in opposition to the intrinsic magnetisation of the particle and tends to demagnetise it. The demagnetising field H_D is calculated according to:

$$H_D=-NM \qquad (2.4)$$

(O'Reilly, 1984), where M is the magnetisation of the particle and N is the demagnetising factor. The demagnetising factor is a function of the pole geometry and is therefore dependent on the particle shape. The demagnetising field acts to disturb the atomic order arising from exchange forces. The competition between the exchange forces and the demagnetising field raises the energy of a particle of volume v by an amount E_m, the magnetostatic self energy, where:

$$E_m=-\frac{1}{2}\mu_0 M.H_D v \qquad (2.5)$$

(O'Reilly, 1984), μ_0 is the permeability of free space.

In order to minimise E_m, the magnetisation tends to align in the direction of the smallest demagnetising field, which depends on the particle shape. This control of the magnetisation direction is termed shape anisotropy.

All magnetic materials have a demagnetising field, and hence shape anisotropy, for example, elongated particles have a shape derived anisotropy which is uniaxial where the easy axis lies along the long axis of the particle. However, shape anisotropy only becomes important for materials which have a high intrinsic magnetisation.

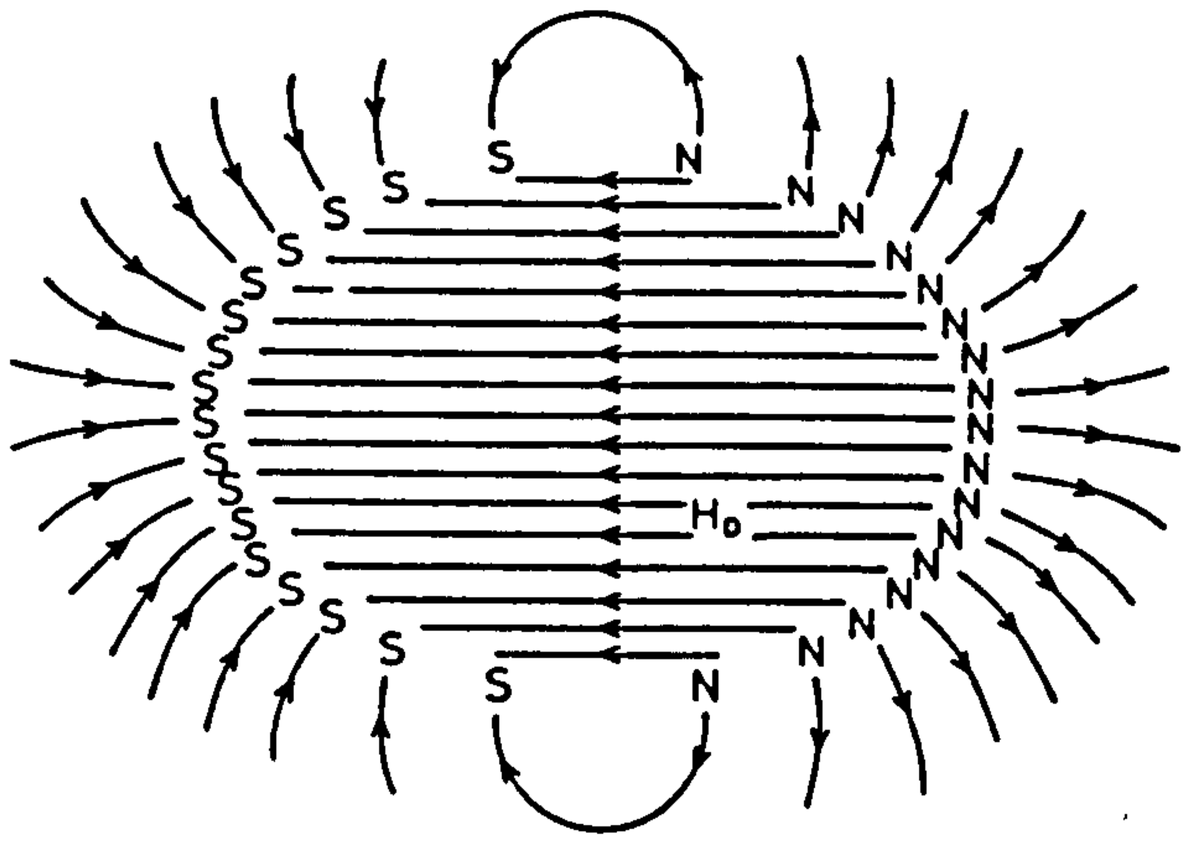

Figure 2.4. An illustration of the surface magnetic poles and the associated demagnetising field in a single domain particle. After O'Rielly (1984).

2.4.3 Magnetocrystalline anisotropy

The intrinsic magnetisation of a material is explicitly linked to its crystal structure. The crystal structure imparts regular order to the electron orbits which in turn, through spin-orbit coupling (Kittel, 1966), define directions where the magnetisation has minimum (the 'easy' axis of magnetisation) and maximum energy (the 'hard' axis). For a cubic lattice (appropriate to magnetite) the energy, E_k, required to magnetise a material in a particular crystallographic direction can be obtained to a good approximation from the relation:

$$E_k=K_1(\alpha_1^2\alpha_2^2+\alpha_2^2\alpha_3^2+\alpha_3^2\alpha_1^2)+K_2\alpha_1^2\alpha_2^2\alpha_3^2 \quad (2.6)$$

(Stacey & Banerjee, 1974), where K_1 and K_2 are empirical constants usually termed the first and second magnetocrystalline anisotropy constants. The α symbols denote the direction cosines of the magnetisation from the

crystallographic axes.

2.4.4 Magnetoelastic anisotropy

The spin-orbit coupling which allows the crystal structure to impose magnetocrystalline anisotropy also allows the magnetisation to be affected by stress applied to the lattice. The application of stress will strain the lattice, which in turn will deform the structure if doing so reduces the magnetocrystalline anisotropy energy (Kittel, 1966). The change in dimensions resulting from deformation is termed the magnetostriction. Magnetostriction imposes anisotropy through its influence upon the magnetocrystalline anisotropy. The anisotropy energy associated with magnetostriction is termed the magnetoelastic energy, E_s. The relationship between magnetoelastic energy and applied stress is described in the simplest form according to;

$$E_s = \frac{3}{2} \lambda_s \sigma \cos^2\theta \qquad (2.7)$$

(Stacey & Banerjee, 1974) where λ_s is the magnetostriction coefficient, σ is the applied stress and θ is the angle between the magnetisation and the applied stress.

2.5 Domain structure

Both the direction and intensity of magnetisation of a particle can be understood when the anisotropy energy terms related to the exchange interactions, particle shape, crystal structure, internal strain and the external field are known. The magnetisation of a particle tends to

configure such that its total energy is minimised. For a small particle, superexchange orders the spin moments parallel throughout the structure forming a single domain (SD). The spin moments are tied to one of a set of preferred directions by the dominant anisotropy term. This may be shape anisotropy in strongly magnetic materials such as magnetite, and magnetocrystalline anisotropy in weak magnetic materials such as haematite. With increasing particle size, the demagnetising field becomes larger. Eventually the demagnetising field reaches a critical value above which a single coherent spin structure (single domain) is no longer the minimum energy condition. In this situation the spin structure is reordered to a minimum energy configuration which has a lower demagnetising field. The simplest way of reducing the demagnetising field in a particle is via the formation of two domains with oppositely directed magnetisations, see figure 2.5a. More complicated domain configurations, which include closure domains, can reduce the demagnetising field further, for example see figure 2.5b. The formation of structures with two or more domains adds a further energy term which is related to the formation of a domain wall between the opposing domains. The domain wall is a transition layer in which the spin structure is incoherent (O'Reilly, 1984). The spin structure through a domain wall is illustrated schematically in figure 2.6 (Crangle, 1977). The thickness of a domain wall is controlled by the exchange energy which favours wider walls, since the angle between adjacent spins

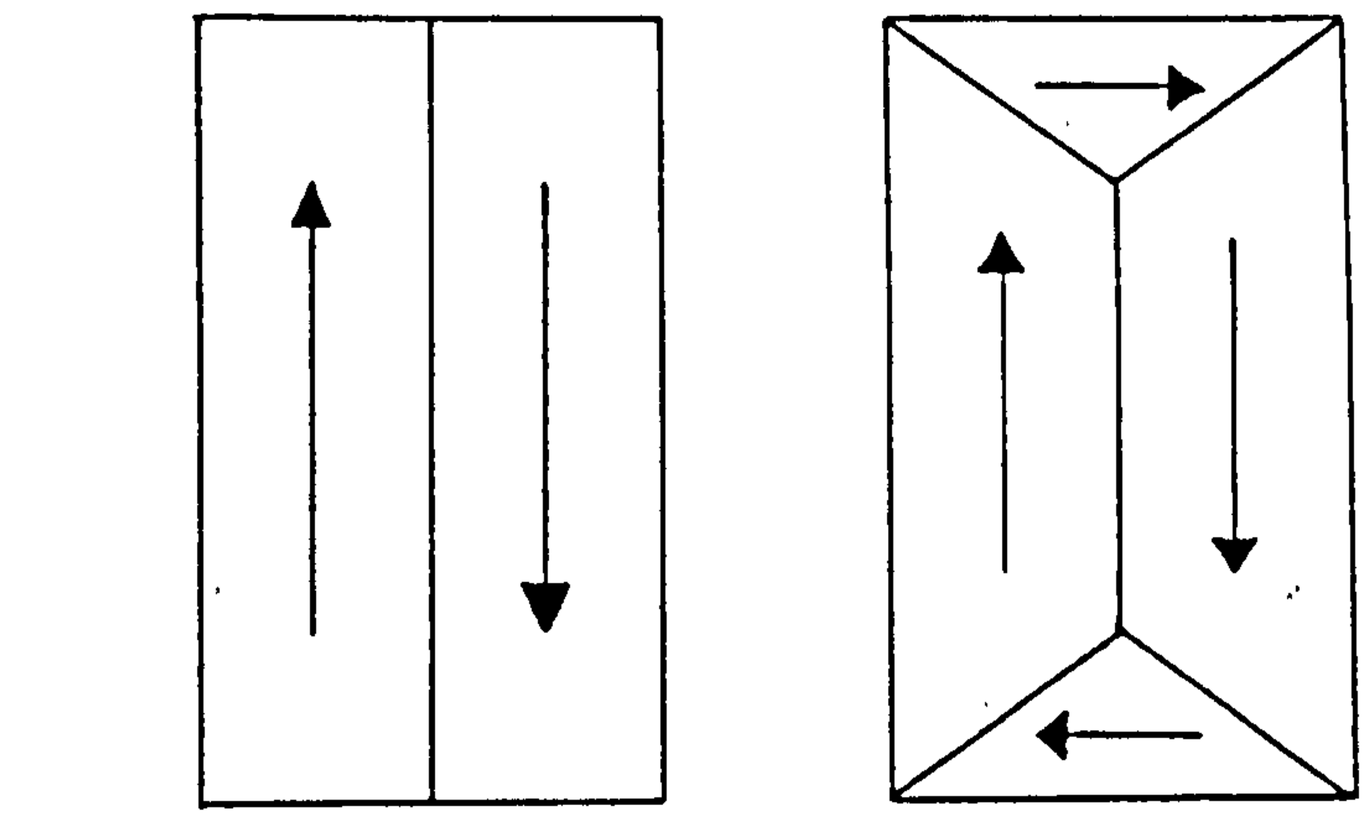

Figure 2.5. An illustration of (a) a simple two domain configuration which reduces the magnetostatic energy of a particle and (b) a more complex domain structure which has closure domains which further reduce the magnetostatic energy.

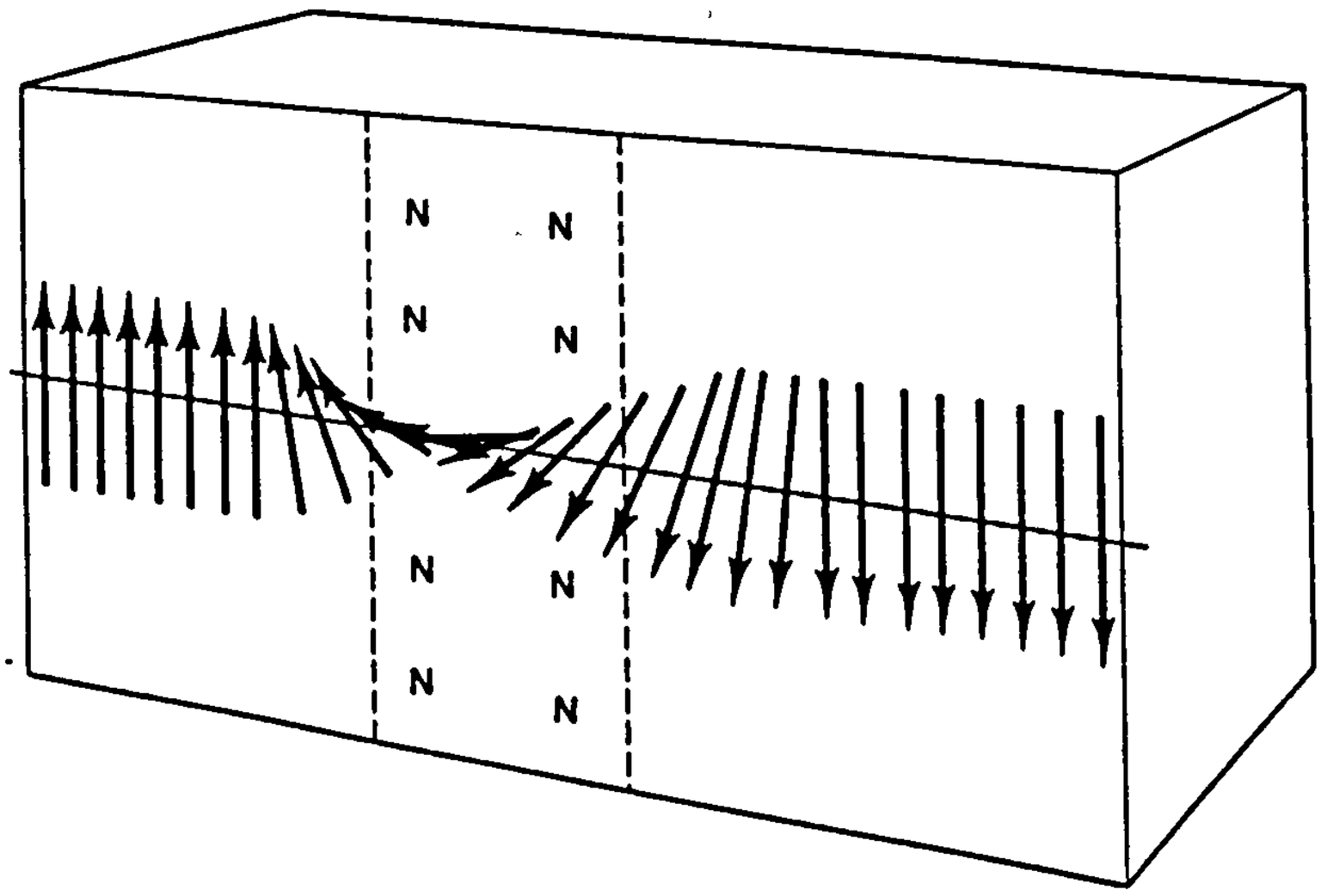

Figure 2.6. A schematic illustration of the spin structure through a domain wall which separates two oppositely magnetised domains. After Crangle (1977).

is reduced, and the anisotropy energy which tends to limit the width (Kittel, 1966). However, despite a particle having minimum energy in a particular multidomain (MD) configuration, it may not achieve this structure. A particle may occupy one of a series of metastable states termed local energy minima (LEM) (Moon & Merrill, 1984), which correspond to different numbers of domains. In such situations additional energy is therefore required to nucleate more domain walls to obtain the lowest energy configuration.

The presence of the metastable state may explain the observations of Soffel (1971), in which particles of similar size were observed to have varying numbers of domains, see figure 2.7.

The particle size at which the single to two domain transition occurs in cubes and rectangular parallelepipeds of magnetite have been calculated by Butler & Banerjee (1975). They obtain values in excess of 0.08 μm for cubes and 0.40 μm for rectangles with a length to width ratio of 2.5:1. However, both Moon & Merrill (1985) and Scherbakov & Lamash (1988) suggest that a metastable single domain state can exist above the critical particle sizes obtained by Butler & Banerjee (1975). These metastable single domain particles can exist up to 0.14 μm for cubes and for any particles elongated beyond the ratio 2.6:1 (Scherbakov & Lamash, 1988).

The particle size for the single to two domain transition in haematite is much larger than that of

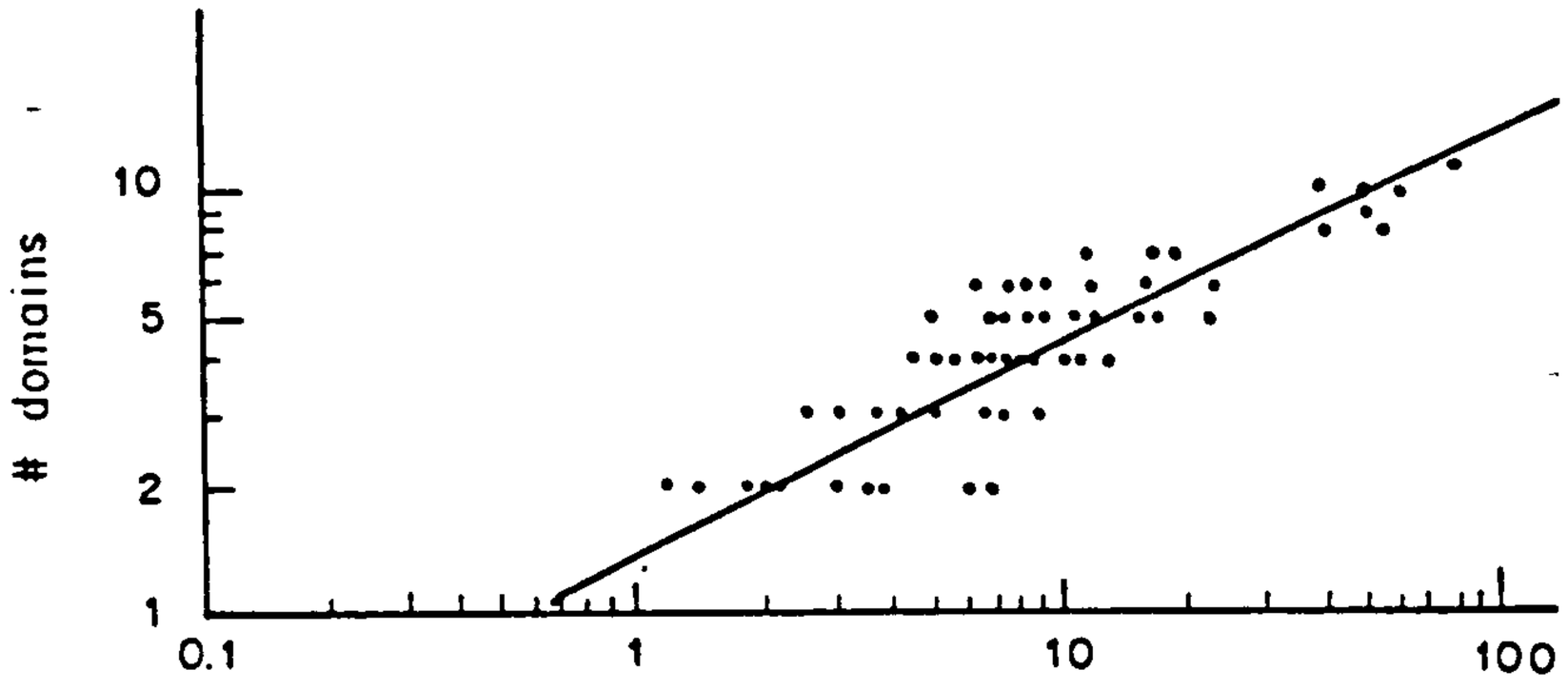

Figure 2.7. The number of domains against particle size for some natural titanomagnetites. After Soffel (1971).

magnetite because the demagnetising field, which depends on the intrinsic magnetisation, is very much smaller. The critical single domain size in haematite has been suggested from experimental work to be in the range 10-100 μm (Dunlop, 1971).

2.6 Coercivity

In order to alter the direction of magnetisation of a particle, energy is required to remove the particle from the potential energy well imposed by various anisotropy terms. This energy can be of magnetic or thermal origin. The magnetic field required to overcome the anisotropy energy of a particle is termed the microscopic coercive force, or coercivity. The magnitude of coercivity depends on the anisotropy terms and therefore upon the mineralogy.

2.7 The effect of temperature

Thermal energy is manifested in solids as vibrations of

the constituent particles. In magnetic solids these vibrations tend to disturb the magnetisation from the minimum energy position imposed by the controlling anisotropy. Increasing the temperature leads to greater disturbance which reduces the coercive force. The coercive force continues to fall as the temperature increases, until thermal energy alone is sufficient to lift the magnetisation from its potential well. The magnetisation of particles in this state is then said to be unblocked, as it has no stable remanant magnetisation. In the unblocked state, the magnetisation of single domain particles with uniaxial anisotropy switches randomly between the two antiparallel energy minima, populating the two energy positions equally in the absence of an external magnetic field. In the presence of a magnetic field, the energy wells parallel to the field become deeper, leading to a dynamic equilibrium in which the parallel state is more highly populated. This produces a magnetisation in the presence of a magnetic field in a process analogous to that of paramagnetism. This behaviour is termed superparamagnetism.

The temperature at which particles unblock and become superparamagnetic depends upon the mineral type, the particle volume and the measuring time. For single domain grains the unblocking temperature increases with increasing particle size. At a given temperature the critical volume below which a particle becomes superparamagnetic can be obtained from;

$$v=\frac{2kT}{MH_c}(Q + \ln t_s) \qquad (2.8)$$

(Stephenson, 1971), where M is the spontaneous magnetisation, H_c is the coercive - force (which is temperature dependent), Q is a constant and t_s is the measurement time.

The particle size for the superparamagnetic - stable single boundary in magnetite, at 20°C and for a measurement time of 100 seconds, is 0.03μm Dunlop (1973).

2.8 Thermoremanence

When a system containing an assemblage of ferrimagnetic particles cools from above its Curie point the magnetisation increases as the electron spins become magnetically ordered. With further cooling the magnetic anisotropy increases, which tends to trap the magnetisation of the particles in one of a set of easy axes. The temperature at which this occurs is termed the blocking temperature. If the particles in an assemblage are identical then their magnetisations are all blocked-in at about the same temperature and time. However, if the particles are different, e.g. if the have different volumes, then they will become progressively blocked-in as the temperature is reduced leading to a distribution termed the blocking temperature spectrum. The orientation of the magnetisation of each particle when it is blocked-in depends on the initial temperature, the cooling rate and the magnitude of the ambient magnetic field. In the case

of an assemblage of single domain particles with uniaxial anisotropy (applicable to single domain magnetite) the magnetic moment of each particle can be blocked into one of two easy directions. In the the absence of an applied magnetic field both orientations are energetically equivalent and so the probability of either state being populated is the same, see figure 2.8a, thus the net magnetic moment of the assemblage is zero. In the presence of a magnetic field, the magnetisation state in which the moments are parallel to the magnetic field is at a lower energy than the opposing state, see 2.8b. In the situation where the magnetic field is small, the two opposing magnetisation states are occupied such that more of the moments reside in the lower (field oriented) energy state, thus giving the assemblage a net magnetisation. In addition, the equilibrium distribution of magnetic moments between the available states depends on the temperature of the system, according to the equation:

$$M_{eq}=vM_s(T)\ \frac{(vM_s(T)H)}{(\ 3kT\ \ )} \qquad (2.9)$$

(Stacey & Banerjee, 1974). The system requires a finite amount of time for this equilibrium to be achieved. As a consequence, the blocking process is complicated by the cooling rate. When the system is cooled rapidly the high temperature equilibrium distribution of magnetisations is blocked-in before the lower temperature equilibrium is acheieved, while for slower cooling a lower temperature

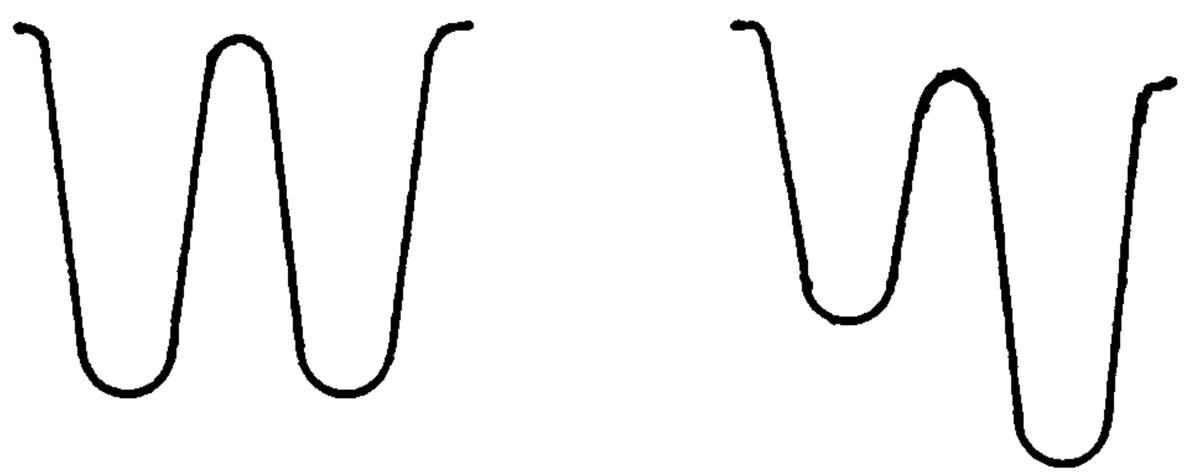

Figure 2.8. A schematic illustration of the energy wells of a particle with uniaxial anisotropy in (a) the absence of a magnetic field and (b) the presence of a small magnetic field.

equilibrium is approached. For single domain assemblages the net magnetisation increases with slower cooling as a lower temperature equilibrium is blocked-in. Conversely, for multidomain particles the magnetisation decreases for slower cooling (e.g. McClelland-Brown, 1984).

3 Thermomagnetic Behaviour

3.1 Introduction

The thermomagnetic behaviour of the sample set has been studied to identify the magnetic minerals present.

Thermomagnetic behaviour describes here the change of the magnetisation of a sample with temperature in the presence of a large magnetic field. These changes can have both physical and chemical origins.

3.2 Physical processes

The Curie point temperature is perhaps the most important physical characteristic by which a magnetic mineral can be identified. The Curie point is a second order phase transition (Crangle, 1977), i.e. it has a latent heat term analogous to the melting point of a solid. Therefore, in the simple case it is a well-defined transition. The Curie point is defined as the transition from an ordered ferromagnetic state (also ferri- and canted antiferromagnetic states, although the transition in these cases is strictly termed the Néel temperature), to a disordered paramagnetic state. The transition is the final stage of competition between the exchange interactions which produce long range order and the thermal vibrations which disrupt it. The thermomagnetic curve represents this competition and is convex in shape to within a few degrees of the Curie point where the breakdown to a paramagnetic state produces an inflexion point as the curve takes on a

concave paramagnetic form. The Curie point temperatures of some commonly occurring natural minerals have been compiled. See table 3.1.

The thermomagnetic curves of natural samples may be the convoluted response of two or more ferrimagnetic (or antiferromagnetic) minerals, various paramagnetic minerals and, less importantly, diamagnetic minerals. This can produce a variety of curves which have multiple Curie point inflexions and/or concave sections resulting from the dominance of paramagnetic minerals which obey the Curie law temperature dependence, see equation 2.2.

3.3 Structural and chemical changes

Various structural and chemical changes can occur as a result of thermal treatment. An important structural change is the inversion of non-stoichiometric (low temperature oxidised) magnetite (maghemite) and titanomagnetite (titanomaghemite). The inversion process is complex and can produce a variety of products and associated thermomagnetic behaviour depending on the initial mineral composition and the extent of the oxidation. A discussion of the mechanisms and products of low temperature oxidation is thus a prerequisite. Low temperature (<350°C) oxidation of (titano-) magnetite proceeds by the diffusion of Fe^{2+} ions to the particle surface, where they becomes oxidised to Fe^{3+} forming a maghemite 'skin' (Ozdemir & Dunlop, 1989). For each Fe^{2+} ion which diffuses to the particle surface, two similar

Table 3.1. Curie points of some natural minerals

Mineral	Formula	Curie Point (°C)	Source
Magnetite	Fe_3O_4	575	O'Reilly, 1984
Titanomagnetite	e.g. $Fe_{2.4}Ti_{0.6}O_4$	150-220	O'Reilly, 1984
Maghemite	γ-Fe_2O_3	645	Ozdemir & Banerjee,1984
Haematite	α-Fe_2O_3	675	O'Reilly, 1984
Goethite	α-FeOOH	80-110	Dekkers, 1988

ions are converted to the 3+ state, to balance the total charge (Stacey & Banerjee, 1974). The presence of water has been shown to play an important role in the formation of maghemite (Elder, 1965). The inversion process involves the transformation from an initial spinel structure phase to a rhombohedral phase in the simplest case, or an intergrowth of two phases, one with a spinel structure and the other with a rhombohedral structure. The inversion products are dependent upon the initial composition of the parent material and on the subsequent degree of oxidation (Readman & O'Reilly, 1970). In the case of maghemite the inversion product is haematite. However if the original oxidation of magnetite produces particles with a magnetite core and a maghemite skin the inversion product will be an intergrowth of magnetite and haematite (Readman & O'Reilly, 1971). In both situations this causes a reduction in the saturation magnetisation. With titanium substitution, the inversion products vary according to the degree of substitution and oxidation. In general, the inversion products of titanomagnetites are a titanium-poor spinel

phase and a titanium-rich rhombohedral phase. In these cases inversion can increase or decrease the saturation magnetisation depending upon the initial mineral composition.

The temperature of the inversion process has been reported by several workers. The range is large, for example Bozorth (1951) reported maghemite stability up to 800°C while Readman & O'Reilly (1970) obtained inversion temperatures around 350-400°C for a range of compositions and oxidation parameters and Ozdemir (1987) reports inversion as low as 250°C. Ozdemir & Banerjee (1984) showed by x-ray diffraction and differential thermal analysis (DTA) studies that their acicular maghemite was stable with respect to haematite up to 510°C and subject to only partial inversion up to their maximum temperature of 660°C. The mechanisms suggested for these discrepancies include the presence of impurities, method of preparation, previous history of the primary mineral and particle shape (Ozdemir & Banerjee, 1984).

Other structural changes which may be important occur when the hydroxide minerals goethite and lepidocrocite dehydrate on heating at 300-350°C forming haematite, and maghemite plus haematite, respectively (Thomas, 1983).

Chemical alteration resulting from heating in air is a long recognised problem. The primary explanation is often that of oxidation. High temperature oxidation of magnetite produces haematite as the end member of the oxidation series (O'Reilly, 1984). The high temperature oxidation of

titanomagnetite forms an intergrowth of a spinel phase with a composition closer to magnetite than the original matèrial and a titanium rich phase towards the composition of ilmenite. With increased oxidation, the spinel phase will alter finally to haematite. The kinetics of high temperature oxidation of titanomagnetite were studied by Kropacek (1974) using natural titanomagnetites heated at rates varying from 1-40°C per minute. It appears from the results of Kropacek that whilst oxidation occurs at all heating rates the degree of oxidation decreases with increasing heating rate. However, since the cooling curves associated with all of the heating rates are similar, it may be that once the temperature has exceeded 600°C the total amount of oxidation is independent of the heating rate.

3.4 The Curie balance

Thermomagnetic behaviour was investigated using a horizontal force Curie balance incorporating a dynamic feedback system. The Liverpool balance is illustrated schematically in figure 3.1. The balance is a relatively simple device. The sample is held in a quartz cup (containing a platinum-platinum/rhodium thermocouple) which is attached to one end of a horizontal beam forming the mass of a long pendulum. The sample is positioned in an electric oven between the pole pieces of an electromagnet. The pole pieces are shaped to provide a field gradient.

In the presence of an applied field the sample becomes

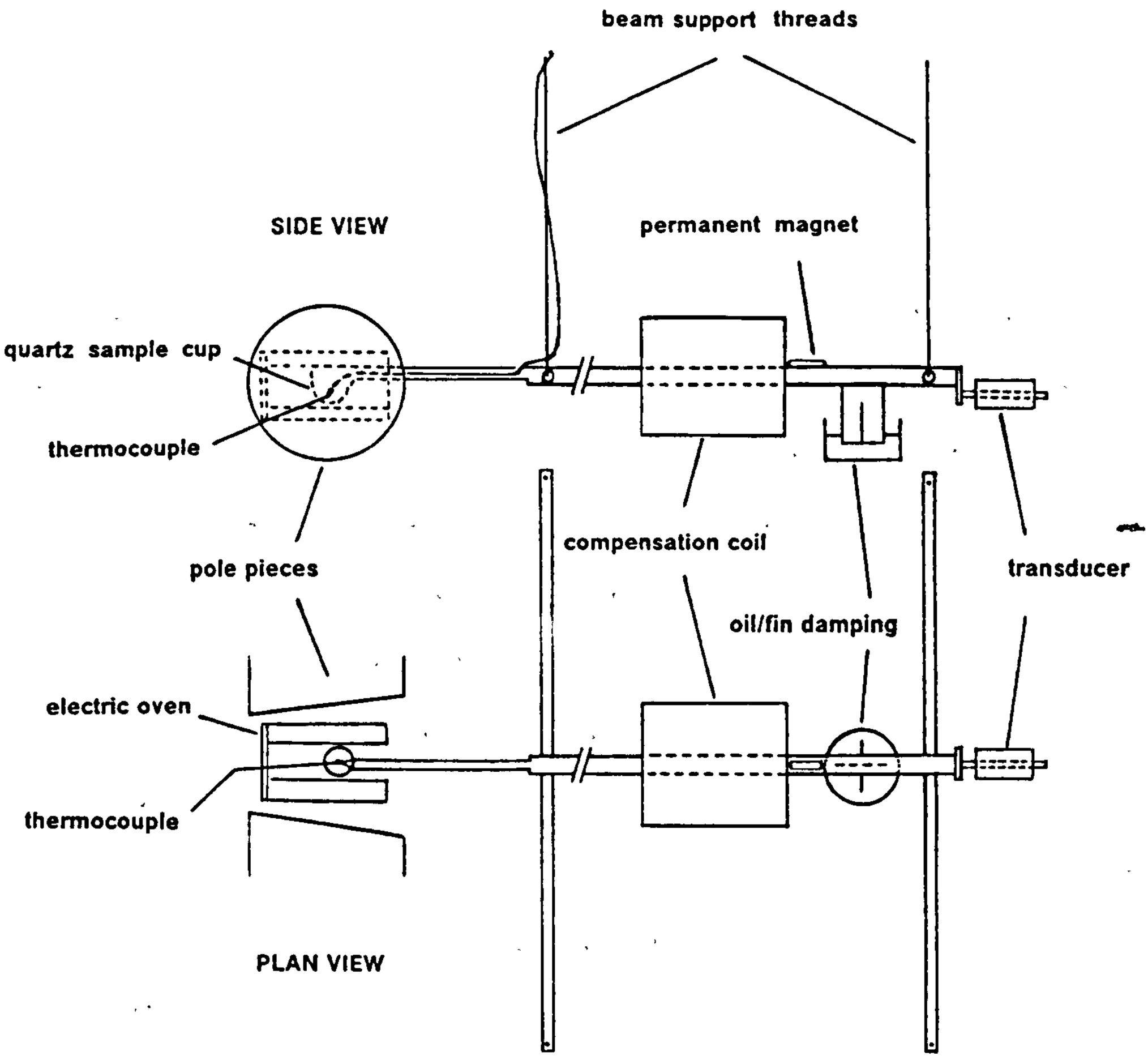

Figure 3.1. A schematic illustration of the Curie balance used in this study.

magnetised, creating a horizontal attractive force that moves the sample up the field gradient. This movement induces a voltage in a transducer placed at the other end of the beam; this voltage is used to supply a correcting current to a compensating coil which interacts with a permanent magnet on the beam to oppose the movement due to the sample. This system of feedback allows the sample position to remain almost fixed relative to the applied field as its magnetisation changes with heating or cooling. The feedback voltage is proportional to the sample's magnetisation. The digitised feedback voltage and a digitised temperature reading are sent via the RS232 port to a BBC microcomputer. The BBC microcomputer provides a real time VDU output of feedback voltage against temperature and a hard plot on completion of an experiment.

The feedback voltage is uncalibrated; instead, the magnetisation is normalised to the first reading. Accurate calibration of the temperature scale is vital for magnetic mineral identification based on Curie point temperature. The thermocouple is a 13% platinum-platinum/rhodium type. The cold junction voltage is compensated using a solid state device. The thermocouple voltage was calibrated to temperature in situ. This was achieved by comparison of the voltage to a standard table (J. Share, pers. comm.). The temperature calibration was additionally checked using a sample of synthetic magnetite, see figure 3.2 (T_C=575°C, O'Reilly, 1984).

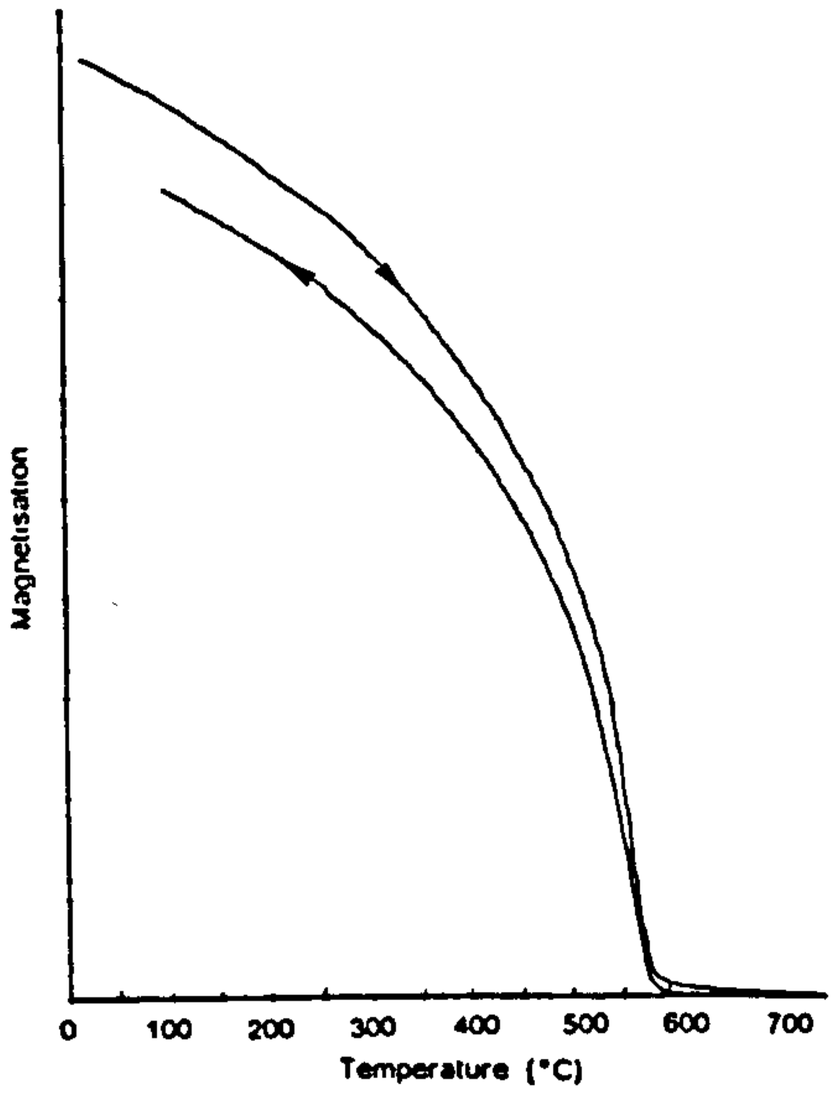

Figure 3.2. The thermomagnetic behaviour of synthetic magnetite measured using the system described. The Curie point temperature is 575°C on heating and 582°C on cooling.

3.5 Experimental procedure

Before each series of experiments the quartz cup was cleaned in an ultrasonic bath.

Samples were prepared by cutting a section of material from the bulk specimen with a diamond impregnated saw. The outer surface (~1mm) of this section was removed to prevent contamination of the bulk composition by surface weathering products which were often visually apparent but may have also been present without being visible (Franklin & Vitali, 1989). Of course, the bulk sample may also be weathered. The prepared section was then crushed. The sample cup was filled with crushed material (~0.1-0.7g); the amount used depending on the expected intensity of magnetisation.

The experimental runs were controlled through the BBC microcomputer. The applied field was controlled from a

separate power supply, it was usually set at ~400 mT in order to saturate any magnetite minerals and to allow direct comparison with data from other samples. However, both lower and higher fields were used for very strong and very weak samples respectively. Each sample was heated in air at atmospheric pressure to 710°C at an approximately linear rate of 100 °C min^{-1}. At 710°C the oven was switched off and the sample cooled freely to 99°C when the run was terminated to reduce the experimental time.

After each run the sample holder was cleaned using a small suction hose.

3.6 Curie point determination

Thermomagnetic behaviour can only provide an estimate of the Curie point temperature because of the appearance of the transition using this method (Crangle, 1977). As described earlier, the transition is from a ferri- or antiferro- magnetic to a paramagnetic state. Curie points have been determined from the intersection of a tangent to the steepest part of the curve and another extended from the paramagnetic 'tail' (see figure 3.3a). This method is similar to that of Grommé et al. (1969). Other inflexion points are estimated in a similar manner.

Curie point temperatures have been obtained from both the heating and cooling curves.

3.7 Results

The Curie point and inflexion temperatures obtained from

both the heating and cooling curves, along with the percentage alteration are compiled for all samples in appendix 2. The following section summarises these figures, gives examples and points out features not apparent from the data. It should be noted that the results are described without any interpretation. The interpretations follow in the discussion section where their basis is explained.

French I

MC01. Five samples from this group (01-05) have thermomagnetic curves of similar shape, see figure 3.3a, but which vary in their estimated Curie point temperatures. The behaviour is further characterised by the broad concave decay of magnetisation at high temperature. The magnetisation on cooling returns to a final value at 99°C between 73 to 93% of the magnetisation at initial heating to 99°C. The value of 93% was obtained from an uncrushed sample. An additional feature of these samples is the difference in the Curie point estimates from the heating and cooling curves. The cooling curve estimates are systematically lower than those from the heating curves by 8-45°C.

The remaining sample of this set (06) differed from the others in both the shape of the heating and cooling curve and the percentage magnetisation change at 99°C. See figure 3.3b. On heating the magnetisation of this sample shows an inflexion at ~300°C. The magnetisation on cooling is slightly greater than on initial heating (101-

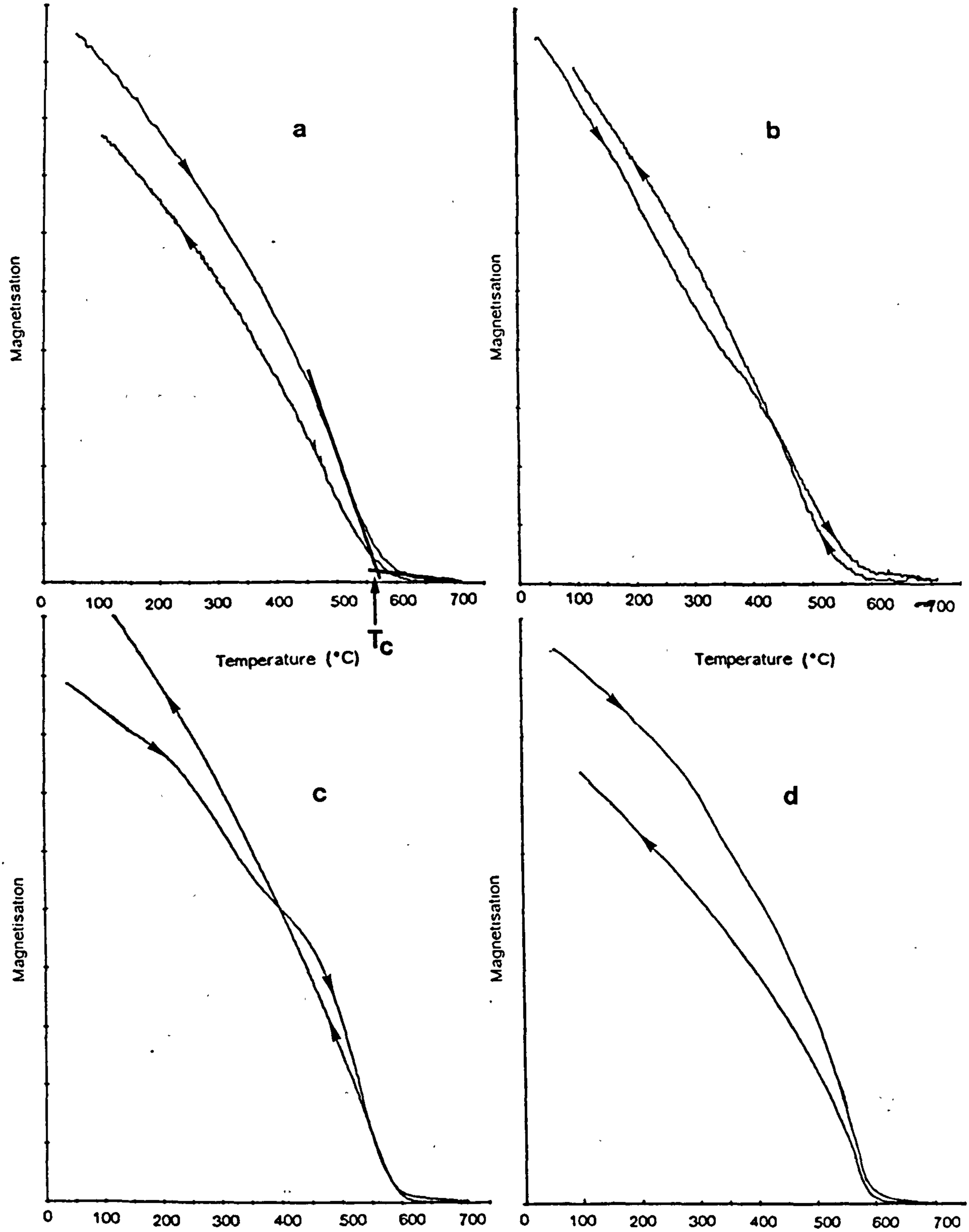

Figure 3.3. The thermomagnetic behaviour of samples (a) MC0104, (b) MC0106, (c) MC0202 and (d) MC0504.

105%, obtained from two subsamples).

British

MC02. The two samples from this group show similar behaviour. Both show irreversible behaviour and exhibit inflexion points at 370 and 335°C respectively on heating and near magnetite Curie point temperatures. The magnetisation on cooling varies smoothly, with the final magnetisation after cooling exceeding the initial magnetisation. See figure 3.3c.

Peruvian

MC05. The thermomagnetic curves of the five samples from this group are similar in shape, percentage alteration, estimated Curie point temperature and in the relatively small differences between the Curie points estimated from heating and cooling.

The heating and cooling curves of all five samples are essentially convex. In addition, samples 01, 02, 03 and 04 all show a slight inflexion between 320°C and 350°C on heating. See for example figure 3.3d. The magnetisation change measured at 99°C ranges between 75-93% of the initial magnetisation. The estimated Curie points from the heating curves are between 0-17°C higher than those estimated from their respective cooling curves.

MC06. The two samples from this set show similar thermomagnetic behaviour. See figure 3.4a. The heating and cooling curves vary smoothly. The Curie point temperatures estimated for the two samples are similar

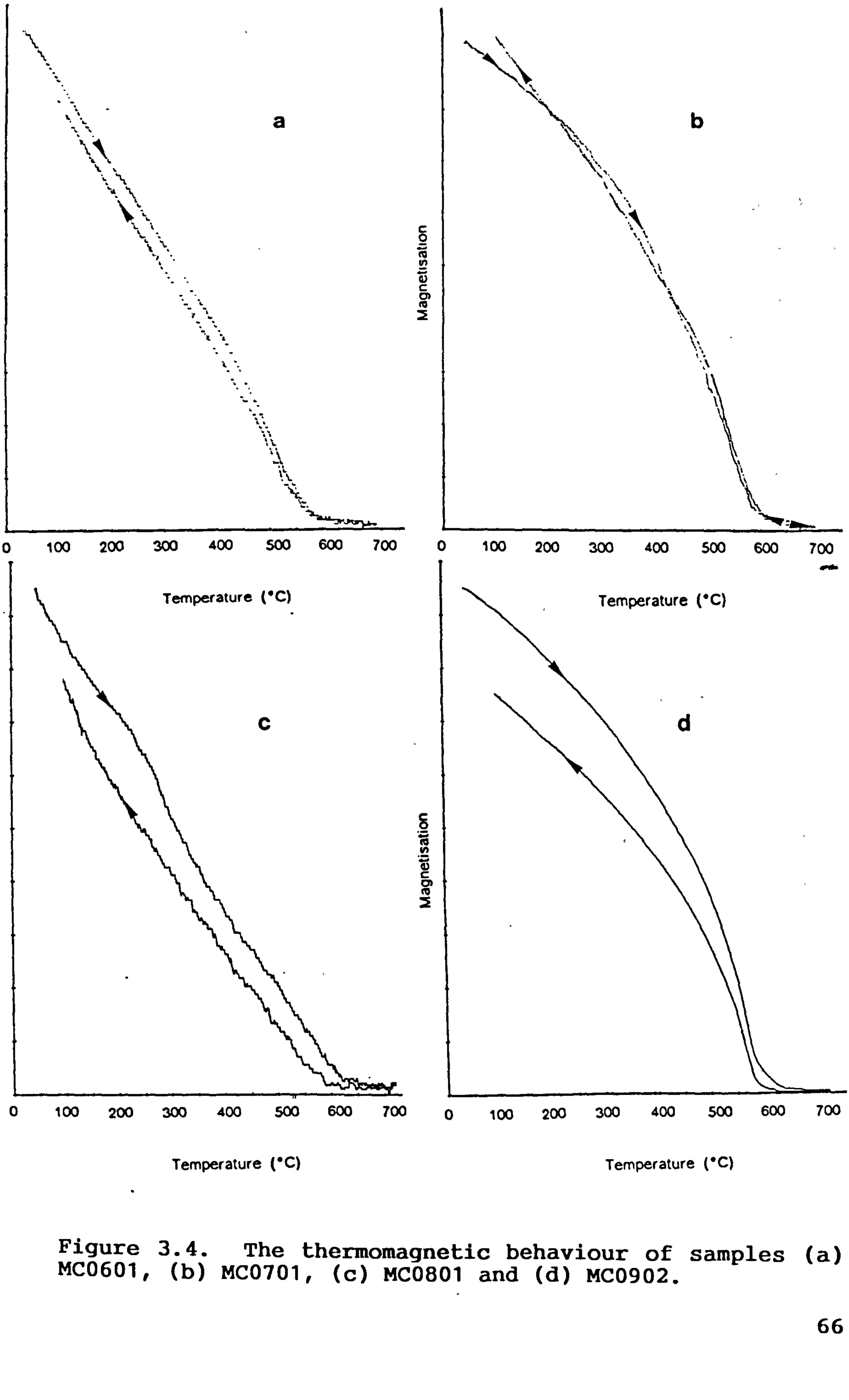

Figure 3.4. The thermomagnetic behaviour of samples (a) MC0601, (b) MC0701, (c) MC0801 and (d) MC0902.

(~560°C). The magnetisation change on cooling to 99°C is very small.

MC07. Of the five samples from this group, 01 and 03 have comparable thermomagnetic behaviour as do 02 and 04. Both 01 and 03 show a slight inflexion on heating and smoothly changing magnetisation on cooling. The magnetisation on cooling to 99°C was greater than the initial magnetisation at 99°C (106% and 107%, respectively). See figure 3.4b. The Curie point temperatures were identical for these samples. The thermomagnetic behaviour of samples 02 and 04 differs from that of 01 and 03 in the smoothly varying nature of both the heating and cooling curves, the percentage alteration (86% and 96%) and also the greater difference between the Curie point temperatures determined from the heating and cooling curves (15 and 25°C).

MC08. All three samples of this set show a broad inflexion in the thermomagnetic curve on heating. On cooling the magnetisation varies smoothly. See figure 3.4c. The magnetisation change due to heating was small; the magnetisation on cooling to 99°C being 84-100% of the initial magnetisation at that temperature. The Curie points estimated from the heating and cooling curves differ by 27-62°C.

MC09. The six sherds of this group show smoothly varying thermomagnetic curves with Curie point temperatures between 580 and 600°C. See for example figure 3.4d. The magnetisation on cooling to 99°C varies from 92% to 53%. Greater alteration is associated with higher Curie point

temperatures.

MC10. The three sherds of this group show different behaviour. The magnetisation of sample 01 varies smoothly with temperature during both heating and cooling. Alteration due to heating is moderate. The two subsamples measured from sample 02 are internally consistent. Both show inflexions on heating and cooling at ~250°C and ~225°C respectively. See figure 3.5a. The remaining sherd (03) has unusual thermomagnetic behaviour. See figure 3.5b. Both the heating and cooling curves are characterised by a large break of slope at ~200°C. The magnetisation is larger after heating.

Egyptian

MC12. The two sherds from Egypt show similar behaviour. The magnetisation varies smoothly during both heating and cooling. The magnetisation decays via a broad tail at high temperature. The high temperature magnetisation decay of sherd 02 suggests the presence of haematite. See figure 3.5c.

French II

MC11. The thermomagnetic behaviour of this group is varied. The behaviour of sherds 01, 02 and 04 is strongly concave. No Curie points can be defined for these sherds. See for example figure 3.5d. Sherds 03, 08 and 10 have irreversible thermomagnetic behaviour which is characterised by an increase in magnetisation after heating. The behaviour of sherd 05 is convex with an inflexion on both heating and cooling. The thermomagnetic

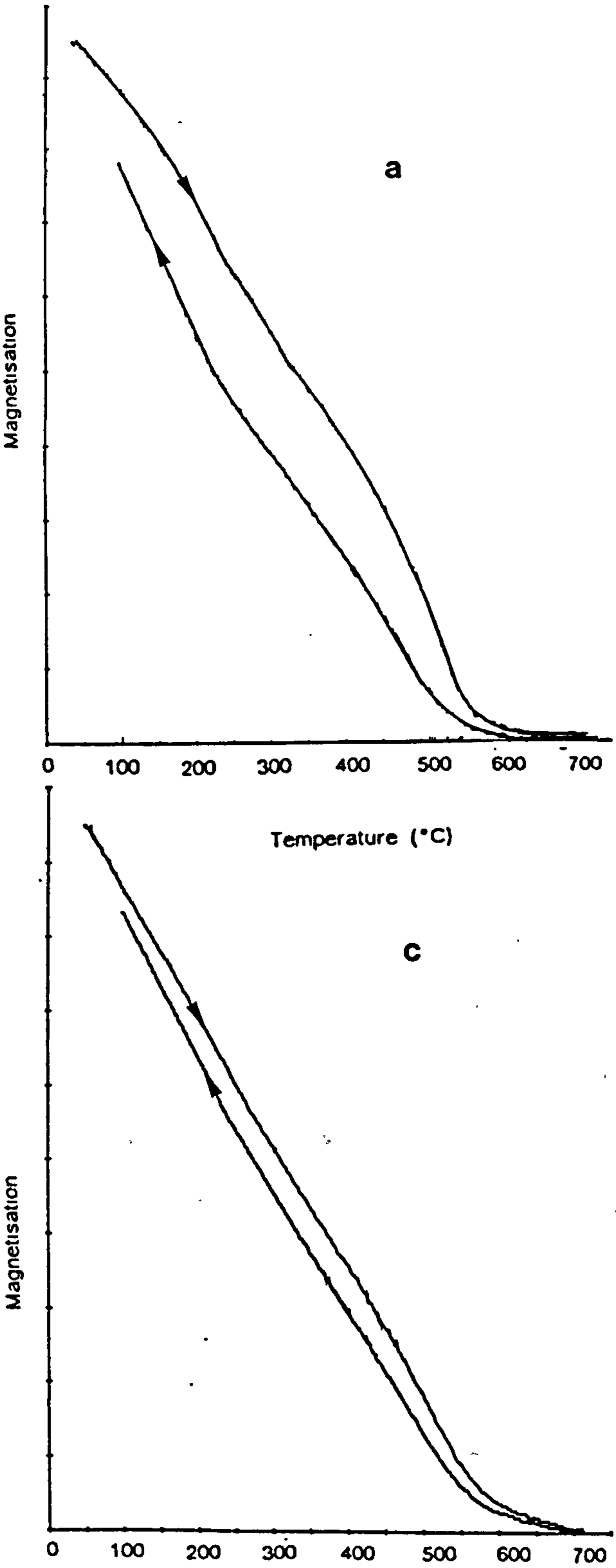

Figure 3.5. The thermomagnetic behaviour of samples (a) MC1002, (b) MC1003, (c) MC1202 and (d) MC1101.

behaviour of sherd 06 varies smoothly from concave at lower temperatures to increasingly convex towards the Curie point.

MC13. The thermomagnetic behaviour of this group is extremely varied. The magnetisation of sherd 01 is the greatest of the whole collection. The thermomagnetic behaviour of this sherd is strongly convex and nearly reversible. The Curie point is well defined at 580°C. In contrast, the magnetisation of sherds 02, 04 and 05 is very weak. The thermomagnetic curves are predominantly concave on both heating and cooling, making the definition of Curie points difficult.

The behaviour of sherds 06, 07, 09 and 10 are similar in that the post heating magnetisation is greater than the initial magnetisation. The more strongly magnetic of these sherds (06, 07 and 09) show a small inflexion on heating and all show smoothly varying cooling curves. See for example figure 3.6a. The Curie points of these sherds are mostly a few degrees above 580°C. The behaviour of sherds 03 and 08 is perhaps related to the previous four, in that an inflexion occurs during heating and the Curie points are just above 580°C. However, the magnetisation of these two sherds is reduced after heating.

The magnetisation of the remaining sherd (11) falls initially in a concave manner and becomes steeper towards the Curie point.

Servian

MC14. The three sherds of this group have very similar

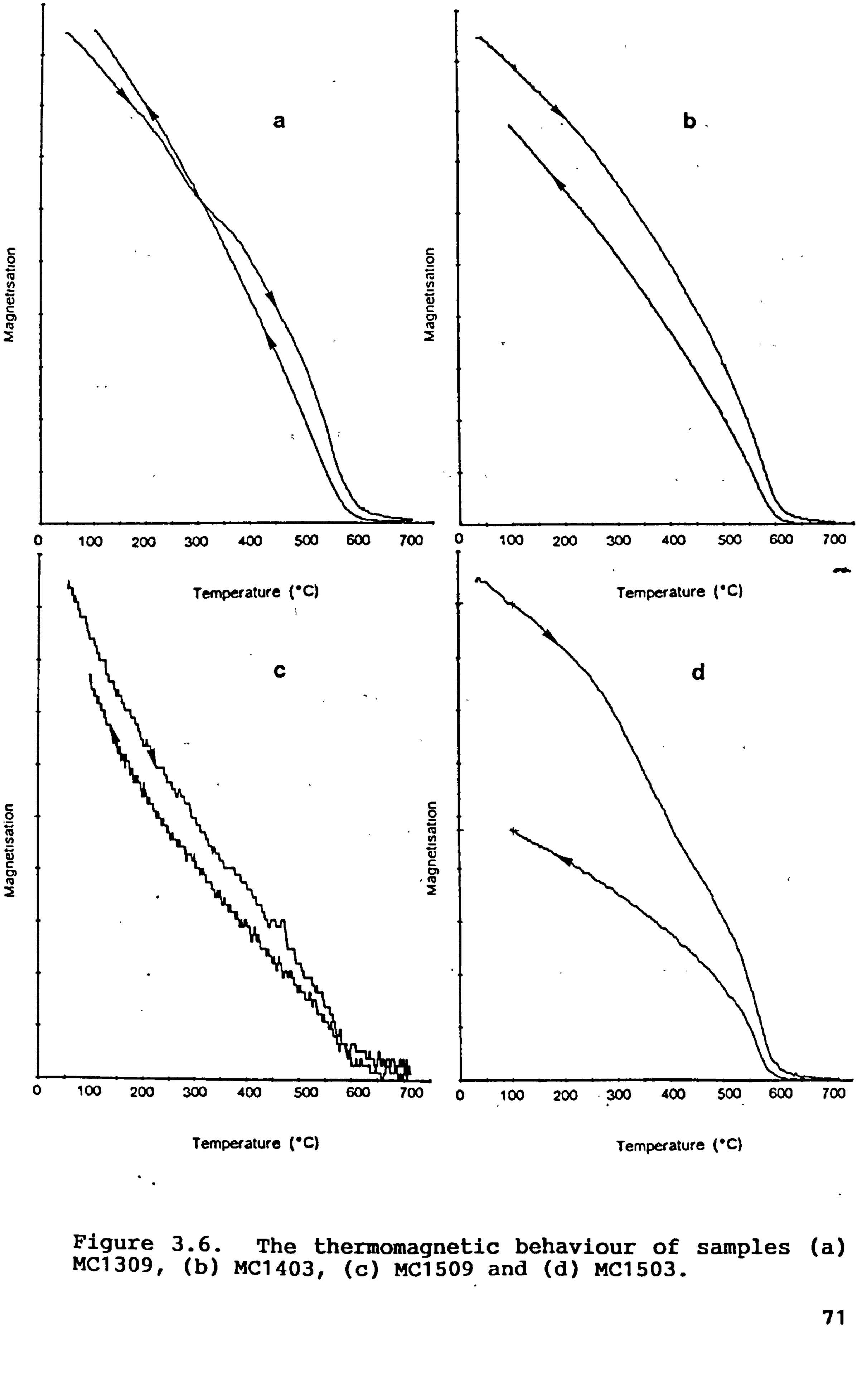

Figure 3.6. The thermomagnetic behaviour of samples (a) MC1309, (b) MC1403, (c) MC1509 and (d) MC1503.

behaviour. See figure 3.6b. The magnetisation varies smoothly, breaking down in all three cases at a Curie point close to 600°C. The alteration after heating is moderate.

MC15. The thirteen sherds of this group exhibit varying behaviour but all have Curie temperatures close to 600°C. The behaviour ranges from smoothly varying convex curves (04, 05, 07, 11 and 13), through to concave paramagnetic dominated curves (06 and 08) with sherds 09 and 10 showing intermediate behaviour. See figure 3.6c. For these samples the magnetisation after heating is at least 82% of its initial value. The behaviour of the remaining four sherds (01, 02, 03 and 12) is characterised by a larger reduction of magnetisation after heating. Sample 03 is exceptional, with a magnetisation after heating of only 54% of its original value. This sherd also shows a broad inflexion during heating. See figure 3.6d.

MC16. The thermomagnetic behaviour of all five samples is quite similar. The behaviour is comparable to that of samples from MC14 except that the Curie point temperatures of the MC14 sherds are slightly higher than those of MC16.

South-West American

MC17.. The thermomagnetic behaviour of the thirteen sherds from this group can be described in three broad subgroups. The first subgrouping includes sherds 01, 02, 04, 09 and 10. These samples are characterised by convex smoothly varying magnetisation curves which have Curie points of 582-620°C. For these samples the magnetisation after heating is 75-99% of the initial value. See for example

figure 3.7a. The behaviour of sherd 08 is similar to this group except for its lower Curie point at ~550°C. A further subgrouping of five sherds (03, 05, 06, 11 and 12) are less strongly magnetic than those of the previous subgroup. The magnetisation curves of these sherds follow a concave path at lower temperatures, becoming convex towards the Curie point. See figure 3.7b. The remaining sherds (07 and 13) are similar in the complexity of their behaviour. During heating the magnetisation falls rapidly in a convex manner to inflexion points of 320°C and 370°C respectively. The magnetisation returns more smoothly on cooling to a final value close to that before heating.

Romano-British

MC18. The thermomagnetic behaviour of the nine sherds of this group is varied. Sherds 01, 02, 03 and 06 are similar with a near linear fall of magnetisation at lower temperatures, more distributed magnetic decay around the Curie point on the heating curve and the absence of significant thermal alteration. See for example figure 3.7c. The Curie point temperatures for these sherds are also similar.

The simplest thermomagnetic behaviour is observed for sherds 05, 07, 08 and 09. The magnetisation of sherds 05 and 09 varies smoothly in a convex manner on heating and cooling with a final magnetisation at 99°C of 87 and 86% respectively. Sherds 07 and 08 also exhibit smoothly varying convex magnetisation curves but the magnetisation after cooling exceeds that before heating, with the cooling

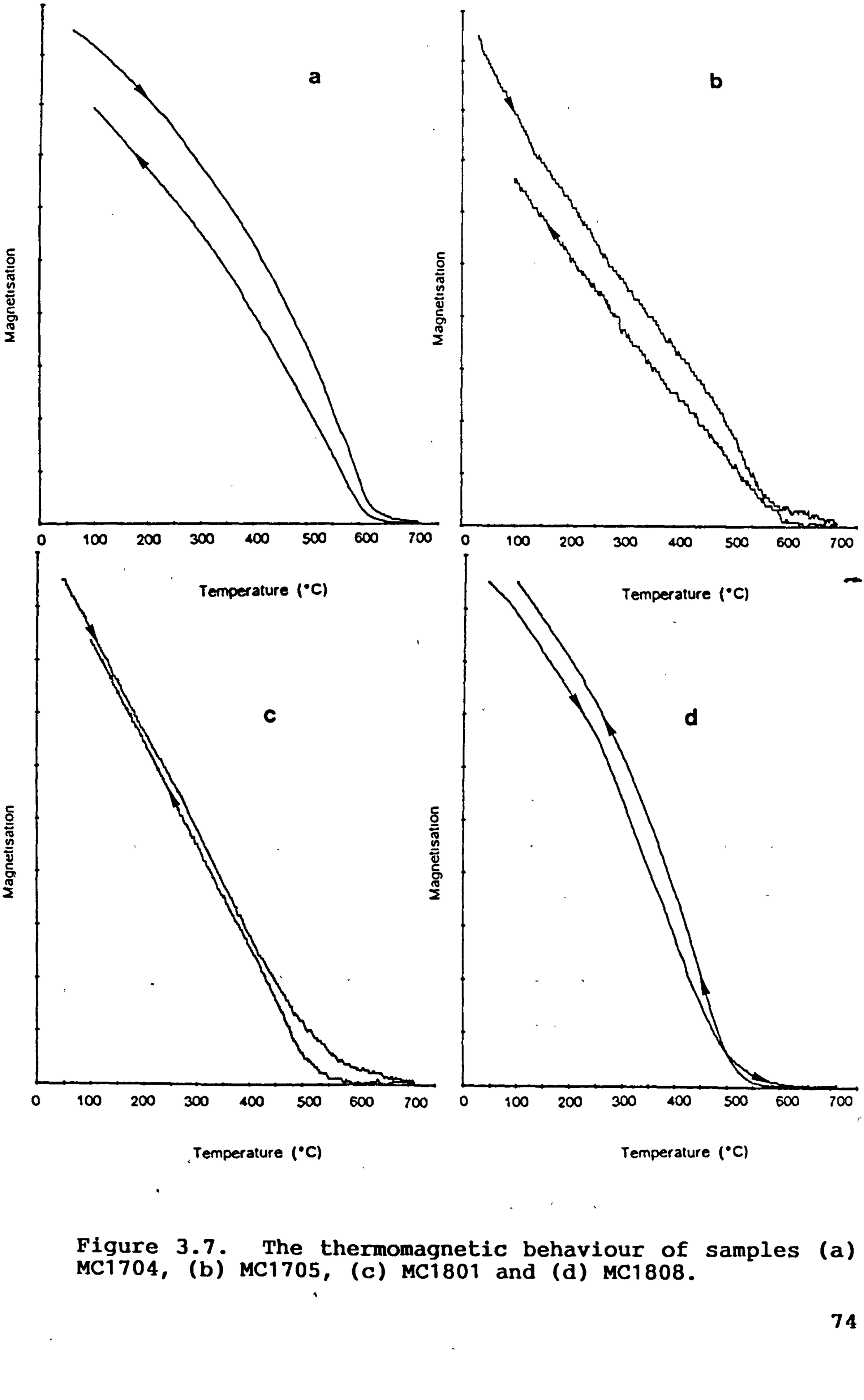

Figure 3.7. The thermomagnetic behaviour of samples (a) MC1704, (b) MC1705, (c) MC1801 and (d) MC1808.

curve crossing the heating curve above 450°C. The Curie point temperatures obtained from the cooling curves are greater than those from the heating curves and the concave decay of magnetisation at high temperature is not as broad. For example see figure 3.7d. The behaviour of sherd 04 is characterised by an inflexion during heating and a smooth magnetisation on cooling. The post heating magnetisation is larger. See figure 3.8a.

MC19. Six of the nine sherds from this group (02, 03, 04, 05, 06 and 09) show simple convex, near reversible thermomagnetic behaviour. See for example figure 3.8b. The Curie point temperatures range from 580/570°C for 02 to 545/552°C for 06 (two subsamples of each). Sherd 08 shows simple convex behaviour, but exhibits greater thermal alteration. The remaining four samples (01, 06, 07 and 09) show varied behaviour. Subsample 01A (the inner part of the sherd) shows irreversible behaviour, but no resultant change in the magnetisation after heating. Subsample 01B (the outer orange part of the sherd) is also irreversible but differs from 01A by the presence of inflexions in the heating and cooling curves. Sherd 07 is relatively weak, and decays in a concave fashion indicating the presence of a dominant paramagnetic fraction. The magnetisation increases after heating.

MC20. The thermomagnetic behaviour of these samples can be described in three subgroups. The first subgroup contains sherds 01 and 07. The behaviour of these samples is shown in figure 3.8c, with a broader decay of magnetisation on

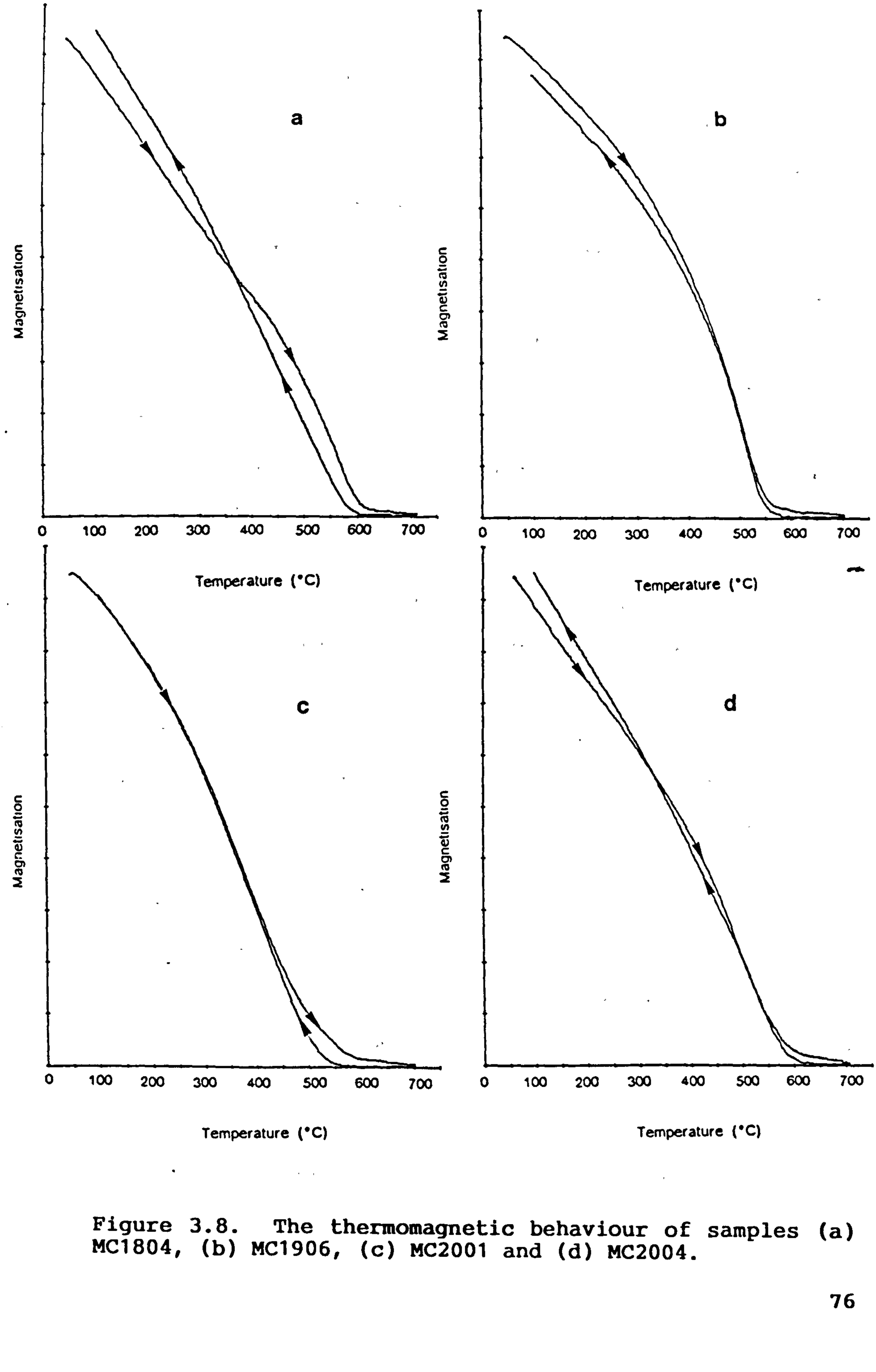

Figure 3.8. The thermomagnetic behaviour of samples (a) MC1804, (b) MC1906, (c) MC2001 and (d) MC2004.

heating than cooling.

The second subgroup is the largest, and contains sherds 02, 05, 06, 09 and 10. The thermomagnetic curves for these samples are convex and vary smoothly. Alteration does not exceed a 10% reduction of magnetisation after heating.

The remaining subgroup (03, 04, 08 and 11) show highly irreversible behaviour, with the cooling curve crossing the heating curve to give an increased magnetisation after heating. A typical example is illustrated, see figure 3.8d.

It is noteworthy that the samples that undergo greatest alteration (08, 11) display inflexion points in the heating curve, with the most pronounced inflexion occurring in the sample that undergoes greatest alteration (11).

MC21. The thermomagnetic behaviour of sherds from this group is quite varied. The behaviour of sherd 01 is illustrated in figure 3.9a. The behaviour is characterised by a change from a lower Curie point with a broad concave decay on heating, to a slightly higher Curie point with a less broad decay on cooling.

Sherds 03, 04 and 09 display simple smooth convex curves with moderate alteration.

Sherds 02, 05, 06, 07 and 08 undergo thermal alteration with an increased magnetisation on cooling. The sherds having the largest increases (07 and 08) also have inflexion points at 315°C and 330°C respectively.

MC22. The thermomagnetic curves of sherds 01, 05 and 07 are similar. The magnetisation is nearly reversible and

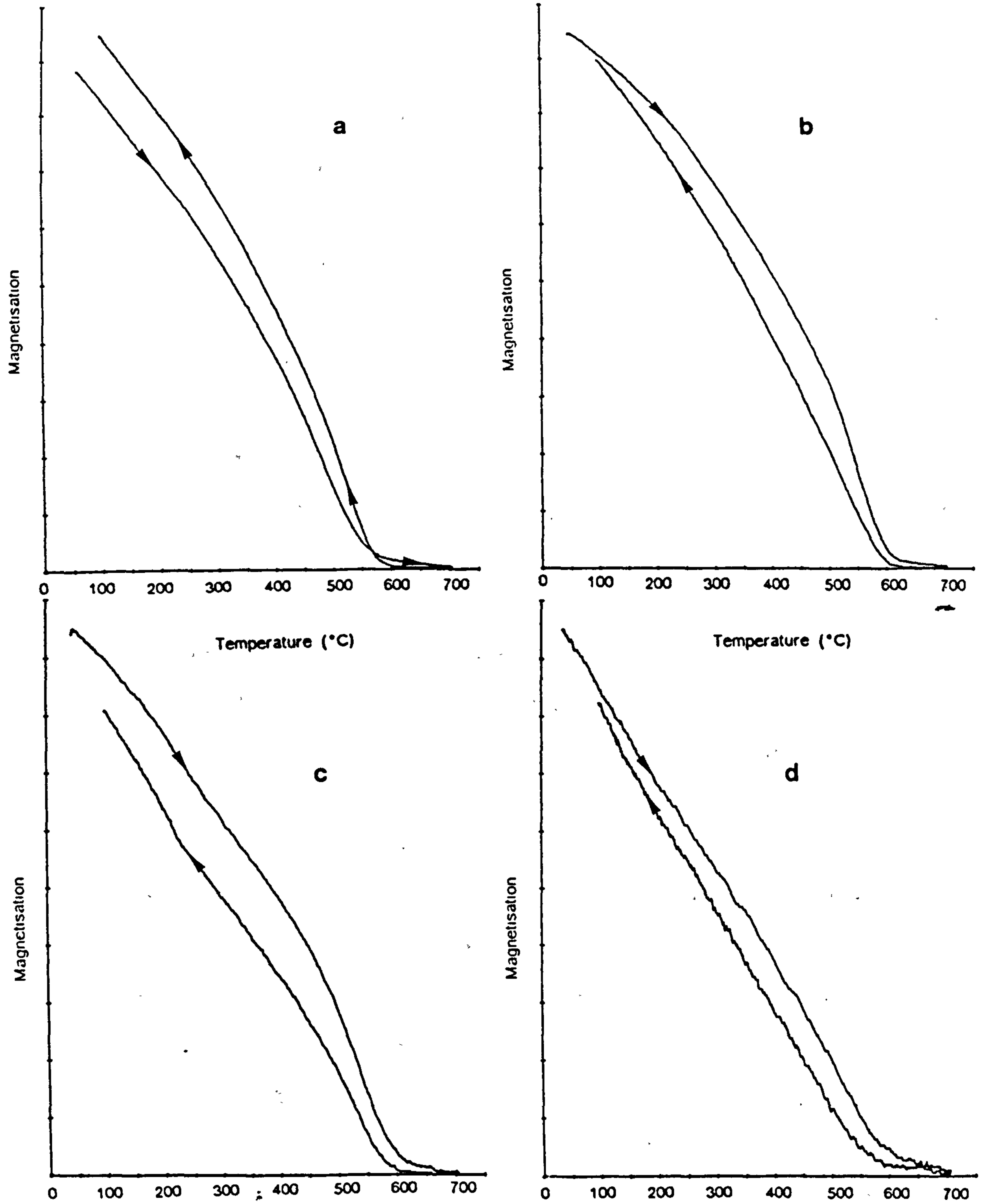

Figure 3.9. The thermomagnetic behaviour of samples (a) MC2101, (b) MC2206, (c) MC2402 and (d) MC2504.

the Curie point temperatures estimated from the heating and cooling curves are within 10°C. Sherds 02 and 09 also have convex smoothly varying magnetisation curves which return on cooling to around 90% of the initial value. However the Curie points estimated from the heating and cooling curves are separated by 15-25°C. The remaining sherds; 03, 06 and 08 show highly irreversible behaviour. Sherd 03 shows an inflexion on both heating and cooling and a considerably reduced magnetisation after the thermal cycle. The thermomagnetic curve of sherd 06 is more strongly convex on heating than on cooling. See figure 3.9b. The thermomagnetic behaviour of sherd 08 shows an inflexion on heating around 220°C and a smoothly varying cooling curve. The magnetisation after heating is larger than initially.

MC23. The behaviour of sherds 01 and 02 is similar in terms of the shape of their respective heating curves, which both show an inflexion, and in the smoothly varying nature of the cooling curves. These sherds also have similar Curie point temperatures, but the degree of thermal alteration differs. The thermomagnetic behaviour of the remaining sherds (03, 04, 05 and 06), is characterised by convex, smoothly varying curves which show moderate (77-86%) alteration after heating.

MC24. Sherd 01 of this group has convex, smoothly varying, near-reversible thermomagnetic behaviour with a Curie point at ~550°C. The behaviour of sherd 02 is irreversible. An inflexion occurs during both heating and cooling. The Curie points estimated from the heating and cooling are

590°C and 580°C respectively. See figure 3.9c. Sherd 03 has convex, smoothly varying magnetisation curves. The Curie point estimates are within 5°C. The final sherd of this group (04) has near-linear behaviour up to about 450°C where the magnetisation decays in a broad concave manner. The magnetisation after heating is 9% larger than the initial value.

MC25. The behaviour of sherd 01 is essentially convex on both heating and cooling, but a slight inflexion occurs during heating. Sherd 02 has smoothly varying thermomagnetic behaviour on both heating and cooling. The magnetisation decay above the Curie point is broader on heating than on cooling. Sherd 03 has convex smoothly-varying magnetisation on both heating and cooling. The magnetisation curves of sherd 04 are approximately linear until close to the Curie point where they become steeper. See figure 3.9d. The final sherd of this group (05) shows irreversible behaviour with magnetisation decaying via a broad concave path. The magnetisation is increased after heating.

Chinese I

MC26. The thermomagnetic curves of all eight sherds vary smoothly on heating and cooling. For sherds 03, 07 and 08 the heating curves are more strongly convex than the cooling curves. See for example figure 3.10a. The magnetisation decay at high temperature is broad. All sherds except 07 show reduced magnetisation after heating. The Curie point temperatures range from 535/552°C for 05 to

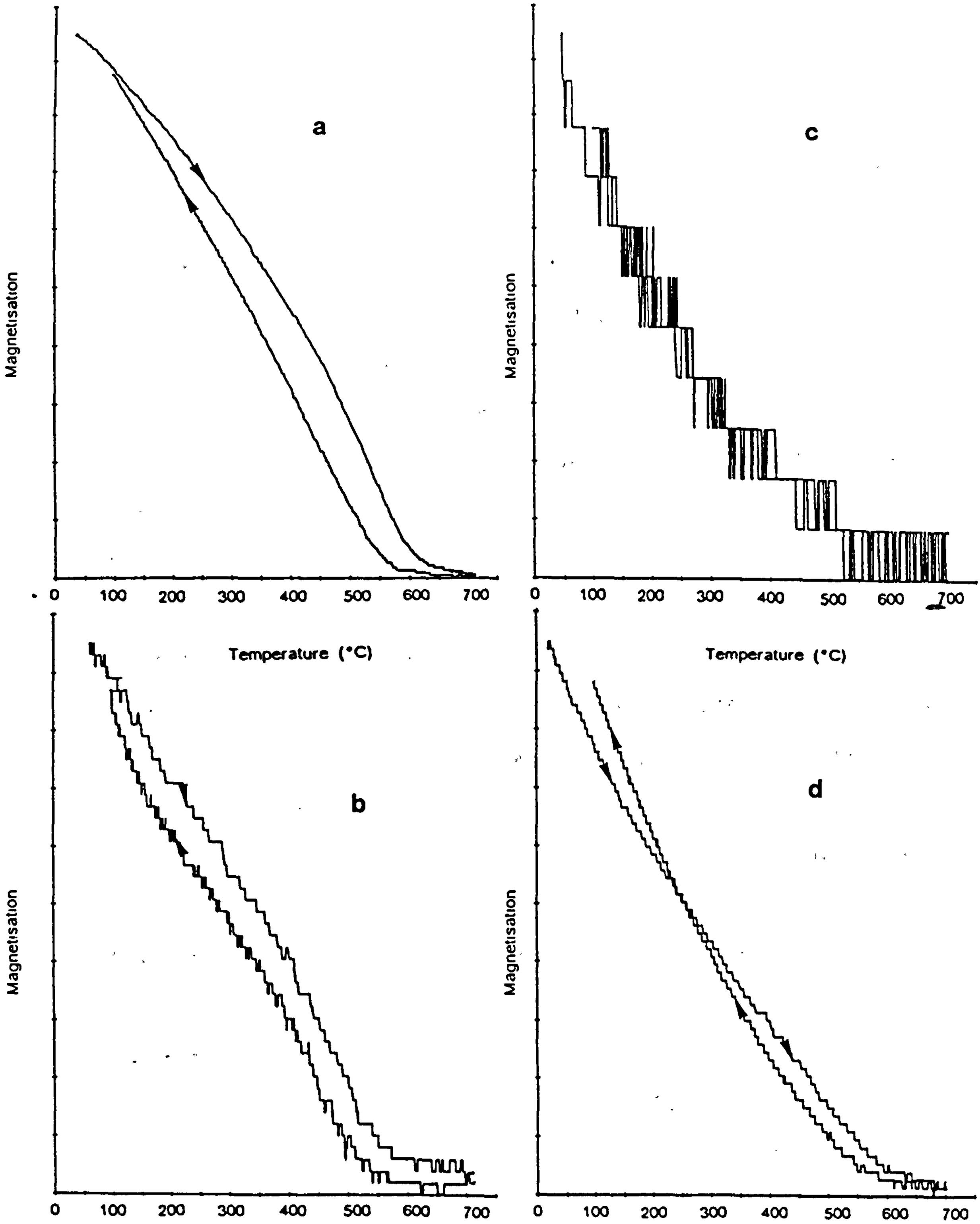

Figure 3.10. The thermomagnetic behaviour of samples (a) MC2607, (b) MC2708, (c) MC2713 and (d) MC2801.

600/608°C for 02.

Chinese II

MC27. The thermomagnetic behaviour of this group is extremely varied. The magnetisation of sherd 01 is strong compared to most of the others in the group. The magnetisation of this sherd falls in a strongly convex manner to a Curie point above 600°C on heating and cools in a less strongly convex fashion with a Curie point of 573°C.

The magnetisation of sherds 05, 06, 07,10 and 11 are much weaker than 01. The thermomagnetic curves of these sherds are concave with no obvious Curie point inflexion. The magnetisation of sherd 08 is strong. The magnetisation falls on heating to an inflexion point at 175°C then falls smoothly to the Curie point at 545°C, see figure 3.10b. The cooling curve has an inflexion at 138°C and a lower Curie point of 485°C. The magnetisation of sherds 09 and 13 are relatively weak. Both have thermomagnetic behaviour which falls initially in a concave manner becoming steeper towards the Curie point. The Curie point cannot be defined for sherd 09 and is only poorly defined for sherd 13. See for example figure 3.10c.

Indian

MC28. The thermomagnetic behaviour for the single Indian sherd is concave during both heating and cooling, preventing the definition of a Curie point. The magnetisation curve is not reversible. The magnetisation is increased after heating. See fig. 3.10d.

3.8 Discussion and Interpretation

The principle aim of studying thermomagnetic behaviour is to identify the magnetic minerals present in the samples. The most powerful diagnostic property is the Curie point temperature.

Some difficulties have been encountered in obtaining the Curie point temperatures in this study. An obvious problem is that many samples are only weakly magnetic, so the Curie point definition is affected by the system noise and the resolution of the plotted curve. A further problem is that for many samples the magnetisation often decays via a relatively broad concave tail at high temperatures (i.e. around the Curie point and above) making the Curie point transition less distinct.

The effect of an increasing paramagnetic component upon the definition of the Curie point has been investigated with a simple model for the thermomagnetic behaviour of a system consisting of paramagnetic and ferrimagnetic (magnetite) components. The ferrimagnetic component is defined by the equation;

$$M(T)=M(0)\left(1-\frac{T^2}{T_c^2}\right)^{\frac{1}{2}} \qquad (3.1)$$

below the Curie point (Williams, 1986) and by the relationship;

$$M(T)=M(0)\ (T-T_c)^{-3/4} \qquad (3.2)$$

above the Curie point (O'Reilly, 1984). Some numerical

adjustment was required in order to match the magnetisation at the cross-over of the two equations. The temperature dependence of the magnetisation of the paramagnetic component follows the reciprocal of the absolute temperature as defined by the Curie Law, see equation 2.2. The thermomagnetic curves for increasing paramagnetic content are illustrated. See figure 3.11. It is clear from figure 3.11 that the Curie point only becomes poorly defined for large paramagnetic contributions and therefore can only provide an explanation for the poor definition of Curie points for curves which are concave, such as figure 3.5d.

A loss of definition of the Curie point has been observed for titanomagnetites with increasing titanium content (Ade-Hall, Wilson & Smith, 1965). In this study a broader decay of magnetisation was observed for sherds with Curie points below ~570°C. See for example figure 3.7d. An explanation for the broader decay of magnetisation is an increasing distribution of Curie point temperatures arising from greater compositional variation with increased titanium substitution.

In this study, Curie point temperatures were obtained from both the heating and cooling curves. It is apparent from appendix 2 that these Curie points are rarely coincident. The Curie points obtained from the heating curves are usually higher than those from the cooling curves. A proper understanding of this discrepancy is necessary for the correct interpretation of the data. A

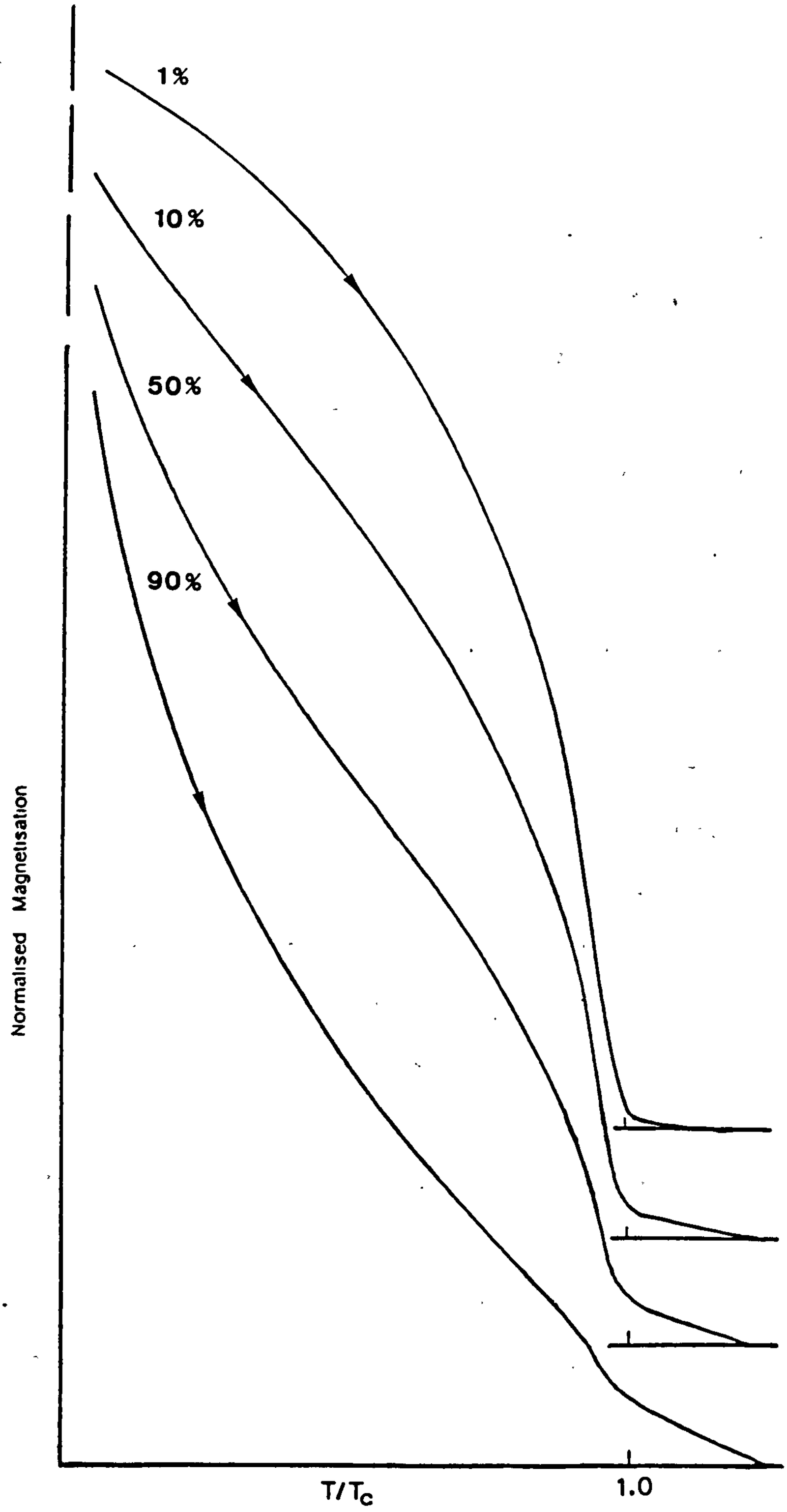

Figure 3.11. Theoretical thermomagnetic behaviour of a system containing varying quantities of a ferrimagnetic and a paramagnetic material. The percentages indicate the contribution of the paramagnetic component to the total magnetisation at room temperature.

suggested cause is that of thermal hysteresis, where the sample, because of its bulk and poor conductivity, lags behind the temperature attained by the thermocouple. This would produce an over-estimate of the Curie point temperature from the heating curve and an under estimate from the cooling curve. If thermal hysteresis is the reason for the discrepancy a simple solution would be to reduce the heating rate. However, this has the disadvantage that thermal alteration will be increased and in the worst case, cause destruction of the original mineral phase. The hypothesis that thermal hysteresis causes the variation in the Curie points has been tested using a fixed amount of synthetic magnetite mixed with increasing amounts of aluminium oxide to provide samples of differing mass. See figure 3.12. The results indicate that increasing sample size does increase the discrepancy between the Curie point estimates. For a reversible sample, the true Curie point must lie between the two estimates. The true Curie point may be closer to one or other of the estimates depending on the heating and cooling rates, but this is difficult to assess. The Curie points discussed in the remainder of this section have been obtained by taking the midpoint between the two estimates (where the estimates are considered, by visual inspection, to represent the same Curie point). For samples where the Curie point estimated from the heating curve is lower than that obtained from the cooling curve, the heating curve estimate is used, although it is accepted that this may be

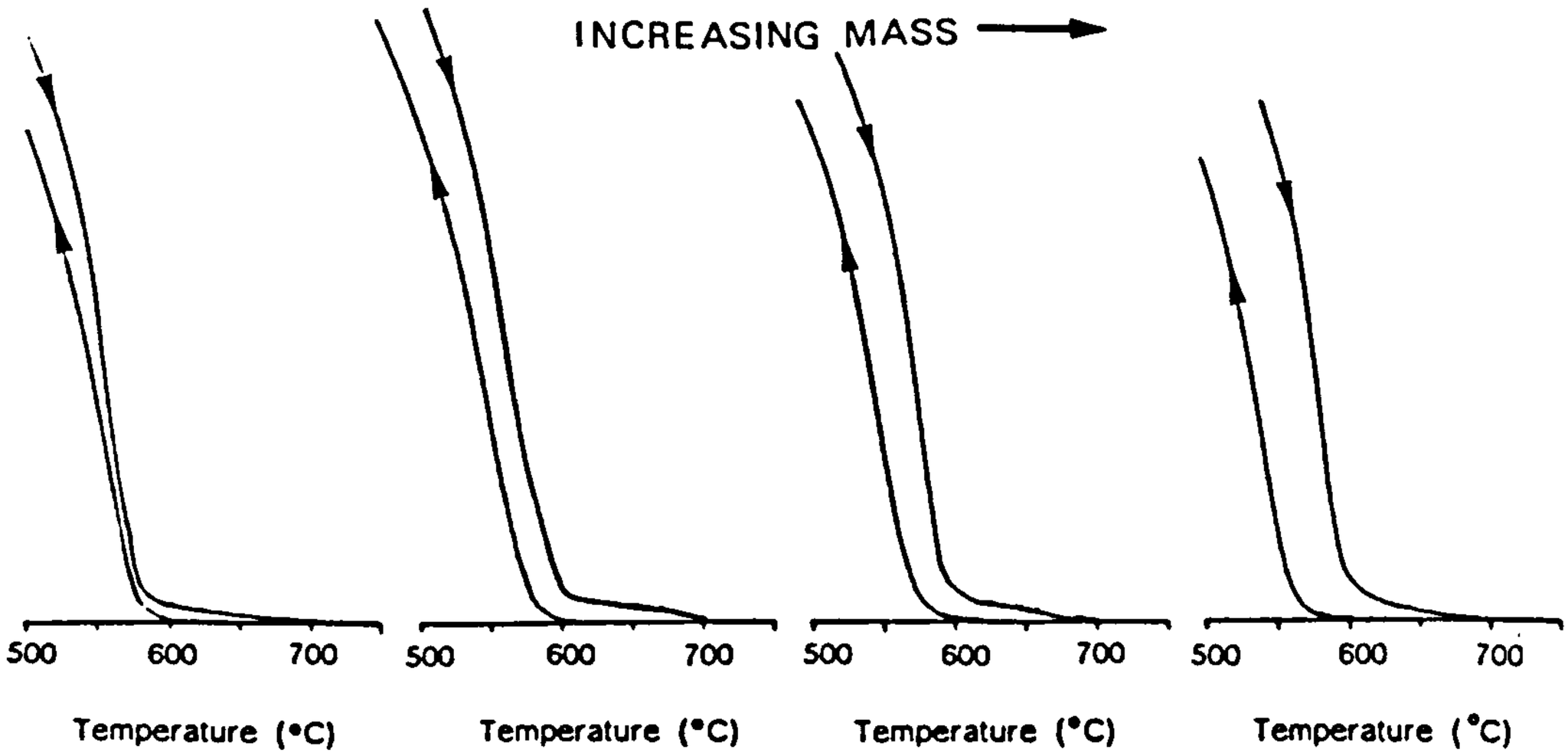

Figure 3.12. The effect of the sample mass on the amount of thermal hysteresis observed in the thermomagnetic behaviour.

an overestimate. Where multiple subsamples have been measured a mean value is taken for the Curie point.

3.8.1 Curie point temperatures

The distribution of Curie point temperatures, and other inflexion temperatures, for the whole collection is compiled in figure 3.13.

Assuming that the Curie points obtained are representative of the original mineral phase present (which may not be the case for samples showing irreversible behaviour and in particular, inflexions) they can be used to identify the minerals. It is clear from the Curie point distribution that the most commonly occurring Curie points are between 570 and 590°C. Considering that the Curie point estimates are probably not more accurate than +/- 10°C (Crangle, 1977) this indicates the presence of magnetite.

The distribution extends to both lower temperatures, down

to 470°C, and higher temperatures, up to 630°C. The lower temperature Curie points suggest the presence of substituted magnetite. Assuming that titanium is the major substitution species, a reasonable assumption considering the prevalence of titanomagnetites in rocks, the degree of substitution can be calculated, assuming the minerals are stoichiometric. According to O'Reilly (1984) the Curie point varies approximately linearly from 575°C for magnetite (x=0) to -153°C for ulvospinel (x=1), where x is the amount of titanium substitution in $Fe_{3-x}Ti_xO_4$. With this linear relationship a simple equation can be obtained for x as follows;

$$x=\frac{575-T_C}{728} \qquad (3.3)$$

Using this equation the maximum titanium content observed in this collection is x=0.13 for T_C=475°C. However, substitution is often less than x=0.03, for 100 of the 147 Curie points fall between 550 and 590°C.

The features of high temperature oxidation of titanomagnetites as discussed in section 3.3 have been observed for several titanomagnetite samples e.g. see figure 3.7d, but not for others, see figure 3.8b.

The distribution of Curie points above the 570-590°C window may be explained in terms of low temperature oxidation of magnetite. The mechanism of low temperature oxidation was described earlier (section 3.3). According to a model proposed by Readman & O'Reilly (1971) the

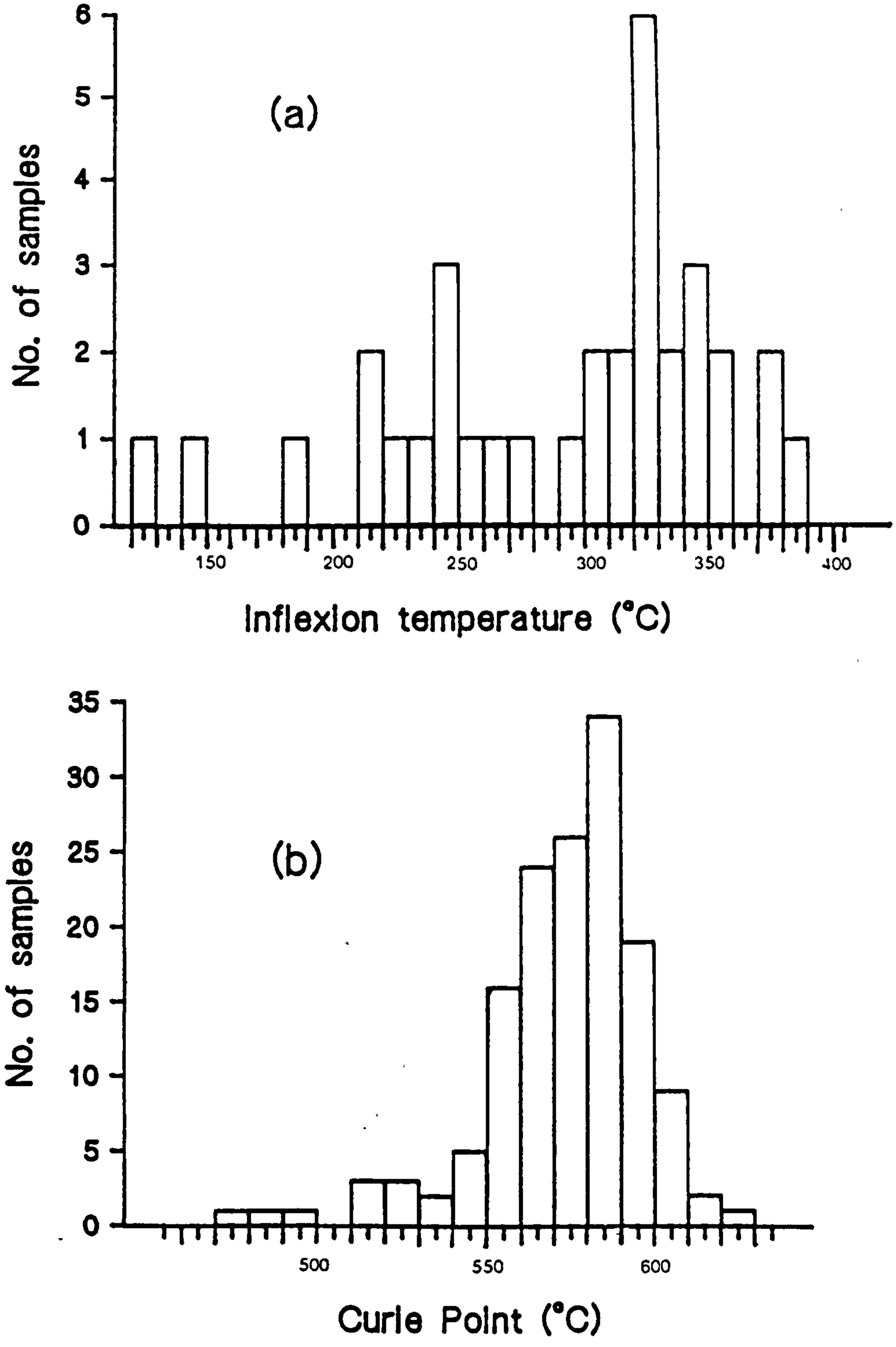

Figure 3.13. Histograms showing (a) the distribution of inflexion temperatures and (b) the Curie point temperatures obtained from the sherds investigated in this study.

maghemite 'skin', arising from oxidation, rapidly becomes homogenised with the unoxidised core, to a composition in the magnetite-maghemite solid solution series, i.e. a cation deficient magnetite. The Curie point temperature of the cation deficient phase increases from that of magnetite towards that of maghemite as the composition approaches that of maghemite. On this basis it is suggested that the thirty-one samples with Curie points above 590°C contain cation deficient magnetite. Other samples may contain cation deficient titanomagnetites which have Curie points not exceeding that of magnetite, and therefore are not identifiable on the basis of Curie point alone. The whole problem of low temperature oxidation, stability to inversion, and inversion products is complex, and may be confused with high temperature oxidation.

3.8.2 Low temperature oxidation

As discussed in the previous section the Curie point temperature of cation deficient magnetite increases as the composition approaches that of maghemite. However, while the structure of magnetite is thermally stable and that of maghemite is unstable, inverting to haematite, the stability of cation deficient magnetite is not well understood. Readman & O'Reilly (1971) suggest that cation deficient magnetites undergo inversion but these workers do not indicate any dependence upon the degree of cation deficiency. The inversion of cation deficient magnetite produces an intergrowth of haematite and magnetite (Readman & O'Reilly, 1971). This would lead to a reduction of the

spontaneous magnetisation and a magnetite Curie point. This can be used to explain the curves which have small inflexions on heating, smooth cooling curves, reduced magnetisation after heating and magnetite Curie points. The situation may be complicated by incomplete inversion or inversion above the Curie point of the cation deficient phase, as observed by Ozdemir and Banerjee (1984). The spontaneous magnetisation of all but three of the cation deficient magnetite samples with Curie points above that of magnetite are reduced by varying amounts after heating to 710°C. See, for example, figures 3.6b & 3.6d. Of these samples, six show inflexion points on heating between 320 and 350°C suggesting that partial or total inversion occurs at these temperatures. The remaining twenty-three samples show no inflexion points suggesting either that inversion does not occur (in which case the reduction in magnetisation is the result of high temperature oxidation to haematite) or inversion occurs above the Curie point of the cation deficient phase.

3.8.3 Titanomagnetites: high and low temperature oxidation

Among the one hundred samples which have magnetite Curie points, sixteen show irreversible behaviour characterised by a generally increased magnetisation (0-27%) on cooling and twelve of these show an inflexion between 220 and 380°C during heating. See for example figures 3.3c, 3.6a & 3.8d. Eleven other samples show similar behaviour but have Curie points less than 570°C. Two possible mechanisms could account for these results. The first mechanism is simply

that of oxidation due to thermal treatment. Oxidation of titanomagnetite tends to segregate the initial, homogenous composition into magnetite and ilmenite, and hence increases the spontaneous magnetisation. This process of oxidation usually occurs at high temperatures (above 600°C) or with low heating rates (see section 3.3). High temperature oxidation is probably the explanation for the behaviour of titanomagnetite-bearing samples, such as in figure 3.9a, where the original composition survives to its Curie point on heating but is oxidised on further heating, giving a higher Curie point on cooling.

However, inflexion points, for the samples that show them, occur at temperatures less than 400°C, suggesting the process is not that of high temperature oxidation. An alternative explanation for the behaviour of these samples is that the minerals are cation deficient titanomagnetites which undergo inversion below 400°C. The magnetisation after inversion and the inversion products of cation deficient titanomagnetite or titanomaghemite depend in a complex way upon the initial mineral composition and the degree of oxidation. The spinel phase formed by inversion has less titanium than the original composition and invariably has a higher intrinsic magnetisation than the initial phase, but the final magnetisation of a sample may be increased or decreased for samples with limited substitution (low x) depending on the degree of oxidation. A high degree of oxidation limits the availability of Fe^{2+} ions which form magnetite, leaving excess Fe^{3+} to be taken

up by non-spinel phases (O'Reilly, 1984). This reduces the final magnetisation after inversion. Conversely, when the degree of oxidation is low there are sufficient Fe^{2+} ions to combine with the Fe^{3+} ions to form magnetite but insufficient to combine with TiO_2 to form ilmenite, leaving an intergrowth of magnetite and anatase (TiO_2). This increases the magnetisation after inversion.

If the samples under discussion are cation deficient titanomagnetites they must, by virtue of their increased magnetisation after heating, be only slightly oxidised. The oxidation parameter, z, can be estimated from;

$$z=\frac{4x/3}{1+x} \qquad (3.4)$$

(O'Reilly, 1984). By assuming a value for the titanium content (x) comparable with that of other samples in the collection i.e. x=0.03, the oxidation parameter obtained is only 0.038, indicating a very limited degree of oxidation for these samples. It is therefore a reasonable conclusion that these samples contain cation deficient titanomagnetites.

3.8.4 Inflexions on heating and cooling

Four samples (MC1002, MC1003, MC2203 and MC2402) and the outer section of two further samples (MC1901B and MC1902B) show well defined inflexions on both heating and cooling. These inflexions occur between 180 and 260°C. The presence of these inflexions suggests that a second ferrimagnetic mineral phase is present which survives heating. An

alternative explanation in terms of the destruction or formation of other phases is unlikely as such changes would be irreversible.

3.8.5 The effect of paramagnetic minerals

The effect of an increasing paramagnetic contribution on the overall shape of the thermomagnetic curves has been modelled. See figure 3.11. It is apparent that the magnetisation changes at lower temperatures are dominated by the paramagnetic component while the ferrimagnetic component becomes dominant at higher temperatures. The transition at intermediate temperatures is, in all cases, smooth. Several of the samples from this study display thermomagnetic behaviour similar to the modelled behaviour (see figure 3.6c) suggesting a similar combination of para- and ferri-magnetic minerals.

3.9 Conclusions

The results of this investigation indicate that thermomagnetic analysis can often be used to identify the ferrimagnetic constituents of ancient ceramics. The thermomagnetic curves are either convex, reflecting the ferrimagnetic minerals or show behaviour consistent with the combination of paramagnetic and ferrimagnetic minerals in various proportions. The spread of Curie points indicates a limited range of mineral compositions from that of magnetite (x=0) to titanium-poor titanomagnetite (x=0.13). In addition, the presence of inflexions in many of the heating curves, suggesting the inversion of cation

deficient phases, and the occurrence of Curie points above that of magnetite, indicate that these minerals have been subject to low temperature oxidation.

From this thermomagnetic investigation the presence of haematite is only indicated in two samples. The apparent absence of haematite is surprising since it is often assumed to be an important mineral in ancient ceramics (Tucker & Thomas, 1983). The presence of haematite may go undetected because of its low magnetisation which may be swamped by ferrimagnetic or paramagnetic minerals, or the system noise.

3.10 Summary of thermomagnetic behaviour

The thermomagnetic behaviour of the sherds investigated can be summarised by assigning them to one of several categories based on their Curie point temperature and the shape of the magnetisation versus temperature curve. The categories are described below.

Category (a) samples have Curie points between 565°C and 585°C, i.e. Curie points within +/- 10° of the Curie point of magnetite (575°C, O'Reilly, 1984) and which are therefore considered to be magnetite. These samples are subdivided on the basis of the shape of the thermomagnetic curve. The heating and cooling parts of the thermomagnetic curve of category a1 samples have a similar form, i.e. nearly reversible, with the magnetisation after heating being reduced by a maximum of 20% from that before heating. See figure 3.3a. Category a2 samples have irreversible

behaviour with the magnetisation either increasing or decreasing after heating, see figures 3.3c and 3.3d.

Category (b) samples have Curie points above 585°C and are considered to represent low temperature oxidised magnetite. This category is also subdivided. Samples in category b1 have near reversible thermomagnetic behaviour with the magnetisation after heating within 20% of that before heating. See figures 3.4d and 3.6b. Category b2 contains samples which show irreversible thermomagnetic behaviour. The magnetisation after heating may be higher or lower than the magnetisation before heating. See figures 3.4b and 3.6d respectively.

Category (c) contains samples which have mean Curie point temperatures less than 565°C, i.e. below the range attributed to magnetite. These samples contain magnetites with limited titanium substitution. The samples are subdivided. c1 samples show nearly reversible thermomagnetic behaviour with the magnetisation after heating being up to 20% less than the magnetisation before heating. See figures 3.4a and 3.8b. Category c2 samples show irreversible behaviour which is characterised by an increase in both the Curie point temperature and the magnetisation after heating. See figure 3.7d and 3.9a.

Category (d) samples have thermomagnetic behaviour which is consistent with the presence of titanomagnetites which have been oxidised to some extent at low temperature. These samples can only be identified by their irreversibility and therefore the category is not

subdivided. See figure 3.8a.

Category (e) samples have two Curie point temperatures which are clear on both heating and cooling. These samples samples contain a near magnetite phase and a high titanium content magnetite phase. See figures 3.5a and 3.5b.

The remaining category (x) simply contains all of the samples for which the ferrimagnetic mineralogy could not be determined from the thermomagnetic behaviour. See figure 3.5d.

The distribution of samples between the categories of thermomagnetic behaviour is shown in figure 3.14.

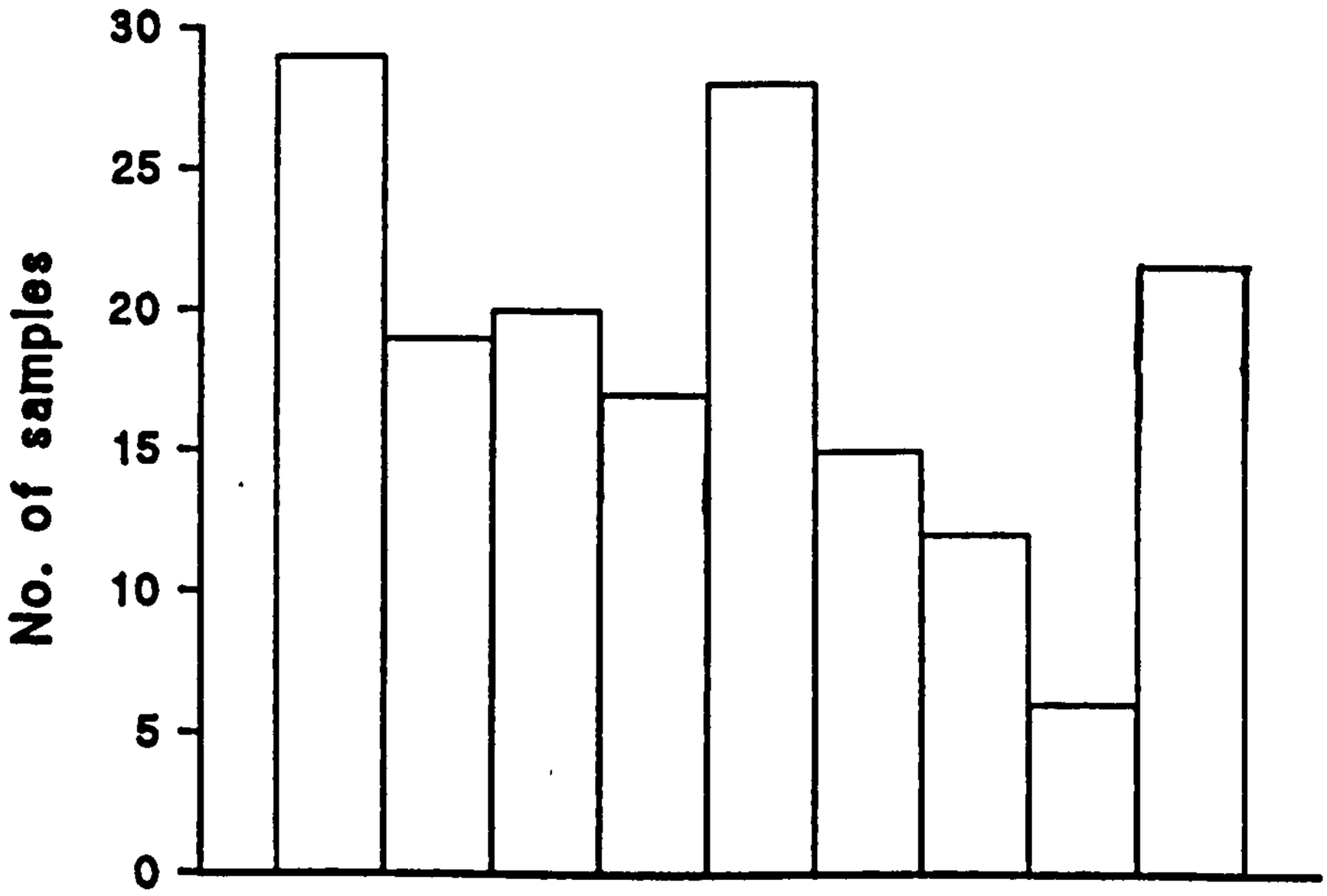

Figure 3.14.. The distribution of samples between the categories of thermomagnetic behaviour described in the text.

4 Isothermal Remanence Acquisition

4.1 Introduction

Stepwise isothermal remanence acquisition (IRM) has been carried out in order to determine the coercivity spectra of magnetic minerals and to use these as an aid to mineral identification. The coercivity spectra have been determined using IRMFIT, a modelling program developed by D. J. Robertson. This method is discussed. IRM acquisition curves have been obtained from selected samples throughout the collection for general investigation. A further series of curves have been obtained for a suite of subsamples from the Servian and Romano-British groups in order to investigate the consistency within both the individual sherds and their respective groups.

4.2 Background

Isothermal remanence is the remanence induced in a material on the application of a magnetic field, without any change of temperature. An individual particle of coercivity, H_c, will become magnetised by an applied field, H, when $H>H_c$. The maximum coercivity is determined by the the composition and morphology of a mineral, for example, magnetite has a maximum coercivity of $2.4x10^5$ Am^{-1} (equivalent to B=300 mT) (McElhinny, 1973), while the value for haematite is $\sim4x10^5$ Am^{-1} (B~500 mT) (Brooks & O'Reilly, 1970) when it is crystalline and $>1.5x10^6$ Am^{-1} (>1.89 T) when it is a fine pigment (Dunlop, 1972a). The

maximum coercivity of crystalline goethite exceeds 1.6×10^6 Am^{-1} (>2.01 T) (Dekkers, 1988). However, maximum coercivities are rarely observed. They occur only for large single domain size particles, the coercivity falls as the particle size decreases owing to thermal disturbance (see section 2.7), and decreases for larger, multidomain particles because magnetisation changes occur principally via domain wall movements which require less energy.

In natural samples the presence of different minerals and different particle sizes leads to a range of coercivities which is termed the coercivity spectrum. During IRM acquisition the remanent magnetisation of a sample increases as increasing applied fields sweep through the coercivity distribution until the maximum coercivity is reached. At which point, the remanent magnetisation increases no further and its value is termed the saturation isothermal remanent magnetisation, SIRM.

4.3 Equipment

Pulsed magnetic fields were used to induce isothermal remanence. A Molspin Pulse Magnetiser provided fields from 10 to 300 mT and a Trilec Pulse Magnetiser provided fields from 400 mT to 4 T. Both systems operate by discharging a capacitor bank through a solenoid which surrounds the sample. The remanent magnetisation was measured using a Molspin spinner magnetometer. This is a development of the magnetometer described by Molyneux (1971). In this system the magnetisation is measured by spinning the sample inside

a circular fluxgate sensor. This induces an alternating voltage, the amplitude of which is proportional to the intensity of magnetisation. The magnetometer is controlled through an IBM compatible personal computer (PC). The magnetometer output is returned to the PC, where corrections for calibration and the mass of the sample are made before the data is saved to a floppy disk.

4.4 Sample preparation and experimental procedure

Samples were prepared in a similar fashion to those for thermomagnetic analysis, except that the samples were not crushed. The samples were packed into 2.5 cm by 2.5 cm cylindrical plastic pots. Orientation of a sample between the pulse magnetiser and the magnetometer was acheived by a lug on the lid of each sample pot.

The initial stage in each series of measurements was the calibration of the magnetometer. This procedure is controlled by the PC, the calibration sample contains a piece of magnetic recording tape with a known magnetisation. In addition, calibration was carried out whenever the magnetometer attenuation wäs increased, to cope with increased sample magnetisation, because the attenuation resistors do not give exactly the stated attenuation and would lead to discrepancies in the data. Calibration was also undertaken at irregular intervals during each series of measurements to check for magnetometer drift. The set of applied fields used was chosen to give a reasonable distribution of data when

plotted on the logarithmic scale used by the IRMFIT software. In order to obtain a smooth acquisition curve the time between the magnetisation acquisition and measurement was kept approximately the same at each field step.

4.5 Data analysis

Isothermal remanence acquisition curves were analysed using IRMFIT. For analysis the data was plotted as isothermal remanence, normalised to the SIRM, against the logarithm (base 10) of the applied field in mT. The aim of the analysis is to fit a curve to the data using either one or two Gaussian (on a log scale) distributions of coercivity. Figure 4.1 shows an example of the method applied to data obtained from one of the sherds investigated. The two coercivity distributions used to model the IRM acqusition are also sketched. The modelled curves were fitted iteratively by adjusting three parameters for each distribution. The parameters which define the distributions are; the mean logarithm of the coercivity, the standard deviation, and the fraction of the normalised SIRM that the distribution accounts for.

Using this technique, the IRM curves for many natural samples can be reasonably well fitted (D. J. Robertson, pers. comm). The physical basis for the observed goodness of fit is not clear.

IRMFIT has been used to identify wether there are one or two mineral components present, on the basis of whether one

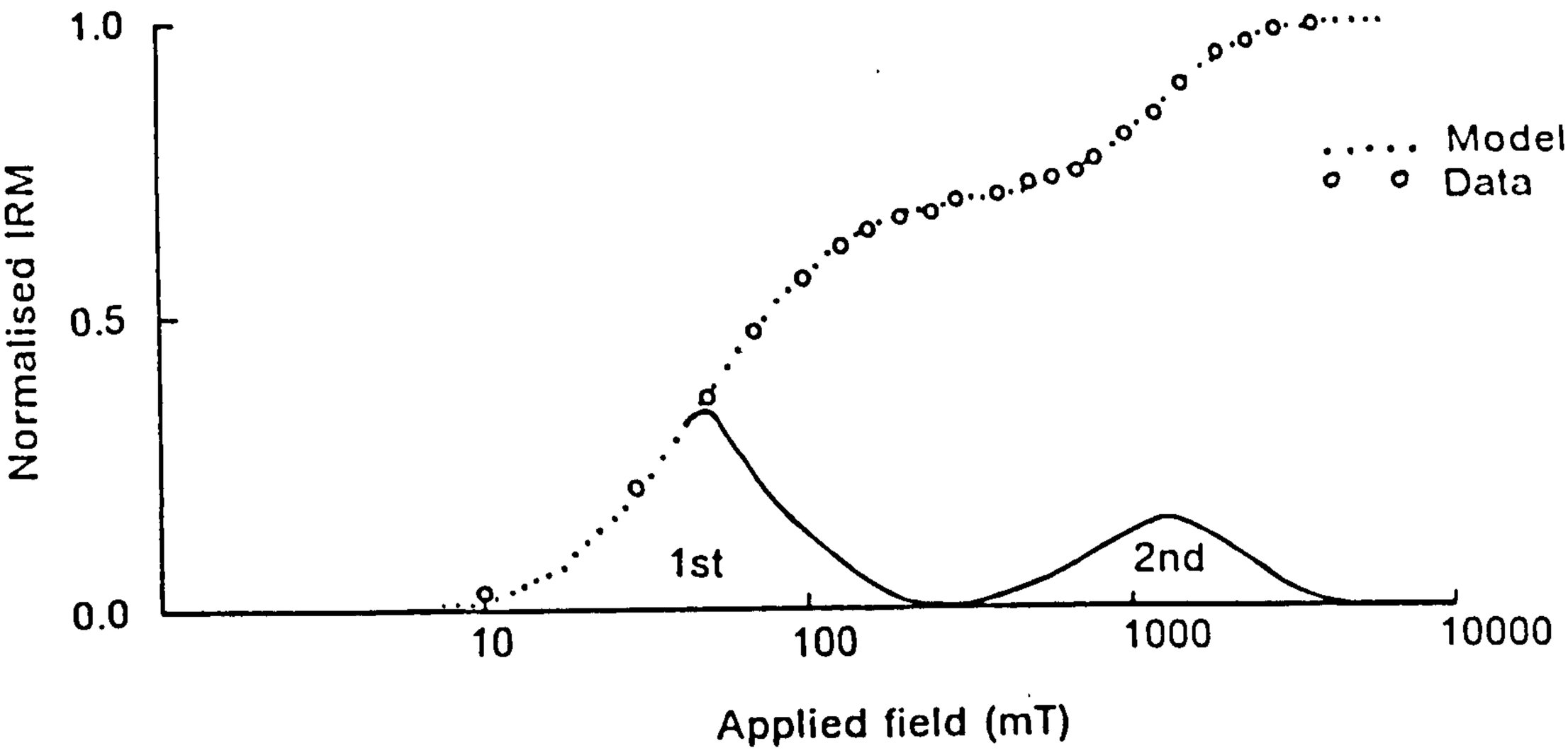

Figure 4.1. An example of the method of data analysis using IRMFIT for sample MC1002. The isothermal remanent magnetisation is plotted cumulatively against the logarithm of the applied field. The two coercivity spectra used to model the experimental data are sketched.

or two Gaussian distributions are required for the best fit. The fit parameters for each distribution are taken as representative of the coercivity spectrum of each mineral component.

4.6 Results

All of the samples investigated were fitted reasonably well using either one or two coercivity distributions. The parameters determined for the best fitting curves are listed in appendix 3.

4.6.1 Identification of the magnetic minerals

The application of IRMFIT allows observed IRM acquisition curves to be broken down into one or two

coercivity distributions. These distributions are interpreted as arising from different magnetic minerals. Separation of the mineral components allows the relative importance of each to be determined even if the coercivity spectra of the two minerals overlap. When one or other of the contributions is small it is not defined well.

The observed IRM acquisition behaviour varies through the collection and within samples. The variations within individual samples are discussed later. The behaviour in the collection varies from samples which have only a single mineral coercivity spectrum, through to samples which have a large low coercivity component and a small high coercivity component, and on, to a sample in which the IRM acquisition is dominated by a high coercivity mineral. Examples of these three types are shown (see figure 4.2).

A low coercivity distribution was fitted to all of curves whereas a high coercivity distribution was not. The number samples with particular fractional contributions to the SIRM contributed by the second, high coercivity, mineral is shown for all of the samples on a histogram, see figure 4.3. Where two or more subsamples are available from a sherd a mean value is shown. The contribution to the SIRM of the second mineral varies from 0-84%, with 92 of 104 sherds having less than 10% of the SIRM attributable to the second mineral.

The two coercivity distributions have been equated with two different minerals. The identification of these minerals is based on the maximum coercivities obtained from

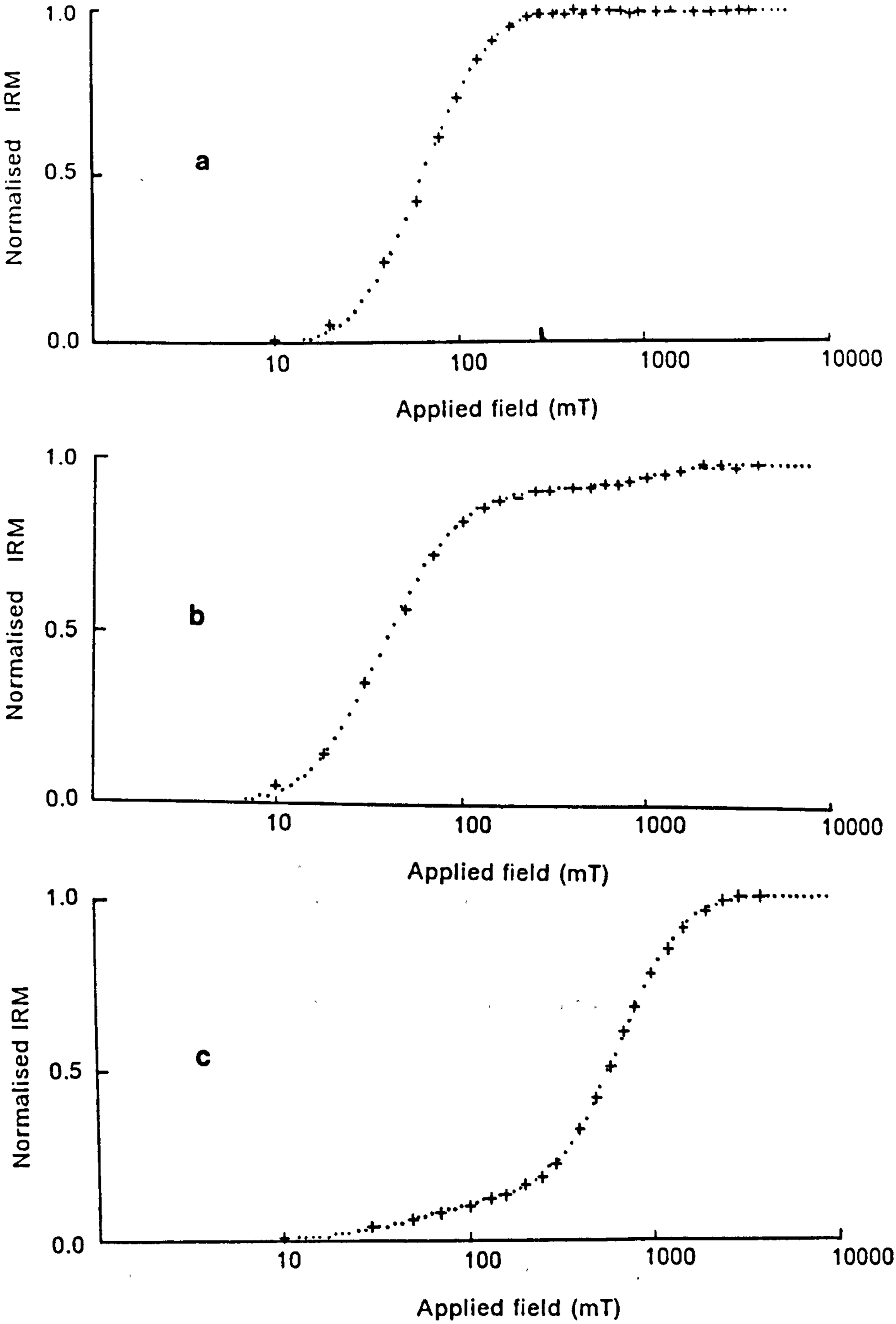

Figure 4.2. Three examples of the isothermal remanence acquisition behaviour obtained from the sherds investigated. The samples show (a) a single low coercivity mineral assembly, MC1706, (b) a large low coercivity component and a smaller high coercivity component, MC1107, and (c) a small low coercivity and a large high coercivity fraction, MC1003.

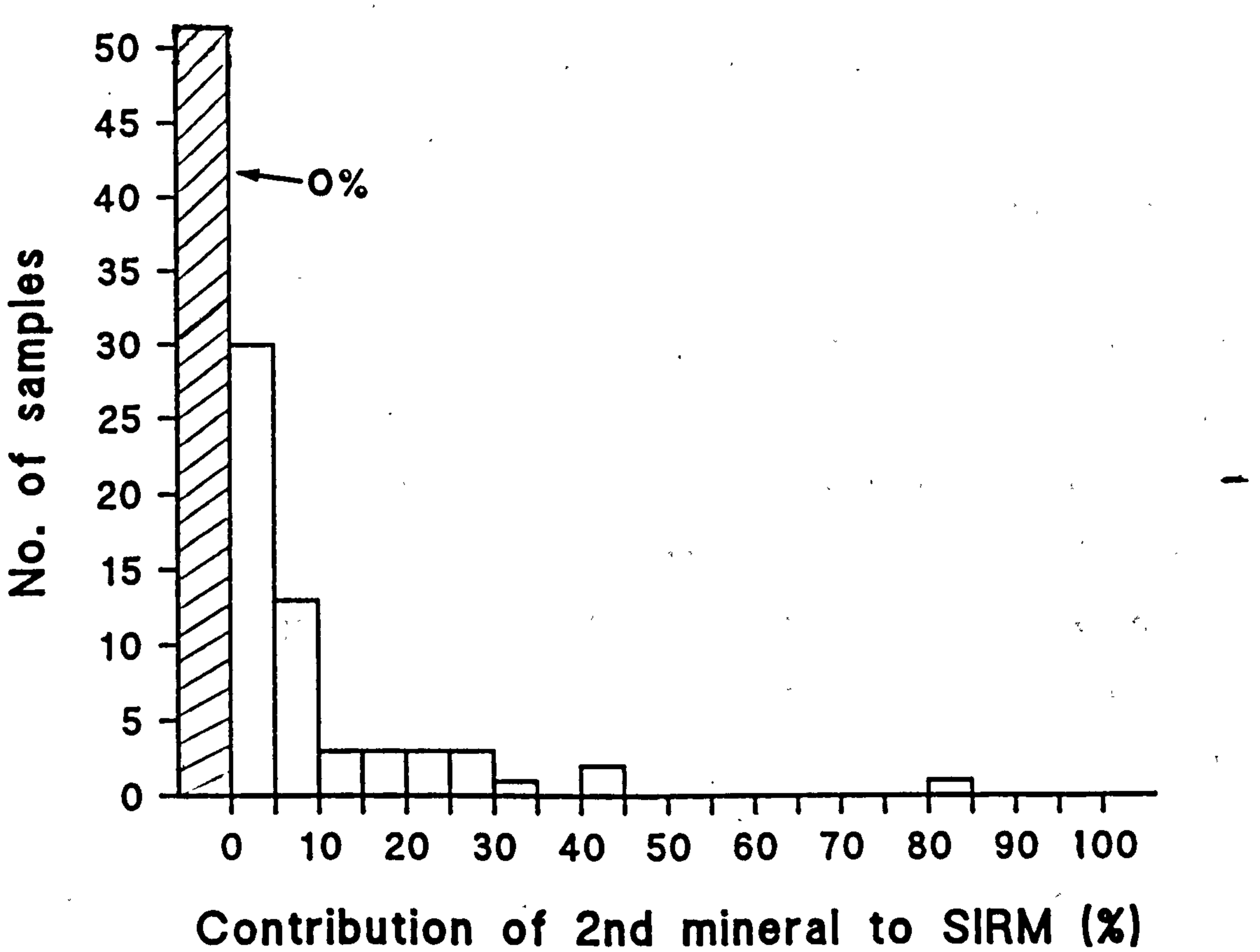

Figure 4.3. A histogram showing the number of samples which have a particular fraction of SIRM which is contributed by the high coercivity mineral.

their respective coercivity distributions. The maximum coercivity (in mT) is calculated as the field at which 95% of a distribution has been magnetised. The limit of 95%,

which is two standard deviations, is arbitrary but leads to values for the saturating field similar to those observed from magnetic hysteresis measurements. Figure 4.4 is a histogram of the maximum coercivities determined from both the low and high coercivity distributions fitted to each of the samples. The histogram shows two concentrations. The maximum coercivities for the first mineral range from 55 mT up to 389 mT, with a peak between 200-300 mT. This peak is close to the maximum coercivity of large single domain magnetite particles (i.e. 300 mT). This suggests that the lower coercivity distribution arises from magnetite or a mineral with a composition close to that of magnetite. The extension of this distribution to lower values probably represents the presence of multidomain or small, near superparamagnetic, single domain particles. The extension of the first distribution above 300 mT may be an erroneous function of the method of calculating the maximum coercivity value, which is extremely sensitive to errors in the gaussian parameters. For example, a difference of 0.05 in the mean log-coercivity value fitted to a particular data set could alter the maximum coercivity by 20-30 mT. Alternatively, the extension above 300 mT may reflect the increased coercivity associated with increasing titanium content magnetite (c.f., sample MC2001 which has a calculated maximum coercivity of 309 mT and Curie point at 513°C, indicating a titanium substituted magnetite with x=0.085). The maximum coercivities of the second mineral are often poorly defined because they account for only a

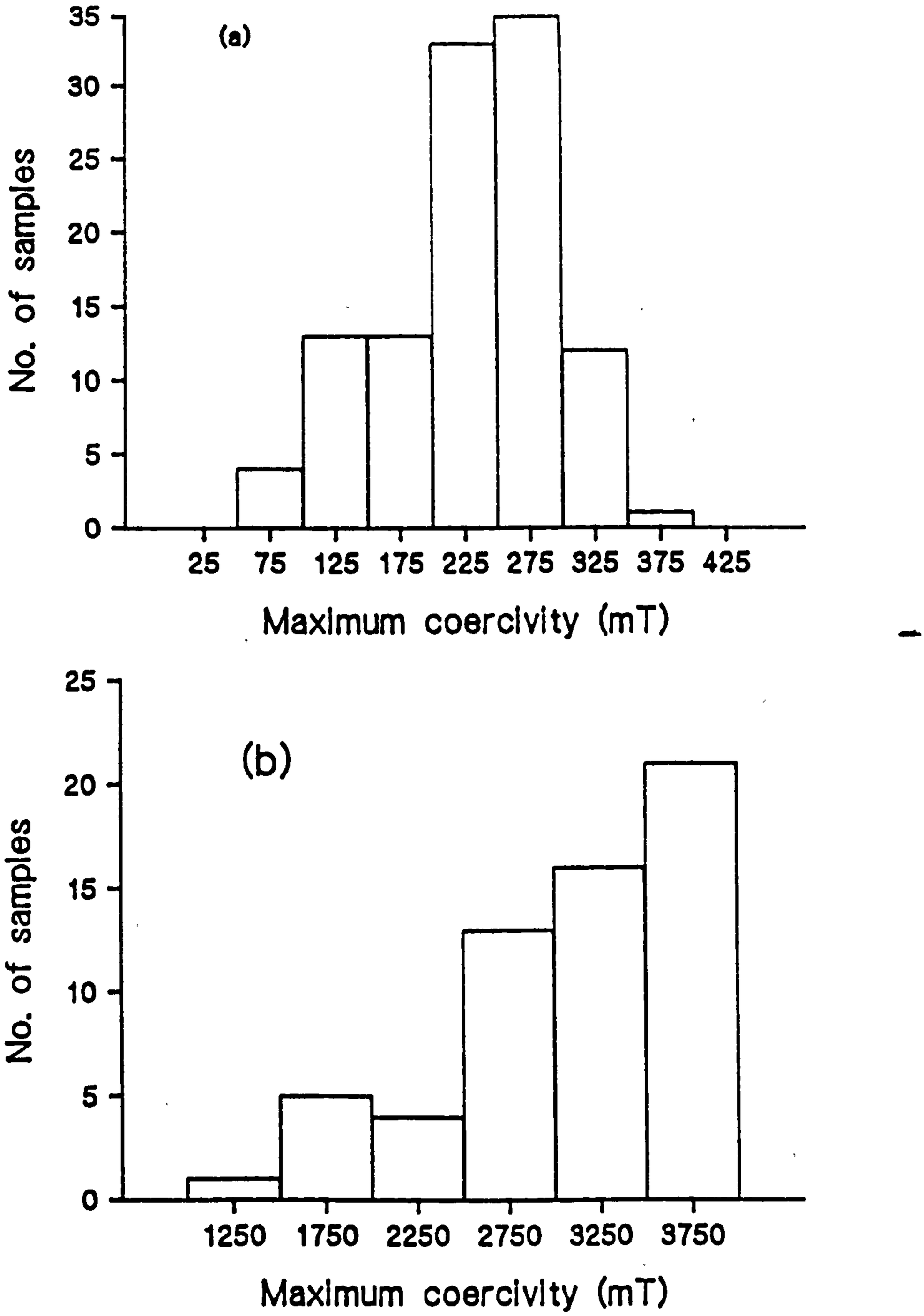

Figure 4.4. Histograms of the maximum coercivities of (a) the low coercivity mineral and (b) the high coercivity mineral.

small fraction of the SIRM which makes them difficult to analyse using IRMFIT. However, inspection of the experimental data showed all of the samples to be saturated below the maximum applied field of 4 T. The range of coercivities for the second minerals suggest the presence of haematite. The presence of goethite is not implied since it rarely saturates below 4 T (France, pers. comm.).

4.6.2 Internal consistency

Both within-sherd and within-group consistency has been tested using Servian and Romano-British pottery. These two groups are most suited to this analysis since both contain a large numbers of sherds from the same site and both span relatively short time periods.

Within sherd consistency was tested using between two to six subsamples from many of the sherds. Where colour differences were observed within a sample the subsamples were taken from the inner (usually black or grey) and outer (usually more orange or brown) parts of a sherd. In other cases no distinction was made between the subsamples.

Comparing the results for these samples is difficult because of the number of parameters. A comparison of the mean log coercivities of the low (first) coercivity distribution for pairs of subsamples has been achieved by plotting the mean of one against the mean of the other. See figure 4.5. The pairs of data should fall on a line of slope=1 if they are internally consistent. It can be seen from figure 4.5 that most of the results plot within 10% of this line. The standard deviations for pairs of data are

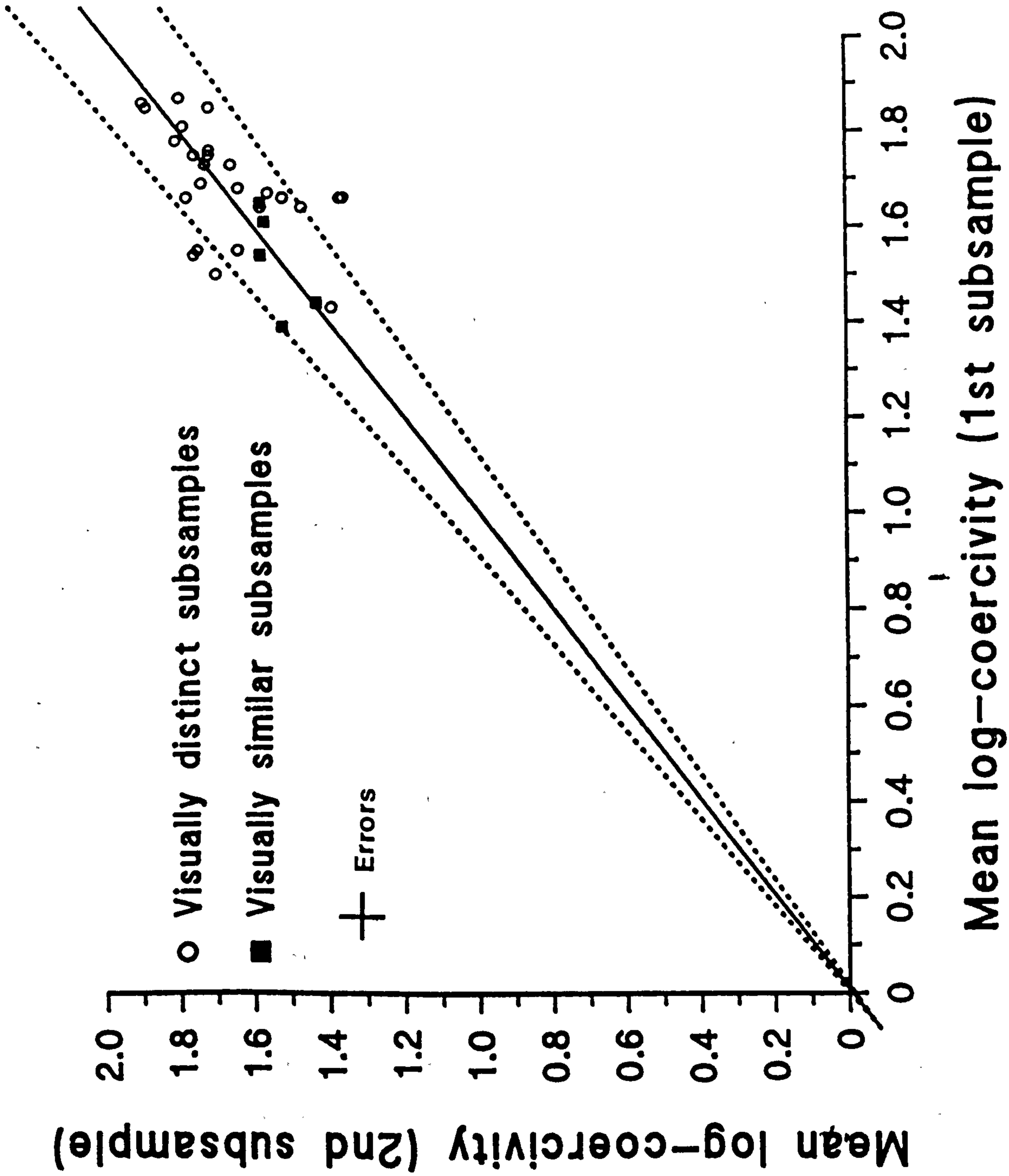

Figure 4.5. A comparison of mean coercivities obtained from the IRM acquisition of pairs of subsamples from the same sherd. Data falling on the line of slope=1 indicates consistency between the pairs of subsamples. The dashed lines indicates slopes of 1.1 and 0.9, i.e. +/- 10%. The error bars are based on the resolution of the fitting method.

usually also similar to within 10%.

The contributions of the two minerals to the saturation isothermal remanence between subsamples has been investigated. Pairs of subsamples have been compared by plotting the percentage of the SIRM held by the lower coercivity spectrum of one subsample against the percentage of the SIRM held by the low coercivity spectrum of the second subsample. These data are shown in figure 4.6. The SIRM of ten of the subsample pairs was entirely accounted for by a single low coercivity mineral. The remainder showed varying contributions of the high coercivity fraction to the SIRM between subsamples. In the case of the pairs of subsamples from the inner and outer parts of the Servian sherds the outer part often contained a high coercivity mineral fraction. In contrast, for the Romano-British pottery, the inner subsamples had a larger high coercivity fraction in five of the ten samples investigated.

4.7 Discussion and conclusion

The acquisition of isothermal remanence has been studied in order identify the magnetic mineralogy of the sherds on the basis of the coercivity. IRM acquisition has also been used to investigate the consistency of the acquisition behaviour both between subsamples from the same sherd and between samples from the same group of sherds. Isothermal remanence acquisition curves have been analysed using IRMFIT. All of the curves obtained were modelled

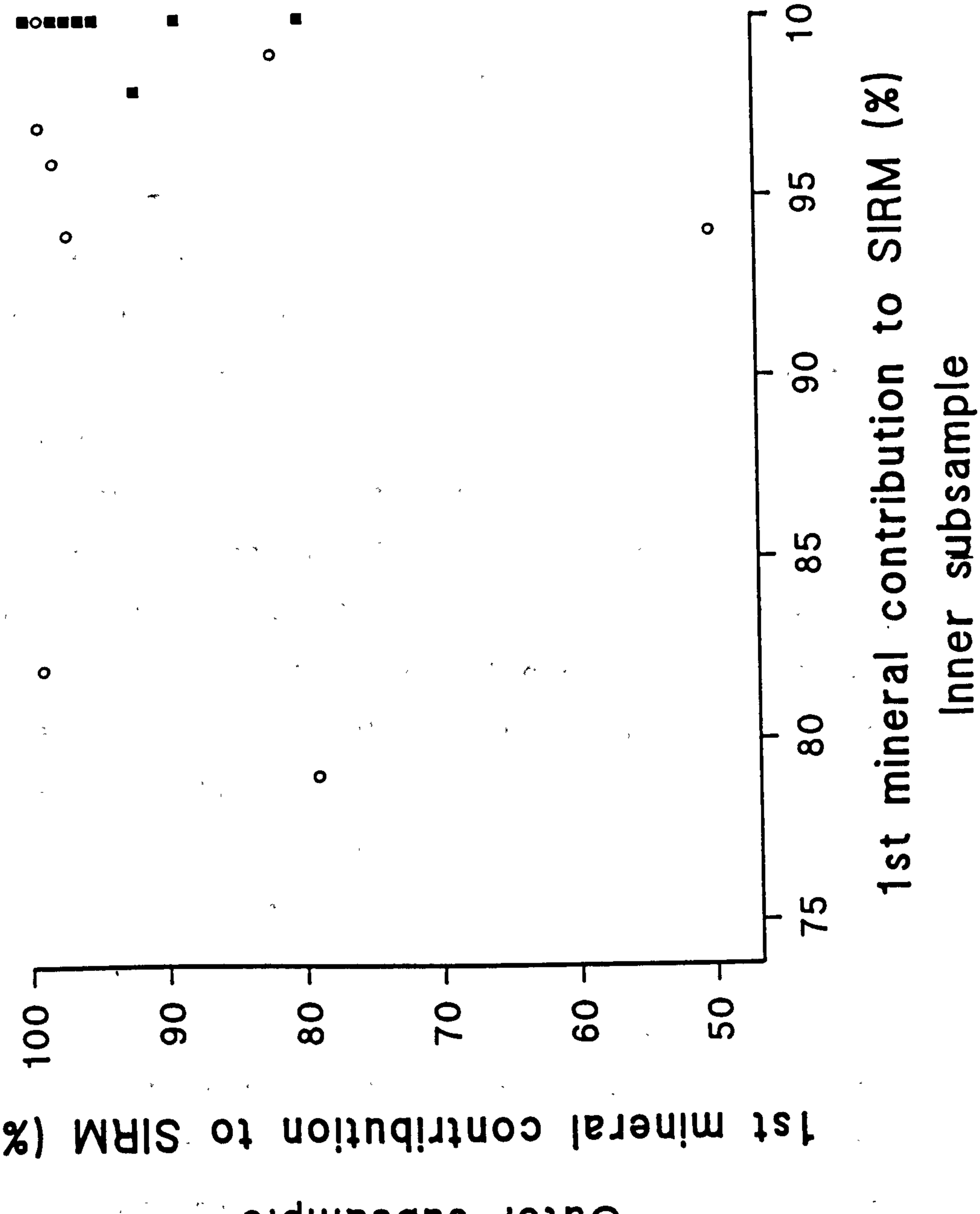

Figure 4.6. A comparison of the fractional contribution of the low coercivity mineral to the SIRM of pairs of subsamples taken from the inner and outer parts of several sherds. The open circles represent pairs of Romano-British subsamples and the solid square represent pairs of Servian subnsamples.

reasonably well using one or two coercivity distributions. The lower coercivity distributions are considered to represent magnetite or titanomagnetite, in agreement with the thermomagnetic analysis. The higher coercivity distributions indicate the presence of haematite. The presence of haematite was not clearly shown by any samples during thermomagnetic analysis, this may reflect the fact that haematite is very weak and often only represents a few percent of the total magnetisation of a sherd and may therefore be swamped by ferrimagnetic and paramagnetic minerals.

Isothermal remanence acquisition revealed that 52 of the 106 sherds investigated contain only magnetite (or a mineral with a composition close to that of magnetite), in agreement with the thermomagnetic results. Other samples show an additional haematite component which is responsible for 1-84% of the SIRM.

The isothermal remanent acquisition characteristics of the sample set can be separated into a series of groups. These groups are based on the fraction of the SIRM which is contributed by the two mineral types. Samples in which the SIRM is entirely attributed to a single low coercivity mineral are designated group (a) while those in which less than 10% of the SIRM is contributed by a high coercivity mineral are label group (b). Groups (c) and (d) are then defined for samples in which the SIRM have high coercivity mineral fractions of 10-50% and >50% respectively. The classification can be further usefully subdivided on the

basis of the mean log-coercivity of the low coercivity mineral which can be obtained for all of the samples. The mean log-coercivities are divided into two groups, namely low (1) and high (2) which have values in the ranges 1.2-1.6 and 1.6-2.0 respectively. The distribution between the groups is shown in figure 4.7.

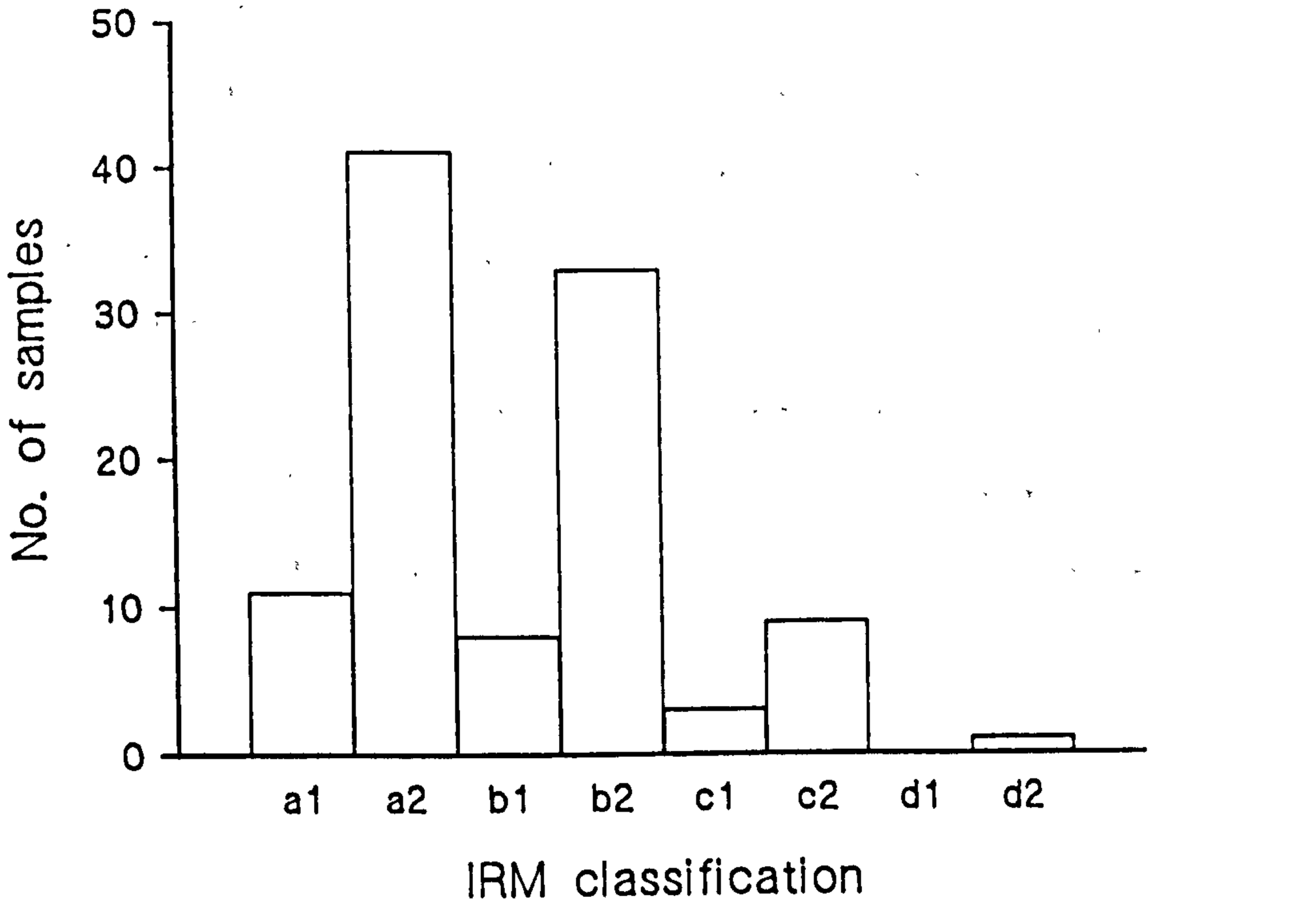

Figure 4.7. The distribution of IRM acquisition behaviour within the groups defined in the text.

The consistency between subsamples from the same sherd was investigated with sherds from the Servian and Romano British groups. Comparing the mean coercivities of the low coercivity mineral indicates that this component is often similar between subsamples. A comparison of the percentage contributions of the low and high coercivity distributions to the SIRM shows that for the Servian pottery the sub-samples taken from the outer part of the sherd often contain more haematite than the inner part. For the Romano-British sherds the haematite content is greater in the outer part for some and the inner part for others. These variations probably reflect the firing processes used to manufacture the pottery. An oxidising environment during firing is suggested for the Servian pottery. The grey and black Romano-British pottery was commonly produced in a reducing environment (White & White, 1961) which may explain the observation of reduced haematite content in the outer part of some sherds. However, as the firing of a replica Romano British kiln showed, an oxidising environment can occur if the kiln is not completely sealed (White & White 1961); this may explain the presence of more haematite in the outer part of some of the Romano British sherds.

5 Magnetic Hysteresis

5.1 Introduction

The magnetic hysteresis behaviour of all of the samples in the collection has been investigated. The principal objective being to obtain information pertinent to the identification of domain states, but also to quantify the mass fraction of the magnetic constituents and to determine the paramagnetic susceptibility.

5.2 Magnetic hysteresis

Hysteresis is defined as the lagging of effect behind cause. In the magnetic case this translates to the lag of magnetic moment changes in response to changes of applied field. Hysteresis is observed for ferro-, ferri- and 'canted' antiferromagnetic materials, except when such materials are in a superparamagnetic state. It is not observed for paramagnetic and diamagnetic materials since neither can have a remanent magnetisation.

Mganetic hysteresis loops are obtained by measuring the magnetisation of a sample in the presence of an applied magnetic field. The magnetic field is usually cycled from zero up to some positive maximum value, the field is then reduced to zero and then increased in the opposite direction up to an equivalent negative maximum from which it is cycled back to the positive maximum.

The process of magnetising an initially demagnetised ferromagnetic material through a complete field cycle is

illustrated in figure 5.1. In low applied fields (region 'a') the magnetisation M increases reversibly , i.e. if the field is removed the magnetisation returns to its initial state. As the applied field increases further the magnetisation continues to increase but in an irreversible way, such that on removal of the field the magnetisation falls along path 'c' to a position with non-zero magnetisation, i.e. an IRM. As the applied field is further increased, the magnetisation increases to a maximum value termed the saturation magnetisation, M_s. The value of the applied field needed to reach M_s is the saturating field, H_{sat}. When the applied field is reduced from H_{sat} the magnetisation falls along path 'e' reaching a value at zero field called the saturation remanent magnetisation, M_{rs} (equivalently termed the SIRM). As the field increases in the reverse direction, the magnetisation continues to fall from M_{rs} down to zero. The value of the applied field needed to reduce the remanence to zero is termed the coercivity or coercive force, H_c. The complete loop is then traced out as the magnetisation increases to saturation in the reverse direction and then returns to saturation in the original direction.

5.3 Hysteresis parameters

The parameters, M_s, M_{rs} and H_c, depend upon the mineralogy, domain state, size, shape and concentration ofthe constituent magnetic particles, and can therefore be used to infer information about the magnetic mineralogy of

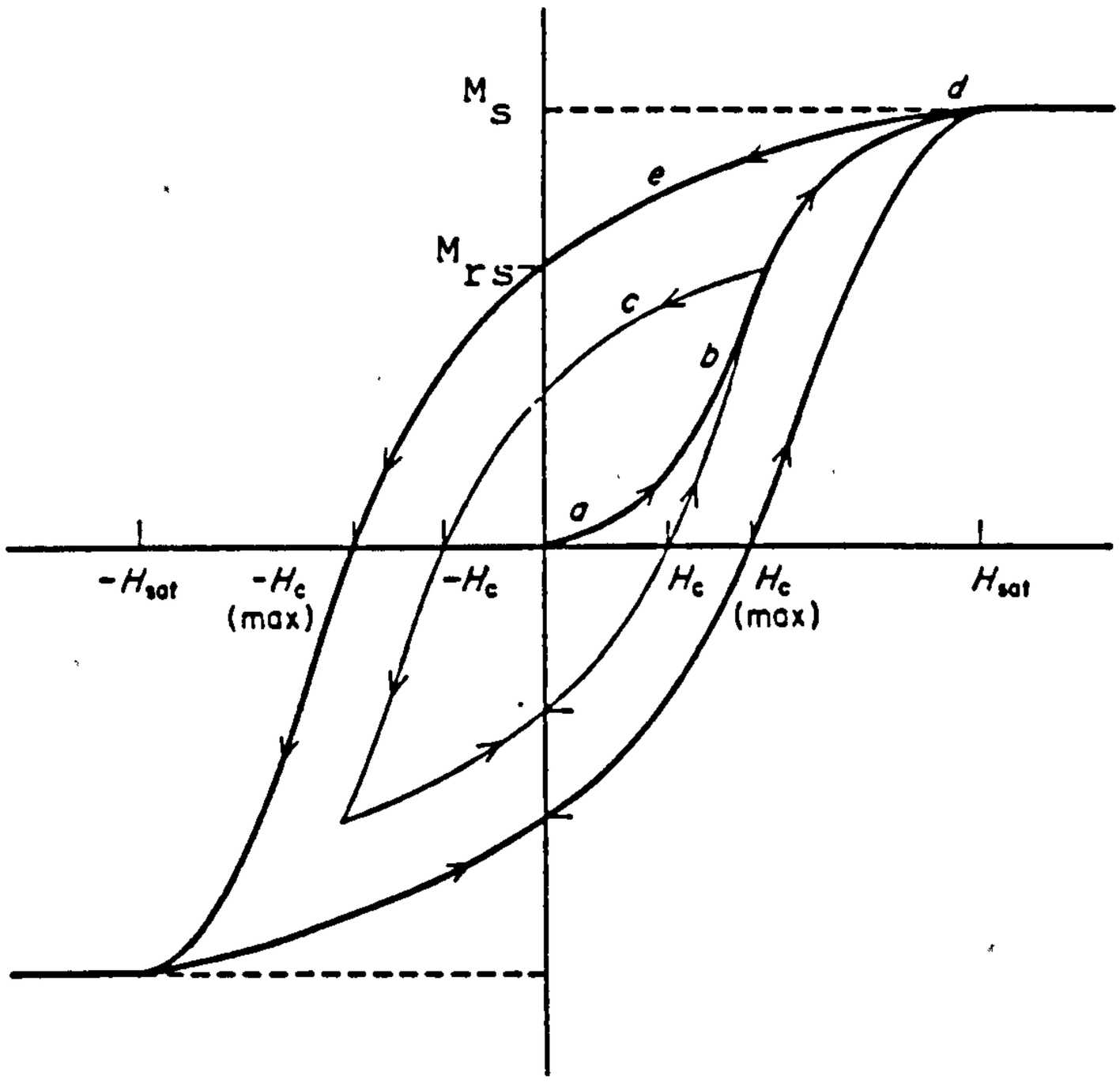

Figure 5.1. An illustration of magnetic hysteresis, after McElhinny (1973). The various regions indicated are discussed in the text. The magnetic hysteresis parameters are also shown.

a sample. To determine these parameters the magnetisation of a material must be saturated.

The saturation magnetisation, M_S, is a function of the magnetic mineralogy and the mass fraction of the magnetic constituents in a material. For example, pure magnetite has a quoted M_S value of 92 Am^2kg^{-1} (O'Reilly, 1984) while haematite has a value of 0.5 Am^2kg^{-1} (Thompson & Oldfield, 1986). The saturation magnetisation of natural materials is reduced by dilution of the magnetic minerals by non-magnetic matrix minerals. The mass fraction of the magnetic minerals in a natural material can be estimated from the value of M_S if the magnetic mineral type is known.

In natural samples the ferrimagnetic signal is often convolved with a paramagnetic signal. The paramagnetic magnetisation must be taken into account in order to obtain the M_s value for the ferrimagnetic mineral.

The saturating field, H_{sat}, is related to the maximum microscopic coercivity and is dependent upon the mineralogy, size and shape of the magnetic particles and the measurement temperature. The maximum value of H_{sat} is determined by the mineralogy. For example, magnetite has a maximum saturation field of 2.4×10^5 Am^{-1} (300mT) (McElhinny, 1973).

The saturation remanence, M_{rs}, is the maximum possible remanence a material can acquire. It is dependent upon the mineralogy, concentration, domain state, size, shape and orientation of the magnetic particles. The dependence upon concentration is the same as that described for M_s, and can be used to remove the effect of the magnetic mineral concentration by normalising M_{rs} to M_s. The ratio M_{rs}/M_s then reflects the domain states, the number of axes of easy magnetisation and any anisotropic alignment of the magnetic particles. For superparamagnetic single domain particles $M_{rs}/M_s=0$ as these particles have by definition no stable remanent magnetisation. The M_{rs}/M_s value for a material containing stable single domain particles depends upon the number of easy axes of magnetisation possessed by the particles and the orientation of these axes within the material. For an assemblage of randomly orientated particles with uniaxial anisotropy (two antiparallel axes

of easy magnetisation) M_{rs}/M_s=0.5 according to the calculations of Stoner & Wohlfarth (1948). A simple illustration of the origin of the ratio of 0.5 for a random assemblage of particles with uniaxial anisotropy is shown in figure 5.2. The ratio M_{rs}/M_s increases when the number of easy axes of magnetisation increases, for example an assemblage of randomly oriented pyrrhotite particles, which have triaxial anisotropy, can have a maximum M_{rs}/M_s ratio of 0.75 (Dunlop, 1971). The ratio also increases if the easy axes are aligned near the direction of the applied field. The M_{rs}/M_s ratio for multidomain particles is low, 0.01, and not single valued since M_{rs} is a function of the domain wall positions which are dependent on variable crystal defects (O'Reilly, 1984). The low values of M_{rs}/M_s of multidomain particles arise as a result of the arrangement of the domains at zero field, which tends to reduce the demagnetisation energy and the associated, externally measurable, remanent magnetisation.

Assemblages of particles in the size range between single domain and multidomain, termed pseudo-single domain, have M_{rs}/M_s values which increase from the low multidomain values (~0.01) towards the higher single domain value (0.5), as the particle size decreases. See, for example, Day, Fuller & Schmidt (1977). This variation has at least three possible explanations. Direct domain state observations made during magnetic hysteresis cycles suggests that the increased ratio is a result of the increasing difficulty of domain wall nucleation (i.e.

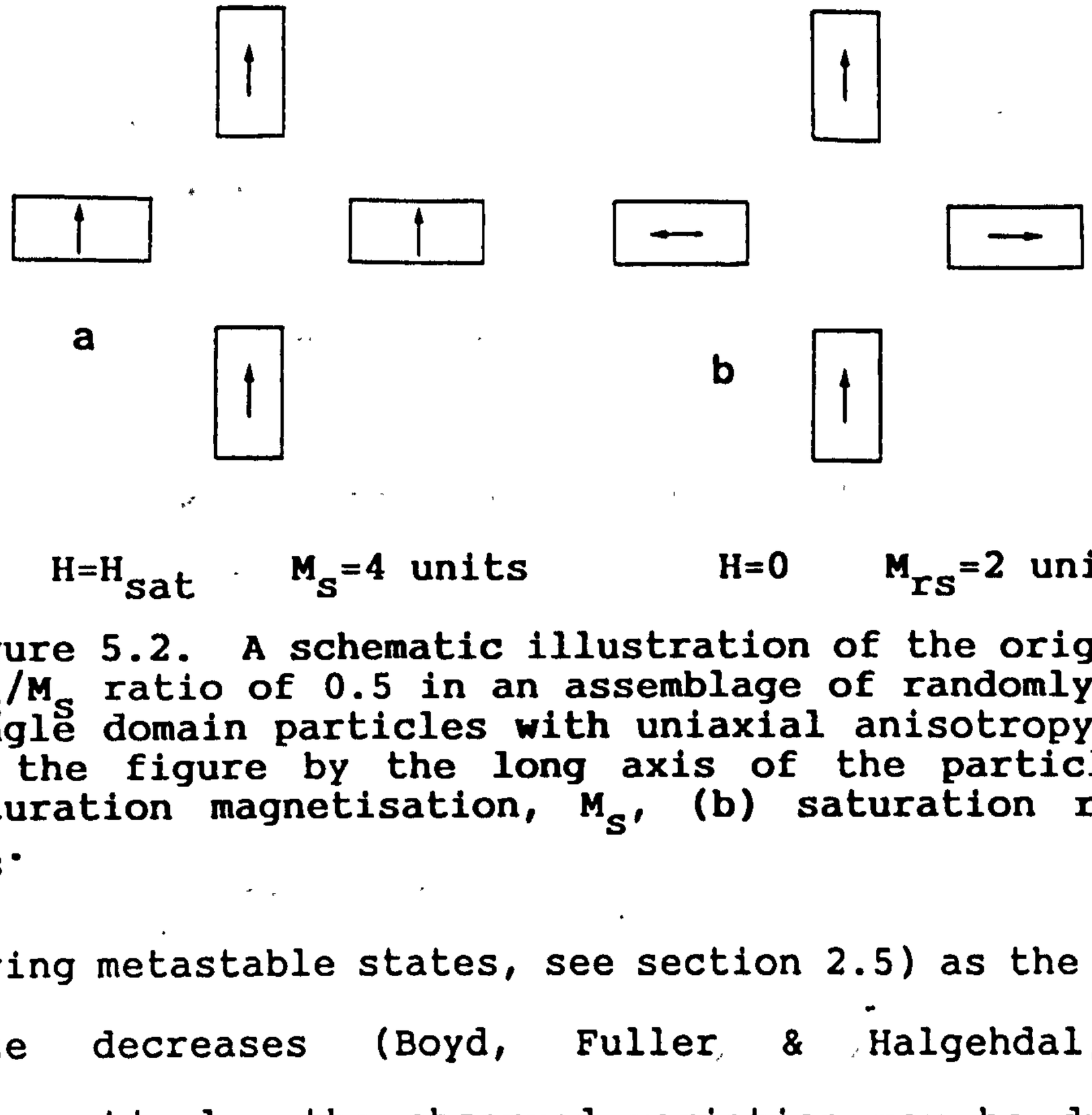

Figure 5.2. A schematic illustration of the origin of the M_{rs}/M_s ratio of 0.5 in an assemblage of randomly oriented single domain particles with uniaxial anisotropy (defined in the figure by the long axis of the particles). (a) Saturation magnetisation, M_s, (b) saturation remanence, M_{rs}.

having metastable states, see section 2.5) as the particle size decreases (Boyd, Fuller & Halgehdal, 1984). Alternatively, the observed variation may be due to the presence of an increasing single domain fraction in the particle size distributions which are closer to the single domain boundary, or, finally, it may be that the remanence value increases due to the relative increase of the contribution from the domain wall moments in small multidomain particles (Dunlop, 1977).

In natural materials the value of M_{rs}/M_s often results from some combination of superparamagnetic, stable single domain, pseudo-single domain and multidomain particles.

The coercivity or coercive force, H_c, is a measure of the magnetic 'hardness' of the material. The coercive force is the field required to reduce a saturation magnetisation to zero, i.e. the field required to reverse half of the magnetisation. Coercivity varies with mineral type. For

a particular mineralogy the coercivity varies with domain state and therefore particle size. See figure 5.3.

5.4 The Vibrating sample magnetometer

Magnetic hysteresis measurements were carried out using a Molspin vibrating sample magnetometer (VSM). The magnetometer consists of a nylon sample holder, one end of which is attached to an oscillating drive. The sample is placed in the free end of the holder which is situated between the pole pieces of an electromagnet. Identical pick-up coils are fixed to the face of each of the pole piece, these coils are wound in series opposition such that with no sample present the pick-up voltage is zero. The system is controlled by a BBC microcomputer. Measurements involve vibrating the sample at a fixed frequency (50 Hz). The magnetisation induced in the sample by the electromagnet induces an alternating voltage in the pick-up coils. A magnetic hysteresis loop is obtained by cycling the field in a stepwise manner between the maximum positive and negative applied fields. The maximum magnetic field produced by the electromagnet of the Molspin system is 1 T.

5.5 Experimental Procedure

Samples were prepared in a similar way to that described in section 3.5. Samples with a mass of 0.6 g or less were placed in a holder which had been cleaned in an ultrasonic bath. The samples were crushed in order to avoid the

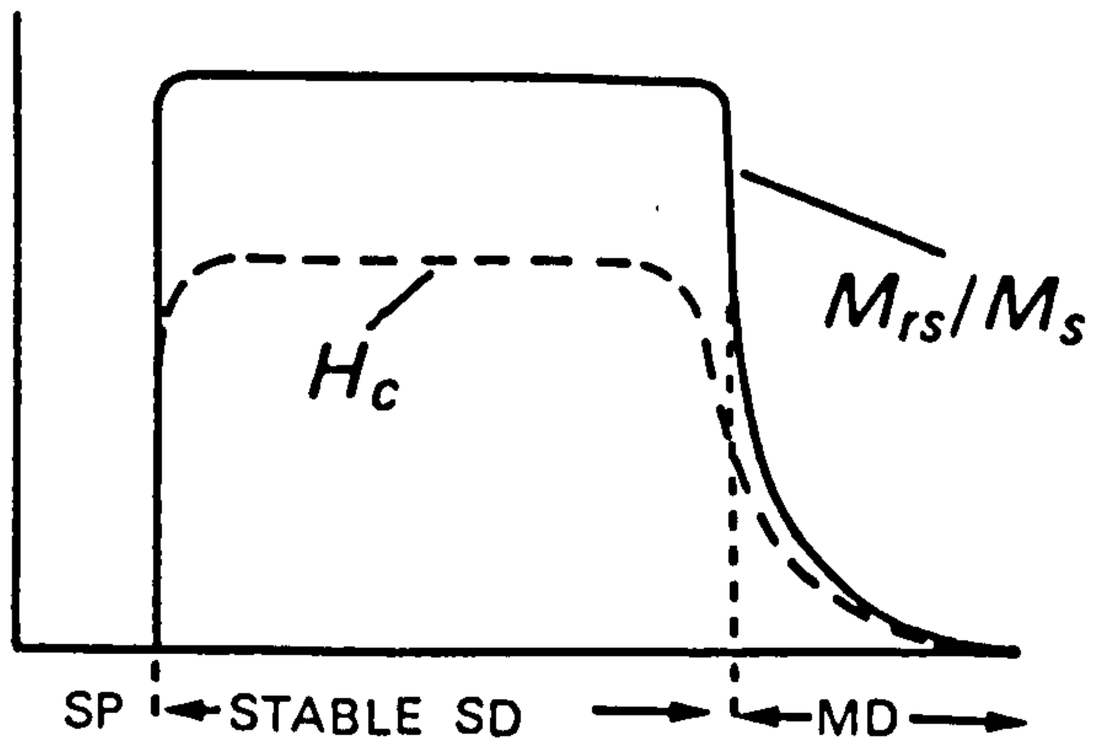

Figure 5.3. A schematic illustration of the variation of coercivity, H_c, and the M_{rs}/M_s ratio with particle size. After O'Reilly (1984).

possibility of magnetic particle alignment due to intrinsic fabric anisotropy (observed in ceramics by Rogers et al. 1979) which would change the M_{rs}/M_s ratio from the value obtained with the same assemblage but in which the particles were randomly oriented.

The experimental runs were controlled through the BBC microcomputer. The system is automated, requiring only a list of field steps and the sample code to be input. The system was calibrated as an initial stage in each series of sample measurements and at intervals during the series. Calibration was undertaken using a known mass of hydrated copper sulphate ($CuSO_4.5H_2O$). All of the measurements were carried out using the same set of magnetic field steps. The results were stored to floppy disk and a hard copy of the hysteresis loop printed.

5.6 Data analysis

To obtain hysteresis parameters, namely M_s and M_{rs}, the raw data was calibrated using the measurement of the known

mass of hydrated copper sulphate. The calibrated data was then corrected to take into account the mass of the sample and to remove the contribution to the saturation magnetisation from any paramagnetic minerals. This analysis was performed using software written by D. J. Robertson. To determine M_s it is necessary to compensate for the paramagnetic component. This is done by fitting a line between the magnetisation at 600 mT and 1 T, this is illustrated in figure 5.4, M_s is the intercept of this line on the magnetisation axis and the paramagnetic susceptibility is given by the slope of the line. This method presumes that the ferrimagnetic magnetisation of a sample is saturated by 600 mT. The coercivity H_c is also affected by the paramagnetic contribution, but this has not been corrected. Since the parameter M_{rs}/M_s shows a particle size dependence similar to that of H_c (see figure 5.3), and because of the presence of a paramagnetic contribution to H_c, this parameter has not been used in this study.

5.7 Results

Hysteresis measurements were made on one hundred and fifty-seven samples. Two or more subsamples have been measured for many of these. The results, as might be expected from such a broad collection, are extremely wide ranging.

All but twenty-one samples and two subsamples have magnetic hysteresis loops that appear to be saturated

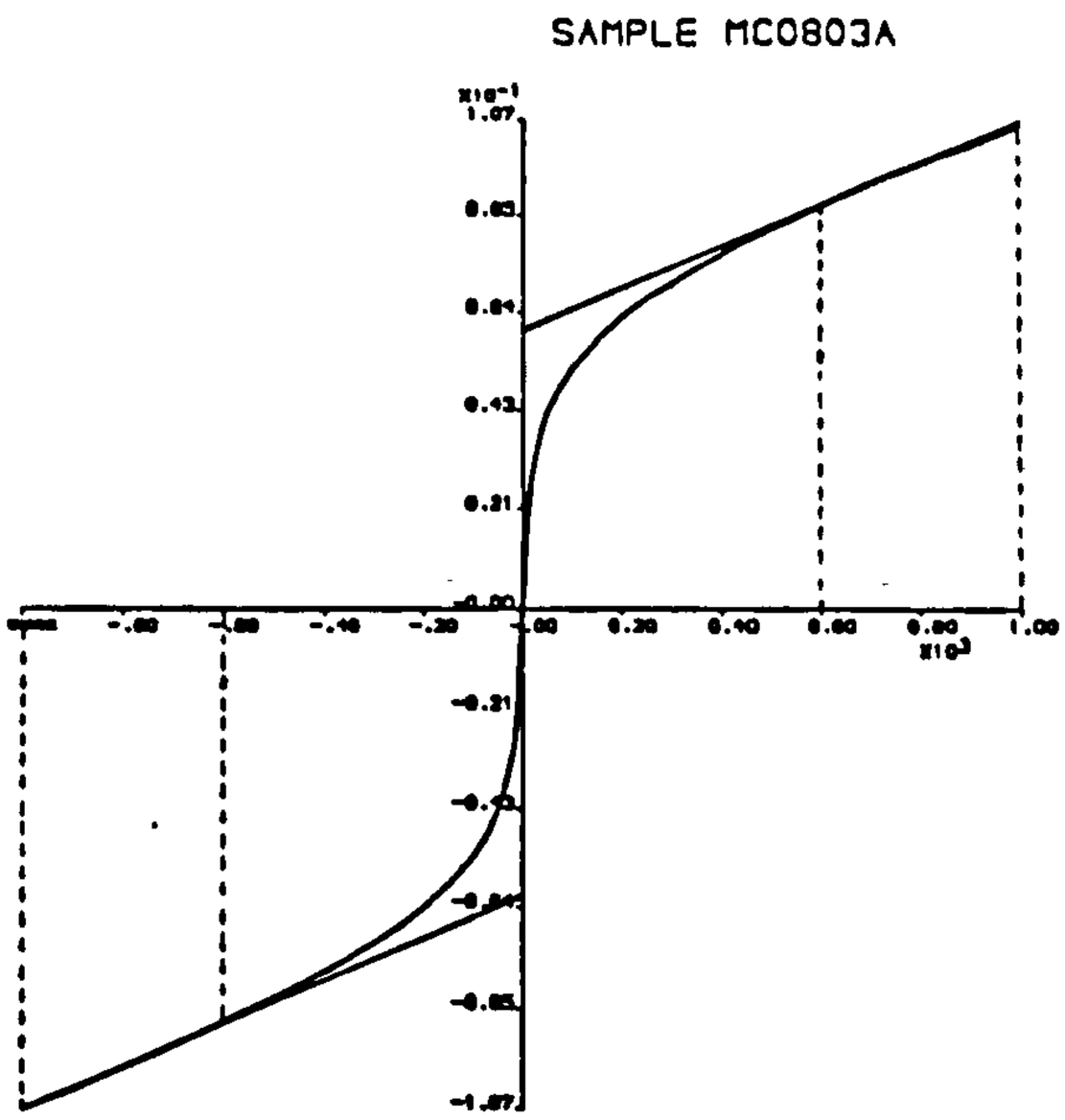

Figure 5.4. Two examples illustrating the method used to correct for the presence of a contribution from paramagnetic minerals.

(closed) by 600 mT, allowing analysis using the software described. The shape of these loops represents the combination of ferrimagnetic minerals of various domain state and differing contributions from paramagnetic minerals. Some examples are illustrated in figure 5.5. The hysteresis loops of the samples which do not saturate by 600 mT can be divided into 'open' and 'constricted'.

Within these groups the behaviour varies. See figure 5.6 for examples. The results obtained from all of the samples are presented in appendix 4.

5.7.1 Internal consistency

The homogeneity of the magnetic particle distribution has been investigated for many samples by determining the hysteresis parameters of two subsamples. Before subsamples can be compared, the precision of the data must be determined. This has been done by measuring many (78) of the samples twice (See appendix 4). The differences between the pairs of M_s and M_{rs} values have been calculated and compiled into histograms. See figure 5.7. Both distributions peak below $3x10^{-3}$ Am^2Kg^{-1} and are skewed. The distribution close to the peak probably represents the true precision of the measurement and analysis techniques, while the higher values may indicate the analysis technique operating on aberrant or poor quality data. The precision of M_s and M_{rs} values expressed as a standard deviation can be estimated from the distributions assuming that 66% of the observed differences fall within one standard deviation. This gives standard deviations of

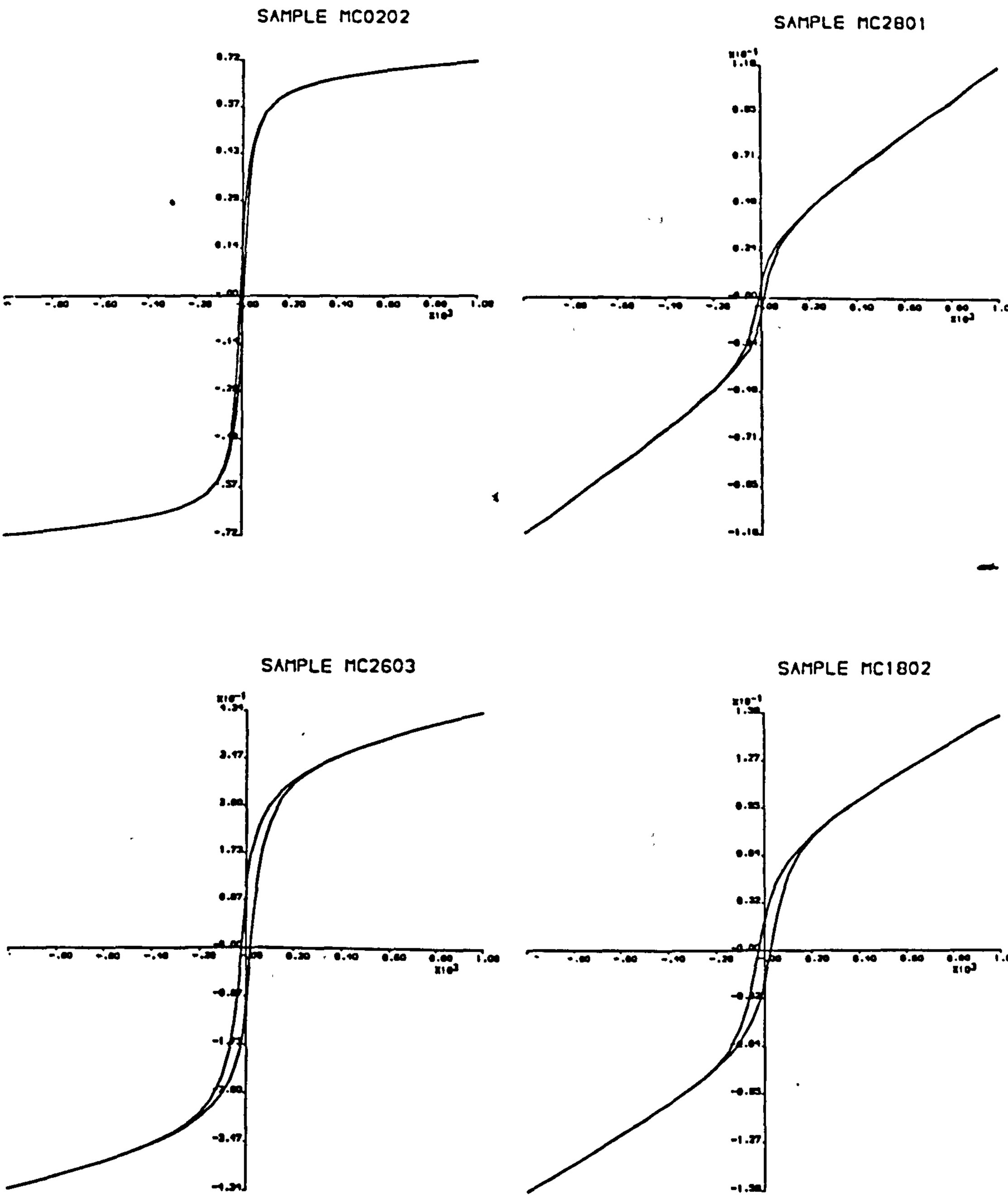

Figure 5.5. Four examples of the types of magnetic hysteresis behaviour observed in the ceramics that were observed to saturate.

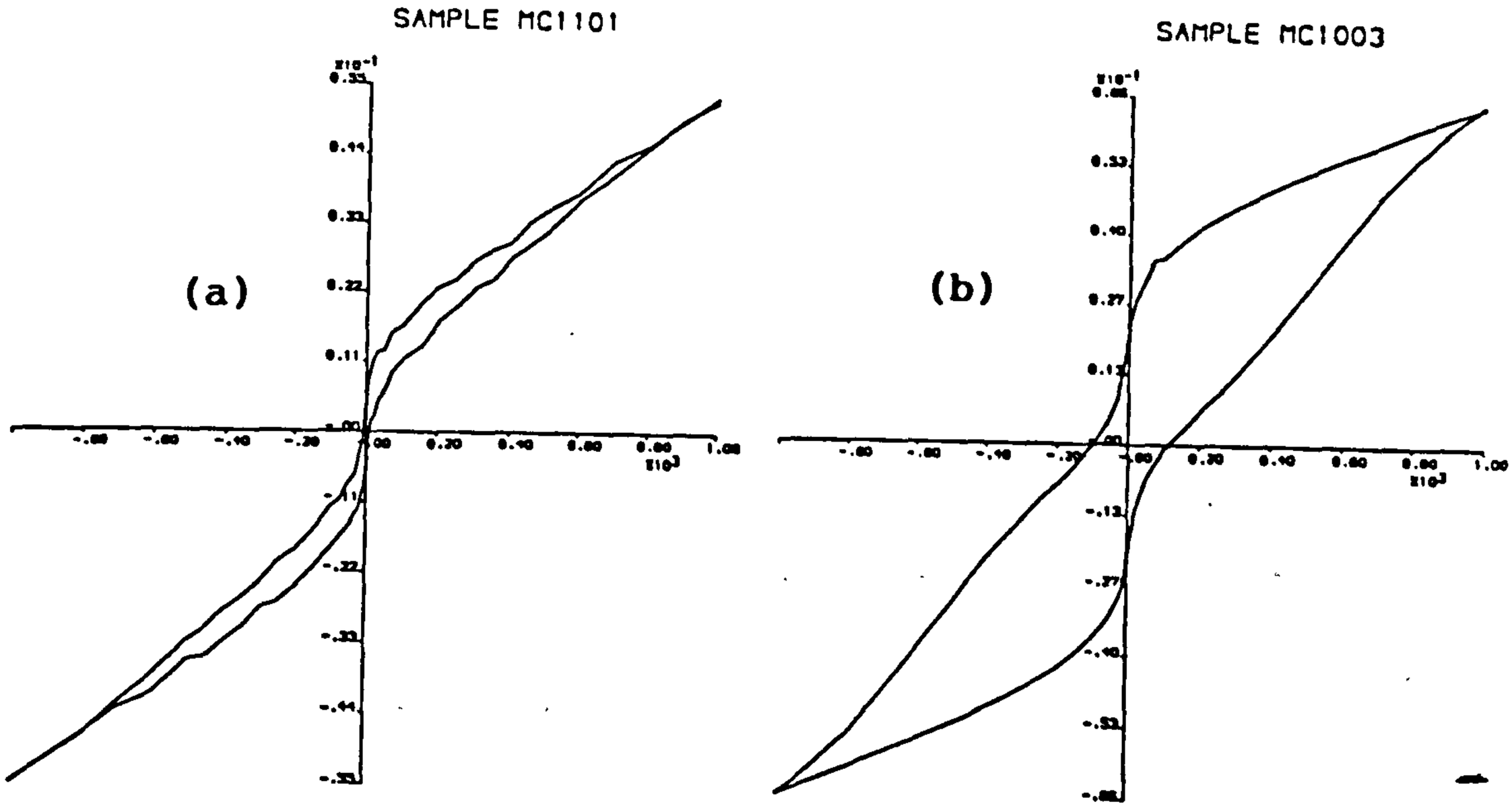

Figure 5.6. Two examples of constricted hysteresis behaviour (a) and (b) and two examples of open hysteresis loops (c) and (d).

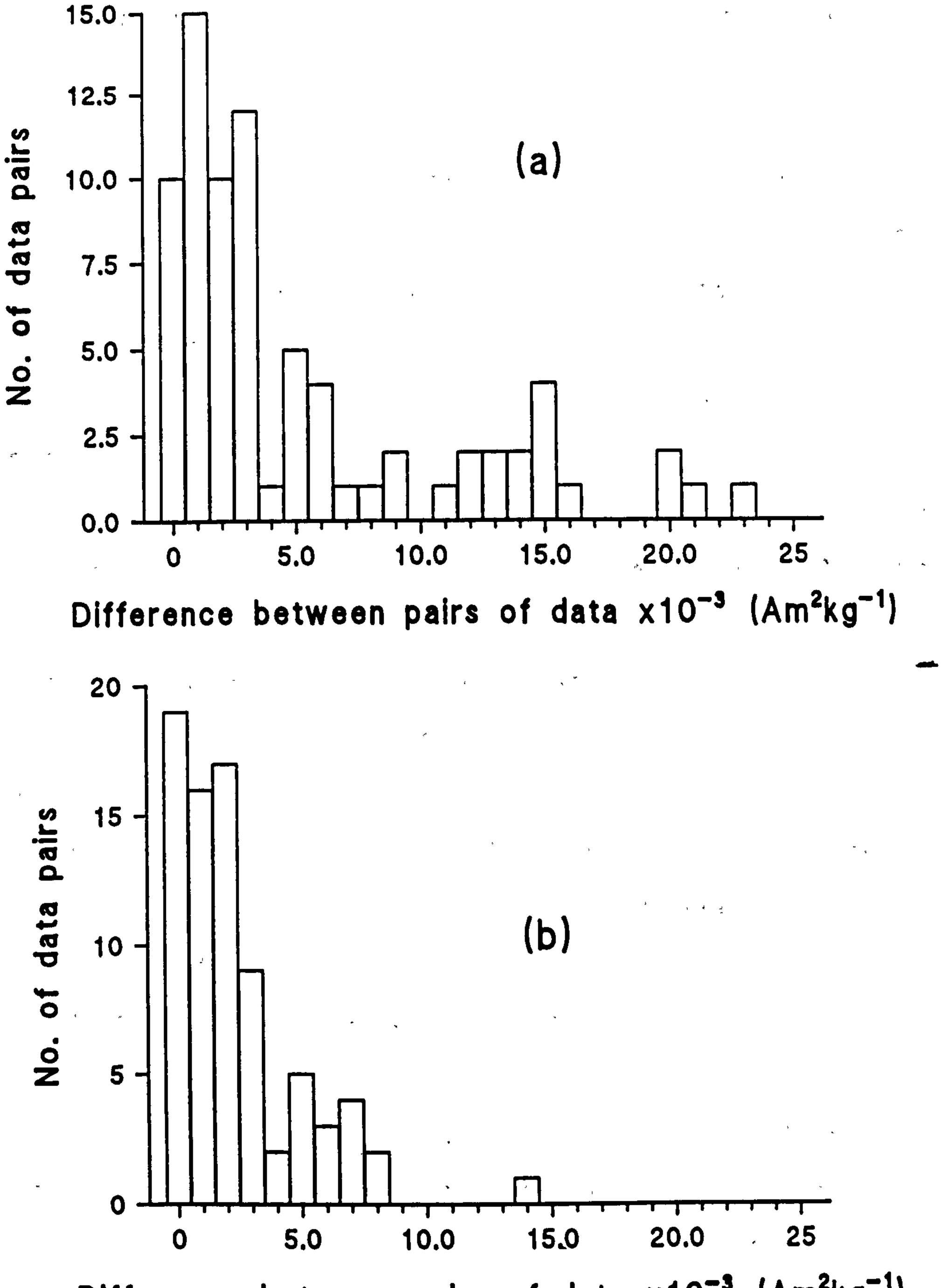

Figure 5.7. Error analysis of both M_s and M_{rs}, the difference between pairs of measurements made on the same sample. (a) The distribution of differences between pairs of M_s values and (b) the distribution of differences between pairs of M_{rs} values.

$6x10^{-3}$ Am^2kg^{-1} and $3x10^{-3}$ Am^2kg^{-1} for M_s and M_{rs} respectively.

Having obtained an estimate of the error associated with the M_s and M_{rs} values, it is possible to compare the values obtained from different subsamples taken from the same sherd and thus get an indication of homogeneity, or lack of it, of the distribution of magnetic particles within the samples. For M_s the comparison of pairs of values has been accomplished

by plotting one value against the other, this has similarly been done for the pairs of M_{rs} values, see figure 5.8. The paired data should plot on a line of slope=1 (within the errors) if the magnetic particles are distributed evenly through the sherds. It is clear from this figure that in many cases the magnetic particles are not homogenously distributed, although 56% of the samples show agreement within 10%. It is also to be noted that where the pairs of data are from the inner and outer parts of a sherd, in all but two cases, the outer part contains the larger magnetic fraction.

5.7.2 Saturation magnetisation & magnetic mineral content

As discussed earlier in this chapter it is possible to determine the mass fraction of the ferrimagnetic constituents from the saturation magnetisation of a sample. The only further information required is the saturation magnetisation per unit mass of the ferrimagnetic minerals present. From the Curie point analysis of this study it is clear that magnetite, titanium-poor titanomagnetites and

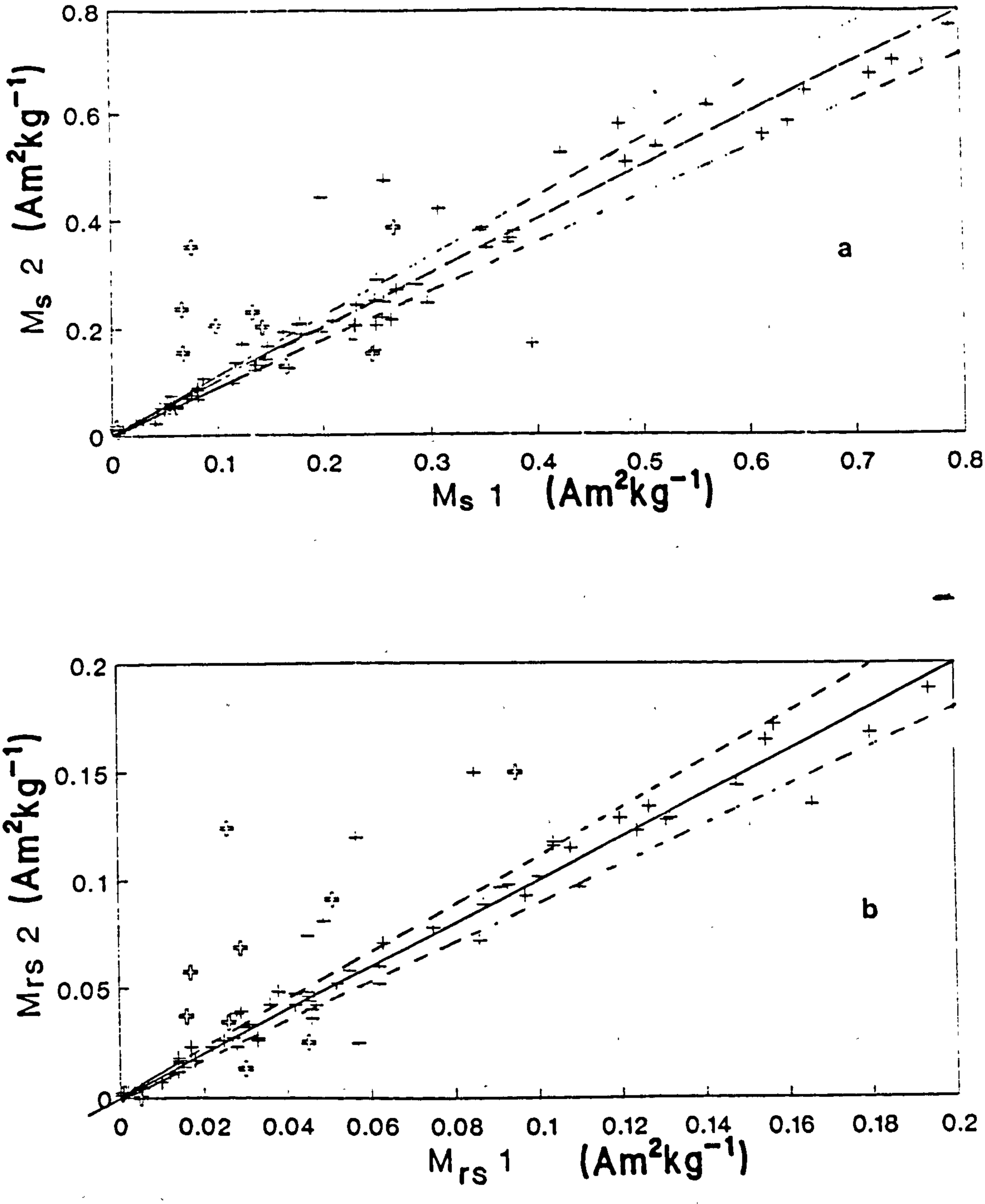

Figure 5.8. A comparison of pairs of (a) M_s and (b) M_{rs} values obtained from pairs of subsamples taken from the same sherds. Homogeneity of the magnetic minerals is indicated where the data fall on a line of slope=1. The solid diagonal line has a slope of 1.0 while the dotted lines have slopes of 0.9 and 1.1, indicating variations of 10%. The crosses on the data indicate the standard deviations. The open symbols indicate pairs of subsamples which are visually distinct.

low-temperature oxidised forms of these minerals are predominant. The variation of saturation magnetisation of titanomagnetites with increasing titanium substitution can be described approximately according to;

$$M_S = 92(1-1.25x) \qquad (5.1)$$

(O'Reilly, 1984), where x is the titanium composition parameter. For the largest titanium content observed in this study, x=0.13, M_S falls from 92 Am^2kg^{-1} (magnetite) to 77 Am^2kg^{-1}, equivalent to a 17% decrease. For the samples which contain low-temperature-oxidised (cation deficient) magnetites the saturation magnetisation will lie between that for stoichiometric magnetite and 75 Am^2kg^{-1} for maghemite (Bate, 1980), since oxidation is unlikely to be complete.

On the basis of these arguments a value for the saturation magnetisation of 92 Am^2kg^{-1}, i.e. that of magnetite, can be used, to a worst approximation of 18% (but often much better), to obtain the mass fraction of the ferrimagnetic minerals. The mass fraction is obtained by dividing the M_S value of a sample by M_S for magnetite. For sherds where two subsamples were measured a mean value for M_S was taken. The distribution of saturation magnetisations and the equivalent mass fractions are shown in figure 5.9. The distribution is strongly skewed to lower values with 95% of the samples having M_S values between 0.001 and 0.60 Am^2kg^{-1}, corresponding to mass

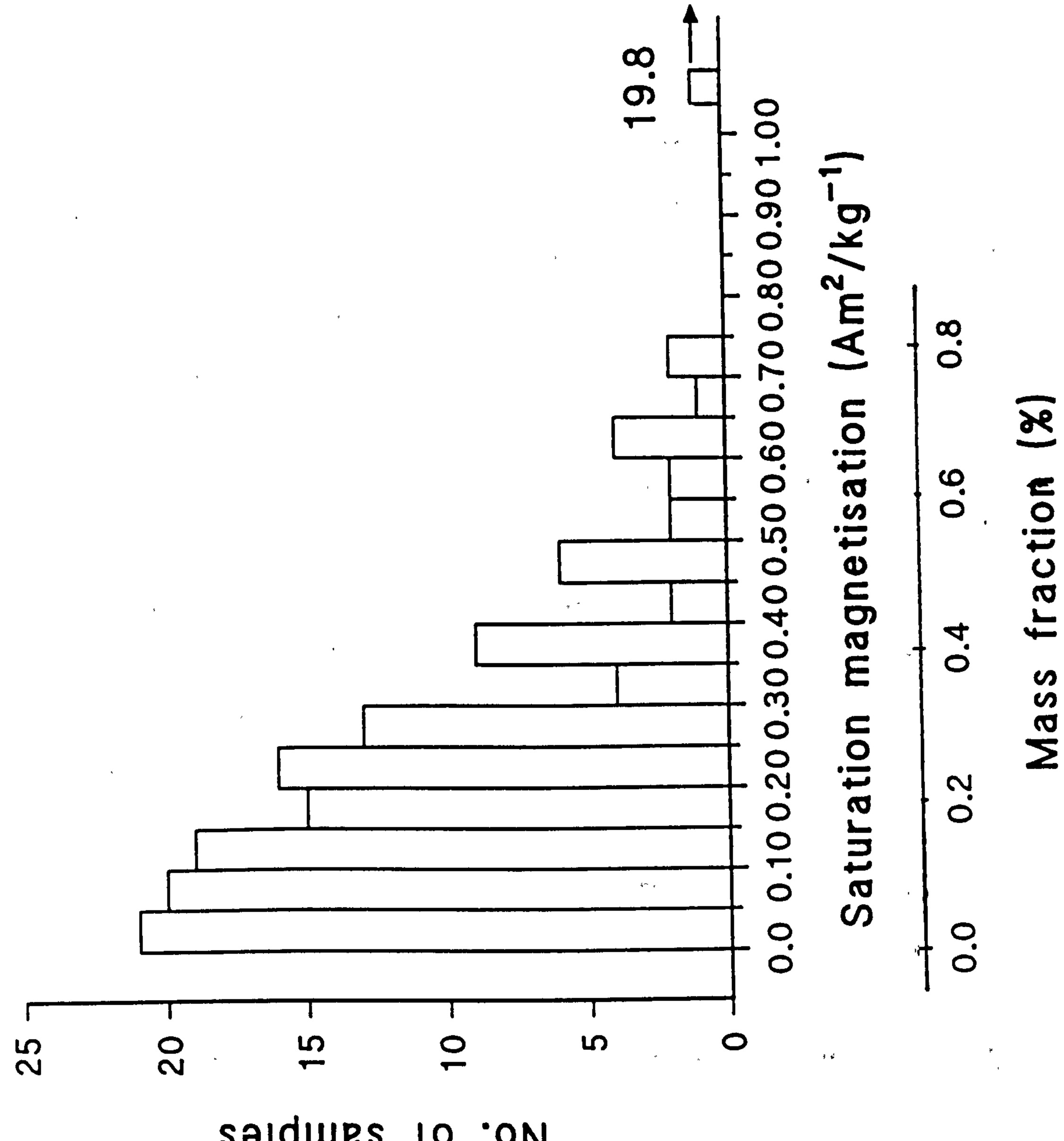

Figure 5.9. The distribution of saturation magnetisation values and the equivalent mass fractions of magnetite for the ceramics investigated.

percentages of magnetite between 0.001 and 0.65%. The maximum value of M_s is 19.8 Am^2kg^{-1} which translates to a mass fraction of magnetite of 21% in this sample (MC1301), this is an extreme exception!

5.7.3 M_{rs}/M_s ratios and domain states

The M_{rs}/M_s ratio can be used to provide some information about the domain states of the magnetic minerals. The M_{rs}/M_s data for all of the samples which saturate before 600 mT are compiled in a histogram, see figure. 5.10. The distribution extends from 0.02 up to 0.50 and has a broad peak between 0.16 and 0.38 in which the data for 84% of the samples fall.

The high percentage of samples with M_{rs}/M_s above 0.16 indicates the common occurrence of either a predominantly pseudo-single domain particle size distribution or a distribution which contains a significant stable single domain size fraction and/or both superparamagnetic and multidomain fractions. Assuming that the distribution is described by the latter then the stable single domain fraction can be estimated. The method of estimation is similar to that used by Dunlop (1972b) taking $M_{rs}/M_s=0.5$ for the stable single domain fraction, $M_{rs}/M_s=0$ for the superparamagnetic fraction and an extreme value of $M_{rs}/M_s=0$ for the multidomain fraction, a necessity of the calculation. The combined contributions of these fractions leads to the observed M_{rs}/M_s ratio;

$$\left(\frac{M_{rs}}{M_s}\right)_{Obs} = X\left(\frac{M_{rs}}{M_s}\right)_{SD} + (1-X)\left(\frac{M_{rs}}{M_s}\right)_{SP\&MD} \qquad (5.2)$$

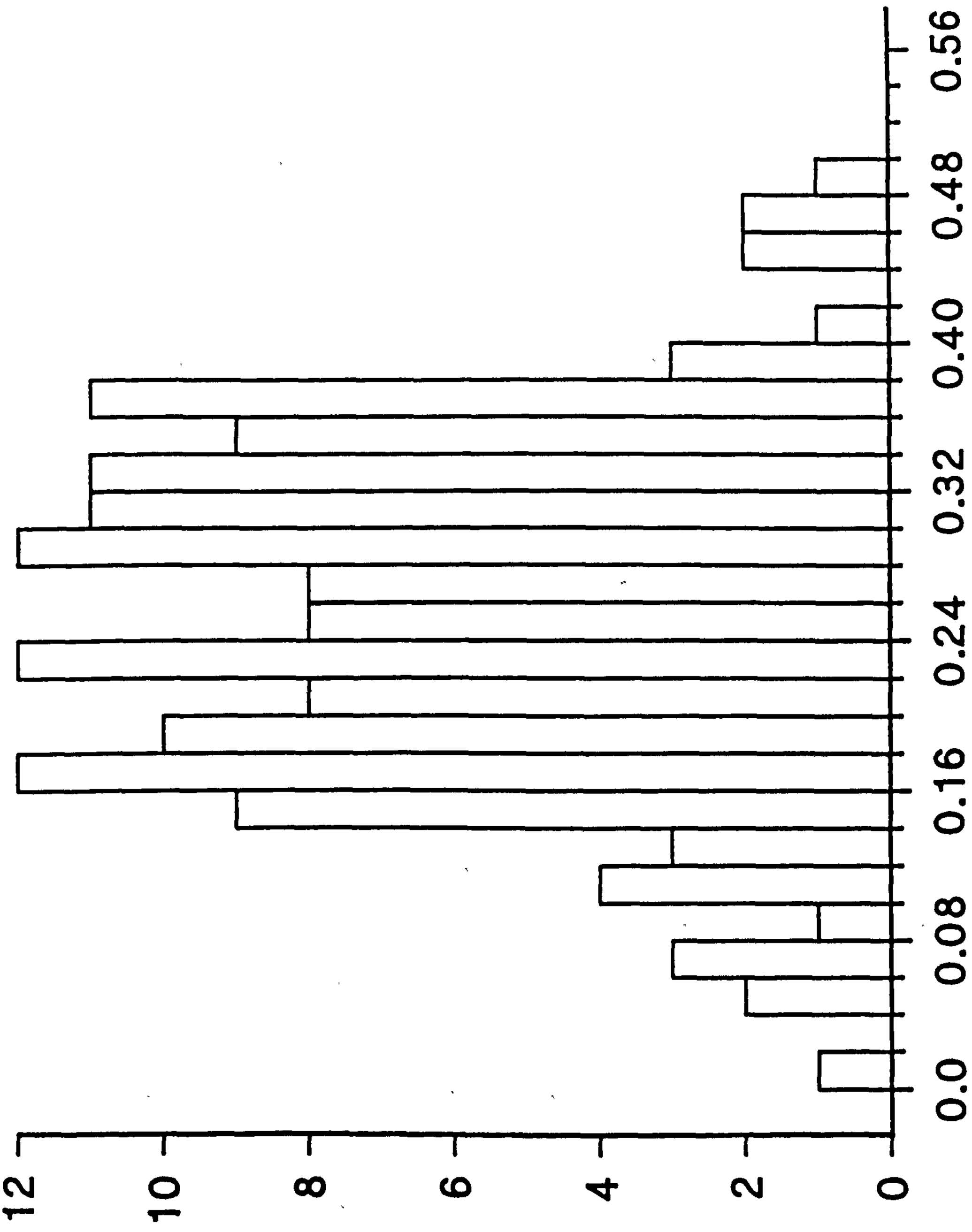

Figure 5.10. A histogram showing the distribution of M_{rs}/M_s values obtained from the sherds for which the ferrimagnetic minerals were saturated below 600 mT.

where X is fraction of single domain particles. The distribution of X, the single domain fraction, is shown in figure 5.11. The single domain fraction varies from 100% for a single sherd down to 1-2%. The distribution shows a broad peak with single domain fractions between 32 and 76% for these sherds.

5.8 Discussion and conclusions

The magnetic hysteresis loops obtained from most of the sherds investigated indicate the presence of a single mineral species which saturates below 600 mT. This is in agreement with the thermomagnetic analysis which showed the predominance of magnetite or minerals with compositions close to that of magnetite. These results conflict with IRM acquisition analysis which showed that for more than 50% of the sherds investigated at least 1% of the SIRM was attributed to haematite. These findings can be reconciled when it is realised that the contribution of haematite to the SIRM is often less than 5%. During measurement of the magnetic hysteresis this small haematite component may be swamped by the stable ferrimagnetic minerals and any superparamagnetic and paramagnetic components, neither of which contribute during IRM acquisition. The haematite contribution would be further reduced since hysteresis measurements were obtained in a maximum field of 1 T, insufficient to saturate the haematite observed during IRM experiments. In samples which have a larger haematite component in addition to a magnetite component, as revealed by IRM acquisition, it is to be expected that the presence

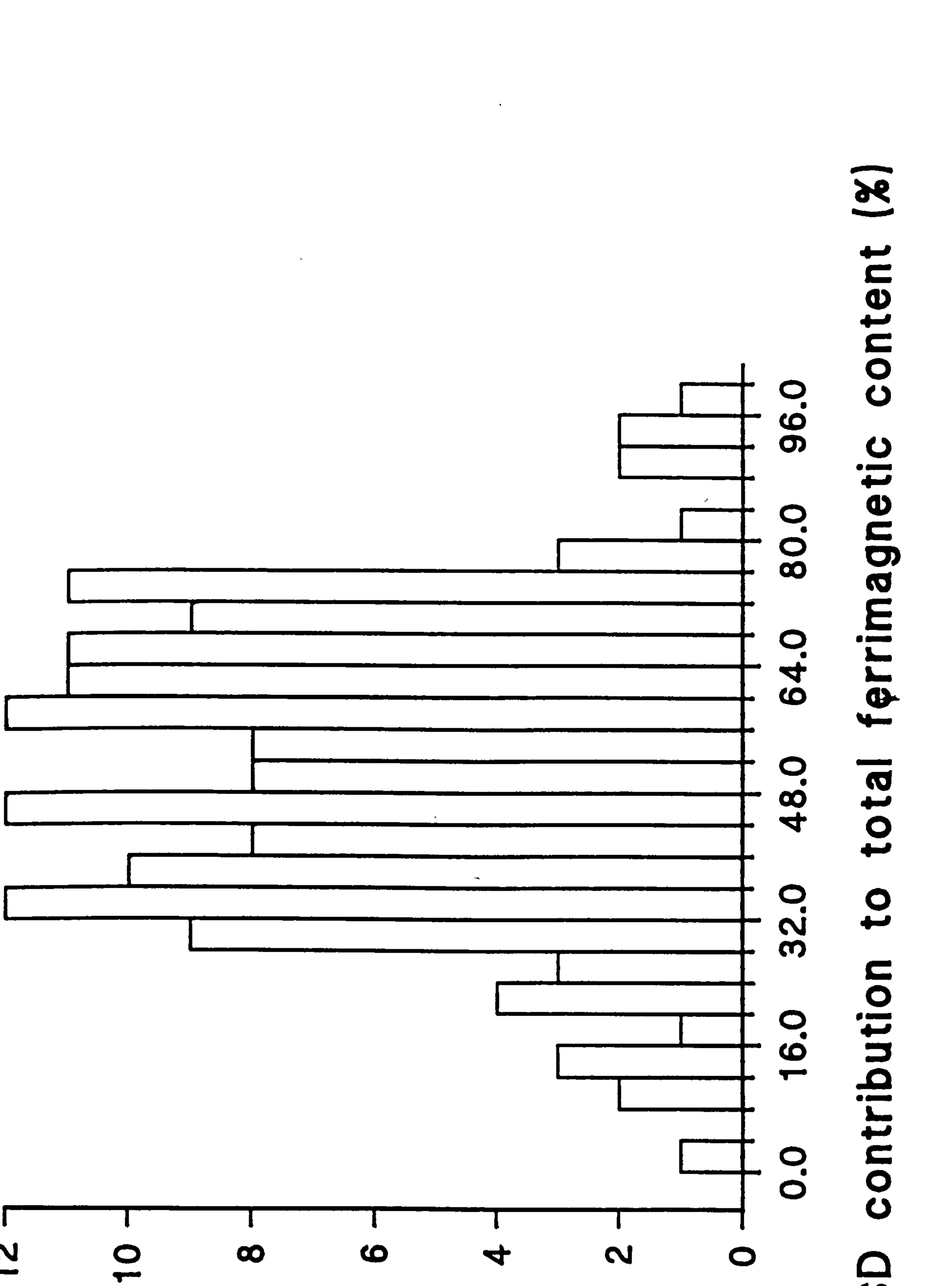

Figure 5.11. A histogram showing the stable single domain content in the sherds which were saturated below 600 mT.

of haematite would also be apparent from the magnetic hysteresis loops. This is the case for twenty-one samples and two subsamples discussed earlier. These samples do not saturate in the maximum applied field of 1 T. Although accompanying IRM acquisition curves are not available for all of these samples it appears that the samples which give a constricted loop show a larger haematite fraction from IRM acquisition than those samples which given an open loop (c.f. MC1901C IRM acq.: haematite %SIRM=50%, hysteresis: constricted, MC1713 IRM acq.: haematite %SIRM=9%, hysteresis: open). The interpretation of the constricted hysteresis loops as arising from mixed assemblages of haematite and magnetite agrees with that suggested by Thompson (1986).

The distribution of magnetic particles within many sherds has been investigated by comparing M_s and M_{rs} values from two subsamples taken from the same sherd. The results indicate that the magnetic particles are often not evenly distributed, although in many cases the differences do not exceed 10%. The distribution of magnetic minerals between the inner and outer parts of the sherds is, in all but one case, uneven, suggesting that the manufacturing process or subsequent usage of the pottery affects the distribution of magnetic minerals.

The values of the saturation magnetisation, determined using a correction for the contribution of paramagnetic minerals, have been used to calculate the mass fraction of the ferrimagnetic minerals. The mass fraction has been

determined approximately using the saturation magnetisation value for magnetite. The mass fraction varies greatly, with 95% of the sherds having mass fractions between 0.001 and 0.65%.

The Mrs/Ms ratio has been used to indicate the domain states present. The distribution of M_{rs}/M_s has a broad peak between 0.16 and 0.38. This suggests either a predominantly pseudo-single domain particle size distribution or a distribution containing single domain particles combined with either, or both, superparamagnetic and multidomain particles. The fraction of the particle size distributions accounted for by single domains particles varies from 32 to 76% for the M_{rs}/M_s range mentioned above. Choosing between the possible distributions requires additional knowledge of the domain states present. In particular the presence of superparamagnetic and multidomain particles must be determined.

5.9 Summary of magnetic hysteresis behaviour

The magnetic hysteresis behaviour of the samples has been classified into series of categories. These categories indicate the general nature of the loops, i.e. group (a) samples have loops which are saturated below 300 mT, while group (b) samples have loops which are open above 300 mT and generally up to 1 T, while group (c) samples show constricted behaviour typical of a combination of magnetically hard and soft minerals. Group (a) has been subdivided on the basis of the remanence ratio (M_{rs}/M_s) to

provide an indication of the single domain fraction of the the total ferrimagnetic content. These subdivisions are (1) 0.0-0.15, (2) 0.15-0.30 and (3) >0.3.

The distribution of samples between the various categories is shown in figure 5.12.

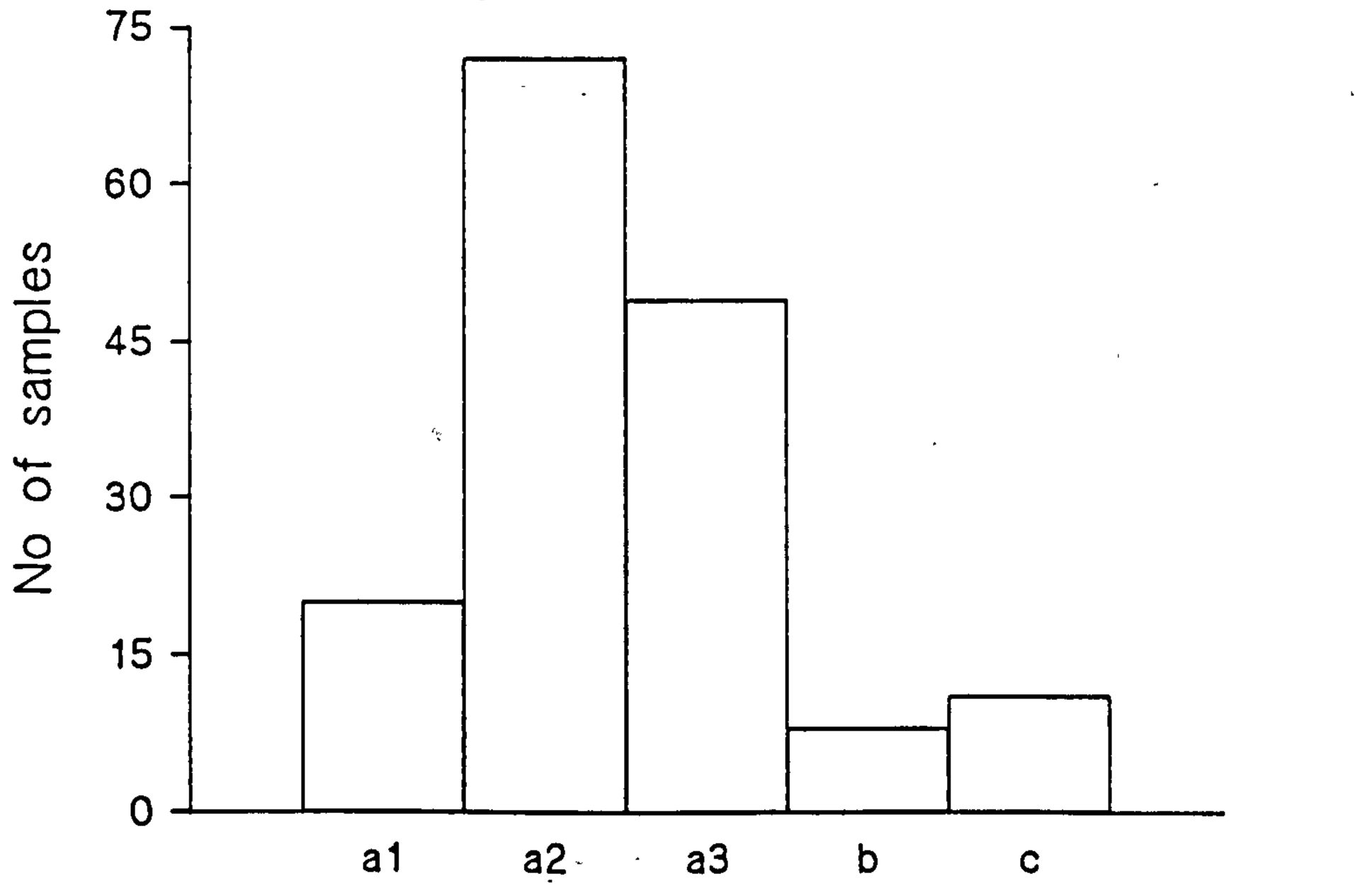

Figure 5.12. The distribution of samples between the different magnetic hysteresis categories described in the text.

6 Low Field Magnetic Susceptibility

6.1 Introduction

Measurements of magnetic susceptibility at low fields have been used primarily to investigate the domain states of magnetic minerals. The methods employed were the measurement of bulk susceptibility at room temperature using two frequencies and the measurement of the variation of susceptibility from approximately -196°C (liquid nitrogen temperature) up to room temperature, termed low temperature susceptibility.

6.2 Physical description

When a weak magnetic field is applied to a material a magnetisation is induced. The ease with which a magnetisation can be induced in a material is termed the magnetic susceptibility. The magnetic susceptibility, X, is defined as the ratio of induced magnetisation M to applied field H;

$$X = \frac{M}{H} \qquad (6.1)$$

For small applied fields ($\mu_o H < 0.1$ mT) the magnetic susceptibility is usually assumed to be independent of the strength of the applied field. However, Smith & Banerjee (1987) have shown that this may not be strictly correct.

Any induced magnetisation will have an associated demagnetising field (see section 2.4.2). The demagnetising field opposes the applied field, reducing its magnitude.

Therefore, to obtain true susceptibilities equation 6.1 must be modified to account for the demagnetising field. The demagnetising field can be obtained if the demagnetisation factor is known, or if it can be estimated by assuming a demagnetisation factor (e.g. see Appel & Soffel, 1985). However, in practice the demagnetising field is often neglected because the induced magnetisation is small and the demagnetisation factor is difficult to determine.

The susceptibility of diamagnetic, paramagnetic and ferrimagnetic materials arises from different physical mechanisms. The mechanisms responsible for diamagnetic and paramagnetic susceptibility have been discussed in section 2.2. The mechanisms responsible for the magnetic susceptibilities of ferro-, ferri- and (canted) antiferro-magnetic materials are similar and depend upon the various energy terms discussed earlier (section 2.4) and upon the domain state. For stable single domain particles, the susceptibility can be explained by invoking a simple model of opposing spins, see figure 6.1. The atomic magnetic moments, represented by the arrows in the figure, are initially antiparallel (figure 6.1a). On application of a magnetic field at some angle to the atomic moments, the moments experience a torque. This torque adds a further energy term to the system, altering the position of lowest energy for the atomic moments to that shown in figure 6.1b. Consequently, a magnetic moment is induced in the direction of the applied field. The magnetic susceptibility of

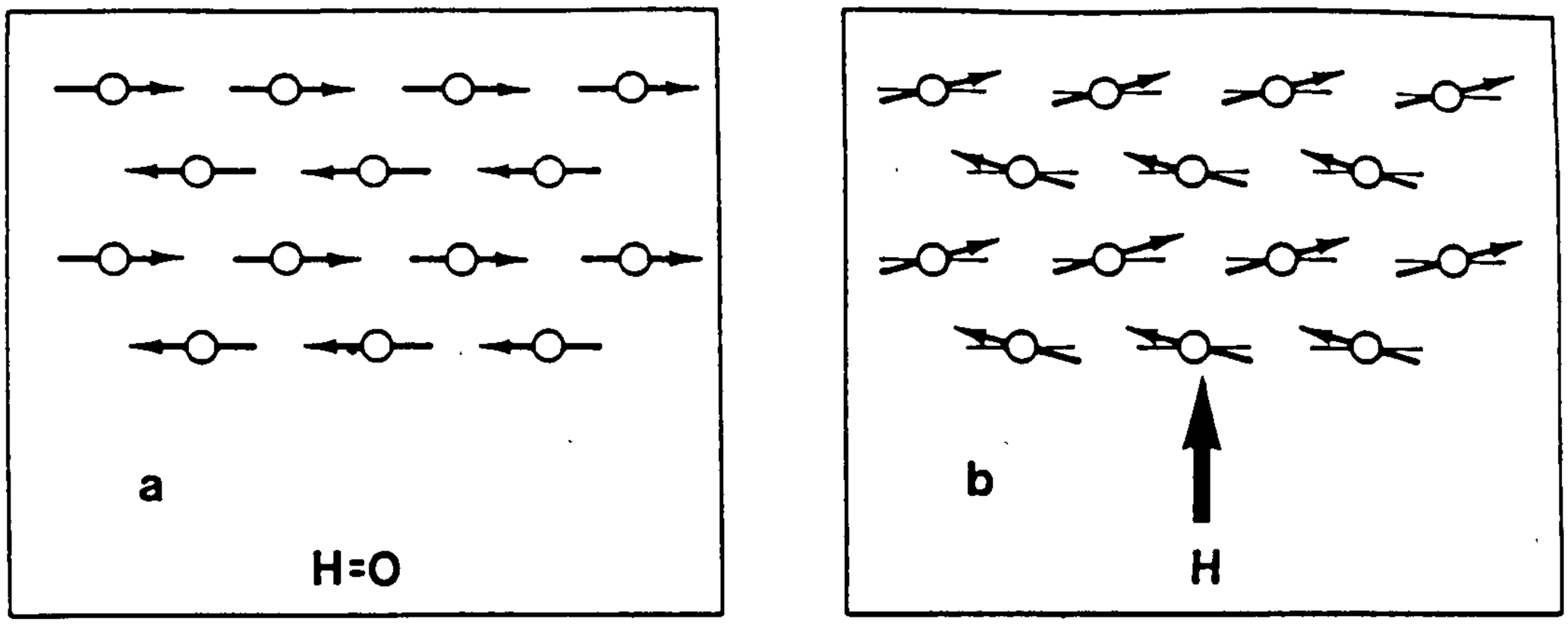

Figure 6.1. An illustration of the mode of magnetisation induced in a single domain particle from (a) zero field to (b) a small applied field. After Crangle (1977).

stable single domain particles is smaller than both the superparamagnetic and multidomain cases because of the relatively large energy required to rotate the aligned spins against the intrinsic anisotropy.

Superparamagnetism was described in section 2.7. The magnetic susceptibility of superparamagnetic particles is dependent on both temperature and the measurement time (Stephenson, 1971). The susceptibility of an assemblage of superparamagnetic particles falls when the frequency of the inducing field equals the relaxation time at which the particles become stable single domain particles. Increasing the frequency of susceptibility measurement in effect shifts the superparamagnetic/stable single domain boundary to a smaller particle size. For magnetite, and a measurement with time constant of 100 seconds, the susceptibility falls by a factor of twenty-five across the boundary from the superparamagnetic to the stable single domain state (O'Reilly, 1984).

The low field magnetic susceptibility of multidomain particles is dominated by the movement of domain walls. On the application of a magnetic field the domain walls move to the new positions of lowest total energy imposed by the field. Such wall movements fractionally increase the size of the domains which are magnetised in the direction of the applied field, and reduce those opposing it, see figure 6.2. The susceptibility of multidomain particles is larger than that for stable single domain particles.

The overall particle size dependence of magnetic susceptibility is illustrated systematically in figure 6.3.

6.3 Dual frequency bulk susceptibility measurements

The measurement of bulk susceptibility at two frequencies was carried out using a Bartington MS2 meter with a dual frequency sensor. This meter operates at frequencies of 0.47 kHz and 4.7 kHz. The Bartington system consists of a tuned inductance circuit. When a susceptible sample is placed in the sensor the system is detuned. The susceptibility is determined from the magnitude of this effect. The effect of the induced demagnetising field was neglected for all susceptibility determinations. In this study the susceptibilities are all mass specific because the mass of the sherds was easier to determine tha are their respective volumes. Equation 6.1 is modified to the mass specific form by division by the density of the sample.

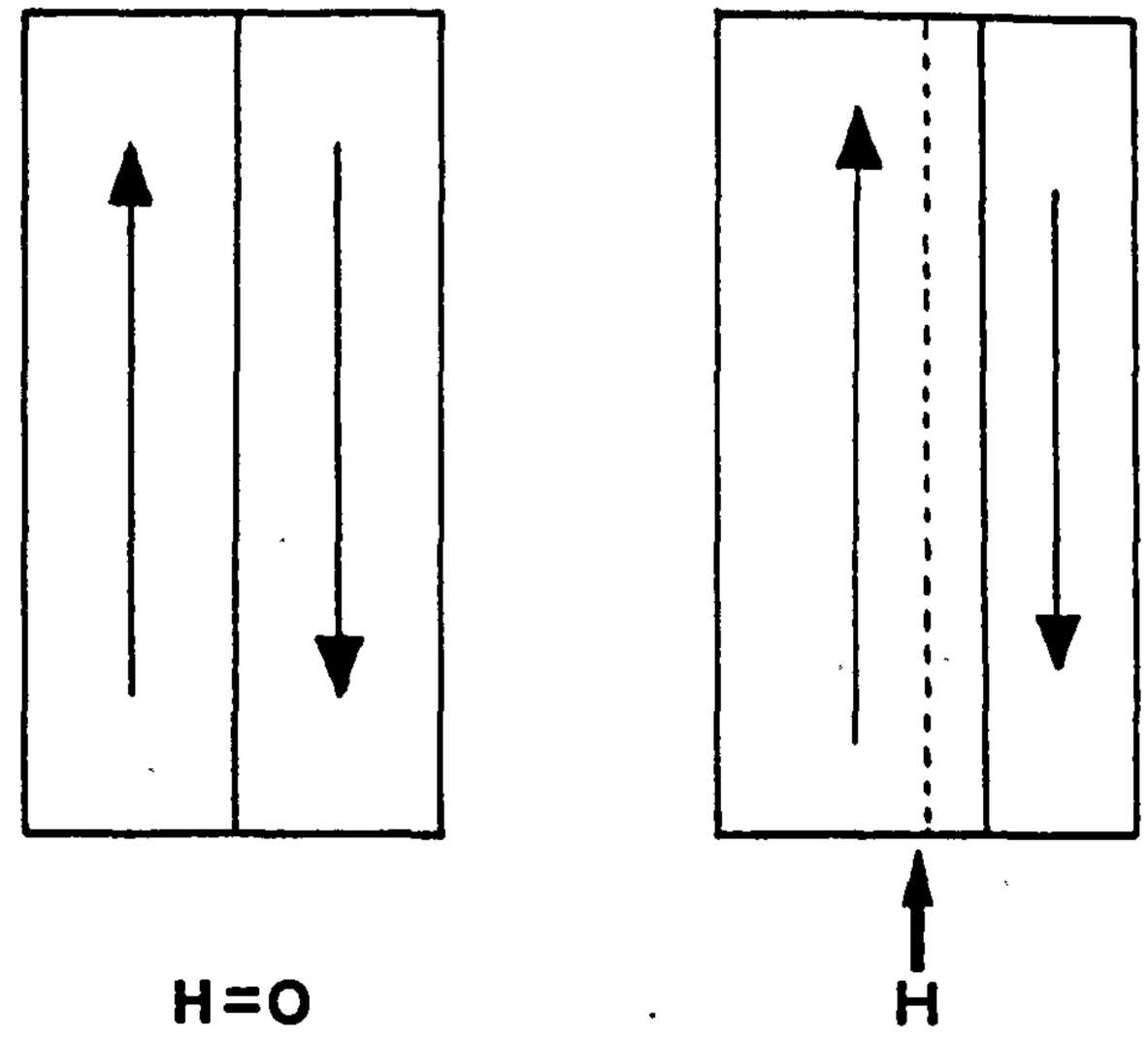

figure 6.2. An illustration of the increase of magnetisation due to domain wall motion on the application of a small magnetic field.

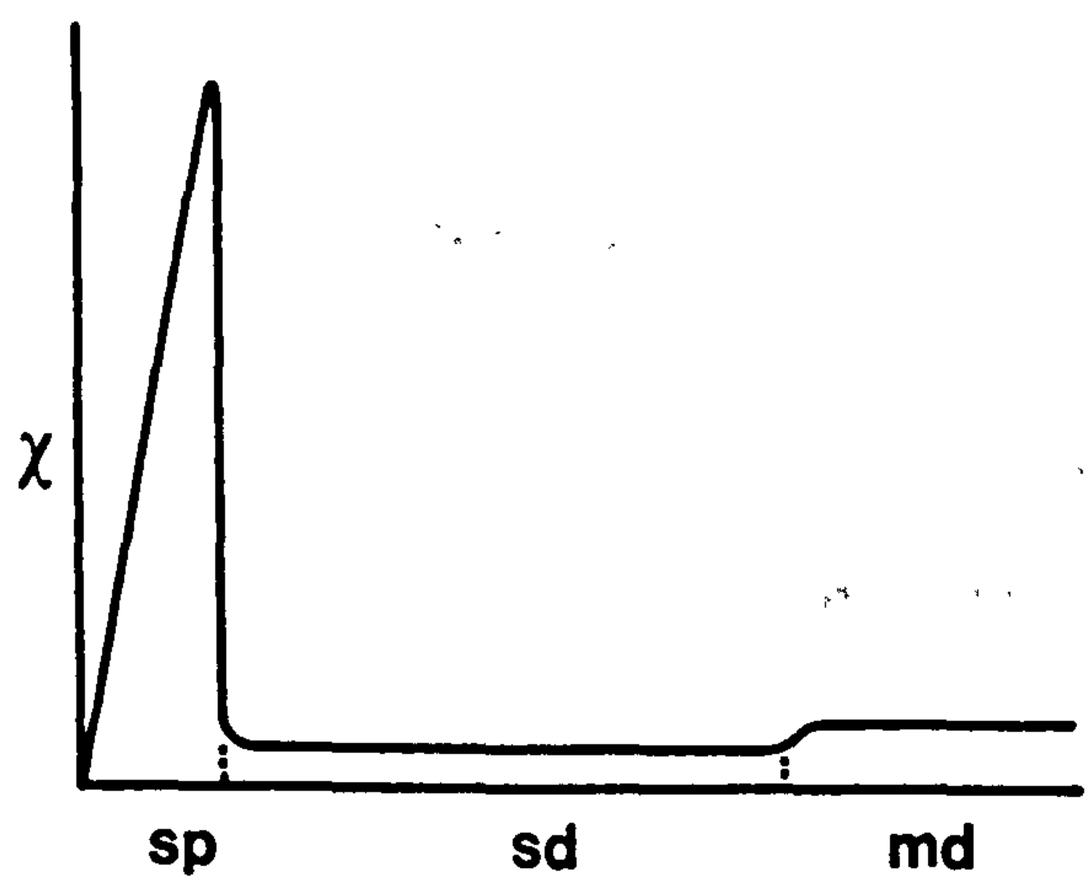

Figure 6.3. The overall particle size dependence of magnetic susceptibility from superparamagnetic through to multidomain size particles. After O'Reilly (1984).

6.3.1 Experimental procedure

Susceptibility measurements were undertaken on the samples that were prepared for IRM acquisition experiments. Susceptibility was measured before IRM acquisition in case any multidomain particles were present, since the susceptibility of multidomain particles falls after exposure to large magnetic fields as the number of domain walls is reduced (Halgedahl & Fuller, 1981).

Susceptibility measurements were carried out using the high sensitivity scale on the Bartington meter which gives a maximum resolution of $1x10^{-9}$ m^3kg^{-1} for the mass specific susceptibility. The system was calibrated before and after each series of measurements and when the frequency was changed. Calibration was achieved using a known mass of paramagnetic manganese (II) oxide. Three repeat measurements were made for measured mass specific susceptibilities of over 10 units (10^{-7} m^3kg^{-1}) and five for those under 10 units. Background readings were taken between successive measurements.

6.3.2 Data analysis

The first stage of data analysis was to correct for the background and drift measurements. The drift of the system was assumed to be linear with time, and was accounted for by taking the background value as the value half way between successive background readings. A mean magnetic susceptibility value was obtained for each sample from the drift corrected readings. These values were then corrected for the calibration before being corrected for the sample

mass to give a final mass specific susceptibility with units of m^3kg^{-1}.

6.3.3 Results

The distribution of bulk susceptibilities measured at 0.47 kHz is shown in figure 6.4. The bulk susceptibility alone provides little useful information since it is dependent upon the concentration and composition of paramagnetic, diamagnetic, ferrimagnetic and canted antiferromagnetic minerals as well as upon the domain states of the latter two mineral types.

Information about the domain states of the ferrimagnetic particles has been obtained from the susceptibility measurements by first subtracting the paramagnetic susceptibility (obtained from magnetic hysteresis measurements) and then by removing the effect of mineral

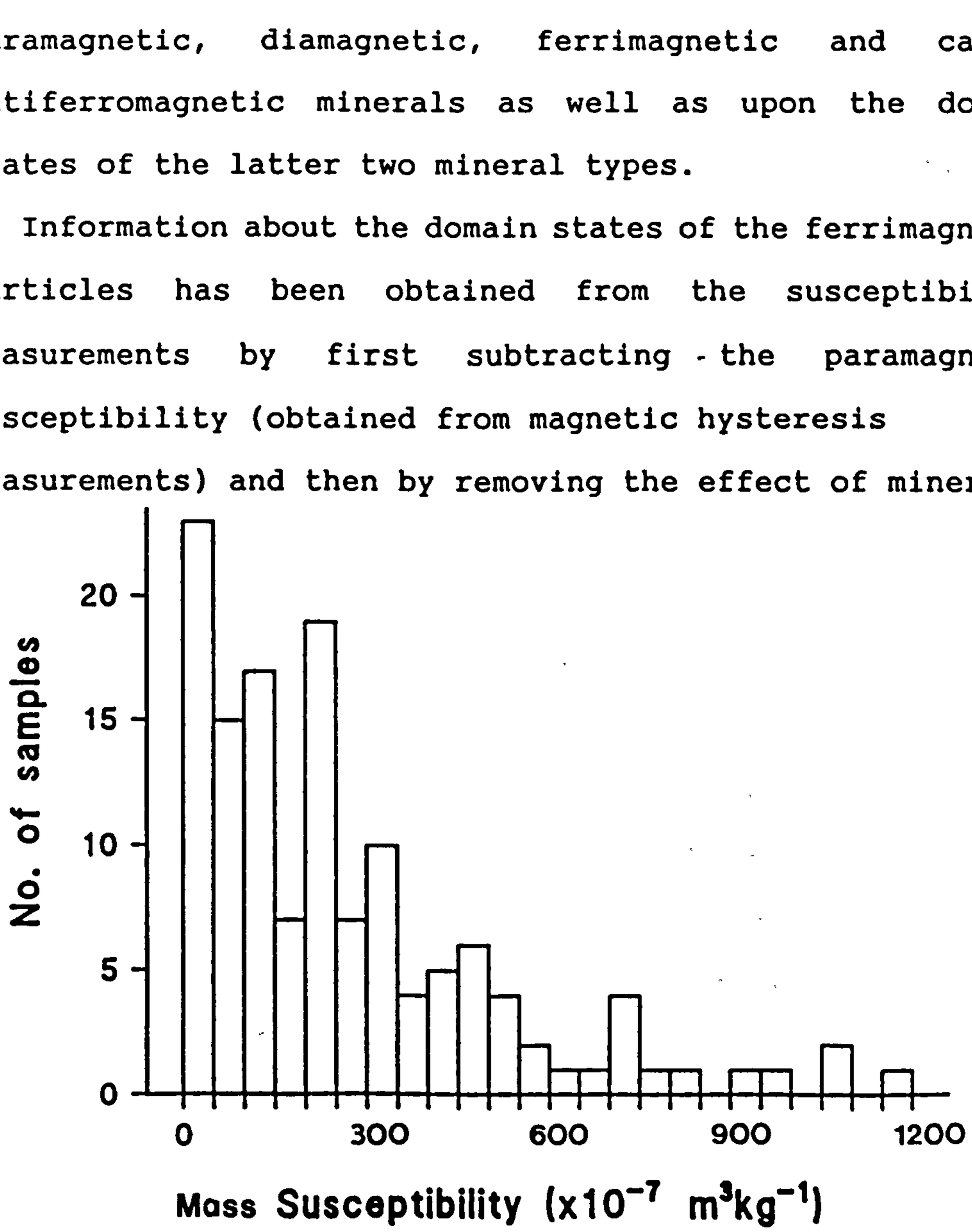

Figure 6.4. The distribution of magnetic susceptibilities in the ceramic collection, measured with an applied field frequency of 0.47kHz.

concentration by dividing the ferrimagnetic susceptibility by the saturation magnetisation (also obtained from magnetic hysteresis). A correction for diamagnetic susceptibility is not required since the only effect of such susceptibility will be to reduce the paramagnetic susceptibility to that observed during magnetic hysteresis measurements. The susceptibility value obtained from this treatment has been termed the reduced ferrimagnetic susceptibility (Dunlop & Prevot, 1982). The reduced ferrimagnetic susceptibility depends only upon the domain states and composition of the ferrimagnetic particles. A histogram of the reduced ferrimagnetic susceptibility obtained from the ceramic collection is shown in figure 6.5. The dashed line in this figure indicates the maximum value of the reduced ferrimagnetic susceptibility of multidomain magnetite particles (0.76 mA^{-1}, calculated from the experimental data of Dankers, 1978), which is the maximum value attainable by any remanence carrying magnetite particle. Any values above this indicate the presence of superparamagnetic particles (Dunlop, 1981). It is clear from figure. 6.5 that almost all of the samples have reduced ferrimagnetic susceptibilities above the maximum susceptibility of multidomain magnetite, indicating the predominance of superparamagnetic particles in the low field magnetic susceptibility of these ceramics. Alternatively, this may indicate a paramagnetic component which was not removed by the correction described earlier, although this explanation is doubtful considering the

extremely low susceptibilities of paramagnetic minerals. The data which fall on or below the maximum multidomain magnetite value may be interpreted as an assemblage containing either none or very little superparamagnetic material or perhaps a mineralogy other than pure magnetite i.e. one with a lower specific magnetisation.

The frequency dependence of susceptibility can be used to infer the presence of superparamagnetic particles irrespective of the mineralogy. The frequency dependence of susceptibility, X_{fd}, has been determined here as the difference between low, X_{lf}, and high, X_{hf}, frequency susceptibility

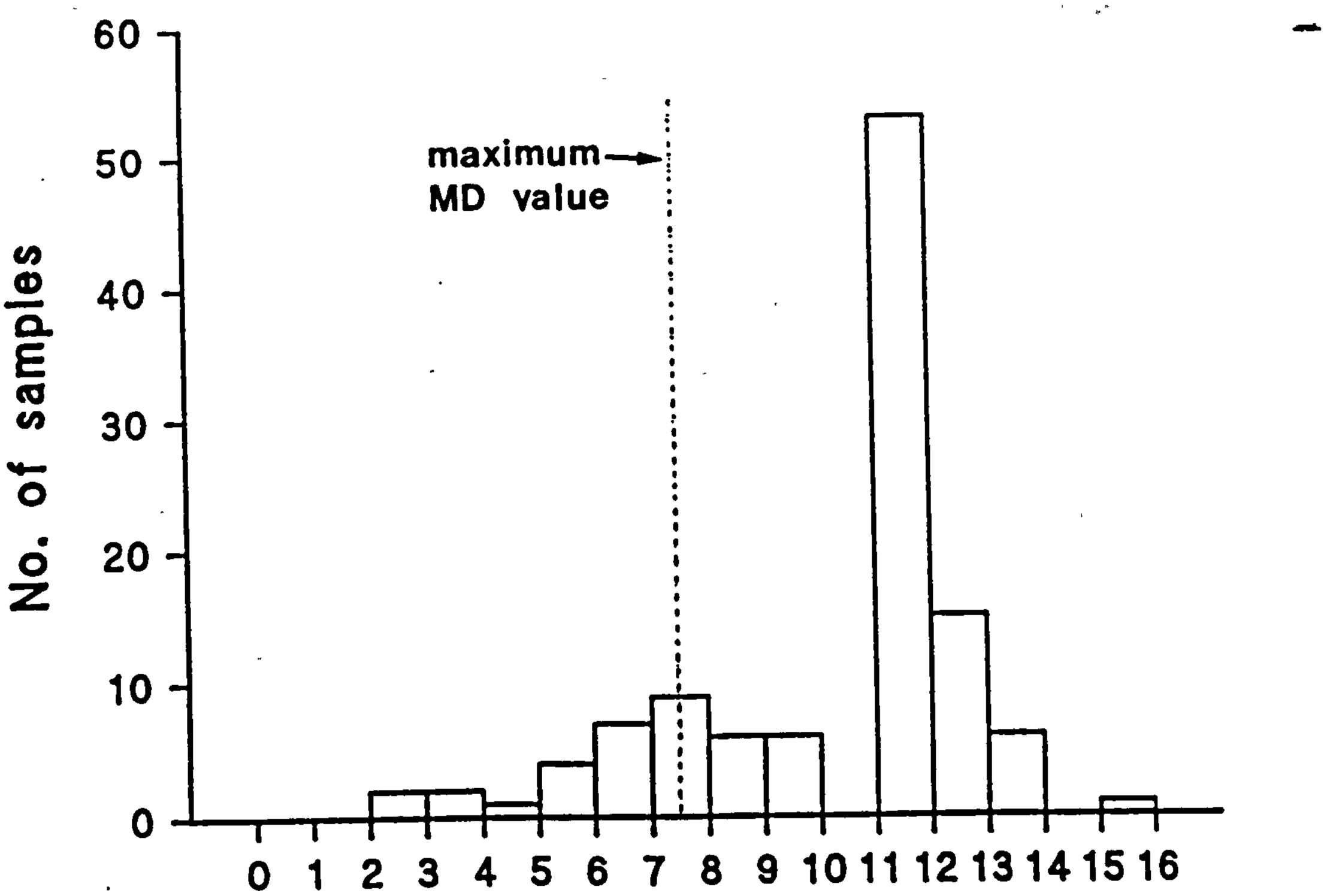

Figure 6.5. A histogram showing the distribution of reduced ferrimagnetic susceptibilities for the ceramics for which the saturation magnetisation was known from magnetic hysteresis measurements, see chapter 5.

measurements expressed as a percentage of the low frequency susceptibility, X_{lf}, i.e.;

$$X_{fd} = \left(\frac{X_{lf} - X_{hf}}{X_{lf}} \right) \times 100\% \qquad (6.2)$$

The frequency dependence of susceptibility has been combined with the reduced ferrimagnetic susceptibility data to investigate the presence of superparamagnetic particles below the maximum ferrimagnetic susceptibility value for multidomain magnetite. See figure 6.6. It is clear that all of the sherds investigated at two frequencies show some frequency dependence of susceptibility, indicating the presence of superparamagnetic particles in these sherds. The occurrence of superparamagnetic behaviour below the magnetite multidomain boundary suggests either the distribution of particles are predominantly stable single domain but with some fraction of particles below the superparamagnetism threshold, or it may indicate that the ferrimagnetic mineral is not magnetite. The second explanation is supported by thermomagnetic analysis which indicates that the data in question is associated with titanium substituted and cation deficient magnetite, both of which have lower reduced ferrimagnetic susceptibilities than stoichiometric magnetite.

6.4 Low temperature susceptibility

The susceptibility of diamagnetic, paramagnetic and ferromagnetic (including ferrimagnetic and antiferromagnetic) materials varies with temperature. The

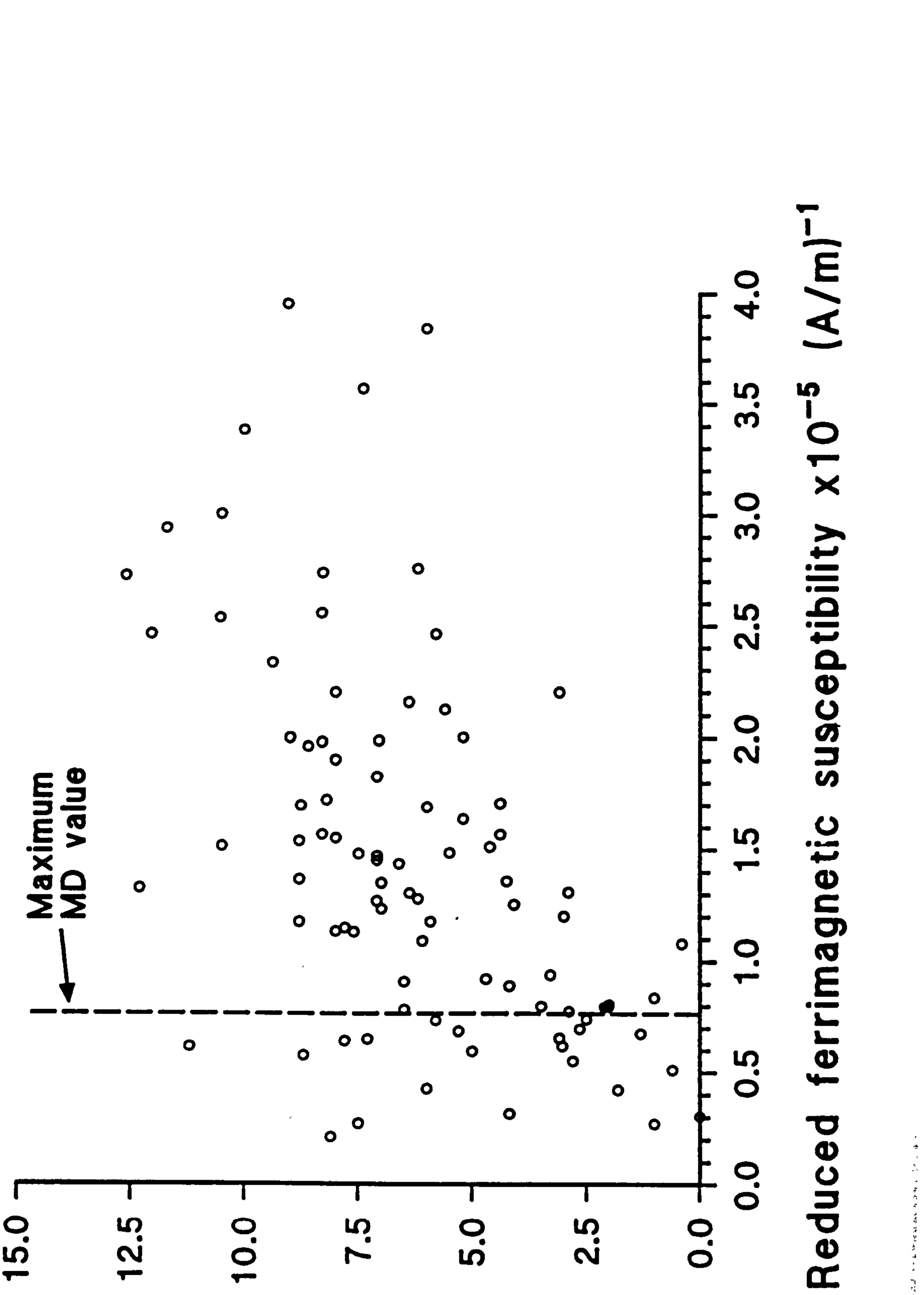

Figure 6.6. A plot of the reduced ferrimagnetic susceptibility against the percentage frequency dependence of the susceptibility for the ceramics investigated.

temperature variation of diamagnetic änd paramagnetic materials has been covered in section 2.2.

The magnetic susceptibility of a ferromagnetic material is controlled by the combination of the anisotropy terms of the magnetic particles. These anisotropy terms are, to varying extent, temperature dependent. The dominant anisotropy term for a particular sample depends upon the mineralogy, microstructure, size and shape of the magnetic particles. The variation with temperature of the anisotropy is expressed in the temperature dependence of the susceptibility. This dependence can therefore provide information diagnostic of the magnetic mineralogy of a sample.

Shape anisotropy

When shape anisotropy is dominant the magnetic susceptibility of a particle varies little with temperature because shape changes due to expansion or contraction of the crystal lattice are very small. Shape anisotropy is dominant in single domain magnetite particles when the particles are elongated by more than 10% (Pullaiah et al., 1975) and may therefore be assumed to be the principal anisotropy in many single domain magnetite particles.

Magnetocrystalline anisotropy

Magnetocrystalline anisotropy is associated with the crystal structure of a mineral. The dominance of magnetocrystalline anisotropy can be identified from the temperature variation of susceptibility if the crystal structure changes with temperature. In the case of

magnetite the crystal structure changes from a cubic to an orthorhombic arrangement between -145°C and -155°C (O'Reilly, 1984). During this transition the magnetocrystalline anisotropy energy changes sign, passing through zero (the isotropic point) between the stated temperatures. The susceptibility of multidomain magnetite is controlled by magnetocrystalline anisotropy (Senanayake & McElhinny, 1981). The anisotropy transition is reflected in the temperature dependent susceptibility of multidomain magnetite which shows a peak at the isotropic point. The transition temperature alters with titanium substitution (Appel & Soffel, 1985) and also becomes frequency dependent (Radhakrishnamurty & Likhite, 1991).

The magnetocrystalline anisotropy of haematite undergoes a similar transition. This is termed the Morin transition and has an isotropic point at -10°C (Dunlop, 1971). The isotropic point is suppressed or pushed to lower temperatures when impurities are present (Collinson, 1983).

Stress anisotropy

When stress anisotropy is dominant the susceptibility decreases with decreasing temperature (Appel & Soffel, 1985). The decrease of susceptibility at low temperatures occurs because the magnetic particles contract which increases the internal stress. The increased stress couples with the magnetostriction to increase the total anisotropy. Thus moment rotation and domain wall motion are more difficult.

The contribution of shape, magnetocrystalline and stress

anisotropy to the temperature variation of susceptibility of multidomain titanomagnetites has been investigated experimentally and theoretically by Appel & Soffel (1985). They infer that stress anisotropy dominates the temperature dependence of susceptibility for titanomagnetites with a titanium content of x>=0.6, while no single anisotropy dominates the temperature dependence of multidomain titanomagnetites with x<0.6.

Superparamagnetism

The phenomenon of superparamagnetism was discussed in section 2.7. The susceptibility of superparamagnetic particles falls on cooling as the magnetisation of the particles becomes progressively 'blocked in', reducing their susceptibility to that of stable single domain particles.

Some of the important temperature dependent susceptibility variations are summarised in figure 6.7. In natural materials the temperature dependence of susceptibility will reflect the combined contributions of the different minerals, domain states and particle sizes present.

6.4.1 Experimental procedure

Susceptibility measurements from liquid nitrogen temperature (-196°C) to room temperature were performed using a Bartington MS2 meter in which the sensor is thermally stabilised with a continuous flow water-jacket. The operating frequency of this system is 0.47 kHz. The sample temperature was monitored using a Cu-Cu/Ni

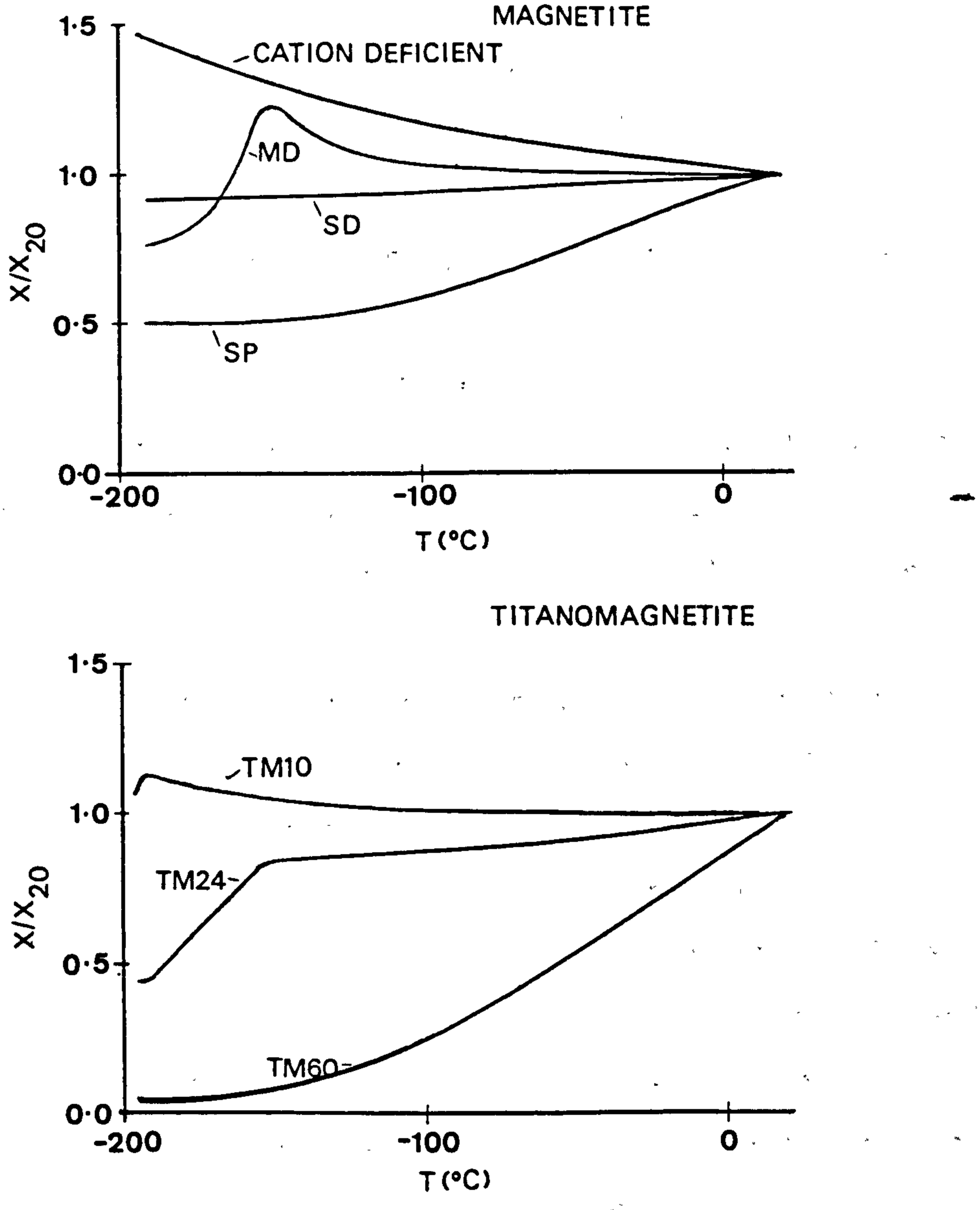

Figure 6.7. Examples of some important types of low temperature susceptibility variations. Adapted from Senanayake & McElhinny (1981) and Appel & Soffel (1985) and Radhakrishnamurty (1986).

thermocouple. The susceptibility meter was interfaced to a BBC microcomputer through which experiments were controlled. Measurements were carried out using relatively large bulk samples in order to maximise the signal to noise ratio. The thermocouple was taped to the surface of a sample which was then surrounded with plasticine for thermal insulation and cooled to -196°C by immersion in liquid nitrogen. The susceptibility was measured as the sample warmed up, with susceptibility readings taken at equal time intervals. The data was corrected for the drifting background of the meter by assuming the drift was linear (in time) between the initial and final background readings. A hard copy of the data, normalised to the room temperature susceptibility value, was plotted for analysis.

6.4.2 Results

One hundred and forty-seven samples were investigated. A range of behaviour was observed. The results have been categorised on the basis of the shape of the curve. The categories are shown in figure 6.8. In many cases the susceptibility behaviour is complex and has been classed as a combination of two categories. The classification and the susceptibility ratio, RS, ($RS=X_{-196}/X_{20}$) of each sample are presented in appendix 6. The interpretation of the categories follows in the discussion section (6.4.4).

French I

MC01 The low temperature susceptibility behaviour of the six French I sherds is dominated by group 1 type behaviour (RS=0.52-0.77) with sherds 02 and 04 displaying a small

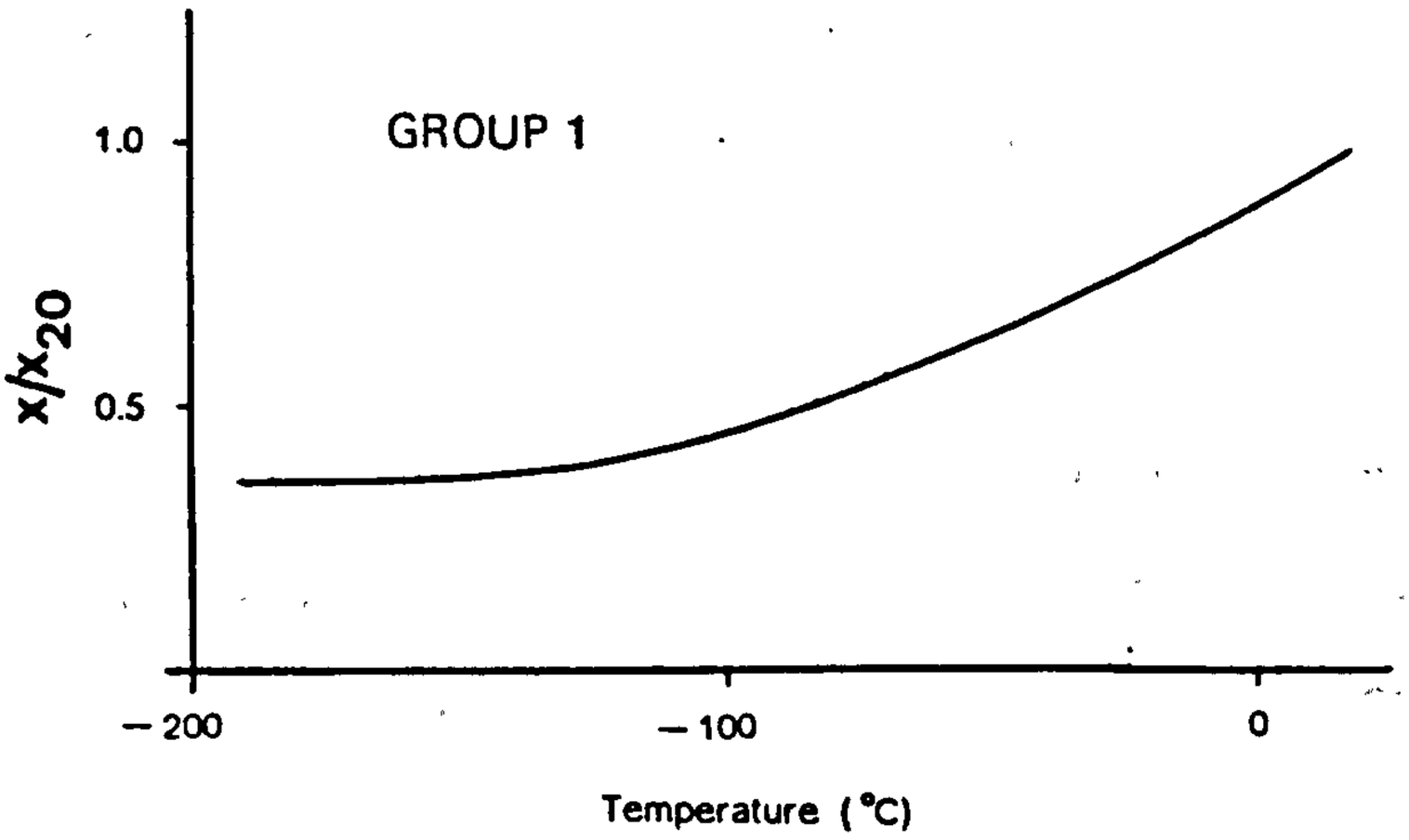

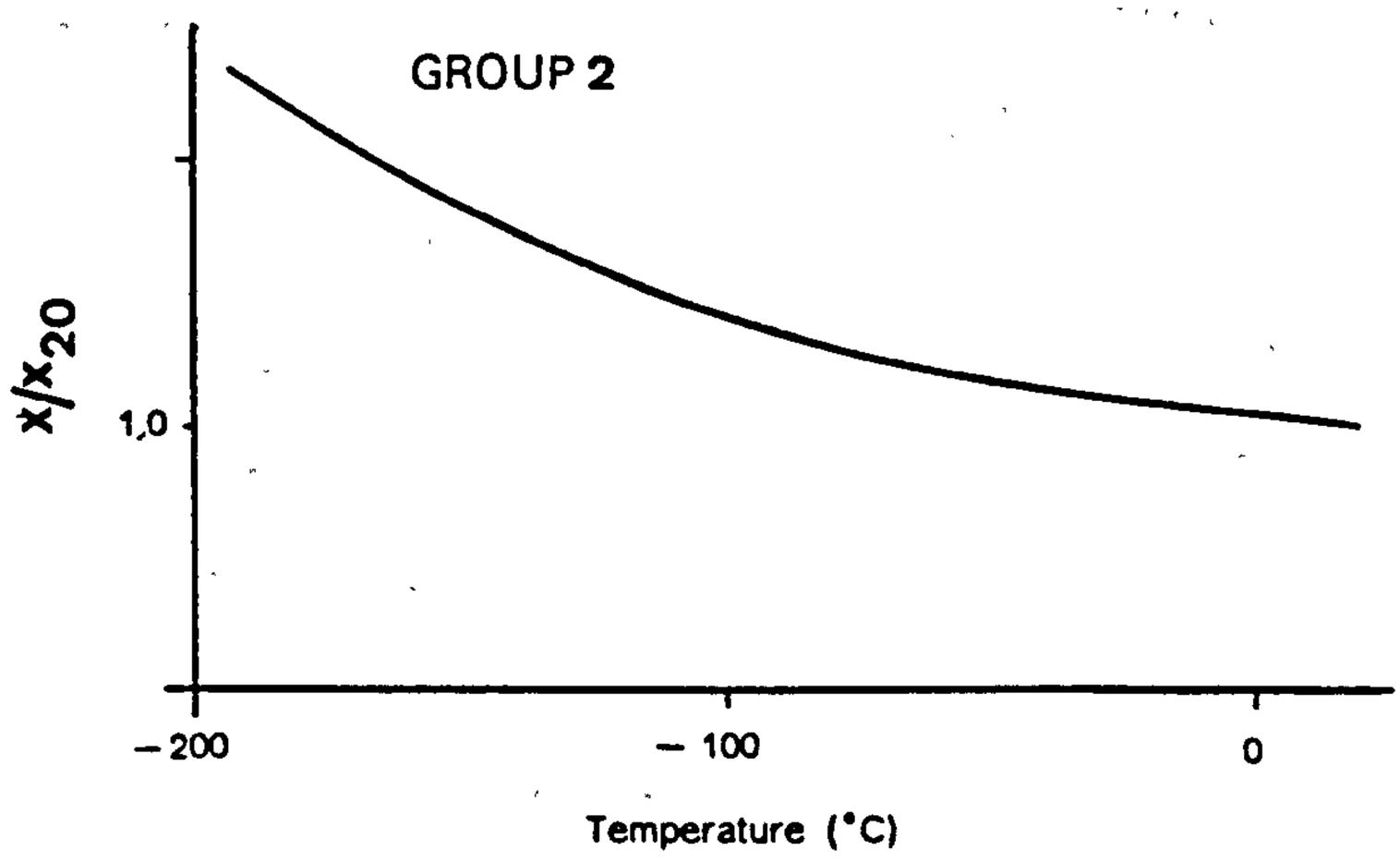

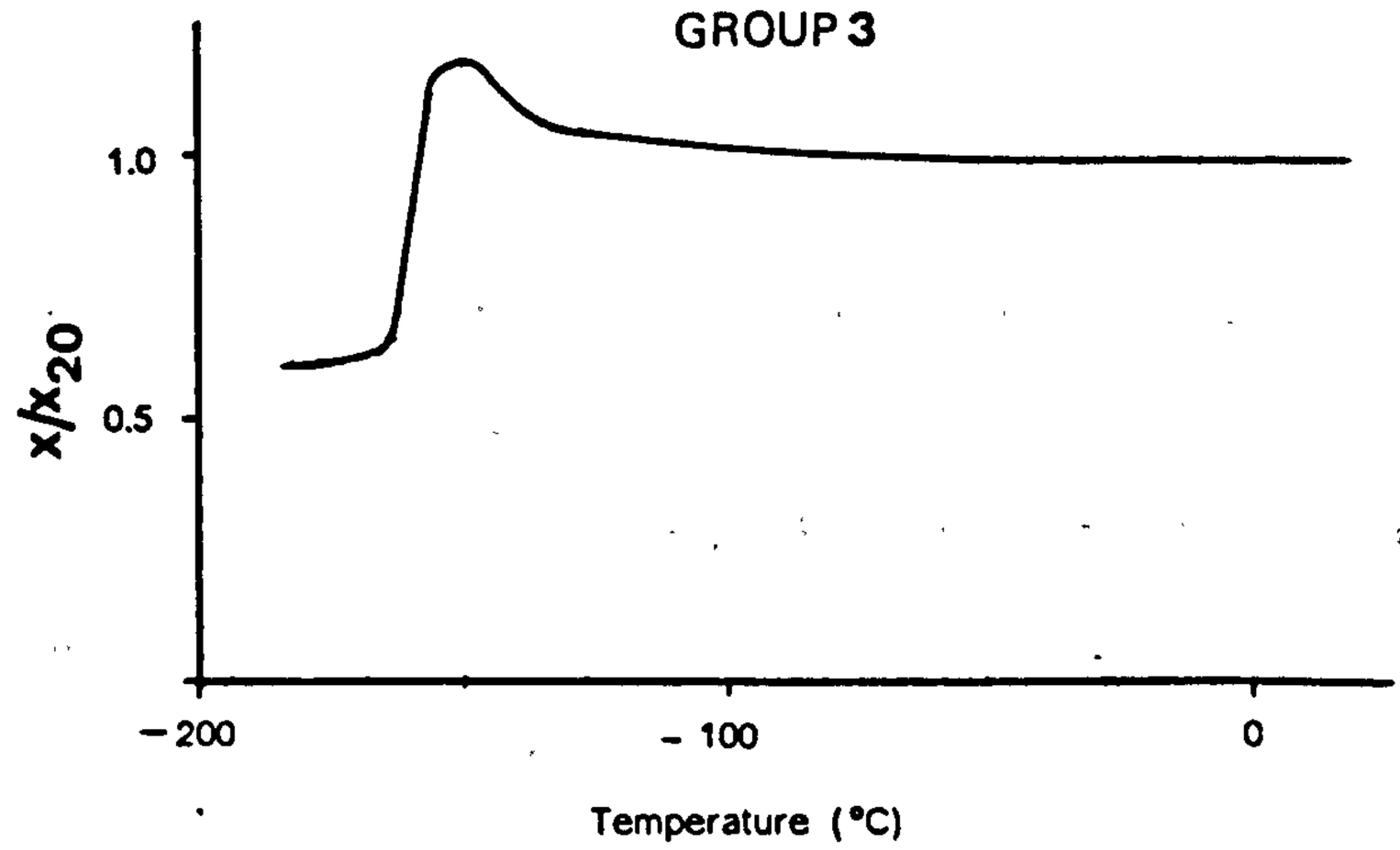

Figure 6.8. The classification of the low temperature susceptibility curves used in this study.

additional group 3 component, see figure 6.9a.

British

MC02 Both of the British sherds display group 1 behaviour with RS values of 0.61 and 0.71 for sherds 01 and 02 respectively.

Peruvian

MC05 All four sherds have a group three component, with 01, 02, and 04 also displaying group 1 behaviour. See for example figure 6.9b. The RS values range from 0.67 to 0.82.

MC06 The behaviour of both sherds is predominantly group 1, but both show a small group three 'hump'. The RS values are similar (0.61 and 0.66).

MC07 Sherds 02, 03 and 04 show similar group 1 behaviour, with RS values between 0.56 and 0.57. See figure 6.9c. The behaviour of sherd 01 has features of both group 1 and the peak of group 3. See figure 6.9d.

MC08 The susceptibility of 01 is relatively weak. The susceptibility of this sample falls initially on warming before rising to the room temperature value. See figure 6.10a. The susceptibility of 01 is of group 1/2 type. The behaviour of sherd 02 is classified as group 1.

MC09 A group 3 type component is observed in all six sherds in this group and is the predominant component in sherds 06, 04 and 02. See figure 6.10b. The behaviour of sherds 01, 03 and 05 is best described as a combination of group 1 and 3 behaviour. See figure 6.10c.

MC10 The behaviour of sherd 01 is a combination of groups

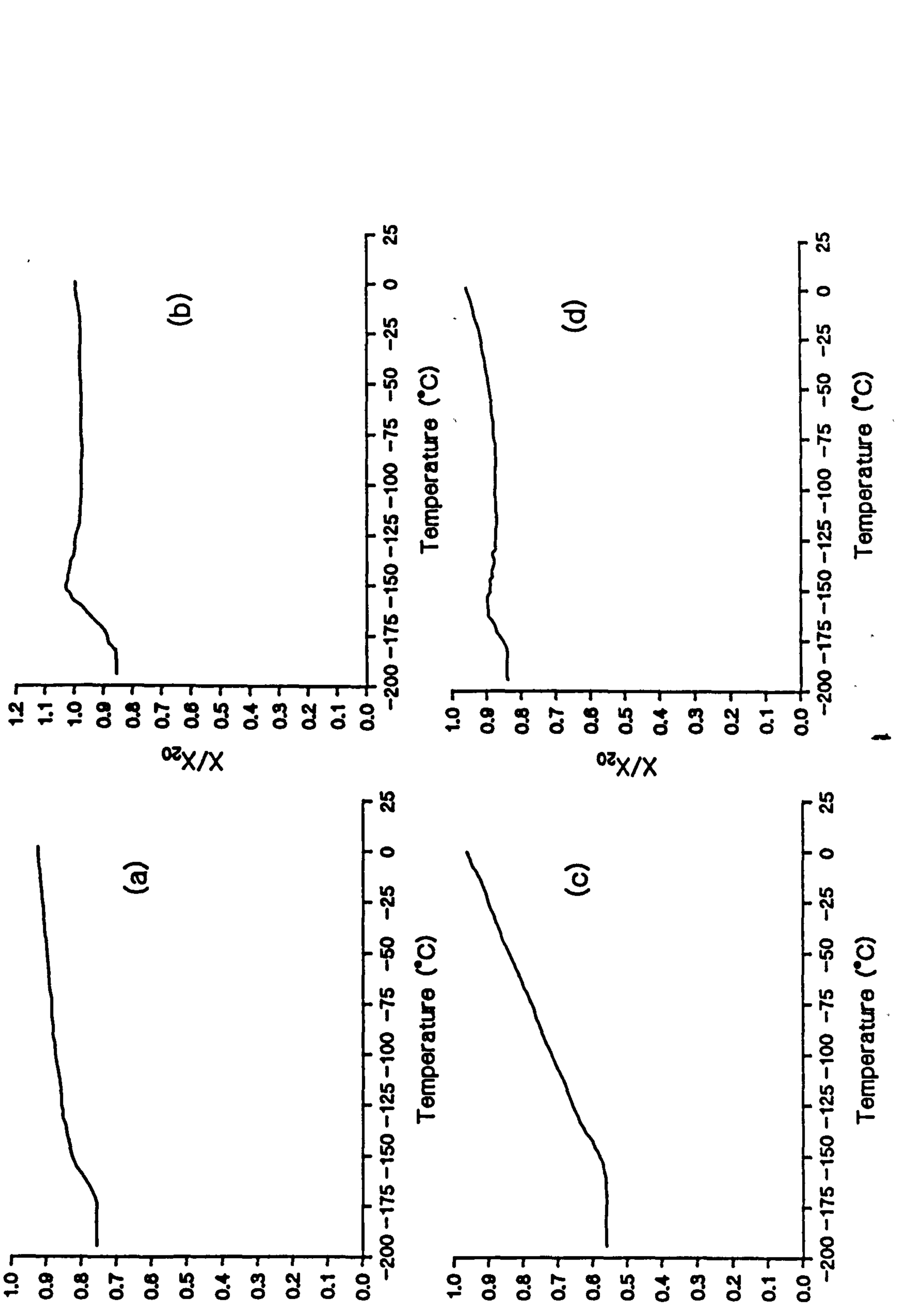

Figure 6.9. The low temperature susceptibility variation of (a) MC0102, (b) MC0504, (c) MC0703 and (d) MC0701.

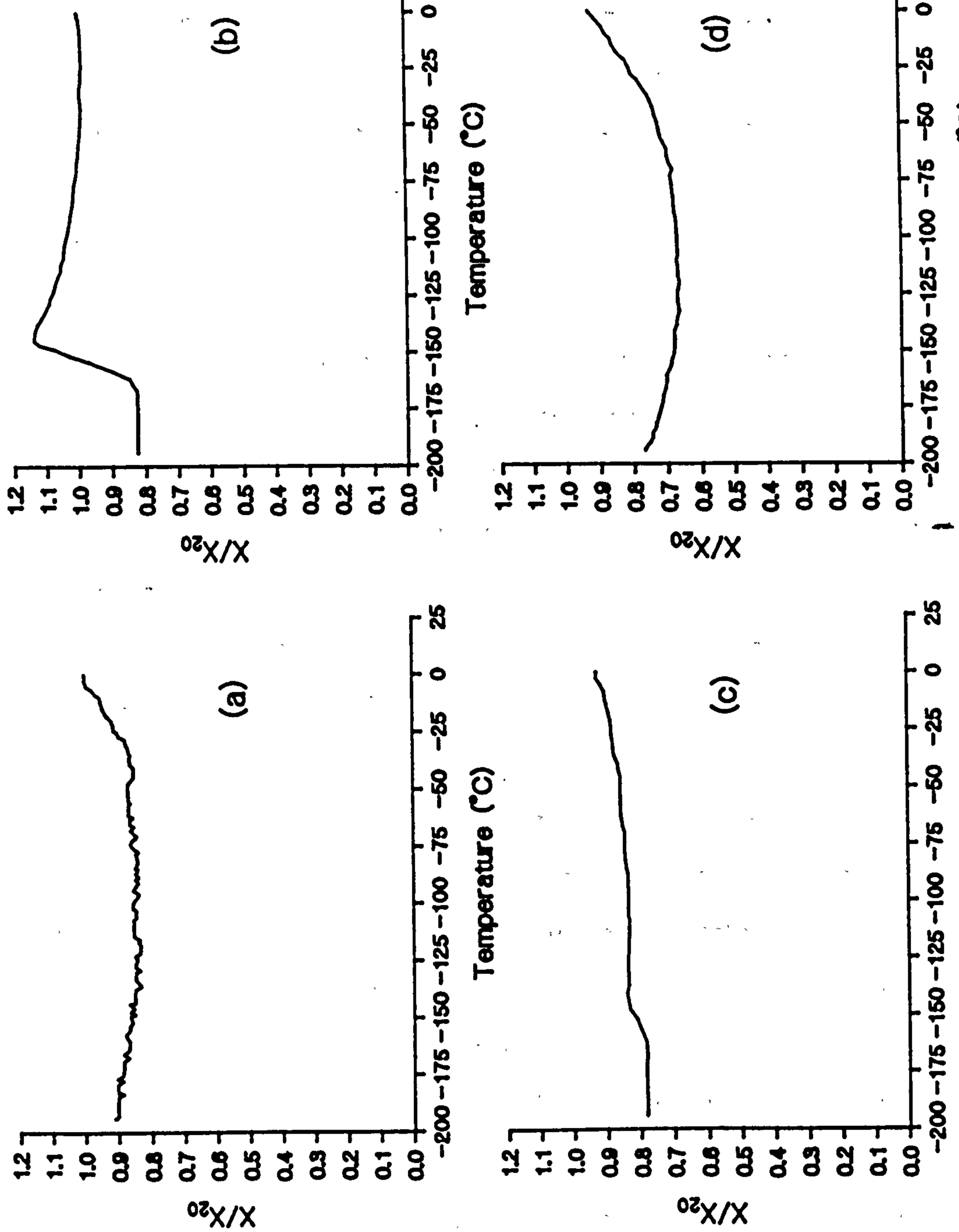

Figure 6.10. The low temperature susceptibility variation of (a) MC0801, (b) MC0904, (c) MC0903 and (d) MC1003.

Egyptian

MC12 Both sherds 01 and 02 display group 1 behaviour, with RS values of 0.91 and 0.73 respectively.

1 and 3. The RS value is 0.54. The susceptibility behaviour of sherds 02 and 03 is similar in shape but differs in the magnitude of the variations (03 showing larger changes). See figure 6.10d.

French II

MC11 Sherds 01, 03, 07, 09 and 10 display group 1 behaviour. The RS values vary from 0.54 for sherd 01 to 0.84 for sherd 09. Sherd 04 shows behaviour suggesting a combination of groups 1 and 3. The susceptibility of sherd 06 is comparatively weak, varying with temperature in a similar way to MC1003 (figure 6.10d).

MC13 Sherd 01 is highly susceptible. The low temperature variation shows a well defined peak indicating group 3 behaviour. See figure 6.11a. The behaviour of 02 and 05 are classified as group 2 but their RS values are vastly different at 1.52 and 2.91 respectively. See for example figure 6.11b. Sherd 10 is categorised as a combination of groups 1 and 2; the susceptibility at liquid nitrogen temperature is higher than at room temperature (RS=1.18) but falls below the room temperature value on initial warming and then recovers on further warming to the room temperature value. The remaining sherds measured (03, 04, 06, 07 and 11) have increasing susceptibility on warming, and are categorised as group 1. The RS values of these sherds vary from 0.56 for sherd 07 to 0.98 for sherd 04.

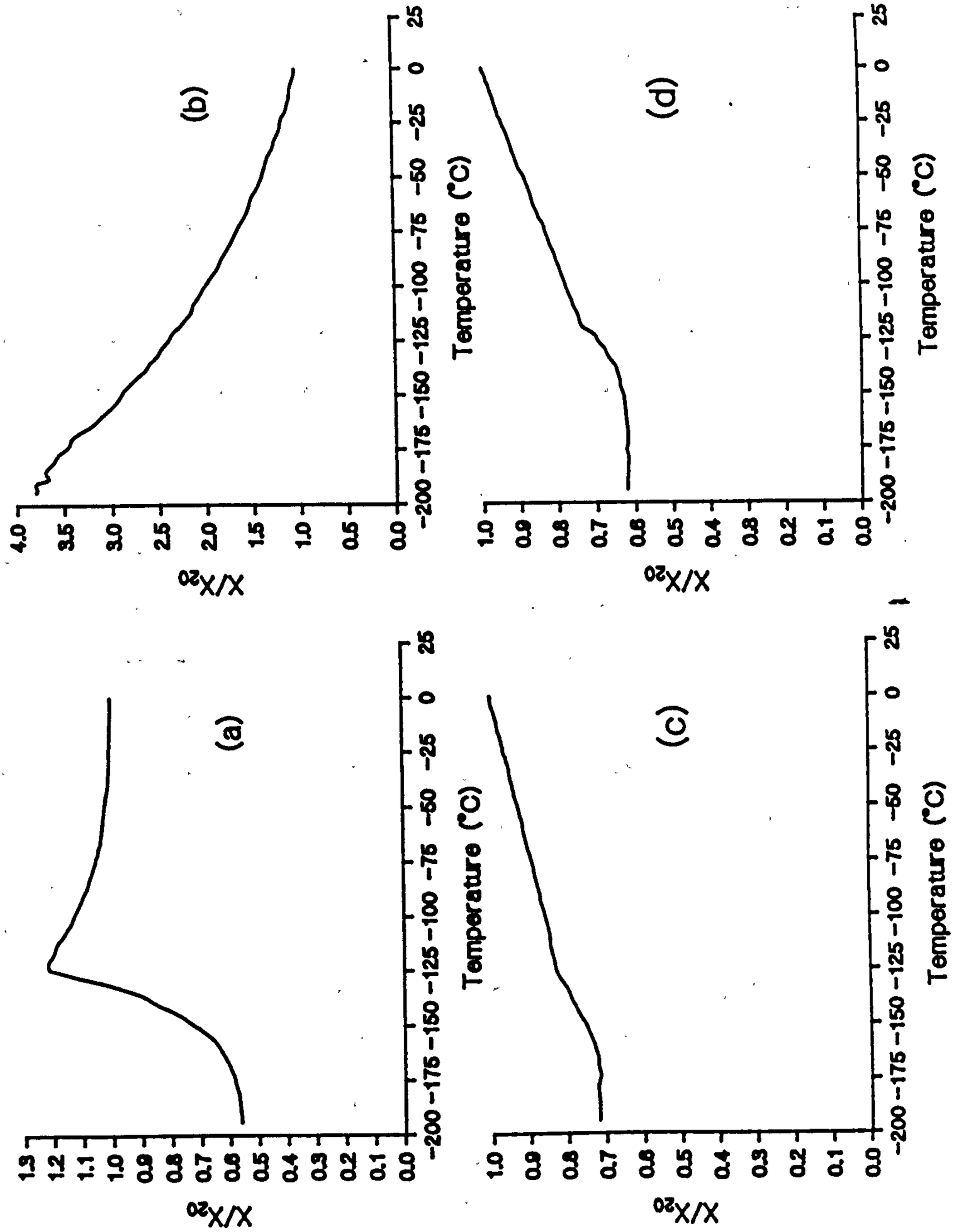

Figure 6.11. The low temperature susceptibility variation of (a) MC1301, (b) MC1305, (c) MC1402 and (d) MC1507.

Servian

MC14 The susceptibility variations of all three sherds are predominantly of group 1 type combined with a small group 3 variation. See for example figure 6.11c.

MC15 Six of the sherds (01, 05, 07, 08,11 and 13) show group 1 behaviour, with RS values varying between 0.61 for sherd 11 to 0.78 for sherd 08. See for example figure 6.11d. Sherds 06, 09 and 12 show type 2 behaviour. The RS value is largest for the sherd with the lowest susceptibility (06) and smallest for the most strongly susceptible sherd (12). The susceptibility of sherd 02 is described predominantly by group 1 but contains a slight hump ascribed to group 3, while the susceptibility behaviour of sherd 03 is best classified as group 3, as shown in figure 6.12a.

MC16 All five sherds showed group 1 behaviour, with RS values between 0.42 (sherd 02) and 0.82 (sherd 04). See for example figure 6.12b.

South West American

MC17 The susceptibility variation of sherds 04, 06 and 13 is of group 1 type, while that of sherds 01, 07 and 10 shows an additional smaller group 3 component and the behaviour of 09 shows predominantly group 3 behaviour. The remaining sherds measured (05, 08 and 12) display susceptibility variations of group 2 type, with the behaviour of sherd 12 showing an additional group 1 component.

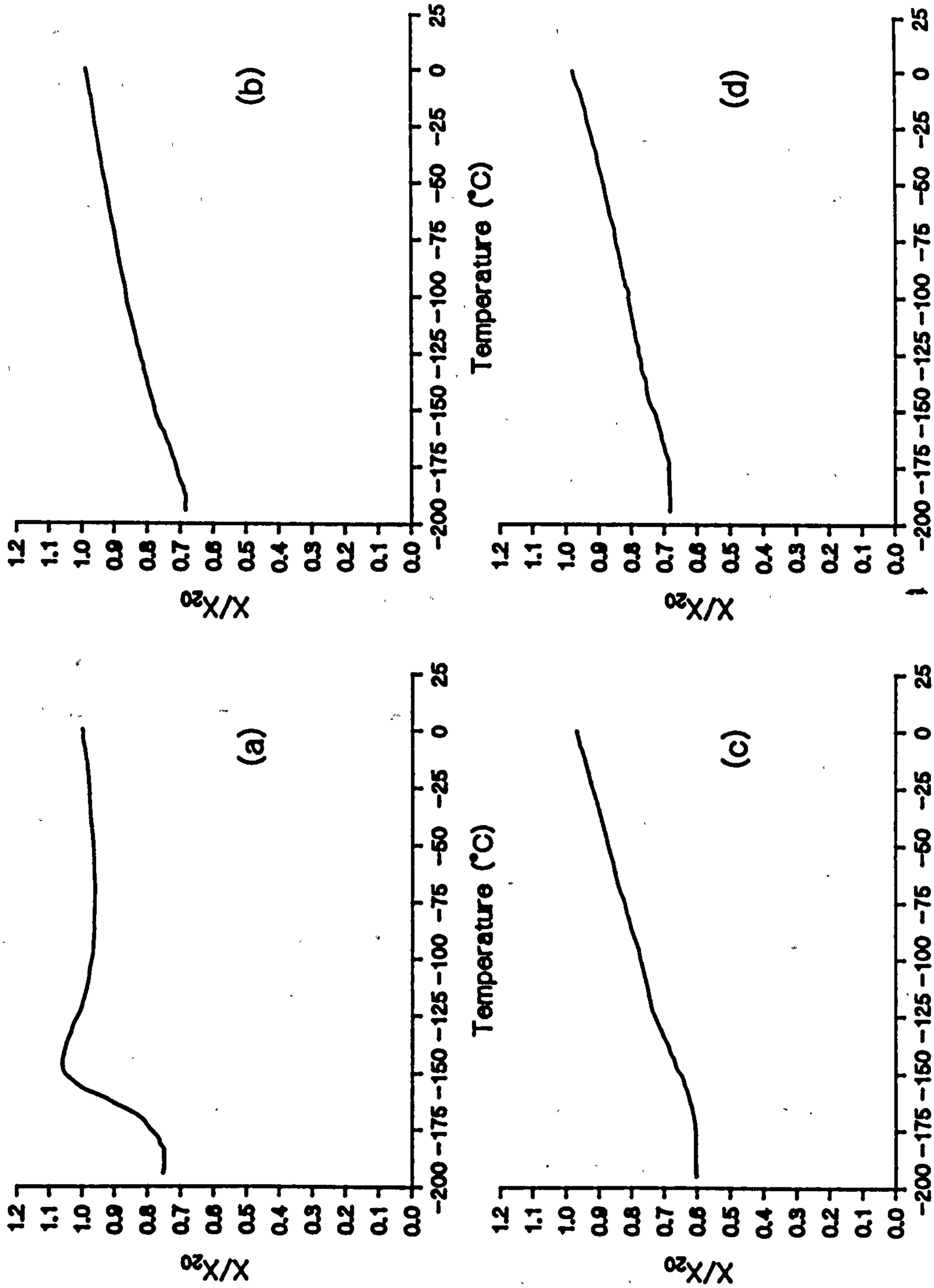

Figure 6.12. The low temperature susceptibility variation of (a) MC1503, (b) MC1603, (c) MC2006 and (d) MC2604.

Romano-British

MC18 The behaviour of sherds 01, 03, 04, 05, 07,08 and 09 shows group 1 type with RS values between 0.56 for sherd 09 and 0.90 for sherd 01. The susceptibility variation of sherd 02 is best described as a combination of group 1 and group 2 type curves. The susceptibility variation of sherd 06 is of group 2 type.

MC19 The behaviour of sherds 01, 02, 03, 04, 05 07 and 09 is of group 1 type. The RS values fall between 0.50 for sherd 03 and 0.99 for sherd 07. The susceptibility behaviour of the remaining sherds (06 and 08) is predominantly of group 1 type with a group 3 component. The RS values of these sherds are 0.61 and 0.59 respectively.

MC20 The susceptibility variation of sherds 01, 02, 04, 07, 10 and 11 is of group 1 type. The RS values range from 0.51 for sherd 11 to 0.75 for sherd 02. The susceptibility variation of sherds 05, 06 and 08 is predominantly of group 1 type with a small group 3 component, see for example figure 6.12c. The RS values for these sherds are 0.56, 0.61 and 0.80 respectively. The susceptibility of sherd 09 is smaller than the others in this group and displays temperature dependent behaviour classified as a combination of groups 1 and 2.

MC21 The susceptibility variation of sherds 01, 02, 04, 05, 07, 08 and 09 is ascribed to group 1 type behaviour; the RS values for these samples ranges between 0.56 (05) and 0.95 (09). The susceptibility behaviour of sherd 03 is

predominantly of group 1 type but has an additional group 3 component. The susceptibility of 06 is the lowest in this group and shows temperature dependent behaviour indicative of a combination of group 1 and 2 types.

MC22 The temperature dependent susceptibility behaviour of sherds 01, 03, 05, 06 and 08 is of group 1 type; the RS values for these sherds are comparatively low, ranging from 0.46 for sherd 06 to 0.74 for sherd 05. The other four sherds of this group (02, 04, 07 and 09) display temperature dependent susceptibility dominated by group 1 behaviour but with an additional group 3 component.

MC23 The temperature dependent susceptibility variation of all six sherds is predominantly of group 1 type with sherd 04 also showing a small group 3 component. The RS values for these sherds varies from 0.62 for sherd 05 to 0.73 for sherd 03.

MC24 The susceptibility behaviour of all five sherds is of group 1 type. The RS values range widely from 0.46 for sherd 05 to 0.91 for sherd 04.

MC25 The susceptibility behaviour of all five sherds is of group 1 type. The RS values range from 0.69 for sherd 01 to 1.00 for sherd 04.

Chinese I

MC26 Sherds 02, 03, 04, 05 and 06 display temperature susceptibility behaviour classified as group 1 type. The RS values for these sherds ranges from 0.59 for sherd 02 to 0.75 for sherd 04, see figure 6.12d. The susceptibility behaviour of sherd 01 is dominated by group 1 behaviour but

also has a small group 3 component. The susceptibility of sherds 07 and 08 is lower than that of the other sherds in this group and displays a temperature dependence indicating the combination of group 1 and group 2 type behaviours.

Chinese II

The susceptibility of several of these samples was very low and as a consequence the temperature dependent variations were below the resolution of the equipment and are therefore not reported.

6.4.3 Interpretation

The primary usage of low temperature variations of magnetic susceptibility, prior to this study, has been to investigate the mineralogy and domains states present in basaltic rocks. Interpretation of the results has been contentious (Radhakrishnamurty et al., 1978 and Senanayake & McElhinny, 1981). The only previous application of low temperature susceptibility to the study of ancient ceramics was reported by Hedley & Wagner (1990), who utilised the interpretations of Senanayake & McElhinny (1981). However, these interpretations were based upon basaltic mineralogy and therefore may be inappropriate to ceramics, although the fundamental properties of the minerals may be the same. The interpretations used here are based upon a combination of previously reported work (Stephenson, 1971, Senanayake & McElhinny, 1981, Appel & Soffel, 1985 and Radhakrishnamurty, 1985, 1986) and also by comparison with the results obtained in this study from other techniques. The following interpretations are best considered as

identifying t[illegible]predominant mineralogy or domain states which contribute to the low temperature variation of the magnetic susceptibility.

Group 1

Group 1 behaviour may arise from the response of an assemblage of superparamagnetic particles which becomes progressively unblocked at higher temperatures, or it may reflect the presence of titanomagnetite particles with composition parameter x>=0.6 (Appel & Soffel, 1985) or x>=0.2-0.3 (Senanayake & McElhinny, 1981); although the values presented by the latter workers neglect the effect of magnetocrystalline anisotropy. The RS values, i.e. the ratio of the susceptibility at -196°C to that at room temperature, for the titanomagnetites with group 1 type behaviour are below 0.4.

For the ceramics investigated, group 1 behaviour has been equated with the unblocking of superparamagnetic particles. The evidence in support of this are the values of reduced ferrimagnetic susceptibilities, the frequency dependence of susceptibility determined at room temperature, and the RS values which are above 0.4. In addition, the observed Curie point temperatures indicate the presence of magnetite with a maximum titanium content of x=0.13; this further opposes an explanation for group 1 type behaviour in ceramics as arising from titanomagnetites with composition parameters of x>=0.6.

Group 2

Group 2 type behaviour can arise from the predominance

of titanium poor magnetite (0<x<0.0.15) (Senanayake & McElhinny, 1981, Radhakrishnamurty, 1986), cation deficient magnetite (Radhakrishnamurty, 1986) or paramagnetic minerals. These possible interpretations can be separated to some extent on the basis of the RS values. Radhakrishnamurty (1986) reports RS values of 1.3 for low titanium titanomagnetites (x=0.1) and 1.5 for cation deficient magnetite. The RS value for susceptibility variations arising from purely paramagnetic minerals has been calculated from the Curie Law (see section 2.2) to be 3.8. Nine samples (1302, 1305, 1506, 1509, 1512, 1705, 1801 and 2003) which display group 2 behaviour, have relatively weak susceptibilities, except for 1708 and 1801. Their RS values range from 1.10 for 1801 to 2.91 for 1305. Four of these samples (1302, 1305, 1506 and 2003) have RS values greater than 1.5, indicating that paramagnetic minerals strongly influence the temperature dependent susceptibility variations of these samples.

The interpretation of the remaining group 2 samples is more difficult. The observed behaviour for these samples may either arise because the signal from paramagnetic minerals is tempered by some ferrimagnetic minerals, or because of the presence of low-titanium-titanomagnetites or cation deficient magnetite. Support for the first of these three possibilities is suggested by samples 1509 and 1705, for which the magnetic hysteresis and thermomagnetic behaviour show a relatively large paramagnetic signal. The explanation in terms of low titanium content

titanomagnetite is suggested for samples 1708 and 1801 which have Curie point temperatures of 550°C and 525°C respectively, while the group 2 behaviour of sample 1512 is best explained in terms of the presence of cation deficient magnetite, on the basis of a Curie point temperature of 620°C.

Group 3

Group 3 behaviour is considered to represent the magnetocrystalline anisotropy transition of magnetite and therefore implies the presence of multidomain particles (Senanayake & McElhinny, 1981 and Radhakrishnamurty, 1985).

More complex susceptibility behaviour may be interpreted as a combination of the groups described above but may also be attributable to the presence of other minerals. The most important category (in terms of common occurrence) of behaviour which must be discussed in this respect is the group 1/3 type. On the basis of the interpretations described above, group 1/3 behaviour arises from the combination of an assemblage of superparamagnetic and multidomain magnetite particles. Alternatively, the observed susceptibility variations could arise from a titanomagnetite of intermediate composition $0.18<x<0.55$. The susceptibility variations for these compositions are affected by the contributions of both stress and magnetocrystalline anisotropy (Appel & Soffel, 1985). This latter explanation is, however, not supported by thermomagnetic analysis which indicates a maximum titanium content $x=0.13$.

6.4.4 Discussion

The distribution of observed susceptibility types is shown in figure. 6.13. Group 1 type behaviour, indicative of superparamagnetic particles, was most commonly observed with eighty-eight of the sherds investigated showing this type of behaviour. The next most common behaviour is of group 1/3 type, which indicates a large superparamagnetic component combined with a multidomain component. In total, these two groups account for the behaviour of 82% of the samples investigated. The fraction of the total ferrimagnetic mineral content which is in a superparamagnetic state can be estimated for sherds which display group 1 susceptibility behaviour. This is done using the M_{rs}/M_s ratio determined from magnetic hysteresis measurements.

The fraction of superparamagnetic particles (M_{rs}/M_s=0) is simply determined as that which, combined with a particular fraction of stable single domain particles (M_{rs}/M_s=0.5), would give the observed M_{rs}/M_s value. The distribution of the fractional contributions of superparamagnetic particles for samples displaying group 1 susceptibility behaviour is illustrated in figure 6.14. Similar fractions cannot be obtained for group 1/3 samples, because the behaviour of the superparamagnetic and multidomain particles cannot be separated in the magnetic hysteresis data. The fraction of the total ferrimagnetic content in the multidomain state may be roughly estimated for samples which show only group 3 susceptibility

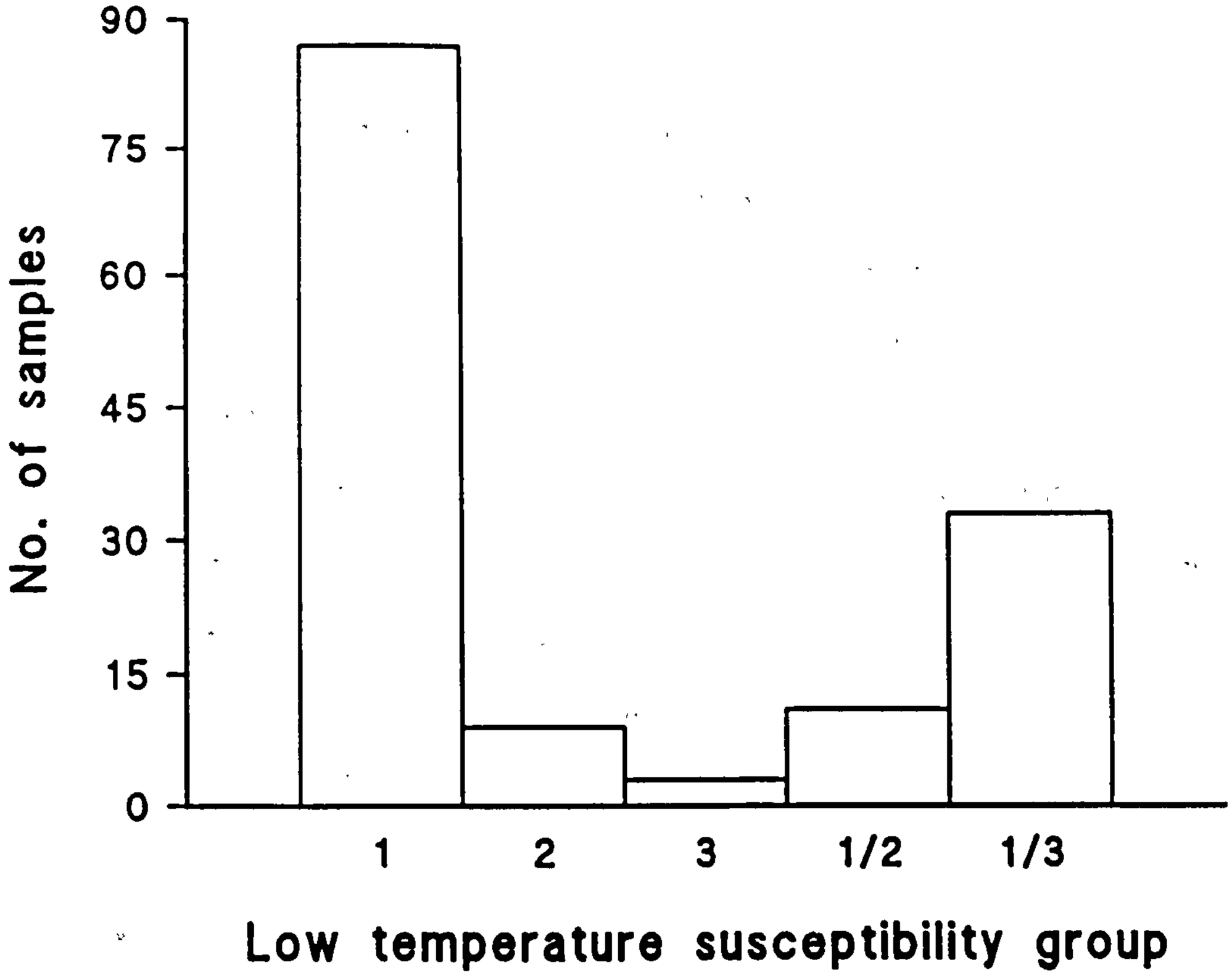

Figure 6.13. The distribution of samples between the different groups of low temperature susceptibility behaviour.

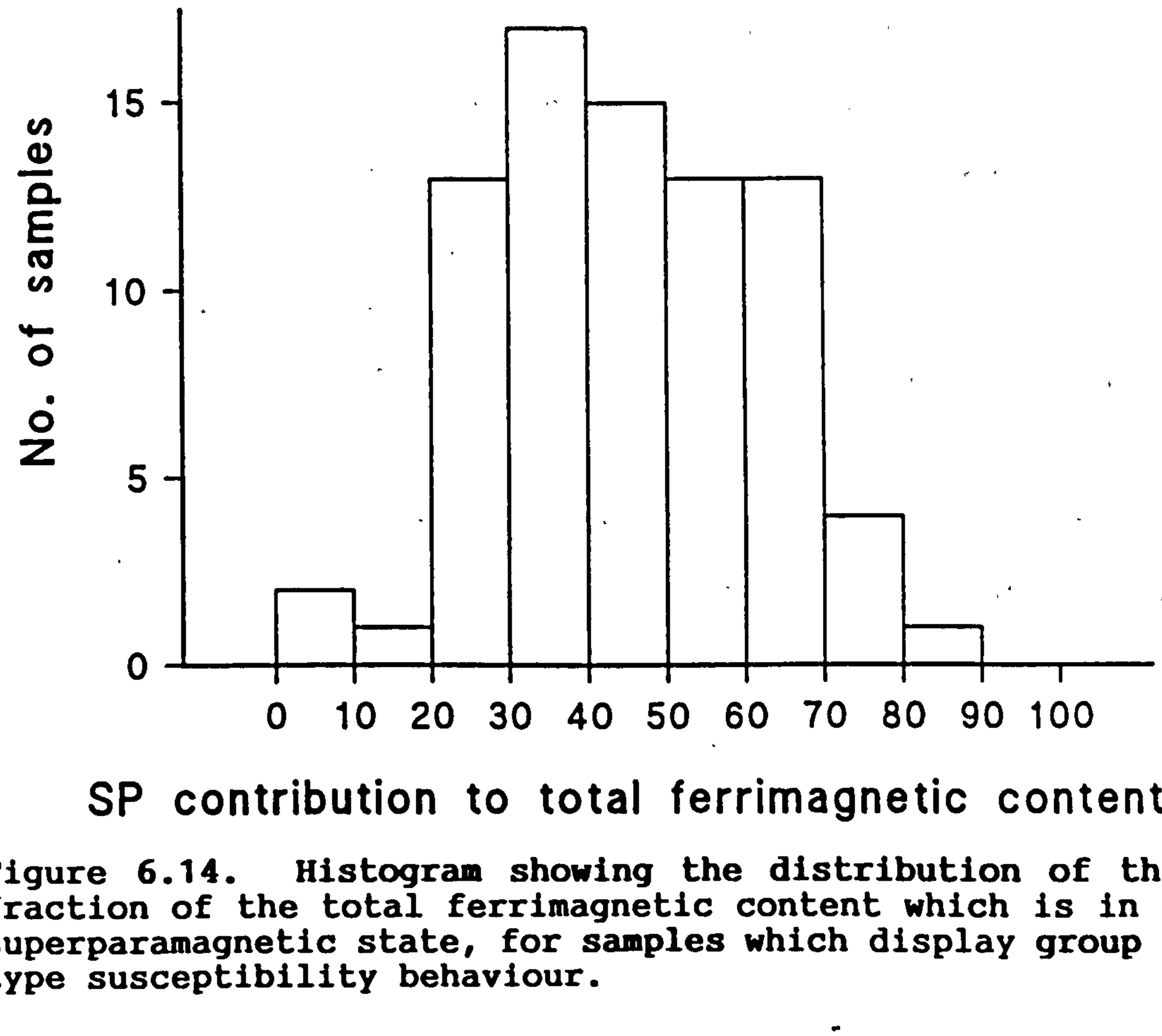

Figure 6.14. Histogram showing the distribution of the fraction of the total ferrimagnetic content which is in a superparamagnetic state, for samples which display group 1 type susceptibility behaviour.

behaviour. This requires that the ratio $Mrs/M_s=0$ is assumed for multidomain particles and it must also be assumed that the sample consists only of stable single domain and multidomain particles. The latter consideration is not strictly fulfilled since all of the samples show some frequency dependence of susceptibility, indicative of superparamagnetic particles. Only four of the samples investigated show group 3 behaviour. The estimated multidomain fractions for these samples range from 70% to 80% of the total ferrimagnetic content.

6.5 Conclusions

Low field magnetic susceptibility has been measured at room temperature using two frequencies, and from -196°C up to room temperature, in order to identify the domain states of the ferrimagnetic minerals present in the ceramics. This analysis indicates that the susceptibility of the ceramics investigated is often dominated by superparamagnetic particles. In several cases, the low temperature susceptibility behaviour is dominated by either a combination of multidomain and superparamagnetic particles or multidomain particles only.

For samples where the low temperature susceptibility variation is attributable to either superparamagnetic or multidomain particles alone (i.e. assuming that the susceptibility variation of stable single domain particles is negligible) the proportions of either the superparamagnetic or multidomain particles in a particular sample can be estimated from magnetic hysteresis data.

This estimate is simply taken as the fraction (x) of the particular domain state (either superparamagnetic or multidomain) that, combined with a fraction (1-x) of stable single domain particles, gives the observed M_{rs}/M_s ratio obtained from magnetic hysteresis measurements. The fractions determined show that superparamagnetic particles can account for as little as 5% or as much as 85% of the total ferrimagnetic particle content, with the distribution peaking between 30% to 50%.

7 Discussion of the Magnetic Mineralogy of Ancient Pottery

7.1 Introduction

A series of experiments has been undertaken to investigate various aspects of the magnetic mineralogy of the collection of ancient pottery sherds. The purpose of these experiments was to elucidate the composition, i.e. the mineral type, the concentration and the domain states of the magnetic minerals present in these sherds. Since the sample set is both geographically and temporally broad, the magnetic mineralogy information obtained may be used to draw some conclusions about the generic similarities and differences in the magnetic mineralogy of ancient pottery. This information will be applicable to archaeomagnetic intensity studies, magnetic provenancing and also to the development of magnetic viscosity dating.

The following sections describe the magnetic mineralogy of the pottery collection investigated here and then go on to discuss the bearing of this upon archaeomagnetic intensity and provenance studies. The effect of the magnetic mineralogy on magnetic viscosity dating is discussed in the following chapter where a full treatment of magnetic viscosity is presented.

7.2 Identification of the magnetic minerals

All magnetic properties depend intimately on the chemistry and structure of the magnetic material under investigation. Unfortunately many magnetic properties are

not single-valued for a particular mineralogy. For example, a measured value of initial susceptibility is dependent upon the mass of magnetic material measured, the domain states of the constituent particles and the ambient temperature, in addition to the intrinsic magnetic properties of the minerals. On the other hand, most magnetic measurements place some constraints upon the magnetic mineralogy, e.g. the maximum coercivity. In addition, the identification of magnetic minerals becomes increasingly complex when more than one mineral species contributes to the observed behaviour. For these reasons, the identification of specific magnetic minerals using magnetic measurements can be ambiguous. However, all ferro-, ferri- and antiferro- magnetic materials can be identified by the Curie point temperature which is a unique temperature above which spontaneous magnetic order is lost.

Since the Curie point temperature depends only on the type of magnetic mineral, it has been used in this study as the principal parameter for the identification of the magnetic minerals. In addition, the maximum coercivity has also been used as an aid to mineral identification, as has the variation of low field susceptibility from -196°C up to room temperature, although the latter only to a limited extent. Curie point temperatures were determined from measurements of the temperature dependence of the high field magnetisation of the samples, the details of which are discussed in chapter 3. Apart from the Curie point temperatures, the shape of the thermomagnetic curves and

the amount of alteration resulting from the heating cycle also provides information which helps towards understanding the magnetic mineralogy.

Thermomagnetic analysis was undertaken on 168 sherds. For several of the sherds more than one sample was investigated. As a result of this work, the Curie temperatures were defined for 147 sherds. The sherds for which no Curie point was defined generally contained a very small fraction of ferrimagnetic minerals and as a result the magnetisation changes with temperature were too small to be measured using the Curie balance. In some samples the signal was swamped by the magnetisation of paramagnetic minerals. Of the 21 samples for which no Curie point was defined 10 were from the Chinese II set, while the remaining 11 were spread among the other sets. The 10 Chinese sherds for which no Curie point could be defined are all very fine white translucent ware, which is usually made from a very pure kaolin and as consequence has an extremely low magnetic mineral content.

The distribution of all of the Curie point temperatures obtained is shown in figure 3.13b. The Curie point temperatures range from 475°C up to 625°C. The distribution between these two extremes is skewed towards the higher temperature and peaks in the interval 580°C to 590°. The Curie points are tightly distributed about this peak with approximately 78% of the sherds having Curie points between 560°C and 610°C. The observed distribution of Curie point temperatures peaks close to the Curie point

of magnetite (575°C, O'Reilly, 1984) which is a commonly occurring mineral. Therefore the magnetic mineral in the sherds for which the Curie point is within about 10°C of the literature value for magnetite may be identified as that mineral. Therefore, approximately 37% of sherds contain essentially pure magnetite. For several of the samples the identification of magnetite is supported by the presence of a peak in the low temperature susceptibility experiments which indicates the isotropic point of multidomain magnetite.

The wider distribution of Curie points about that of magnetite may be interpreted as arising from deviations of the mineralogy from that of pure magnetite. The distribution of Curie points below that of pure magnetite suggests that the mineralogy of these sherds contains magnetite in which some of the iron is substituted by other cation species. Substituted magnetite commonly occurs in basalt, in which the substitution species is predominantly titanium, although others such as aluminium and magnesium can occur in very small quantities (e.g. Appel & Soffel, 1985). Increasing titanium substitution leads to a progressive decrease of the Curie point temperature. Therefore, the sherds with Curie point temperatures below that of pure magnetite are likely to contain titanomagnetite. The amount of titanium substitution can be determined from the Curie point temperature and is quantified by the composition parameter x which is obtained from equation 3.3. The maximum titanium substitution

observed in this study is x=0.13, for the Romano-British sherd MC1807. The identification of titanomagnetite is supported for some of the sherds by the low temperature susceptibility behaviour. For such samples, e.g. MC1806 and MC1708, the susceptibility at -196°C is greater than that measured at room temperature as expected from previous work on titanomagnetite (Appel & Soffel, 1985).

The Curie points observed above that of pure magnetite are more difficult to interpret; the details of the interpretation are presented in chapter 3. It is suggested that these Curie points result from the presence of non-stoichiometric magnetite. Such minerals have the same structure as magnetite but the unit cell of the material does not have exactly the same composition because it lacks a fraction of the cations (Fe ions in magnetite) and is consequently referred to as cation-deficient. The Curie point temperature of the non-stoichiometric form of a mineral is greater than that for the stoichiometric form. Non-stoichiometric (titano-) magnetites are formed as a result of low temperature oxidation of an original magnetite or titanomagnetite particle, for further details see chapter 3. The Curie point temperature, the shape of thermomagnetic curve and the amount of thermal alteration are all dependent on the initial composition of the particle and the extent of oxidation. Thus, the interpretation of thermomagnetic behaviour is difficult, and may be impossible, if the cation deficient mineral is destroyed (inverted) before its Curie point temperature is

exceeded. However, the results obtained here suggest that for some of the samples the cation deficient minerals are at least partly stable to temperature or invert at temperatures above the Curie point as also observed for synthetic maghemite (Ozdemir & Banerjee, 1984).

Alternative explanations can be postulated, for example, the higher Curie point temperatures may represent a mineral in the haematite-ilmenite series, described by the formula $Fe_{2-y}Ti_yO_3$ (O'Reilly, 1984). The observed Curie points of 600-630°C indicate values for the composition parameter, y, of 0.085-0.051 (using an equation reported by Nagata & Akimoto, 1956, quoted in O'Reilly, 1984). However, this explanation would require about one hundred times more material than a cation-deficient magnetite to produce an equivalent intensity of magnetisation. This explanation is not supported by the isothermal remanence acquisition data, presented in chapter 4, which show that the largest fraction of the saturation remanent magnetisation is associated with coercivities that are typical of magnetite-type minerals rather than haematite-type minerals.

The isothermal remanence acquisition data indicates that 49 of the 108 sherds investigated contain a single distribution of coercivities, while the isothermal remanence acquisition of the remainder could be resolved into two coercivity distributions. Each coercivity distribution has been interpreted as representing a single mineral with a distribution of coercivities resulting from a distribution of particle sizes. The maximum coercivity

of each mineral present has been determined from its coercivity distribution. Since the maximum coercivity is ultimately determined by the chemical structure, and hence the composition of a material, it can constrain the choice of possible minerals which would give rise to an observed coercivity spectra. In this respect the sherds which have only a single coercivity spectrum, and the lower coercivity spectrum of the sherds which contain two spectra, indicate a maximum coercivity close to that of magnetite, i.e. 300 mT (McElhinny, 1973), see figure 4.4. This result supports the mineral identification based on the Curie point temperatures. However, in many of the sherds a second coercivity distribution was observed; the maximum coercivity of which exceeded 1 T and was commonly greater than 3 T. These higher coercivity distributions must be equated with a mineral other than a magnetite-type mineral, conflicting with the thermomagnetic data which indicates only a single magnetic mineral type in all but a few of the samples investigated. The isothermal remanence acquisition and the thermomagnetic behaviour may be reconciled when it is considered that the higher coercivity mineral in most cases contributes only a small fraction to the saturation isothermal remanence and also that the field applied during thermomagnetic measurements (~400mT) is below that required to saturate the second mineral. Thus the magnetisation of the higher coercivity mineral will most likely be swamped by that of magnetite during thermomagnetic measurements. The high coercivity mineral in all of the sherds

investigated is considered to be haematite. An alternative explanation, in terms of the presence of goethite, cannot explain the results because its maximum cöercivity usually exceeds 4 T (France, pers. comm.).

Isothermal remanence acquisition experiments were undertaken on subsamples taken from sherds of variegated colour from different regions. These sherds were invariably orange on the surface and grey or brown towards the centre. The IRM experiments showed a clear difference between the orange and grey/brown, with the saturation IRM of the orange subsamples showing a larger contribution from haematite.

The magnetic mineralogy of the sherds investigated is dominated, in terms of the intensity of magnetisation, by ferrimagnetic magnetite-type minerals. The compositions vary from that of magnetite to titanium substituted magnetite and to low temperature oxidised (cation-deficient) forms of both magnetite and titanomagnetite. The maximum titanium content has a value for the composition parameter, x, of 0.13. The degree of low temperature oxidation is very difficult to establish from the thermomagnetic behaviour because the thermomagnetic response depends on the original composition as well as the degree of oxidation. However, the oxidation parameter, z, (O'Reilly, 1984), see eq. 3.2, was estimated for a substituted titanomagnetite composition typical of those observed in this study, at about 0.038, indicating a very small degree of low temperature oxidation.

7.3 Concentration of the magnetic minerals

For many of the sherds investigated the concentration of the ferrimagnetic minerals has been estimated. The concentration, or more specifically the mass fraction, of the ferrimagnetic minerals was determined from the measured values of saturation magnetisation combined with the literature value for the saturation magnetisation of magnetite.

The saturation magnetisation values for the sherds were obtained from measurements of the magnetic hysteresis, see chapter 5 for details. By this method it was possible to obtain the saturation magnetisation from sherds in which the magnetic hysteresis loop was 'closed', i.e. reversible, above 600 mT. The mass fractions were estimated by dividing the measured saturation magnetisation by the value for the saturation magnetisation of pure magnetite. The mass fraction of the magnetite-type mineral ranges from 10^{-3} up to 21 % of the total mass for the sherds investigated. Ninety-five percent of the sherds investigated have mass fractions between 10^{-3} % and 0.65 %.

The typical mass fractions obtained for the sherds are below the typical values of 1-5% reported for rocks (Collinson, 1983).

The homogeneity of the distribution of magnetic material within a particular sherd was investigated by measuring the saturation magnetisation of pairs of subsamples. A comparison of the mass fractions determined from such pairs indicates that in most of the sherds which are visually

homogeneous the mass fractions are similar to within 10%, while for subsamples from sherds which are visually distinct, the mass fractions are dissimilar by more than 10%. In the latter situation the greater mass fraction resides in the outer part of these sherds.

7.4 Domain states

The precise nature of the size distribution and the domain structure of the ferrimagnetic particles present cannot be elucidated. However, using the remanence ratio obtained from magnetic hysteresis measurements and the classification of the variation of low field susceptibility from -196°C up to room temperature, some information about the domain states can be obtained.

The results show that sherds may contain superparamagnetic-single domain particles, stable-single domain particles and multidomain particles. Stable single domain particles can account for less than 2% up to nearly 100% of the total ferrimagnetic content of a sherd, although in 121 of the 147 sherds studied the stable single domain fractions are distributed between 32 and 76%.

The low temperature susceptibility study indicates that the remaining ferrimagnetic material is predominantly in a superparamagnetic state (supported by the frequency dependence of the susceptibility), although in many of the sherds a multidomain fraction is also apparent. Multidomain material was identified from the low temperature variation of the magnetic susceptibility. 38

of the 147 sherds investigated contain some multidomain material. However, the amount of multidomain material cannot be estimated from the available information because of the presence of superparamagnetic particles.

In general, the particle size distribution of the ferrimagnetic minerals in ancient ceramics extends from the superparamagnetic size through the stable single domain region, in which 34-76% of the particles reside, and often extends into the multidomain size region. The contribution of pseudo-single domain particles is difficult to assess because the mechanisms responsible for the observed behaviour of such particles is not well understood, also these particles may not be important since the size range for the transition from single to multidomain particles is relatively narrow.

7.5 Correlation of magnetic parameters

In the previous chapters the sample set was summarised by dividing the samples between a series of categories depending on their behaviour. In this section the different categories of behaviour obtained from the various techniques are compared and the observed correlations are discussed.

The descriptions of the various categories are given in the relevant chapters, for the thermomagnetic behaviour see section 3.10, for the isothermal remanence behaviour see section 4.7, for the magnetic hysteresis behaviour see section 5.9 and for the low temperature susceptibility

behaviour see section 6.4.4.

Table 7.1 shows the relationship between the thermomagnetic and the isothermal remanence acquisition behaviour. These are generally consistent with the predominance of magnetite or titanomagnetite, although the isothermal remanence acquisition also reveals the presence of haematite (b,c, & d), usually as a small fraction of the saturation isothermal remanence, in many of the samples (b). Table 7.1 also shows that there is little correlation between the specific thermomagnetic behaviour and the isothermal remanence acquisition characteristics.

Table 7.2 shows the relationship between the magnetic hysteresis and the isothermal remanence acquisition behaviour. The magnetic hysteresis behaviour is consistent with the isothermal remanence acquisition and the thermomagnetic behaviour in that the magnetic mineralogy is dominated by magnetite or titanomagnetites, as witnessed by the predominance of samples in the hysteresis group (a).

Table 7.1. Correlation of thermomagnetic and isothermal remanence behaviour.

	Isothermal remanence behaviour							
Thermomagnetic behaviour	**a1**	**a2**	**b1**	**b2**	**c1**	**c2**	**d1**	**d2**
a1	3	5	0	7	0	1	0	0
a2	1	3	1	2	0	0	0	0
b1	1	7	7	0	1	0	0	0
b2	2	4	1	0	0	0	0	0
c1	0	8	0	12	0	0	0	0
c2	0	10	0	2	0	0	0	0
d	0	5	0	4	1	0	0	0
e	0	0	0	1	0	4	0	1

Table 7.2. Correlation of magnetic hysteresis and isothermal remanence behaviour.

Magnetic hysteresis	Isothermal remanence behaviour							
	a1	a2	b1	b2	c1	c2	d1	d2
a1	2	2	3	2	0	0	0	0
a2	7	19	3	17	2	2	0	0
a3	0	21	2	13	0	3	0	0
b	0	0	0	2	0	1	0	0
c	0	0	0	0	0	1	0	0

However, as with the thermomagnetic behaviour, the magnetic hysteresis measurements rarely indicate the presence of haematite which is revealed by isothermal remanence acquisition.

The subdivisions of the hysteresis categories on the basis of the remanence ratio (M_{rs}/M_s) correlate with the subdivision of the isothermal remanence acquisition behaviour which is dependent on the mean coercivity of the low coercivity (magnetite) distribution. The subdivision of category (a) magnetic hysteresis behaviour into 1, 2 and 3 indicates increasing values for the remanence ratio. These subdivisions correlate with the increasing subdivisions of the isothermal remanence acquisition behaviour into 1 and 2 which indicates in an increase in the mean coercivity.

Table 7.3 shows the relationship between the low temperature susceptibility and the magnetic hysteresis behaviour. This table shows that the low temperature susceptibility behaviour of the samples investigated is predominantly of group 1 type, which is indicative superparamagnetic behaviour. Group 1 samples are mostly

Table 7.3. Correlation of low temperature susceptibility and magnetic hysteresis behaviour.

	Magnetic hysteresis behaviour				
Low temperature susceptibility	a1	a2	a3	b	c
1	4	39	34	3	3
1/2	2	5	3	1	1
2	5	4	0	0	0
1/3	3	16	10	1	3
3	4	1	0	0	0

associated with intermediate and high remanence ratios, i.e. hysteresis groups a2 and a3. This contrasts with group 3 susceptibility behaviour which, although the number of samples is small, is predominantly associated with group a1 hysteresis behaviour. The association between group 1/3 susceptibility behaviour and the magnetic hysteresis categories is intermediate between that observed for group 3 and group 1, although it is closer to the distribution of latter.

7.6 Inter-site comparisons

An understanding of the similarities and differences between sherds from the same site and between those from different sites is useful to archaeologists for determining the provenance of artefacts and for defining trade routes (e.g. Tarling, 1983). The magnetic mineralogy of artefacts is potentially useful in this respect.

Various aspects of the magnetic mineralogy may be compared. The composition of the magnetic minerals can be compared with parameters obtained from the thermomagnetic behaviour. Figure 7.1 shows an example of a comparison of the Curie point temperature and the percentage change in

magnetisation after heating for the Romano-British sherds from the same site and the Servian sherds also from the same site. It can be seen from figure 7.1 that there is some separation of the two groups of sherds, with the Servian sherds having, in general, a higher Curie point and never showing a higher magnetisation after heating. However, there is some overlap between these two culturally distinct groups which suggest that using this comparison leads to ambiguities in the identification of a sherd.

The coercivity spectrum is another potential tool for distinguishing between sherds of different origin. The isothermal remanence acquisition behaviour of the sherds studied here has been analysed by fitting a log-normal distribution of coercivities to the experimental data, see chapter 4 for details. This analysis describes each coercivity in terms of a mean log-coercivity and a standard deviation about this mean. A comparison of these parameters, again between the Romano-British and Servian sherds, is shown in figure 7.2. The two groups can be distinguished on the basis of these parameters but there is some overlap, leading to possible ambiguity in the identification of sherds.

Magnetic hysteresis provides information about the total ferrimagnetic content via the saturation magnetisation value and a measure of the single-domain fraction via the remanence ratio. These parameters may also provide a means of distinguishing between groups of sherds. Figure 7.3 shows a plot of the remanence ratio against the saturation

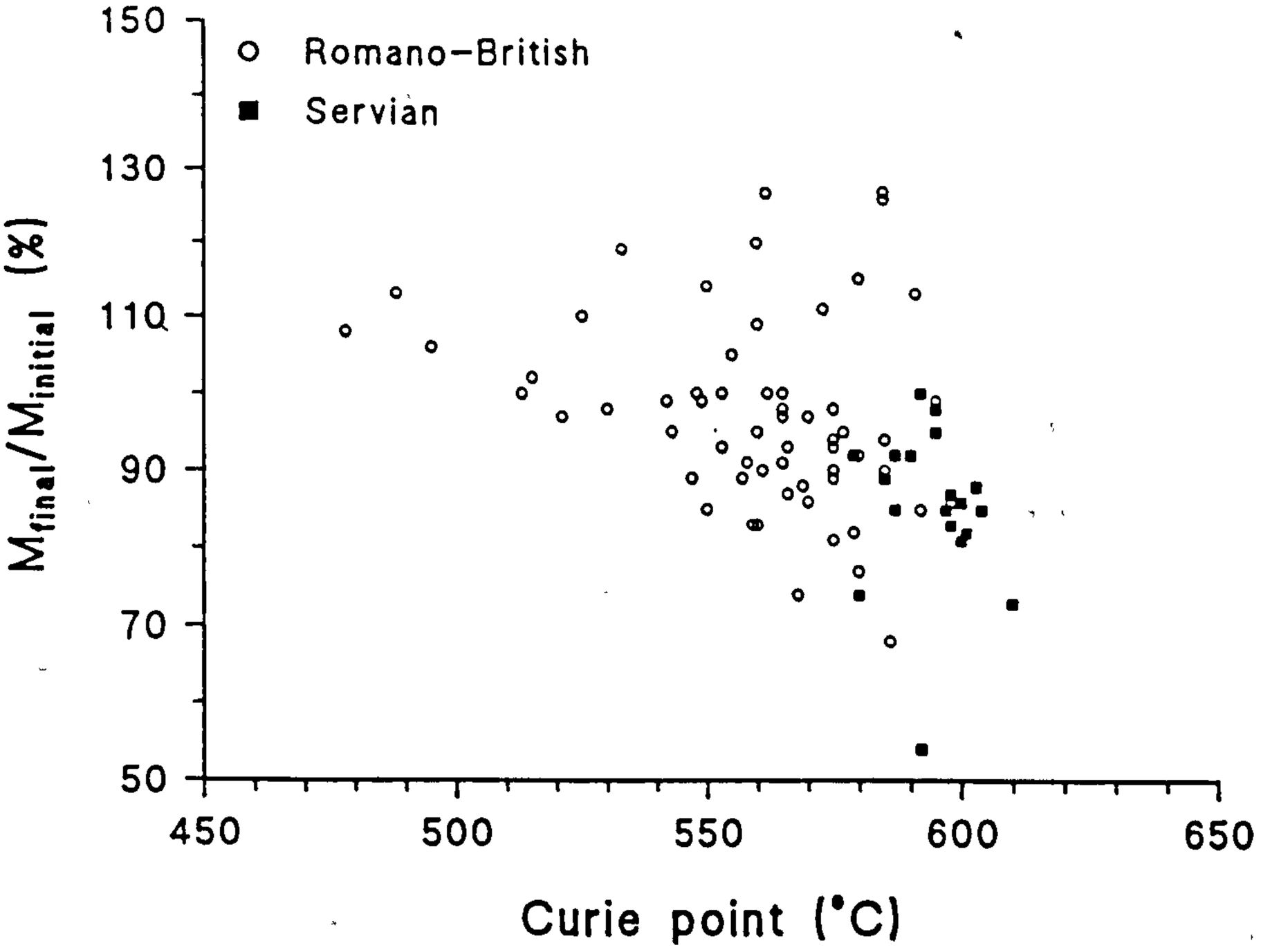

Figure 7.1. A plot of the Curie point temperature against the percentage alteration for a comparison of these parameters between and within the two groups of sherds.

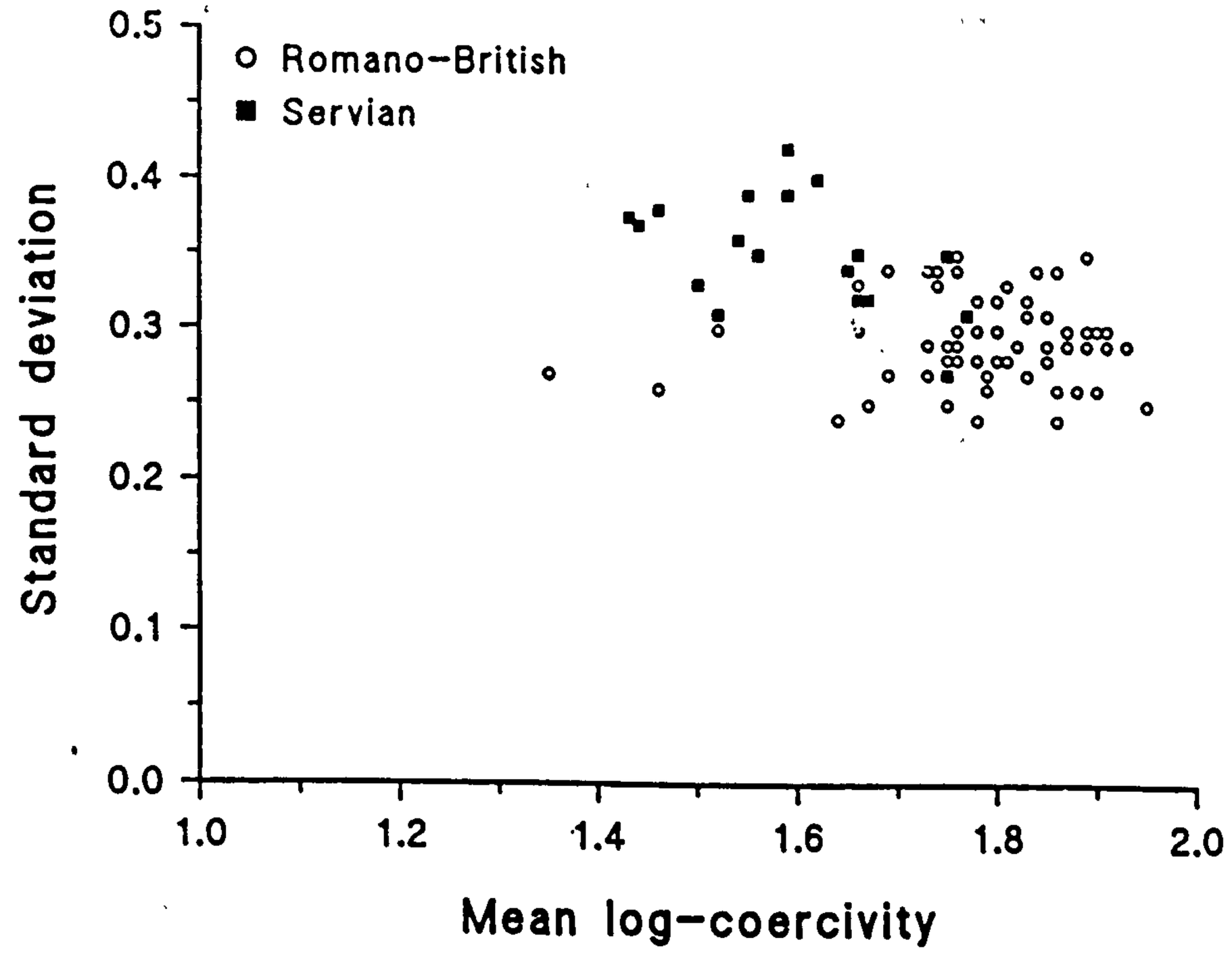

Figure 7.2. The standard deviation against the mean log-coercivity for sherds from the Romano-British and the Servian groups.

magnetisation for the Romano-British and the Servian groups of sherds. It is apparent from figure 7.3 that the remanence ratio provides a better means of separating the two groups than the saturation magnetisation.

For the two groups of sherds discussed, the isothermal remanence acquisition parameters and the remanence ratios provide the best method of distinguishing between them. Other methods, not included in the examples described here, may be better. In conclusion, the most appropriate method may depend on the particular sherds under study. However, multivariate analysis of all of the magnetic parameters discussed is likely to provide the best method for distinguishing between different groups of sherds.

7.7 Implications for archaeointensity determinations

The mineralogy and the domain states of the magnetic particles present in a material affect the original acquisition of remanence in antiquity, the alteration of this remanence over time and the retrieval of the ancient magnetic field intensity from the material.

The thermomagnetic analysis of the sherds indicates that the magnetic minerals have compositions close to that of magnetite. However, for many of the sherds there is evidence of some low temperature oxidation, while in others the magnetite contains a limited titanium substitution.

The effect on archaeointensity determinations of particles which have undergone partial low temperature oxidation is difficult to assess. If the oxidation

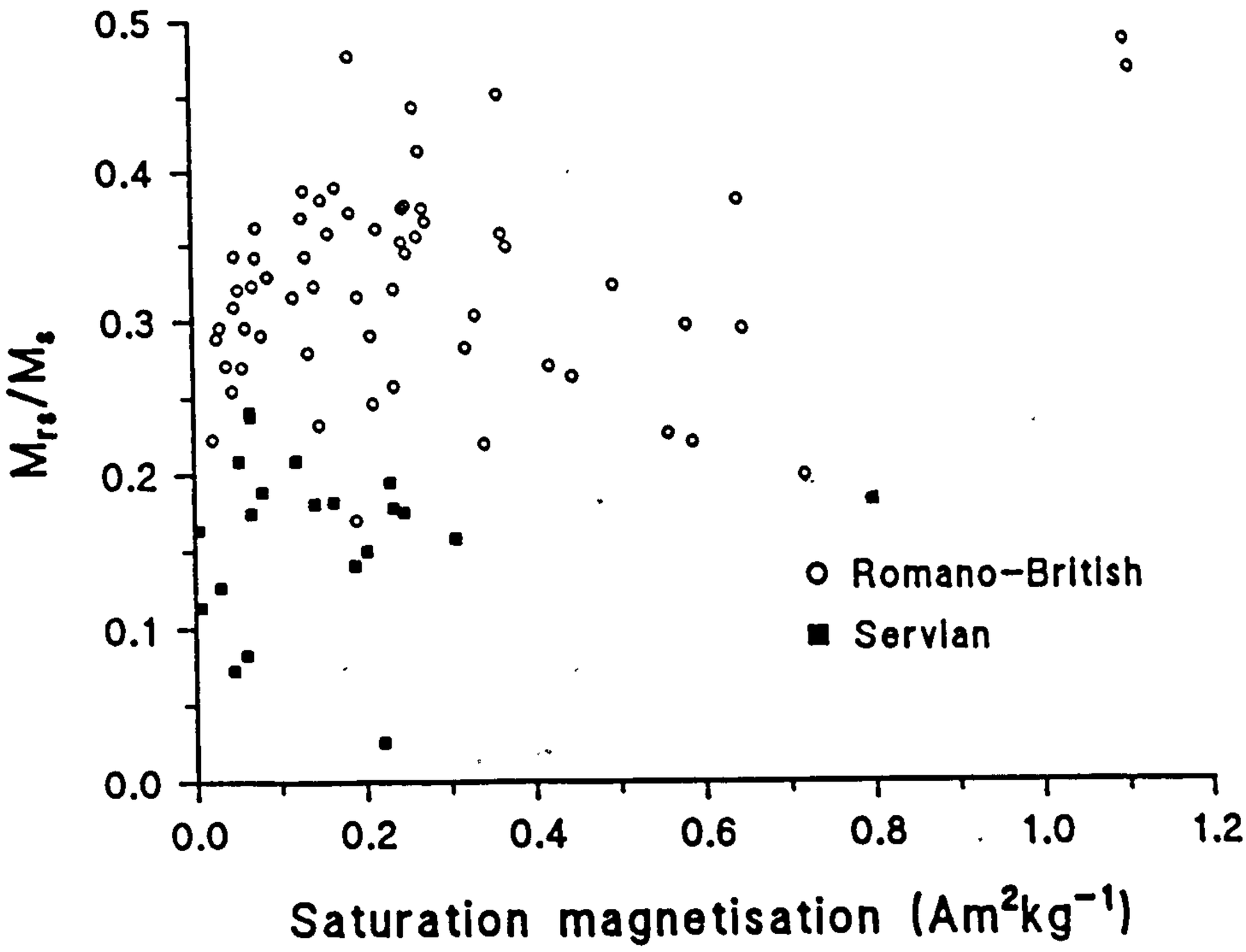

Figure 7.3. The remanence ratio (M_{rs}/M_s) against the saturation magnetisation (M_s) for sherds from the Romano-British and Servian groups.

occurred in the final stages of cooling, during the manufacture of a pot in antiquity, then the mineral may acquire a chemico-viscous remanent magnetisation (Ozdemir & Dunlop, 1989) in the same direction as the thermoremanent magnetisation. Such a chemico-viscous remanence would be difficult to distinguish from that of thermal origin and could lead to erroneous archaeointensity estimates. If the oxidation occurs over time, subsequent to the final deposition of an artefact, then the chemical remanence may be identifiable from its direction, although the original remanence direction of the particle may be retained if the magnetic moments of the electron spins in the oxidised region of a particle remain exchange coupled to the unoxidised core of the material. These problems are in

addition to that of inversion or partial inversion of cation-deficient magnetite which leads to a considerable reduction of the remanent intensity.

The sherds which contain titanomagnetite may be problematic if they oxidise during high temperature laboratory treatment as this can significantly change the mineralogy. High temperature oxidation is more of a problem for single heating intensity techniques, such as the alternating field method of Shaw (1974), since the heating is carried out at a single high temperature.

The domain states of the magnetic minerals are also important for archaeointensity determinations. The results of this study show that the ferrimagnetic content of ancient pottery is often made up of a large fraction of superparamagnetic and stable single domain particles. This distribution suggests that ancient pottery contains a considerable fraction which is susceptible to viscous activation across the superparamagnetic-stable single domain boundary.

The variation of susceptibility from -196°C up to room temperature indicates that many of the sherds investigated contain a measurable fraction of multidomain particles in addition to single domain particles. This may lead to problems for two reasons. Firstly, it has been shown experimentally that for samples which contain multidomain magnetite the NRM-TRM intensity plot can be curved without the presence of thermal alteration (Levi, 1977). This problem is probably associated with the complex mechanism

of distributed unblocking (e.g. Dunlop, 1983). The second problem associated with a mixed assemblage of single- and multi-domain particles is that they exhibit opposite cooling rate effects. Thus, for a laboratory cooling rate which is faster than the original, then the single domain fraction will acquire a less intense magnetisation, while the multidomain magnetisation will be more intense than that acquired in antiquity.

This discussion points out some of the more well understood problems which are associated with archaeomagnetic intensity determinations. However, several other problems which cannot be easily and unambiguously defined, contribute to the difficulties of obtaining accurate archaeointensity estimates (e.g. Gubbins & Roberts, 1983, Sternberg, 1989). For example, inaccuracies in the dating of artefacts or the occurrence of rapid secular variation (e.g. Shaw, 1979) can lead to erroneous interpretation. For such reasons a detailed archaeointensity study of the sherds investigated here is of little value because many of them are poorly dated, making comparisons with existing secular variation curves (where such curves exist) difficult. However, a limited comparative archaeointensity study has been carried out using the alternating field demagnetisation technique of Shaw (1974) with the addition of the anhysteretic remanent magnetisation (ARM) correction method of Rolph & Shaw (1985). The experiments were carried out using the integral squid magnetometer and demagnetisation system

described by Shaw et al.(1985).

The data are extremely varied which makes the definition of an archaeointensity result very difficult and of only limited value.

The internal consistency of the archaeointensity data has been tested by measuring two, nominally similar, subsamples from some sherds. The archaeointensity data of the two subsamples from the Servian sherd MC1603 is similar with both showing nearly linear NRM-TRM behaviour and both having similar values for the archaeointensities obtained. On the other hand, the archaeointensity behaviour of the two sub-samples from the Romano-British sherd MC1904 differs considerably in the degree of non-linearity of the NRM-TRM plot, see figure 7.4, and also the intensity values obtained from linear portions of the NRM-TRM plots are considerably different.

Within site comparisons have been made for sherds from the Servian and Romano-British groups since the sherds within each of these groups are geographically and temporally related. Thus, the sherds within each group may be expected to have been fired in the presence of an ambient magnetic field of similar intensity, therefore allowing variations in the intensity behaviour to be related to difference between the magnetic mineralogies of the sherds. Three Servian sherds, MC1602, MC1603 and MC1604 were investigated. These sherds all have similar Curie point temperatures, group 1 type low temperature susceptibility behaviour, as well as having similar

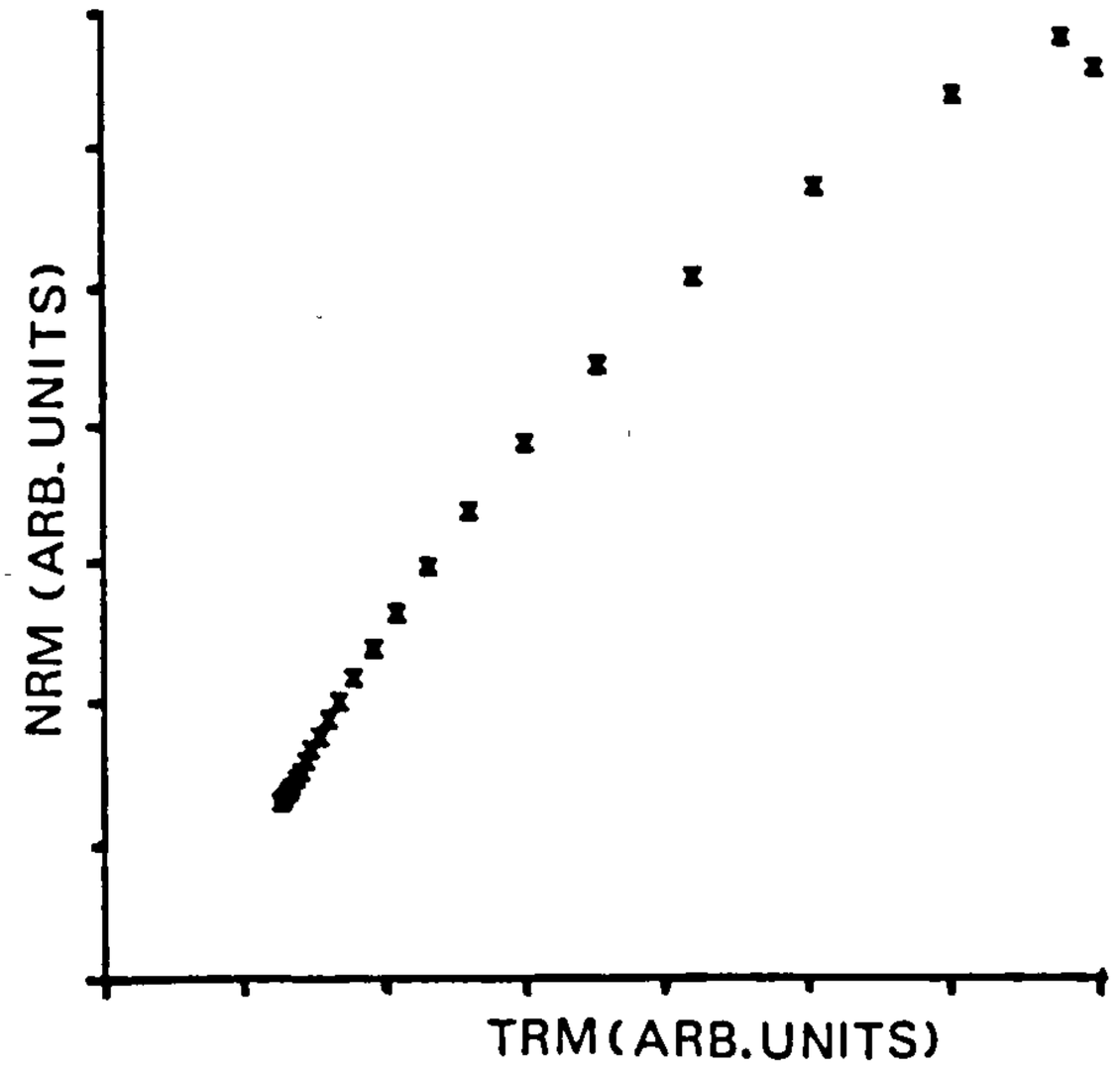

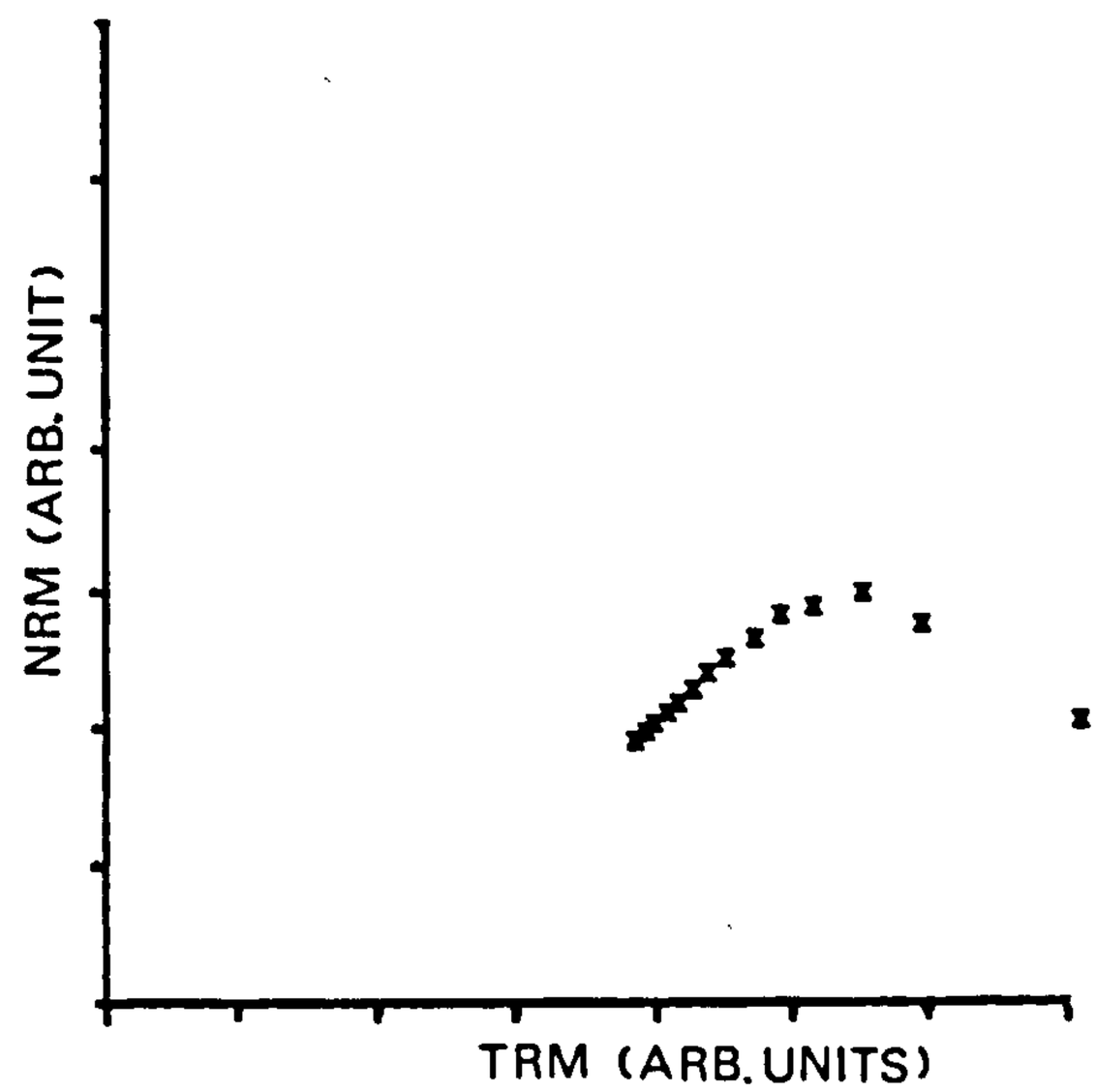

Figure 7.4. The NRM-TRM plots for two subsamples from sherd MC1904, obtained by alternating field demagnetisation of the original ancient NRM, and of a laboratory induced TRM.

magnetic hysteresis and isothermal remanence characteristics. However, the archaeointensity determinations vary considerably with values of 88.4 +/- 3.4 μT for MC1602, 51.2 +/- 0.5 μT for MC1603 and 35.2 +/- 0.6 μT for MC1604. The only apparent differences in magnetic behaviour occur in the form of the thermomagnetic behaviour. The thermomagnetic behaviour of MC1602 shows a slight increase in the magnetisation after the heating cycle, while the behaviour of MC1603 is essential reversible in form and the thermomagnetic behaviour of MC1604 is irrevrsible, having a inflexion on heating and a reduced magnetisation on cooling.

The archaeointensity behaviour of the Romano-British sherds MC2002 and MC2104 is similar in the shape of the NRM-TRM plots and also in that the field intensities obtained from the linear region of the NRM-TRM plots are similar, i.e. 43.3 +/- 0.8 μT for MC2002 and 40.1 +/-1.1 μT for MC2104. These samples have similar magnetic mineralogy in all but the fact that the Curie point temperature of MC2002 suggests that this sherd contains slighly titanium substituted magnetite while MC2104 contains essentially pure magnetite, thus indicating that under suitable conditions both types of magnetic mineral give acceptable results. The behaviour of other Romano-British sherds was more complex and could not be obviously related to any of the measured parameters.

The archaeointensity data of almost all of the sherds investigated shows some non-linearity in at least part of

the complete NRM-TRM plot which may be attributable to thermal alteration. However, the NRM-TRM relationship of the single sherd investigated from the Chinese II set (MC2705) is very closely linear throughout the data set, see figure 7.5. The ferrimagnetic minerals in this sample are in very low concentration compared to the bulk of the samples investigated here and as a consequence little information could be obtained. However, it is suggested that the fundamental reason for the improved archaeointensity data lies in the manufacture of the Chinese sample. In contrast to all of the sherds in the other groups, which are medium or fine ware, some of the Chinese II set sherds , including the MC2705, are very fine white ware which suggests a very high firing temperature. This heat treatment probably lead to the stabilisation of the magnetic minerals and the very fine structure probably gave the sherd greater protection from subsequent environmental attack during burial, thus preserving the original stable mineralogy.

7.8 Conclusions

The magnetic mineralogy of the ancient pottery investigated is dominated, in terms of the intensity of magnetisation, by magnetite-type minerals. These minerals are slightly titanium-substituted in many of the samples and also in many cases show behaviour which is consistent with limited low temperature oxidation. The presence of haematite was identified in 59 of the 98 sherds which were investigated using isothermal remanence acquisition.

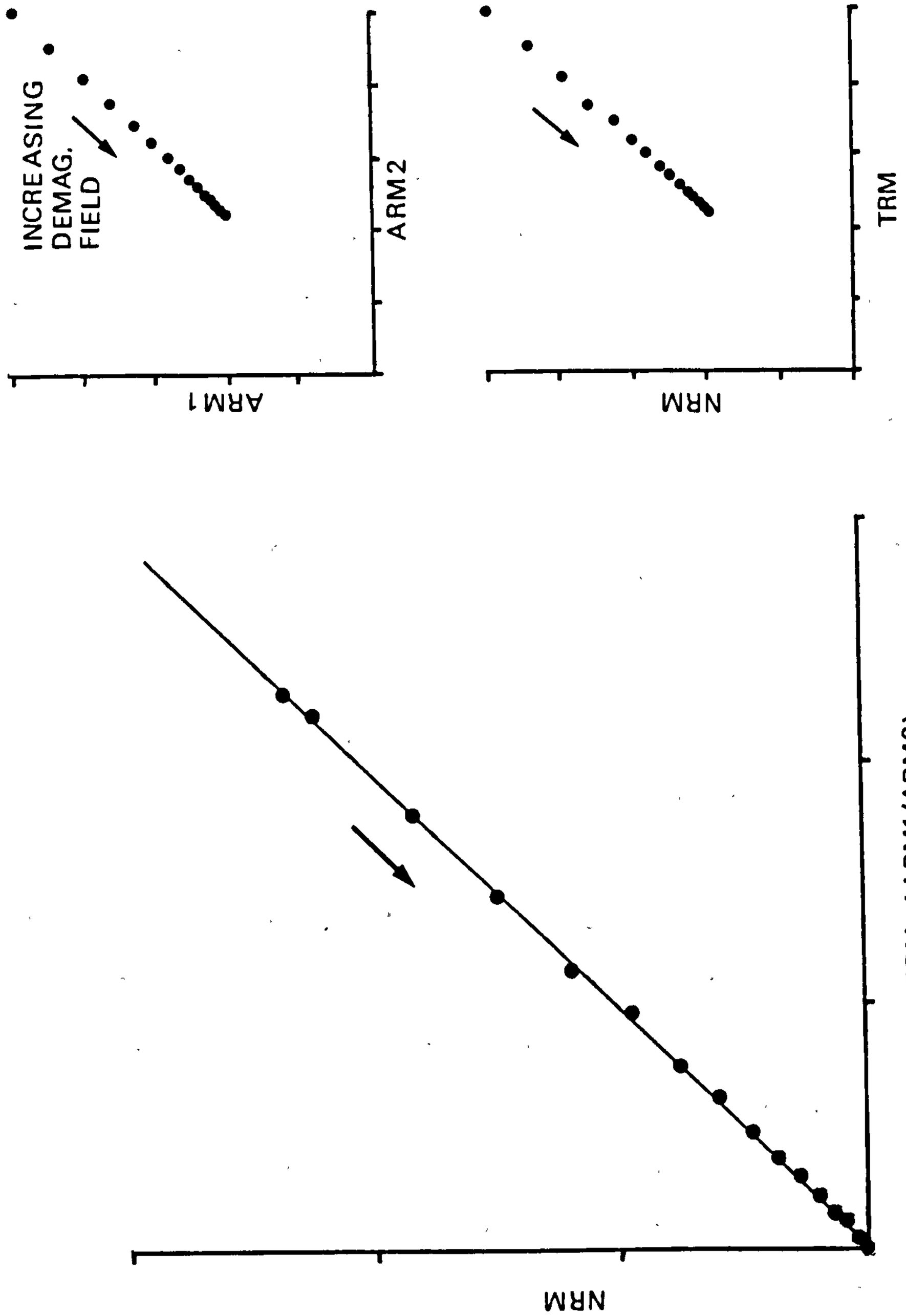

Figure 7.5. The NRM-TRM, ARM1-ARM2 and the ARM corrected NRM-TRM plot for the Chinese samples MC2705.

However, haematite accounted for less than 10% of the total SIRM in 43 of these sherds.

The Curie point temperature and the amount of thermal alteration of the magnetic minerals can be characteristic of a particular group of sherds, for example the Romano-British sherds often have Curie points indicative of titanomagnetite. However, the distribution of Curie points (see figure 3.13b) indicates that considerable overlap occurs between the Curie point distributions of the different groups. This limits the use of the Curie point temperature for distinguishing between groups of sherds.

The distribution of the mean log-coercivity against the standard deviation of the coercivity distribution provides another way of distinguishing between groups of sherds. The two groups of sherds could be separated by this method although there was some overlap of the two data sets. A comparison of the remanence ratio and the saturation magnetisation, obtained from magnetic hysteresis measurements for the same two groups of sherds, showed that the these groups were most easily separated on the basis of the remanence ratio alone. The distributions of saturation magnetisation in the two groups were similar, providing no indication of the origin of a sherd. This is in contrast to the work of Coey et al. (1979) who found that the various groups of sherds they investigated could be identified according to the value of their saturation magnetisation.

Some of the sherds containing titanomagnetite or low

temperature oxidised magnetite may be problematic for archaeointensity determinations because they are especially susceptible to thermal alteration. Some of the sherds which contain titanomagnetite show signs of high temperature oxidation in the thermomagnetic behaviour, e.g. figure 3.7d and 3.9a, while the low temperature oxidised magnetite may be inverted on heating, e.g. figure 3.3d and 3.6d.

The particle size distributions of the pottery samples investigated show that the ferrimagnetic particles occur, in a variety of superparamagnetic, stable-single domain and multidomain configurations. Superparamagnetic and stable single domain particles dominate the ferrimagnetic mineralogy of many of the sherds, although the presence of multidomain particles is evident from the low temperature susceptibility behaviour.

8 Magnetic viscosity: An alternative dating tool?

8.1 Introduction

A time dependent change in the magnetisation of a ferromagnetic material, in the presence or absence of a magnetic field, is termed magnetic viscosity, following the nomenclature of Ewing (1885).

Demagnetisation data obtained from palaeomagnetic investigations of a variety of lithologies, including basalt (e.g. Piper et al., 1991) and loess (Rolph, et al., 1989), often reveal the presence of a secondary component of magnetisation which has a low unblocking temperature and/or a low coercivity spectrum and is usually directed towards the present geomagnetic field direction. Such components are commonly attributed to the effect of magnetic viscosity (see Wilson & Smith, 1968) and are termed viscous remanent magnetisation (VRM). Viscous magnetisation has also been identified in archaeomagnetic directional investigations of in-situ kilns, hearths and burnt floors, and walls (e.g. Thellier, 1937, Schurr, Becker & Soffel, 1984, Sternberg, 1989) and by the presence of a low temperature component of differing slope observed on Arai plots during archaeointensity studies of materials not in-situ such as pottery sherds (Aitken, 1983).

The time dependent nature of magnetic viscosity and its contribution to the magnetic remanence of many natural materials has led to the suggestion of its use as a dating tool. This possibility was investigated by Creer (1957) and Heller & Markert (1973); both studies reported reasonable

success. The development of a dating method based on magnetic viscosity appears, therefore, to be a distinct possibility. However, recent developments in both experimental and theoretical work on magnetic viscosity require a reappraisal of the previous work and may lead to the development of an alternative magnetic viscosity dating technique. This requires an understanding of the theoretical and experimental aspects of magnetic viscosity.

8.2 A review of theoretical and experimental magnetic viscosity

8.2.1 Introduction

Time dependent changes of the isothermal magnetisation of a variety of materials have been investigated by many workers (for a review up to 1973 see Dunlop, 1973). Viscous magnetisation has often been observed to vary linearly with the logarithm of time (t) (e.g. Street & Woolley, 1949, Creer, 1957, Shimizu, 1960 and Prevot, 1981) and consequently the growth or decay of viscous magnetisation, M(t) is often described by the expression:

$$M(t)=S \ln(t) \qquad (8.1)$$

where S is the coefficient of viscous acquisition or decay (see for example Tarling, 1983). However, there are also many reports of viscous magnetisation changes which are non-linear with the logarithm of time (e.g. Tivey & Johnson, 1981, 1983, Chantrell, Hoon & Tanner, 1983, Dunlop, 1983 and Moskowitz, 1985); the viscosity coefficient in such cases is the slope of the magnetisation-against-time curve and is itself time

dependent. From the theoretical treatments of magnetic viscosity, which are discussed later, it is clear that both linear and non-linear log time relations may be expected, although the mechanisms of some viscous changes, e.g. those in multidomain magnetite particles (Dunlop, 1983), are not fully understood.

The physical mechanisms suggested to account for the phenomenon of magnetic viscosity include thermal fluctuations, diffusion of cations and vacancies, chemical changes and eddy currents (see Moskowitz, 1985). The effect of eddy currents is of most importance in electrically conductive materials such as steel. Eddy currents are therefore ignored in the following discussion which is restricted to naturally occurring minerals, in particular magnetite, which is a poor conductor. Chemical changes are also omitted here, although their importance in natural materials is recognised and has been discussed earlier.

8.2.2 Theory

The first theoretical description of magnetic viscosity was presented by Richter (1937) as part of a study of magnetic after-effects in steel. Richter's model, although phenomenological, suggesting no physical mechanism for moment changes, brings in the concept of viscosity as a relaxation process. The relaxation process is characterised by the relaxation time, τ, which is a measure of the time required for the magnetisation of a particular fraction of an assemblage to change. τ is analogous to the

half-life in radioactive decay. Richter presents the time dependence of the relaxation of magnetisation as the following expression:

$$M(t)= \beta \int f(\gamma)\exp(-t/\gamma)d\gamma \qquad (8.2)$$

where M(t) is the magnetisation at time t, $f(\gamma)$ is the distribution of log relaxation times and ß is a constant related to the magnetisation at t=0. Richter used equation (8.2) to model his data by using a truncated distribution function of the form illustrated, see figure. 8.1. The Richter model gives an observed time dependence for viscosity which is linear with respect to the logarithm of time (t) when t is well within the limits of the relaxation time distribution, i.e. $\gamma_{min} < t < \gamma_{max}$.

By analogy with dielectrics, Becker & Doring (1939) also described viscosity as a relaxation process and also predicted log t dependence in some situations (quoted in Street & Woolley, 1949). In 1949, two important contributions were made to the theory of magnetic viscosity. Street & Woolley (1949) described magnetic viscosity as an activation energy process, appealing to the mechanism of moment rotation in single domain particles as described by Stoner & Wolhfarth (1948) for changes of magnetisation. They suggested that in the case of magnetic viscosity, discontinuous moment rotation results from stress fluctuations arising from thermal agitation. Street & Woolley successfully applied their theory to experimental data from an alloy of aluminium, nickel, cobalt and copper.

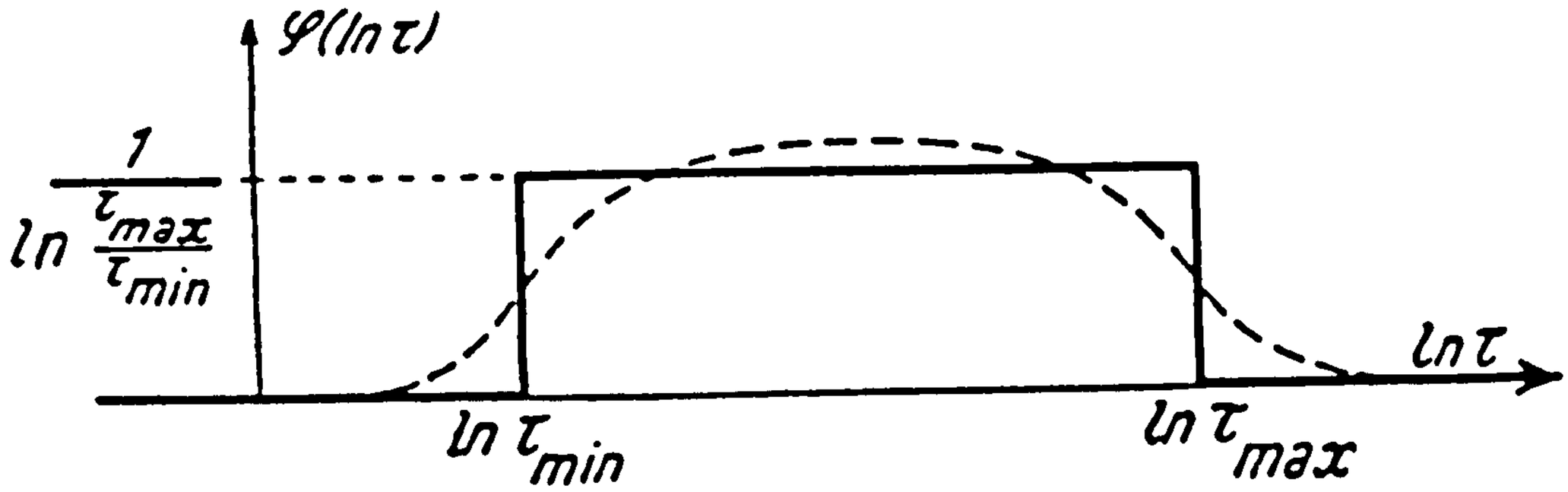

Figure 8.1. Distribution function of relaxation time constants. The dashed line is the actual function within the limits of the integral in equation 8.2 and the solid line is the distribution used in calculations. From Richter (1937).

They obtained a log-time dependence for the acquisition of viscous magnetisation, but made no attempt to define the activation energy, and hence relaxation time, in terms of other physical properties. Néel (1949) similarly suggested that magnetic viscosity was a thermal activation process in single domain assemblages and also that the activation energy and relaxation time are dependent on perturbing couples which "arise from elastic deformations of the grain by thermal agitation" (Néel, 1955). However, Néel (1949) went further than Street & Woolley (1949) by considering the effect of the thermally induced shape changes on the demagnetising field and magnetoelastic energy, from which the relaxation time for uniaxial single domain particles was described. Néel (1949) described the relaxation time

in terms of the absolute temperature, T, the saturation magnetisation, M_s, the particle volume, v, and the microscopic coercivity of the particle, H_c, according to the expression:

$$\frac{1}{\tau} = C \exp\left(\frac{-vH_cM_s}{2kT}\right) \qquad (8.3)$$

where C is a rate constant and k is Boltzmann's constant. Equation (8.3) is strictly applicable only to situations in which thermal relaxation occurs in zero magnetic field. The relaxation time for an assemblage of particles is altered in the presence of an applied magnetic field, h, such that the rate of transition from the field oriented easy direction to the field opposing (-) easy direction, and the rate of transition from the field opposing, to field oriented (+) easy directions, are modified from equation (8.3) to:

$$\frac{1}{\tau^+} = C \frac{(1-h)\ (1-h^2)^{0.5}}{(H_c)\ (H_c^2)} \exp\left(\frac{-vM_s(H_c-h)^2}{2H_ckT}\right) \qquad (8.4a)$$

$$\frac{1}{\tau^-} = C \frac{(1+h)\ (1-h^2)^{0.5}}{(H_c)\ (H_c^2)} \exp\left(\frac{-vM_s(H_c+h)^2}{2H_ckT}\right) \qquad (8.4b)$$

with the overall relaxation time given by:

$$\frac{1}{\tau} = \frac{1}{\tau^+} + \frac{1}{\tau^-} \qquad (8.5)$$

In the context of single domain particles of minerals such as magnetite, the change in the relaxation time due to h is negligibly small when the magnitude of h is of the

same order as the geomagnetic field. As a consequence, h has been ignored in subsequent theoretical treatments of magnetic viscosity (e.g. Walton, 1980, Worm & Jackson, 1988). The relaxation time equations derived by Néel have formed the basis of most time-temperature work, on single domain systems, such as thermal demagnetisation and magnetic viscosity. Equation (8.3) has recently been shown to be identical (except for the constant C) to the expression obtained from a more fundamental approach by Walton (1986).

Theoretical modelling of thermally activated magnetic viscosity in assemblages of single domain particles, has principally involved determining the magnetisation changes produced by the spectrum of relaxation times associated with the distribution of particle sizes in the assemblage. Stephenson (1971) considered the growth of viscous magnetisation in terms of the superparamagnetic-stable single domain boundary sweeping, with time, through a distribution of particle volumes. The viscous magnetisation acquired in a small field h, was defined from this according to:

$$M(t) = \int \frac{1}{3} v M_s N(v) \; v \frac{M_s h}{kT} \, dv \qquad (8.6)$$

where N(v) is the particle size distribution to which Stephenson put $N(v)=Bv^r$ and obtained from (8.6) by substituting for v and v_1 the expression:

$$M(t)=\frac{M_s^2 hB}{3kT}\frac{2kT}{M_s H_c}(Q+\ln\tau_o)^{r+3}+\frac{1}{r+3}\frac{(1+\ln\tau-\ln\tau_o)^{r+3\cdot1}}{Q+\ln\tau_o} \qquad (8.7)$$

where Q=ln C. According to this expression and providing γ is well away from its maximum or minimum value, the time-dependence of viscous magnetisation depends on the volume distribution and is logarithmic only when r=-2, with M(t) increasing more quickly than log t for values of r>-2 and more slowly for r<-2, see figure 8.2. Stephenson's treatment has been criticised for taking the microscopic coercivity as a constant which is independent of the particle volume (Dunlop, 1973) although it has been pointed out that the particle volume varies more rapidly than the coercivity (Williams, 1986). The theoretical treatments of Walton (1980), Williams (1986) and Worm & Jackson (1988) are similar to that of Stephenson (1971) in their inclusion of a volume distribution of the form $N(v)=v^r$ and a single valued microscopic coercivity H_C, and consequently these models produce a similar dependence time which varies with r and is logarithmic only for r=-2. However, these more recent treatments also consider the effect of temperature and involve the temperature dependence of the saturation magnetisation and the microscopic coercivity. Worm et al. (1991) have considered a more realistic model which includes the distribution of microscopic coercivities as well as the volume distribution.

8.2.3 Single domain viscosity experiments

Experimental investigation of single domain systems is difficult because of the relative difficulty of producing

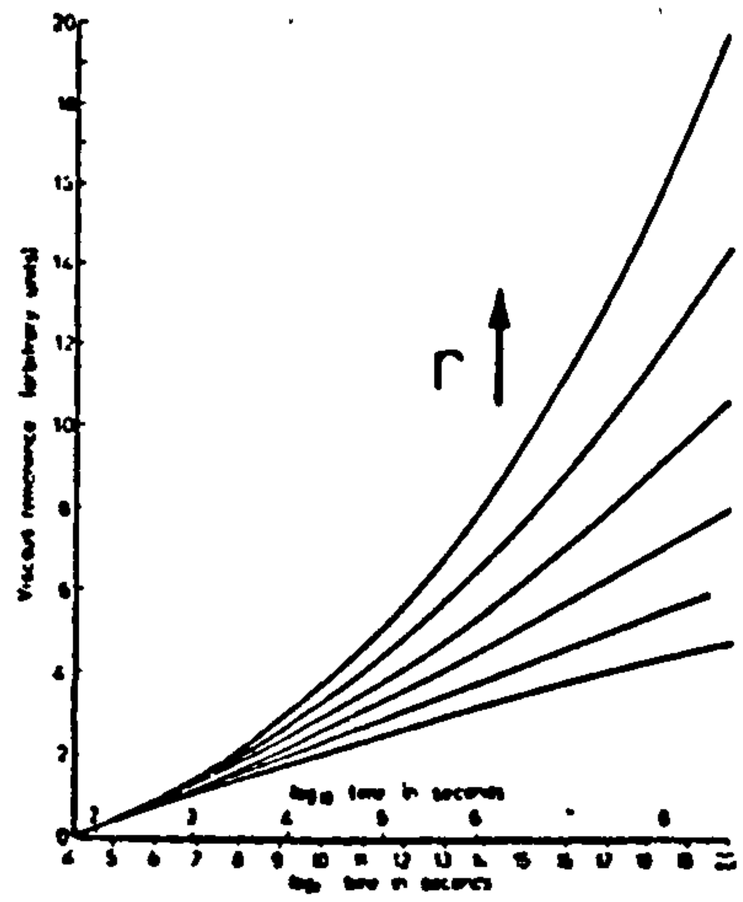

figure 8.2. The growth curves of viscous remanent magnetisation for different particle volume distributions described by N(v)=vr. From Stephenson (1971).

and characterising assemblages which contain sufficiently small particles. For magnetite, of particular interest to this study, the critical size for the transition from single domain to multi-domain in cubic particles has been calculated to be 0.08 um (Butler & Banerjee, 1975), although it has been suggested that metastable single domain configurations may exist in larger particles (Moon & Merrill, 1985, Scherbakov & Lamash, 1988) see section 2.5. Also, the critical size is dependent on the particle shape through its effect on the magnetostatic energy which leads to an increase in the maximum single domain size with increasing particle elongation. Experimental work on the magnetic viscosity of single domain magnetite is limited. Tivey & Johnson (1981, 1984), Dunlop (1983), Williams (1986) and Worm et al. (1991) report experimental work on single domain or near single domain size particles. The particle sizes (including standard deviations where given),

coercivity and M_{rs}/M_s ratios for the samples investigated in these studies are given in table 8.1. In all of the studies discussed, viscous magnetisation was measured in the presence of the applied field. The particle sizes given in table 8.1 are, in most cases, greater than the theoretical maximum value for cubic particles. Also, the remanence ratio, M_{rs}/M_s, is, in all but one case, less than the theoretical value of 0.5. However, the reported sizes may be single domain if the particles do not have cubic geometry. This is clearly the case for sample TODA, and the irregularity of shape has been suggested by Williams (1986) to support his argument that samples 63F and 69B contain single domain particles. The samples of Dunlop (1983) are reported to have cubic geometry and therefore should have a maximum single domain size close to that expected from Butler & Banerjee (1975), suggesting that both the 0.037 um and the 0.076 um samples contain predominantly single domain particles and that the 0.221 um sample mostly contains particles slightly above single domain size. The measured M_{rs}/M_s values, shown in table 8.1, are in excess of those expected for an assemblage of multi-domain particles (except for sample z) which can be interpreted as resulting from particle size distributions which range from superparamagnetic through stable single and pseudo-single to small multi-domain sizes, with a significant fraction of particles in the stable single domain size region. The M_{rs}/M_s ratios and H_c values may be further reduced by particle interactions (Davis & Evans,

Table 8.1. Particle sizes and magnetic parameters from investigations of viscosity in single domain magnetite.

Code	Size (μm)	Standard deviation (μm)	H_c ($\times 10^3$ Am^{-1})	M_{rs}/M_s	Reference
Z	0.016	-	1.3	0.0025	Tivey & Johnson (1981)
LR	0.110	-	10.3	0.135	" "
CC	0.210	0.06	13.9	0.177	" "
TODA	0.35x0.04 rods		33.4	0.430	" "
	0.037	0.015	13.9	0.254	Dunlop (1983)
	0.076	0.025	14.3	0.270	" "
	0.100	0.029	13.1	0.262	" "
	0.221	0.042	10.7	0.174	" "
63F*	0.300	-	37.0	0.440	Williams (1986)
69B*	0.100	-	39.0	0.500	" "
*	0.025-0.100		46.6	0.467	Worm et al. (1991)

* indicates samples prepared by the glass ceramic method of Worm & Markert (1986), the other samples were prepared by dispersion of powders.

1976). This is supported to some extent by the data for samples prepared by dispersion of magnetite powders, which are likely to have interacting clusters, having lower M_{rs}/M_s ratios than samples with similar particle sizes where the particles were grown in separation by the glass ceramic method described by Worm & Markert (1986).

Tivey & Johnson (1981, 1984) investigated four samples with particle sizes or remanence ratios that indicate they contain a predominance of single domain particles. The samples were obtained from various sources with varying details provided. Information about the particle size distribution is only presented for sample CC, in the form of a standard deviation. The viscosity experiments were carried out at room temperature and involved the

acquisition of viscous remanent magnetisation in a field of 100 μT over a period of 16 hours and the zero field decay of viscous remanence over 8 hours, with the first data taken after about six minutes giving approximately two decades of log-time. Under these experimental conditions Tivey & Johnson investigated the effect of magnetite concentration, varying the proportion of magnetite from less than 1% to greater than 20% and concluding that, within their experimental capacity, the gross concentration of particles has no first order effect. This is suprising since McClelland-Brown (1984) observed a large difference in the cooling rate dependence of thermoremanent magnetisation of single domain magnetite for concentrations of 0.19 and 2.14%. Unfortunately, the coercivities and remanence ratios for the different concentrations are not given by Tivey & Johnson, so the effect of interactions, which may be expected to increase with concentration, cannot be tested. Tivey & Johnson also describe the effect of zero field storage, after a pretreatment involving the induction of a thermoremanence by cooling from 620°C and alternating field demagnetisation at 80 mT, prior to the acquisition of viscous remanence. They report that for increased storage time, the rate of viscous acquisition decreases. This effect is not predicted by the thermal activation theory discussed. Williams (1986) supposes that the storage time effect is an artefact of the alternating field demagnetisation prior to zero field storage which, it is suggested, does not remove all of the viscous remanence

remaining from previous experiments. This is incorrect since according to Tivey & Johnson (1981) the samples were given a thermoremanence after each experiment and prior to demagnetisation, therefore imposing the same initial conditions each time. However, the effect may be attributable to contamination by multi-domain particles for which the acquisition rate can be affected by the diffusion of defects (discussed later) which is also a thermal activation process controlled by time and temperature (Kronmuller, Schutzenauer & Walz, 1974, Moskowitz 1985). An alternative mechanism suggested by Moskowitz (1985) is that the observed effect arises from moment changes due to defect diffusion in single domain particles. Unfortunately the lack of detailed particle size information leaves this to speculation. Further, the lack of detailed particle size distributions and experiments at high temperature does not allow the theoretical models to be tested, although the time dependence of viscous acquisition which was observed to be non-linear with the logarithm of time indicates a particle size distribution defined by $r>-2$ in those models.

The experimental work of Dunlop (1983) is more comprehensive and systematic than that of Tivey & Johnson (1981, 1984). Dunlop (1983) reports the time and temperature dependence of acquisition and decay of viscous magnetisation in single domain samples as part of a wider study of the magnetic viscosity of magnetite. The submicron magnetites were obtained by precipitation which produced cubic particles with a high degree of

crystallinity and small spread of sizes. The particle size distributions are presented in the form of mean particle size and standard deviation. The magnetic viscosity of four samples, containing approximately 1.0% by volume of magnetite dispersed in high purity kaolin, were investigated at temperatures from 9°C up to 500°C over acquisition (in a field of 100 μT) and decay times of 20 minutes. The time dependence of viscous magnetisation acquisition is similar to that reported by Tivey & Johnson (1981, 1984) with viscous magnetisation growing faster than the logarithm of time for all samples and at all experimental temperatures. Dunlop analysed the acquisition and decay curves in terms of a best fitting quadratic in log t of the form:

$$M(t) = a \log t + b (\log t)^2 \qquad (8.8)$$

where a and b are constants. The viscosity coefficients, S_a (acquisition) and S_d (decay), defined as the slope dM(logt)/dlogt are thus:

$$S_{a,d} = a + 2b \log t \qquad (8.9)$$

this reveals that the viscosity coefficient changes linearly with the logarithm of time.

The temperature dependence of the viscosity coefficients, S_a and S_d, for three of the four samples is shown in figure 8.3. Both of the viscosity coefficients

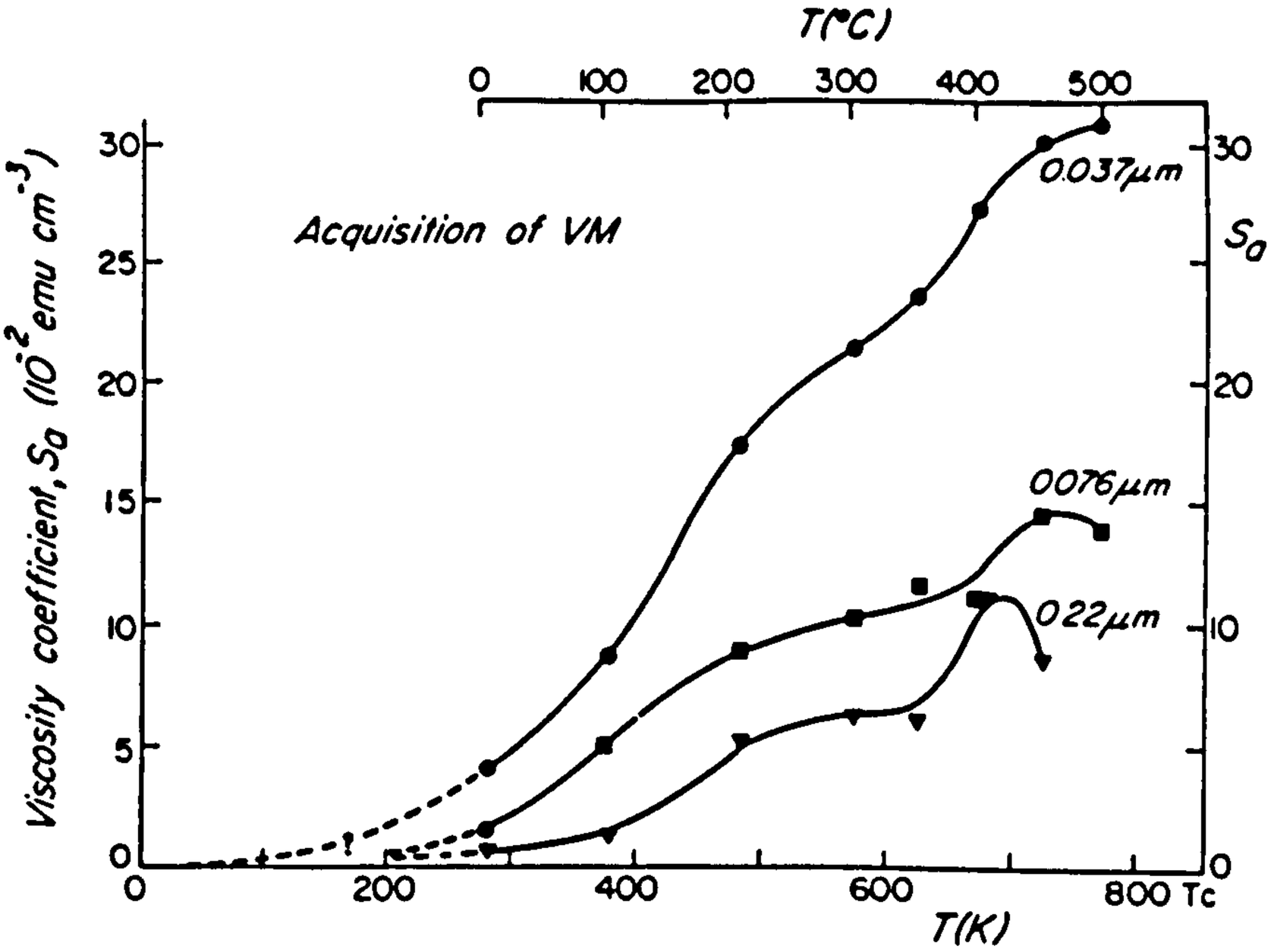

Figure 8.3. The temperature dependence of the average viscosity coefficient for a set of magnetite samples. From Dunlop (1983).

increase with temperature in qualitative agreement with thermal activation theory. However, for the samples containing the 0.076 μm and 0.22 μm particles, the viscosity coefficients peak around 450°C to 500°C and then fall at higher temperatures. Dunlop attributes this to a decrease of all of the relaxation times to the timescale of the experiment or less, i.e. the particles become superparamagnetic.

The particle size dependence of room temperature viscosity coefficients was also investigated by Dunlop (1983). The acquisition coefficient decreases with increasing particle size for sub-micron particles, in agreement with the findings of Tivey & Johnson (1981, 1984) although the data of Dunlop does not show the linear relation between the acquisition coefficient and the logarithm of particle size reported by Tivey & Johnson

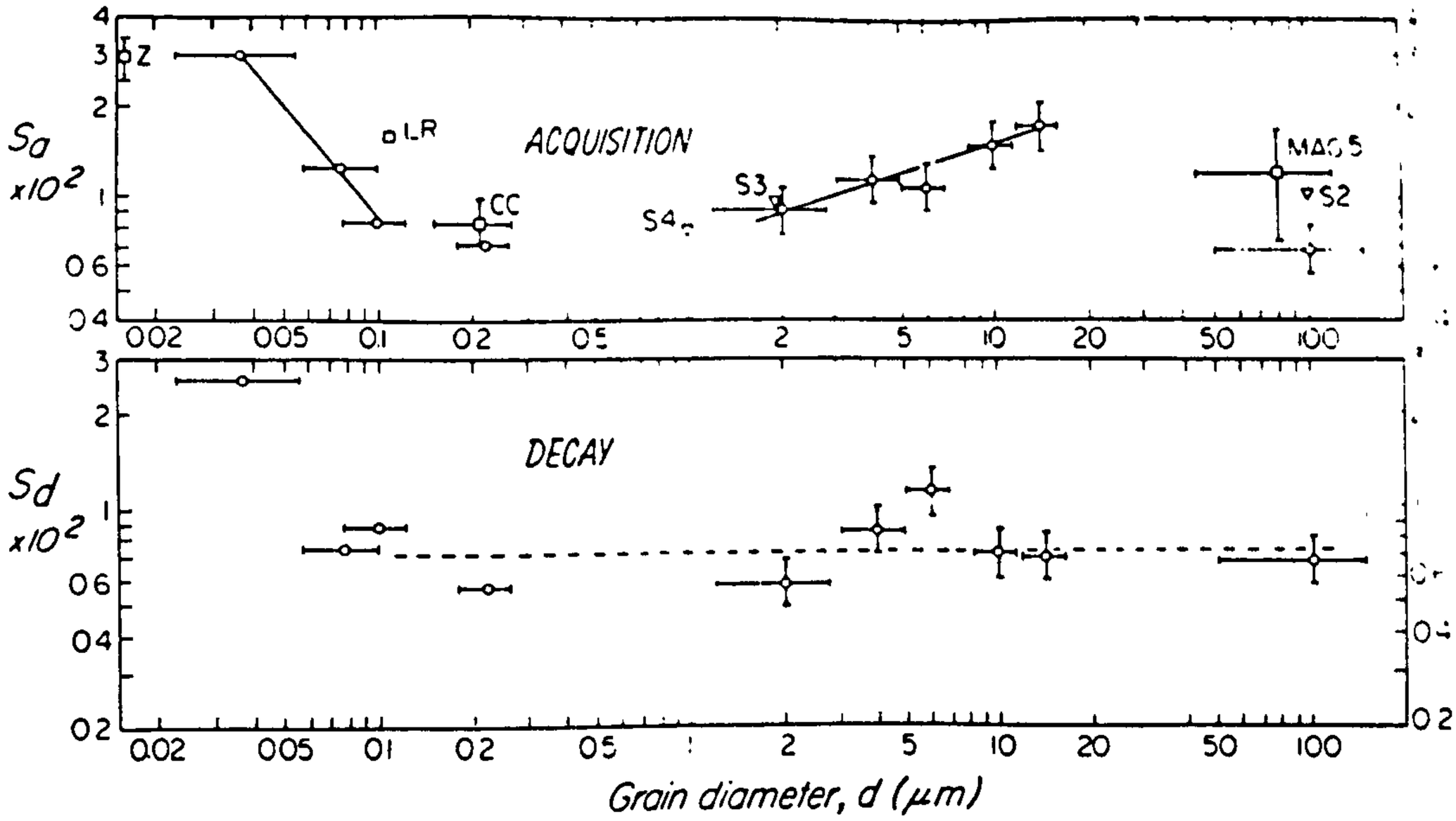

Figure 8.4. The particle size dependence of the average viscosity coefficient measured at room temperature. After Dunlop (1983).

(1981, 1984). See figure 8.4.

The comprehensive data set obtained by Dunlop (1983) allowed Walton (1983b) to test the thermal activation theory presented by Walton (1980). The primary requirement of Walton's theory is a knowledge of the particle size distribution. Walton (1983b) used a log-normal distribution which had the same mean and variance as the particle size distribution, measured using a transmission electron microscope (TEM). The theory also requires knowledge of the average anisotropy of the particles, K, which is obtained from:

$$K = \frac{M_s}{2} H_c \qquad (8.10)$$

where M_s is the saturation magnetisation of magnetite and H_c is the measured coercivity of the sample. Walton (1983) points out that equation (8.10) is derived for elongated

particles and is therefore not strictly applicable to the cubic geometry of the experimental particles. A further requirement for the calculation of the expected viscous moments is the concentration of magnetic particles in the sample; this was unknown and left as an adjustable parameter. Figure. 8.5 compares the theoretically predicted viscous acquisition at different temperatures with that obtained experimentally. The agreement is quite good for both the time and temperature dependence. The temperature dependence of S_a is also in good agreement with the experimental data. However, the theoretically derived time dependence of the acquisition coefficient, S_a, does not agree with the experimental data, although both theory and experiment indicate a log-t dependence for S_a. Walton (1983) suggests that the inconsistency indicates that the experimental time dependence may be incorrect.

Williams (1986) studied the time and temperature dependence of magnetic viscosity of two single domain magnetite samples as part of a study including samples containing multidomain particles. The samples were prepared by the glass ceramic method described by Worm & Markert (1988). No particle size distributions were presented for these samples because of the difficulty of locating a sufficient number of particles. Sample 69B contains chains of elongated interacting particles. Williams carried out two series of expëriments. Short period tests with acquisition times of 30 minutes and decay times of 42 minutes at temperatures ranging from 40°C to

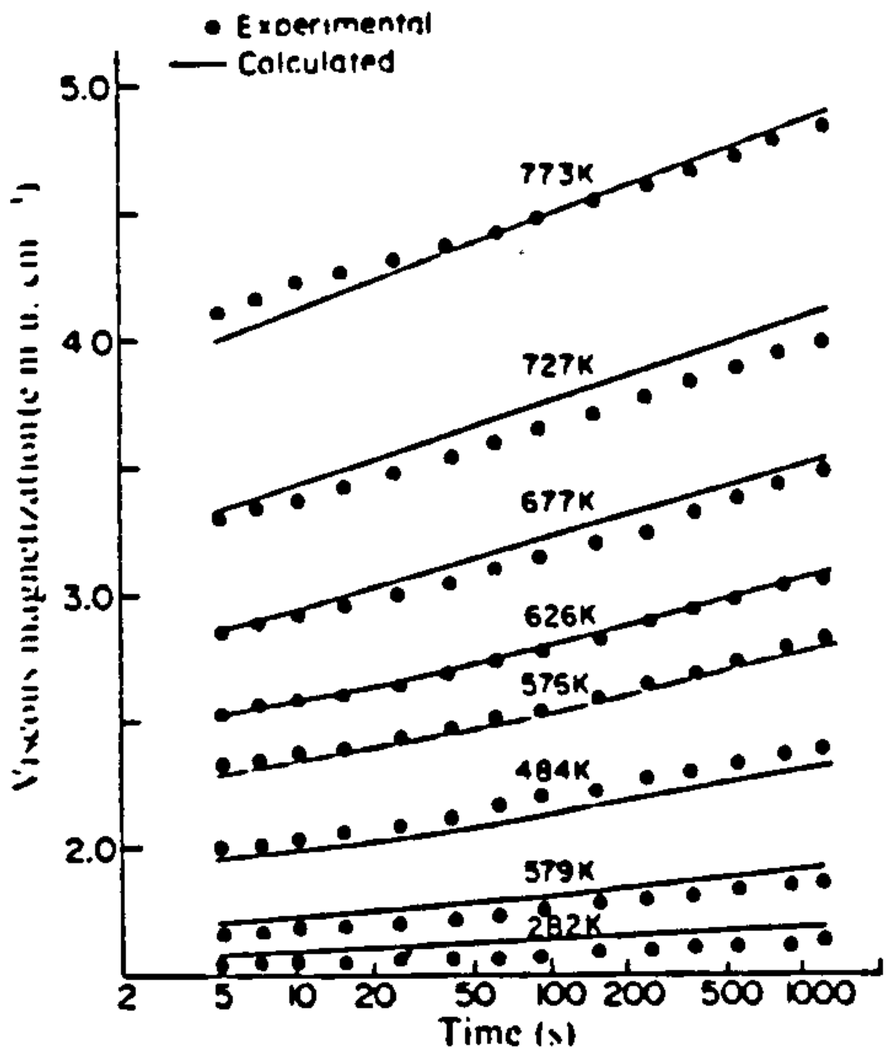

Figure 8.5. A comparison of the theoretical acquisition of magnetic viscosity using the theory of Walton (1980) with the experimental, data for magnetite obtained by Dunlop (1983). After Walton (1983b).

about 500°C. Details of the applied field during acquisition are not given. These experimental conditions are comparable with those of Dunlop (1983). Sample 63F which contained non-interacting particles was subjected to a second set of experiments which involved acquisition over 16 hours and decay times of 15 minutes.

The short period viscosity experiments reveal only a slight curvature, which increases with temperature, in the acquisition coefficient with time for sample 63F, in comparison with the curvature observed for sample 69B. Williams attributes the increased curvature to the effect

of particle interactions. Williams fitted the theory of Walton (1980) to both the time and temperature dependence of the acquisition coefficient S_a in order to obtain separate estimates of the particle size distribution N(v) for sample 63F. The theoretical fit to the time data indicates a particle size distribution of the form $N(v)=v^r$ with r between 0 and -2. The theoretical fit to the temperature dependence of S_a is more precise, see figure 8.6, giving a value for r of -1.4, in agreement with the range obtained from the time dependence. The longer period acquisition experiments on sample 63F were designed to test Walton's theory by comparison of long duration, low temperature viscous acquisition with shorter duration, higher temperature decay. The agreement between the theory and experiment is again quite good.

The most recent experimental study of magnetic viscosity in single domain magnetite was reported by Worm et al. (1991); they investigated a single sample containing 4% of magnetite with particle sizes between 0.025 μm and 0.1 μm. The particle size distribution within this sample is not included although it, and the measured distribution of microscopic coercivities are used in the theoretical treatment. The acquisition of viscous magnetisation was measured over about 50 minutes at temperatures ranging from -193°C up to 57°C. The acquisition field ranged from zero up to 154 mT. Worm et al. compared their experimental results with theoretical predictions based on both the experimentally derived particle size and the microscopic

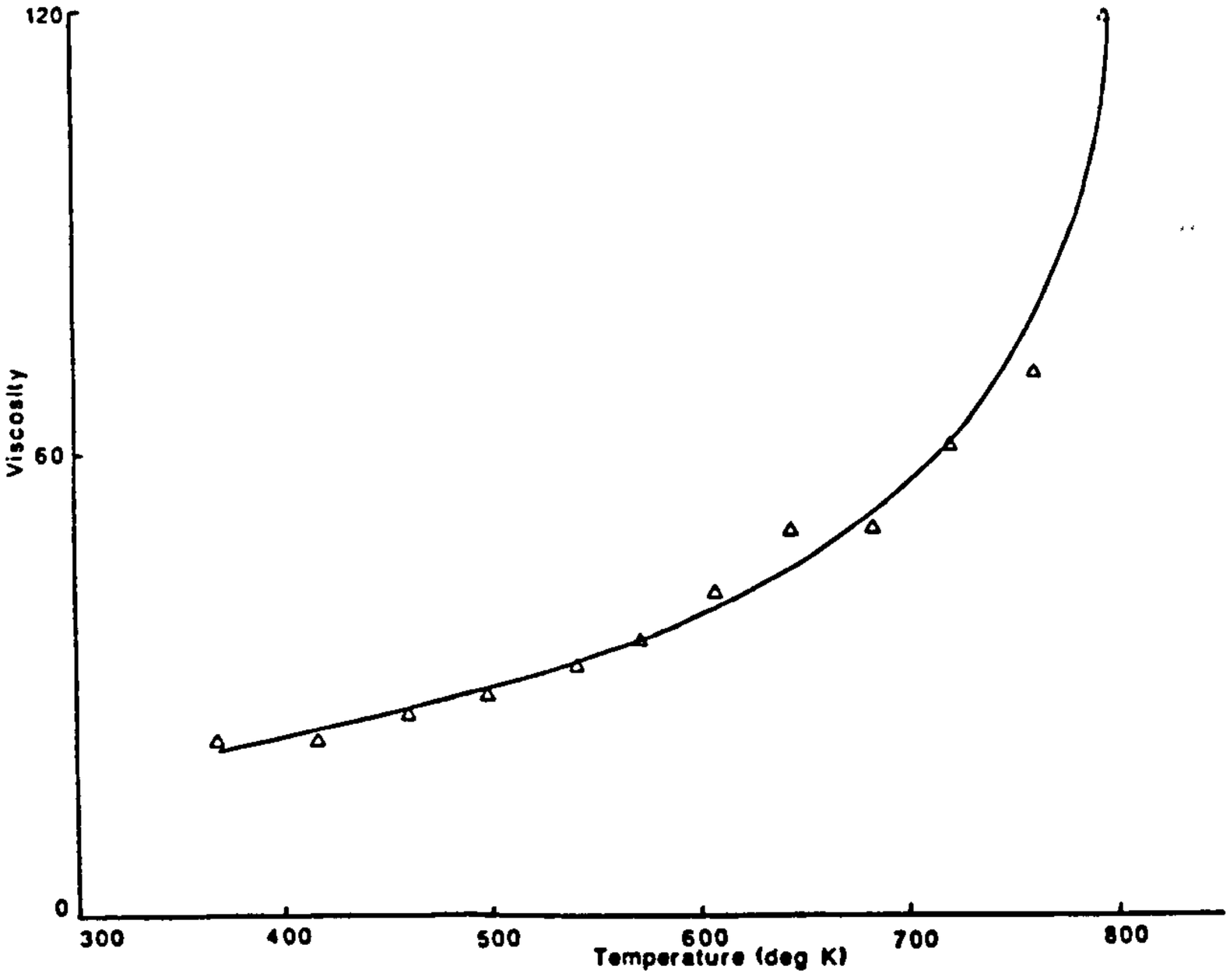

Figure 8.6. The theoretical best fitting curve to the temperature dependence of the viscosity coefficient S_a for a glass-ceramic magnetite sample. From Williams (1986).

coercivity distributions, rather than just the former as in most previous analysis. The use of such large fields complicates the analysis, requiring a precise relation rather than the low field approximation for the relaxation time. Worm et al. (1991) report a "significant quantitative gap" between the experimental observations and theoretical predictions. They suggest that magnetostatic energy is more important than the Néel (1949) formulation predicts.

8.2.4 Demagnetisation of viscous remanence

Investigation of the magnetic viscosity of single domain particles over much longer times than those described necessitates the use of rocks. Such investigations have been able to test the thermal activation theory of single

domain viscosity by comparing experimental demagnetisation times and temperatures with those predicted theoretically. Pullaiah et al. (1975) developed a set of time-temperature curves to relate the demagnetisation time and temperature to the duration of burial and metamorphism at a particular temperature. The theoretical curves were obtained by rearranging the low field approximation to the relaxation time, τ, proposed by Néel (1949) into the form:

$$\frac{T_2 \log C\tau_2}{M_s(T_2)\ H_c(T2)} = \frac{T_1 \log C\tau_1}{M_s(T_1)\ Hc(T_1)} \qquad (8.11)$$

where T_1 and τ_1 are taken as the temperature and time of magnetisation acquisition during burial and T_2 and τ_2 as the temperature and time of thermal demagnetisation. In practice, the temperature dependence of the microscopic coercivity, H_c, is accounted for by using the assumption that $H_{c(T)}$ is proportional to $M_{s(T)}$. This approach assumes that all particles with a particular relaxation time, τ, will be demagnetised when the demagnetisation time, t, equals the relaxation time. This is not strictly correct since τ is defined as the time to activate (in this case to demagnetise) only 63% of such particles. The experimental results of Pullaiah et al. disagree with their theoretical predictions; the experimental demagnetisation temperatures were consistently higher than predicted. Walton (1980) suggests that this is to be expected if no account of the particle size distribution is taken. Walton (1980) derived an alternative equation, also based on the low field

approximation, for relating time and temperature pairs, which includes the effect of the particle size distribution through the parameter r described earlier, viz;

$$\frac{(T_1 J(T_2)^2)}{(T_2 J(T_1)^2)}^{2+r} = \frac{(\ln Ct_1)}{(\ln Ct_2)}^{3+r} \qquad (8.12)$$

Middleton & Schmidt (1982) used this equation to construct time and temperature curves for both magnetite and haematite with which they compared experimental demagnetisation of magnetite and haematite components of the same age. The predicted ages of the geological remanence obtained from the demagnetisation data of the two minerals are in agreement, supporting the assertion of the importance of the particle size distribution. However, the theoretical relation derived by Walton (1980) has been questioned by both Enkin & Dunlop (1988) and Worm & Jackson (1988). Both suggest that the relation is flawed because it relates the time and temperature necessary to produce a magnetisation of the same intensity as that resulting from a different time and temperature, not the t-T relation for relating thermal demagnetisation with viscous acquisition. Enkin & Dunlop (1988) suggest that the observed discrepancy may be due to the application of the low field approximation to the relaxation time. They suggest that for larger particles (~0.1 μm for magnetite), the medium field approximation to the relaxation time may be more appropriate. This leads to closer agreement between theory

and experiment, although Enkin & Dunlop (1988) suggest that the 'higher than expected' demagnetisation temperatures for viscous magnetisation are associated with domain wall moments or wall segments, i.e. sections of a domain wall separating adjacent domains. Worm & Jackson (1988) consider that the medium field approximation is not applicable to single domain magnetite because the particle size above which this approximation is appropriate exceeds the maximum single domain size, although it should be noted that this is not the case for elongated particles. Worm & Jackson (1988) investigated the low field approximation similar to that of Pullaiah et al. (1975) but took into account the particle size distribution and set the demagnetisation time t equal to three times the relaxation time τ, equivalent to demagnetising 95% of the particles with relaxation time of τ. This analysis reveals that particle size distribution is not a major influence on the demagnetisation time and temperature, contradicting the supposition of Walton (1980). Worm & Jackson also suggest that larger particles with pseudo-single or multi-domain configurations give rise to the generally higher demagnetisation temperatures and are of importance in rocks.

8.2.5 Magnetic viscosity of multidomain materials

It is generally agreed that magnetic viscosity occurs in multidomain materials, although there remains some debate about the mechanisms responsible for this behaviour. Changes in the magnetisation of multidomain materials in

small fields ($<< H_c$) are considered to arise from domain wall motion and it is commonly agreed that viscous magnetisation in multidomain magnetite can be explained on this basis. However, the mechanism which causes the release of walls from their pinning sites is unresolved with some workers considering that magnetic viscosity in multidomain magnetite arises from thermal activation alone (Néel, 1950, Stacey, 1963, Averyanov, 1967, Sholpo, Belokon & Sholpo, 1972), while others have suggested that the diffusion of vacancies, defects and impurities may be important (Tropin & Vaslov, 1966, Shashkanov & Metallova, 1970, Moskowitz, 1985).

Néel (1950, 1955) suggested that magnetic viscosity in multidomain materials such as magnetite is essentially a thermal activation process and that it could be described in terms of a randomly varying 'viscosity field', H_f, resulting from changes of the free energy produced by thermal fluctuations of the spontaneous magnetisation. The viscosity field is considered to aid domain walls in overcoming the energy barriers imposed by their pinning sites and hence allow them to move into positions of lower energy with respect to the ambient conditions. The viscosity field was defined as;

$$H_f = S\ (Q + \ln t) \qquad (8.13)$$

where S is the viscosity coefficient and Q is a constant. The magnetisation after time t is described by;

$$M(t)=M(t=0)+CH_f \qquad (8.14)$$

where C, in this case, is the irreversible susceptibility. Néel's theory predicts a temperature dependence for the viscosity coefficient of the form;

$$S \propto T/M_s(T) \qquad (8.15)$$

$M_s(T)$ is the saturation magnetisation at the temperature T. The temperature dependence of M_s is weak at temperatures considerably below the Curie point and leads to an approximately linear relationship between S and T over such temperatures and a more complicated one close to the Curie point (Dunlop, 1983). Néel's theory also predicts that for small applied fields, and after the initial induction of an isothermal remanence which is proportional to H^2, the viscosity coefficient varies linearly with H.

Averyanov (1968) has criticised Néel's formulation since it neglects the spin exchange contribution to the free energy. Averyanov (1968) also showed that the probability of overcoming an energy barrier, and hence the rate of viscous activation, depends on the total free energy arising from thermal fluctuations and not just the magnetic free energy suggested by Néel (1950). Dunlop (1973) suggested that Néel's theory is also flawed by its neglect of the effect of self-demagnetisation.

The contribution of diffusion processes to the magnetic viscosity of natural and synthetic samples has been discussed extensively by Moskowitz (1985). In multidomain materials, viscous magnetisation results from the

activation of domain walls from pinning sites to positions of lower energy (Dunlop, 1983). The pinning sites arise from point defects, dislocations, lattice vacancies and impurity atoms which interact with the walls altering their energy. The diffusion of such features and the hopping of electrons through a material will change the potential energy profile of a domain wall, which will influence the time dependence of the magnetisation of a material. Diffusion processes are highly dependent upon the number of the diffusion species. Two processes which affect the viscosity are associated with diffusion; firstly, the magnetisation of a material can change with time if it is altered by the diffusive movement of defects or impurities such that a particular wall is no longer in a minimum energy configuration. This is termed the diffusion after-effect. Secondly, the diffusive migration of cationic vacancies can stabilise a particular domain wall configuration, making further magnetisation changes more difficult. This process is also associated with a decrease of susceptibility with time (Kronmuller et al., 1974, Moskowitz, 1985, Schmidbauer & Fassbinder, 1987) and is termed susceptibility disaccommodation. Diffusive processes are also thermally activated with the relaxation time, τ, for the diffusion of a particular species defined as:

$$\tau = \tau_o \exp(E_a/kT) \qquad (8.16)$$

where τ_o is a time constant, τ_o 10^{-12}s for magnetite (Schmidbauer & Fassbinder, 1987)), and E_a is the activation

energy of the diffusion process (Schmidbauer & Fassbinder, 1987). The magnetisation change resulting from the diffusion after-effect is given by:

$$M(t) = M_{eq}-(M_{eq}-M_o)\exp(-t/\tau) \qquad (8.17)$$

where M_{eq} is the equilibrium magnetisation of the diffusion process and M_o is the magnetisation at t=0. The stabilization of magnetisation with time is related to the disaccommodation of susceptibility, X(t), which is given by:

$$X(t) = X_{eq}-(X_{eq}-X_o)\exp(-t/\tau) \qquad (8.18)$$

where X_{eq} is the equilibrium susceptibility and X_o is the susceptibility at t=0.

The importance of diffusion processes to the magnetic viscosity of multidomain magnetite can be understood by considering the activation energies involved and their associated relaxation times. The activation energies have been determined from disaccommodation studies of slightly non-stoichiometric magnetite by Kronmuller et al., (1974) and magnetite and titanomagnetites by Schmidbauer & Fassbinder (1987). The earlier of these studies considered that the two diffusive processes occur together and gives activation energies for these of 0.82 and 0.87 eV respectively. Schmidbauer & Fassbinder (1987) recognise that two process may occur but present only a single activation energy of 0.87 eV which is increased to 0.91 eV to correct for the change in vacancy concentration. These

values are somewhat lower than the 1.12 eV obtained by Grimes (1972) using a equation developed for diffusion in metals, although Schmidbauer & Fassbinder (1987) suggest that the formula may not be strictly applicable to the spinel structure. Taking the range of the values for the activation energy discussed, i.e. 0.8< Ea <1.15, the range of relaxation times, τ, calculated using equation 8.16 with $\tau_o=10^{-12}$s from Schmidbauer & Fassbinder (1987), is 10s < τ < 2 years at 20°C. Diffusion processes are somewhat different for titanium substituted magnetite even when the substitution is very small, e.g. x~0.025 (Hohne et al., 1975). The maximum activation energy for diffusion in a particular titanomagnetite depends on the amount of substitution. Schmidbauer & Fassbinder (1987) obtained activation energies of 1.17 eV for x=0.025 up to 1.6 eV for x=0.1. This equates to relaxation times of ~40 years and 10^6 years respectively.

In magnetite the diffusion processes discussed operate over relatively short times compared to geological and archaeological timescales, although they are significant on the laboratory time scale. However, the diffusion processes described consider only the movement of vacancies or cations over distances of a few atoms rather than over longer distances for which the activation energies are larger, e.g. 1.4 eV (Nakamura et al., 1978) and consequently have longer relaxation times of the order of 10^4 years. The diffusion of cations and vacancies in even slightly substituted titanomagnetite is characterised by

relaxation times which are important on both geological and archaeological timescales.

Shimizu (1960) conducted the first systematic study of the magnetic viscosity of multidomain magnetite. Four samples were prepared from natural magnetite by crushing and sieving to give narrow particle size distributions with approximate particle sizes of 1, 2, 100 and 270 μm. The temperature dependence from -183°C up to 550°C and the field dependence from 25 μT up to 1 mT of magnetic viscosity were investigated. The acquisition of viscous magnetisation was measured continuously between 30 and 2000 seconds. The temperature dependence of the viscosity coefficient for three of the samples is shown, see figure 8.7. In all three cases the viscosity coefficient increases linearly with temperature from -73°C up to 50-200°C below the Curie point, above which the viscosity coefficient rises steeply, reaching a peak just below the Curie point before rapidly falling to zero at the Curie point. In addition, for the sample containing the largest particles the temperature dependence of the viscosity coefficient is given down to -196°C. This data shows a peak in the acquisition coefficient which occurs around the magnetocrystalline isotropic point (-150°C) associated with the change of sign of the magnetocrystalline anisotropy constant.

The linear temperature dependence of the viscosity coefficient supports the theory of Néel (1950, 1955) when

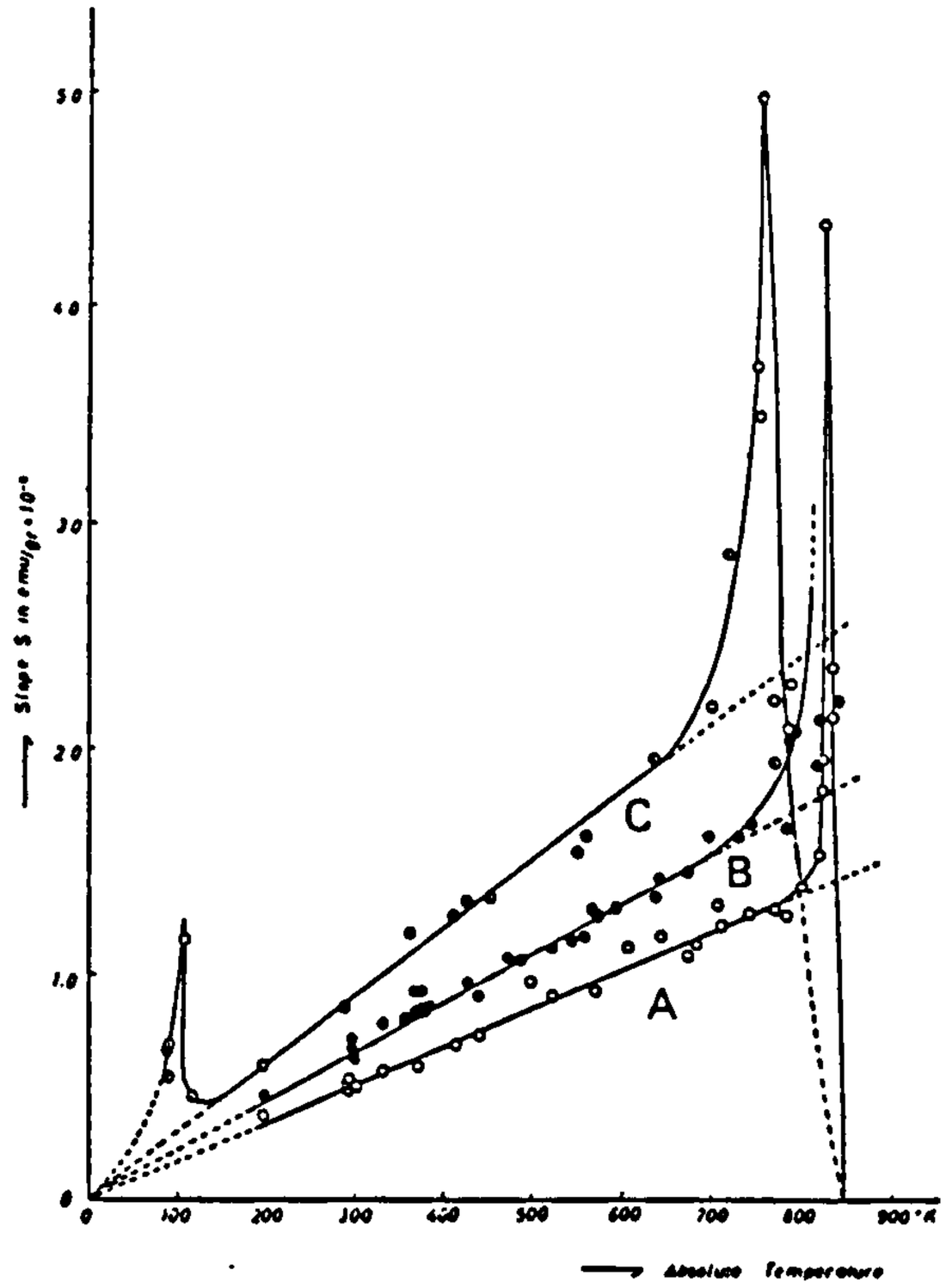

Figure 8.7. The temperature dependence of the viscosity coefficient for three multidomain magnetite samples reported by Shimizu (1960). The three samples have mean particle sizes of (A) 2 μm (B) 100 μm and (C) 270 μm.

thermal agitation causes fluctuations in the height of the pinning site energy barriers rather than thermal agitation causing changes in the internal field due to changes of the spontaneous magnetisation from its mean value. Shimizu (1960) suggests that the rapid increase in the viscosity coefficient towards the Curie point can be explained in terms of the particles becoming single domain-like and thus have a larger net magnetisation than equivalent size multidomain particles. These single domains arise at high temperatures because the magnetocrystalline anisotropy falls rapidly towards the Curie point which leads to increasing domain wall size, producing an essentially single domain configuration which is controlled by the

shape anisotropy. The rapid fall of the viscosity coefficient at the Curie point reflects the loss of ferrimagnetic order.

Shimizu (1960) also reports that the viscosity coefficient increases linearly with the acquisition field over the range investigated, which is also qualitatively in agreement with the thermal activation model of Néel (1950, 1955). The results of Shimizu (1960) show no indication of the diffusion effects.

Since the study of Shimizu (1960), a considerable volume of work on the magnetic viscosity of multidomain magnetite has been produced. Shashkanov & Metallova (1970) studied the temperature dependence of the viscosity coefficient of natural magnetite crystals. Their experiments involved the acquisition of viscous magnetisation at temperatures from room temperature up to the Curie point of magnetite. Skovorodkin et al., (1975) carried out similar, but more detailed, experiments which included the effects of various annealing temperatures and atmospheres to control the degree of non-stoichiometry. The temperature dependence of the viscosity coefficient reported by both of these groups shows two peaks, one around room temperature and the other at about 150°C. It has been suggested that these peaks indicate that magnetic viscosity proceeds by a mechanism arising from the diffusion of defects, in particular cation vacancies. However, Bolshakov (1975) states that the presence of such peaks cannot be taken as confirmation of the existence of diffusion based viscosity since a similar

result may be observed by thermal activation of a suitable distribution of relaxation times. Sholpo et al. (1972) dismiss the idea of diffusion based viscosity since "no working theory" had been proposed. Both Sholpo et al. (1972) and Bolshakov (1975) favour the explanation of viscosity in multidomain magnetite as a thermal activation process with diffusion leading only to disaccommodation of susceptibility and a stabilisation of domain walls to further viscous changes.

A mechanism for a diffusion after-effect has been described by Sporer (1984) and Moskowitz (1985). They suggest that the interaction of the spontaneous magnetisation with the lattice defects will alter the energy barriers to viscous magnetisation changes and consequently lead to a diffusion after-effect.

More recent experimental work by Tivey & Johnson (1981, 1984) and Williams (1986) on synthetic multidomain magnetite and Sporer (1984) on synthetic multidomain titanomagnetite suggests that diffusion effects are important. Both Tivey & Johnson (1981, 1984) and Sporer (1984) report the effect of increased zero field storage time on the subsequent acquisition of viscous magnetisation at room temperature. With increasing storage time the magnetic viscosity is reduced. This result indicates a stabilisation of the initial demagnetised state during zero field storage which is consistent with the diffusion of defects associated with disaccommodation. Sporer (1984) also presents the titanium content dependence of the

viscosity coefficient, from which the presence of a systematic diffusion after-effect is concluded. Williams (1986) observes peaks in the temperature dependence of the viscosity coefficient measured in three samples and suggests that this is the result of disaccommodation.

8.2.6 Summary

Experimental observations of magnetic viscosity of single domain magnetite particles on timescales of many minutes to several hours are, in many situations, reasonably well explained by thermal activation models which take into account the particle size distribution within a sample. In some cases, the mechanism of particle interactions has also been required to account for the observed behaviour. The larger discrepancies between thermal activation theory and experiments conducted in large applied fields, reported by Worm et al (1991), may be attributed to magnetostriction which is relatively large in magnetite (78×10^{-6}; Stacey & Banerjee, 1974), and which becomes important at larger applied fields. Therefore this discrepancy is unlikely to be significant in fields of the order of the geomagnetic field as used by other workers and of particular interest here. However, the effect of zero field storage upon low field viscous acquisition in single domain assemblages is contrary to the expectations of thermal activation theory, and requires further investigation. The application of single domain theory to determine the demagnetisation times and temperatures required to erase geological age viscous remanence has

produced mixed results. Walton (1980) suggests that the distribution of particle sizes is an important factor, contributing to the maximum time and temperature necessary to remove viscous moments. This view is supported by the experimental work of Middleton & Schimdt (1982). However, Worm & Jackson (1988) also considered the effect of the particle size distribution and concluded, in contrast to Walton (1980), that it has only a small effect on the demagnetisation conditions. This seems intuitively correct since the maximum time and temperature of the demagnetisation depends primarily upon the largest single domain particles that have been activated rather than the distribution of particles below this size. The latter will be demagnetised below the maximum time and temperature, while the distribution of larger particle sizes will not have been viscously activated. The experimental findings of Middleton & Schmidt (1982), supporting the supposition that the particle size distribution is important, can be questioned since the time-temperature relations presented by them required knowledge of the particle size distributions in the samples. These were unknown and therefore essentially used as an adjustable 'fit' parameter. An alternative explanation proposed by both Worm & Jackson (1988) and Enkin & Dunlop (1988) to account for the 'higher than expected' demagnetisation temperatures is that these temperatures are associated with the viscous magnetisation of small multidomain particles.

Experimental observations of magnetic viscosity in

multidomain magnetite have produced conflicting results which has lead to disagreement about the mechanisms responsible. Qualitative agreement between the experimental data of Shimizu (1960) with the theoretical treatment of Néel (1950, 1955) supports the assertion of Néel (1955), Sholpo et al. (1972) and Bolshakov (1975) that magnetic viscosity in multidomain magnetite is a thermal activation process. However, the studies of Shashkanov & Metallova (1970) and Skovordkin et al. (1975) and Sporer (1984) suggest that an additional process arising from the diffusion of cationic vacancies also contributes to the magnetic viscosity in multidomain magnetite and titanomagnetite. Aside from the mechanism leading to viscous magnetisation, it is more widely agreed that the diffusion of cations and vacancies increases the energetic stability of domain walls and leads to a reduction of susceptibility, termed disaccommodation (Sholpo et al., 1974, Kronmuller et al., 1974, Schmidbauer & Fassbinder, 1987 and Moskowitz, 1985) . Such increases of wall stability increase the relaxation time of the wall, which means that subsequent viscous activation of the domain wall will require a longer time for activation than it required have prior to stabilisation.

The combination of thermal and diffusion effects gives rise to complex viscosity behaviour in multidomain magnetite which is dependent on the stoichiometry of the minerals in a sample. In consequence, quantitative theoretical modelling of experimental data from multidomain

samples has been much less successful than it has for the single domain case.

8.3 Magnetic viscosity as a dating tool

The occurrence of magnetic viscosity in natural materials suggests its possible use as a tool for dating such material. Previous attempts at retrieving the age of viscous remanence have been made by Creer (1957) and Heller & Markert (1973).

Creer (1957) investigated the time dependence of the magnetisation of some samples from the Keuper Marls of Sidmouth as part of a wider study of these rocks. This included a study of the effect on the magnetisation of the duration of exposure to a constant laboratory field, h, and the effect of varying h while keeping the duration of exposure fixed. From these results Creer (1957) found that at a constant temperature the magnetisation ,M, acquired was obtained from:

$$M = ah \log t \qquad (8.19)$$

where 'a' is a constant and t is the acquisition time. It was also shown that equation 8.19 holds for t at least up to 10 days and for h equivalent to about 50 μT. Using this equation and knowing the magnitude of the geological age viscous remanence and by assuming that both the temperature and the Earth's magnetic field have remained constant, the time that has elapsed since the last reversal of the Earth's magnetic field was estimated. A value of 97800

years was obtained with limits calculated from the standard error in log t of 10500 and 250000 years. This value is lower than the commonly reported date for the Bruhnes-Matuyama reversal of about 710000 years ago (e.g. Roberts & Piper, 1989), although the upper limit of this estimate is much closer to the accepted age. This approach highlights the problems of extrapolating room temperature laboratory time scale experiments to geological timescales. Firstly, a small error in determining the magnetisation acquired after a particular time in the laboratory can amount to a very large error in the estimated geological time because of the dependence of the magnetisation upon the logarithm of time. Secondly, the form of the viscous acquisition that was measured on the laboratory timescale, in this case it was linear, may not hold for the entire duration (geological time) of the viscous acquisition. This depends upon the relaxation time distribution which may lead to an increase or decrease of the acquisition rate with time. The underestimated age for the Bruhnes-Matuyama reversal obtained from the Keuper Marls suggests that the relaxation time distribution is of the form $N(\gamma)=\gamma^r$ where r is less than -2.

An alternative approach to retrieving age information was explored by Heller & Markert (1973). They developed a method based on the fluctuating field model of multidomain viscosity proposed by Néel (1950). They applied their model to some quartz dolerite rocks obtained both from outcrop and from Hadrian's Wall, where some blocks were

included in the original construction. The composition and Curie points of the magnetic mineralogy of the samples were well characterised. It was assumed that multidomain titanomagnetite was responsible for the magnetic viscosity in these samples. The essence of the dating method involves a comparison of the alternating field required to erase the ancient viscous remanence with the theory proposed by Néel (1950, 1955). This theory was outlined earlier in the review of multidomain viscosity. To obtain a date, the various parameters in equation 8.13 were determined. A measurement of $X_{irr}S$, where X_{irr} is irreversible susceptibility and S is a viscosity coefficient, was obtained from the slope of the viscous acquisition in experiments carried out in the laboratory on samples which were initially completely demagnetised. The irreversible susceptibility was determined by subtraction of the reversible susceptibility from the differential susceptibility measured in a field appropriate to the acquisition field of the original ancient viscous remanence, i.e. equivalent to 50 μT. . The fluctuating field, H_f, was calculated by subtracting the ancient field from the peak alternating field needed to erase the original viscous remanence. The remaining requirement to obtain a date is a value for the constant Q. Q depends upon the number of attempts per second made by a domain wall to overcome a pinning induced energy barrier. This is the frequency constant, C, in the relaxation time formulation of Néel (1949) . Heller & Markert (1973)

question the validity of the accepted value of Q=23, derived using the Larmor frequency. This is the fundamental precession frequency of an electron in a magnetic field. They resolved this problem by calculating Q from their viscosity experiments.

The results were obtained for three samples from Hadrian's wall and one sample from the original outcrop. The ages for samples from Hadrian's wall are 1600, 1800 and 2400 years before present (BP), in quite good agreement with the date of construction which is known to extend from 1850 to 1600 years BP. The sample obtained from outcrop was expected to have viscous magnetisation associated with the period of Normal polarity since the Bruhnes-Matuyama reversal which occurred about 710000 years BP. In the event the estimated age of viscous remanence was 818000 years BP, which is about 15% longer than expected. Heller & Markert (1973) point out that their analysis lacks any statistical treatment and as such their data must be treated with caution.

The results obtained by Heller & Markert (1973) suggests that their approach and hence the multidomain viscosity model proposed by Néel (1950, 1955)) are valid to a reasonable extent. Their approach and the Néel (1950, 1955) model may be criticised on a number of points. The method will be flawed if the samples dated contain a significant fraction of viscous single domain particles. As discussed in the review section the theoretical model has been criticised by both Averyanov (1968) and Dunlop

(1973) for neglecting the exchange portion of the free energy of the thermal agitation of the spontaneous magnetisation and the demagnetising effect due to particle shape. This imposes limitations on the quantitative application of the model. The approach used by Heller & Markert (1973) requires knowledge of the rate of growth of viscous magnetisation, which was determined from laboratory experiments. As a consequence, the dating method suffers in a similar way to that used by Creer (1957) since the acquisition rate may vary with time depending on the distribution of relaxation times making extrapolation of room temperature viscous acquisition rates invalid. The laboratory viscosity experiments were also used to determine Q, which is crucial to the age determination, and which is related to the frequency constant, C, in the relaxation time equation, by Q=-ln (1/C). Using the expressions and data given by Heller & Markert (1973), 1/C has been calculated to be ~1.7-1.8 seconds which is equivalent to a frequency C of 0.55-0.59 sec^{-1}. This is much lower than the maximum theoretical value of 10^{12} sec^{-1} for thermal activation of a domain wall (Gaunt, 1977) and more importantly it is several orders of magnitude smaller than the minimum values calculated for other materials. However, the minimum value of C depends on the size and morphology of the pinning sites (Gaunt, 1977), the specifics of which are unknown in titanomagnetite. Therefore, while it cannot be shown that the value of Q determined for thermal activation of a domain wall in

titanomagnetite is incorrect it must be considered questionable upon further investigation. -

In addition to these points, diffusion processes must be considered with regard to the acquisition and stability of viscous remanence in multidomain titanomagnetite. The role of diffusion was discussed in the review section. The diffusion of defects, in particular cation vacancies in magnetite and titanomagnetite, is considered by some workers to lead to a change in the magnetisation, termed the diffusion after-effect, while it is more commonly agreed that the diffusion of such defects leads to increased stability of domain walls after they have been thermally activated. In the latter case diffusion leads to a change in the relaxation time spectrum of a sample. Diffusion increases with the number of the vacancies and therefore the degree of oxidation. The samples investigated by Heller & Markert (1973) contained oxidised titanomagnetite and as such are likely to be affected by diffusion to some extent. This will have affected their experimental work. First, increased stability of the domain walls would lead to an increased resistance to alternating field demagnetisation, as has been observed by Prevot (1981), giving a larger than expected value for the fluctuating field, H_f, and a consequent over estimate of the age of viscous remanence. Second, if the relaxation time spectrum in the sample has changed, as seems likely, since the acquisition of the original viscous remanence, then subsequent laboratory acquisition experiments will not

be wholly representative of the original behaviour.

The reliability of both of the dating methods discussed suffers because they rely upon the assumption that the viscosity coefficient, measured in the laboratory at room temperature, is constant over geological and archaeological time scales. It is clear from the theoretical and experimental review that such constancy is not an inherent feature of magnetic viscosity but requires, for example in single domain assemblages, a particle size distribution of the form $N(v)=v^{-2}$. In addition, the reliability of the method of Heller & Markert (1973) also suffers because the importance of diffusion processes to the viscosity of the samples is not assessed and therefore remain as an unknown variable which may lead to additional errors. More reliable methods of dating which utilise magnetic viscosity must address these problems. The effect of diffusion processes on the time-dependent magnetisation in multidomain particles remains poorly understood and as such suggests that materials in which viscous magnetisation is attributed to multidomain magnetite or titanomagnetite should be avoided at present. The following suggested methods are therefore considered applicable to samples containing single domain assemblages.

As discussed, the extrapolation of short term, room temperature viscosity experiments to archaeological and geological time scales will be successful only for a linear dependence of the magnetisation on the logarithm of time. This problem may be approached in two ways. First, the

requirement of the form of the time dependence of the total viscous magnetisation, which is related to the particle size distribution, can be circumvented by determining only the time required to viscously activate the most stable part of the viscous remanence. The time and temperature for the thermal activation of a single domain particle was given, see equation 8.11. In an assemblage of single domain particles thermal activation will sweep through the distribution of particle sizes from smallest to largest with increasing time. The largest particles have the longest relaxation times and thus will be activated last and will have the highest demagnetisation temperature. By using the relaxation time equation 8.11, with the demagnetisation time and temperature required to erase the most stable part of the original viscous remanence, the acquisition time of the original viscous remanence, acquired at around 10-20°C, can be calculated. This method has been used to estimate the temperature and duration of geological burial processes (Pullaiah et al., 1975). This method assumes that the relaxation time of the most stable particles has been reached. This may not be the case since the relaxation time represents the time elapsed for the activation of 63% of the particles, in an assemblage of identical particles, so particles are therefore activated both before and after the relaxation time. Aside from this, the method suffers because it relies on the quantitative use of the relaxation time equation, which may not be strictly correct because of factors such as the

neglect of the magnitude of the applied field (Enkin & Dunlop, 1988). This problem and the one discussed earlier could be avoided if the time dependence of viscous acquisition was determined by reactivating, in the laboratory, all of the magnetic moments activated over archaeological or geological time. This necessitates viscosity experiments at high temperatures. A dating method using this approach would involve a series of viscous acquisition experiments on a sample at different temperatures in which a magnetisation was grown which was equivalent in magnitude to that acquired since antiquity. An average acquisition coefficient for each temperature could then be calculated for this magnitude of magnetisation, which includes correcting for the reduction of M_s with increased temperature. The average acquisition rate for the original viscous remanence acquired since antiquity would then be determined by extrapolation of a curve fitted to the high temperature data. With knowledge of the magnitude of the original viscous remanence and having determined the average acquisition rate, the age of the original viscous remanence can be calculated.

More complex dating methods also involving a series of high temperature experiments could be developed. Such methods could use the theoretical time and temperature relations, such as those of Walton (1980), from which the particle size distribution may be determined and used to model the acquisition of viscous remanence. Unfortunately, some experimental observations, in particular the time

dependence of the viscosity coefficient, are not in agreement with the theoretical treatment and therefore suggest that an empirical approach would be most useful.

8.4 Magnetic viscosity dating of ancient ceramics

It is apparent from the previous sections that a dating method based on either the demagnetisation of viscous remanence or extrapolation of high temperature viscous acquisition experiments may be possible in samples containing single domain particles. However, the discussion assumes that the original viscous remanent magnetisation was acquired at a constant temperature and in a constant ambient magnetic field, and this may not be an approriate assumption.

The suitability of the magnetic mineralogy of ancient ceramics for magnetic viscosity dating must also be considered. The study of the magnetic mineralogy of archaeological ceramics forms the bulk of the present work, and in the context of viscosity dating the particular features of the magnetic mineralogy that are of importance are; that the particles responsible for the viscous magnetisation are single domain particles and that the relaxation time spectrum of these particles has not changed since they were viscously activated. The magnetic hysteresis results indicate that a high proportion of the samples investigated contain a large stable single domain fraction, while the investigation of the susceptibility reveals that the remainder of the particle size

distribution is predominantly in the superparamagnetic single domain region with about a quarter of the samples also showing behaviour attributable to the presence of multidomain particles. The results vary quite considerably and therefore any investigation of magnetic viscosity must include a thorough study of the magnetic mineralogy. The second point concerning the mineralogy is the requirement for the relaxation time spectrum of a sample to have remained unchanged over time. The problem associated with stabilisation of domain walls by the diffusion of defects does not apply to single domain particles. However, the relaxation time of a particle will change if the particle has undergone chemical alteration over time. The thermomagnetic analysis undertaken in this study indicates that low temperature oxidation is widespread in ceramics. Whether this oxidation occurred at ambient temperatures over time since the burial of the ceramics, or whether it was formed during modest temperature heating (100-300°C) in antiquity, is unknown. Therefore, the occurrence of such changes must be considered as a potential problem with respect to the alteration of the relaxation time spectrum of a sample. Indeed, if oxidation does occur over time then the time dependent magnetisation may have both viscous and chemical origins leading to a chemico-viscous remanence (Ozdemir & Dunlop, 1988).

The method of dating based on the time and temperature needed to demagnetise a viscous remanent magnetisation, and using single domain theory, has been tested with a pottery

sample of known age. The sample investigated is a pottery sherd of Saxon age (440-1066 AD, later part) kindly supplied by the Grosvenor Museum, Chester. In order to date the sample the relaxation time at the demagnetisation temperature is equated to the relaxation time at ambient temperature, according to the equation 8.11 derived by Pullaiah et al. (1975). In addition to the demagnetisation time and both the demagnetisation temperature and the ambient temperature, a number of other factors which depend on the mineralogy must be assumed or evaluated. Thermomagnetic analysis of this sample indicates a Curie point temperature of about 550°C, suggesting that the magnetic mineral present is a titanium substituted magnetite with a composition parameter x=0.03. Magnetic hysteresis measurements indicate that the sample is saturated below 500 mT showing no evidence of haematite. The M_{rs}/M_s value of 0.285 indicates a large stable single domain component (~57%). In addition, the variation of low field susceptibility from -196°C up to room temperature is typical of those observed for many of the other samples investigated in this work and which is considered to represent the progressive unblocking of superparamagnetic particles. There is no convincing evidence for the presence of multidomain particles but their presence cannot be ruled out. The temperature dependence of the spontaneous magnetisation and the microscopic coercivity are also required for the evaluation of equation 8.11. According to Pullaiah et al. (1975), shape anisotropy is

dominant over magnetocrystalline anisotropy at room temperature for single domain magnetite particles when the particle is elongated by as little as 10%. Shape anisotropy imposes a coercivity which is directly proportional to the saturation magnetisation of the particle, leading to a similar form for the temperature dependence of both the coercivity and the saturation magnetisation. The remaining requirement, aside from the experimental data, is a value for the frequency factor C, this is of the order of 10^{10} s^{-1} (McNab et al., 1968).

Only three 9 mm diameter samples could be drilled from the sherd. Stepwise thermal demagnetisation and remanence measurements were carried out using the automated SQUID magnetometer system described by Shaw et al. (1985). This system enabled the sample to remain in zero field during the entire process. The demagnetisation time for each heating step was approximately twelve minutes, although the precise demagnetisation time is not of great importance. The demagnetisation data was analyzed using orthogonal vector plots, an example of which is shown in figure 8.8. The demagnetisation temperatures required to completely erase the viscous remanent magnetisation were determined to be between the two data points which mark the change of direction from the viscous component to the primary component. The demagnetisation temperatures for the three samples are given in table 8.2. The demagnetisation temperatures obtained from the three samples are not in

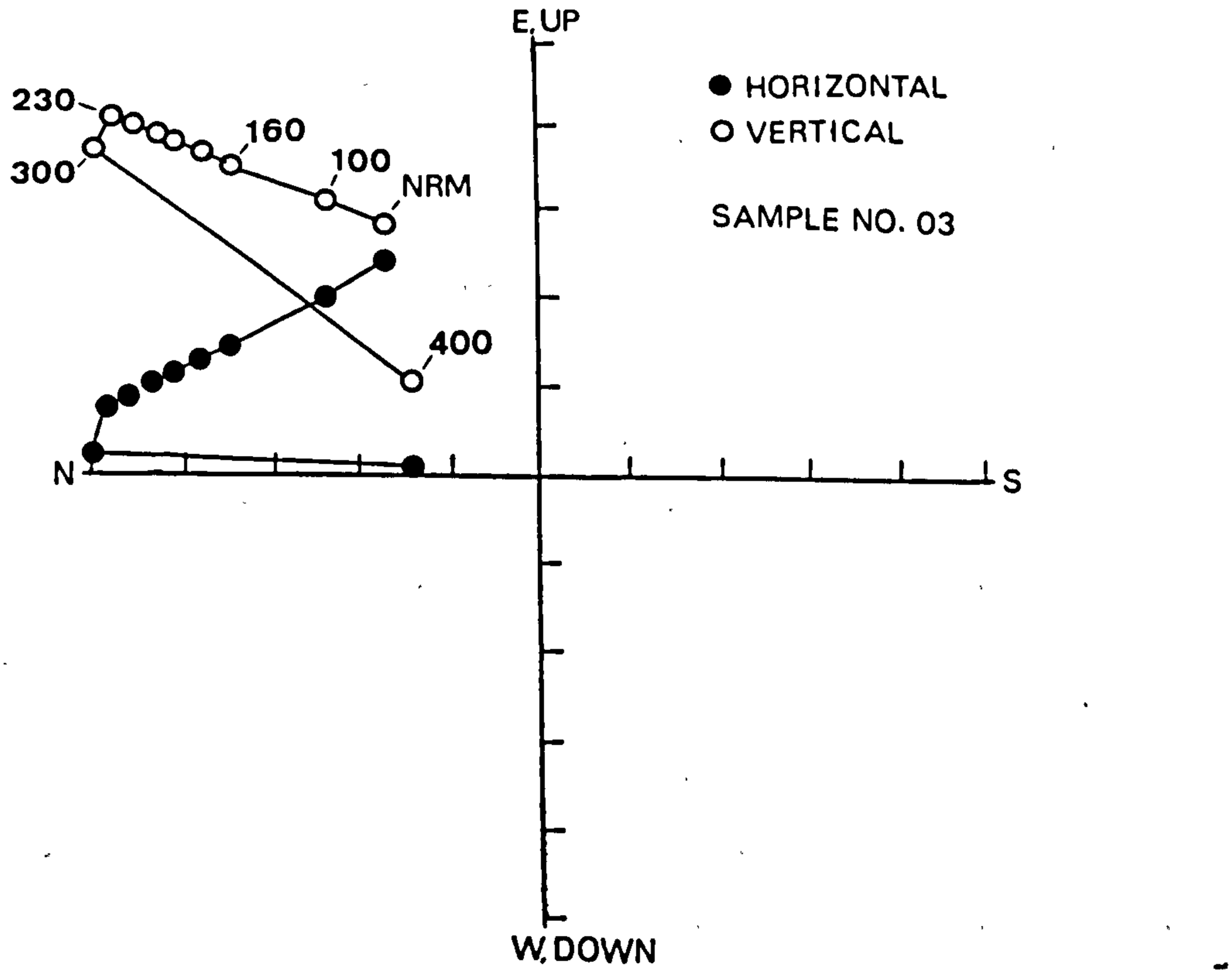

Figure 8.8. An example of the thermal demagnetisation behaviour obtained from the Saxon pottery sherd, the numbers indicate the demagnetisation temperatures in °C.

Table 8.2. Demagnetisation temperatures and times obtained from three subsamples of Saxon age pottery sherd.

Sample no.	Demag. temperature (°C)	Demag. time (minutes)
01	175-200	12
02	230-250	12
03	230-300	12

good agreement, the reason for this is not obvious. Despite the poor agreement, an age for the viscous remanence can still be determined using the observed temperature range. Equation 8.11 has been evaluated using the values for the various required parameters shown in table 8.2. The estimated ages obtained from the minimum and maximum demagnetisation temperatures are 4.6×10^7 and

$3.9x10^{22}$ years respectively. The estimated ages are represented graphically in figure 8.9. These ages are considerable overestimates of the true age. This result is similar to that noted previously by Pullaiah et al (1975) and Enkin & Dunlop (1988) for rock samples. The reason for this overestimate is not clear since the samples investigated do not contain a large multidomain fraction although pseudosingle domain particles may play an important role.

Table 8.3. Values for parameters used to evaluate the demagnetisation time-temperature relationship eq.8.11.

Parameter	Value	Description
C	10^{10}Hz	Fundamental attempt frequency of thermal fluctuations.
t_1	720 seconds	Laboratory demagnetisation time, equivalent to relaxation time, τ, at demagnetisation temperature.
T_1	448-573 K	Range of demagnetisation temperatures, in Kelvin, needed to remove viscous remanence.
$\frac{M_s(T_2)}{M_s(T_1)}$	1.105-1.230	Ratio of saturation magnetisation at the ancient acquisition temperature to that at the demag. temperature.
$\frac{H_c(T_2)}{H_c(T_1)}$	1.105-1.230	Ratio of microscopic coercivity at the ancient acquisition temperature to that at the demag. temperature.
T_2	278 K	The temperature at which the ancient viscous remanence was assumed to be acquired, i.e. 5°C.
t_2	REQUIRED	This is time required for the acquisition of the original viscous magnetisation.

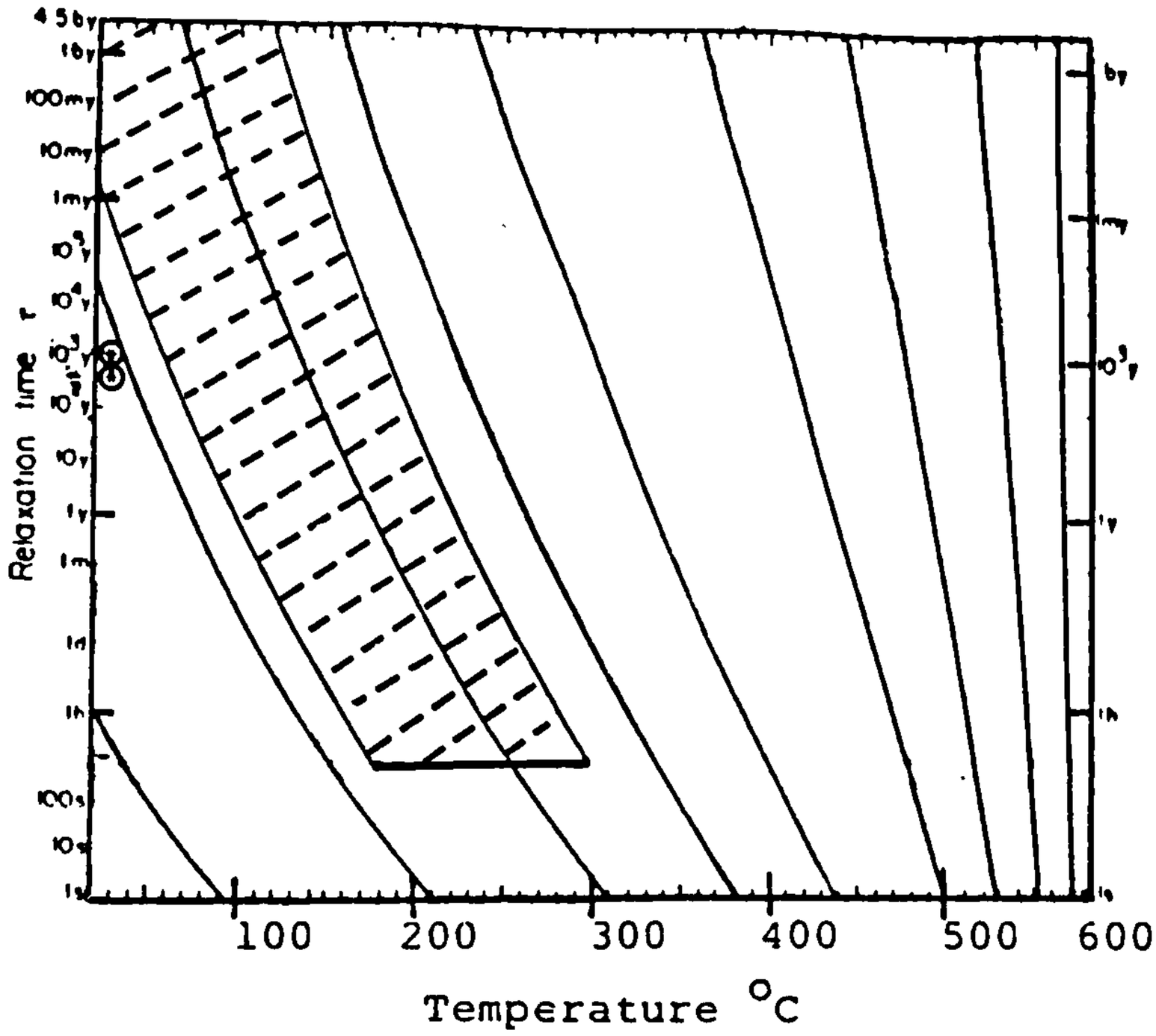

Figure 8.9. Graphical representation of the temperature dependence of the relaxation time after Pullaiah et al. (1975). The demagnetisation time and temperatures obtained in this study are represented by the thick horizintal line draw on the graph. The variation of the relaxation time with temperature for the sample investigated in this study is shown by the hatched area on the graph. The true age of the sherd investigated is indicated by two stars on the graph at the assumed VRM acquisition temperature. The calculated relaxation times, based on the observed demagnetisation temperatures, are not coincident with the true age of the viscous remanence.

An investigation of the magnetic viscosity of ancient ceramics at elevated temperature is difficult because the magnetisation of these materials is relatively weak. A cryogenic SQUID magnetometer was used in this study to investigate the magnetic viscosity of ceramics. The aim of this investigation was to obtain the temperature dependence of the acquisition coefficient, which could then be used to date the age of viscous remanence of a sherd. The magnetometer utilised was capable of heating a sample and applying a small magnetic field while the sample was

positioned in the measuring position (Share, 1986). This arrangement reduced the overall sensitivity of the system because of the increased separation between the sense coil and the sample as a result of the thermal insulation required. The sensitivity was sufficient to measure the viscous remanent magnetisation of many of the ceramic samples investigated in this study, see figure 8.10.

However, the magnetometer system performance was poor when measurements were made in the presence of an applied field or when the furnace was in operation, i.e. the conditions required for the high temperature viscosity experiments. These problems were not overcome during the course of this study and therefore the experimental evaluation of alternative dating methods wasn't undertaken.

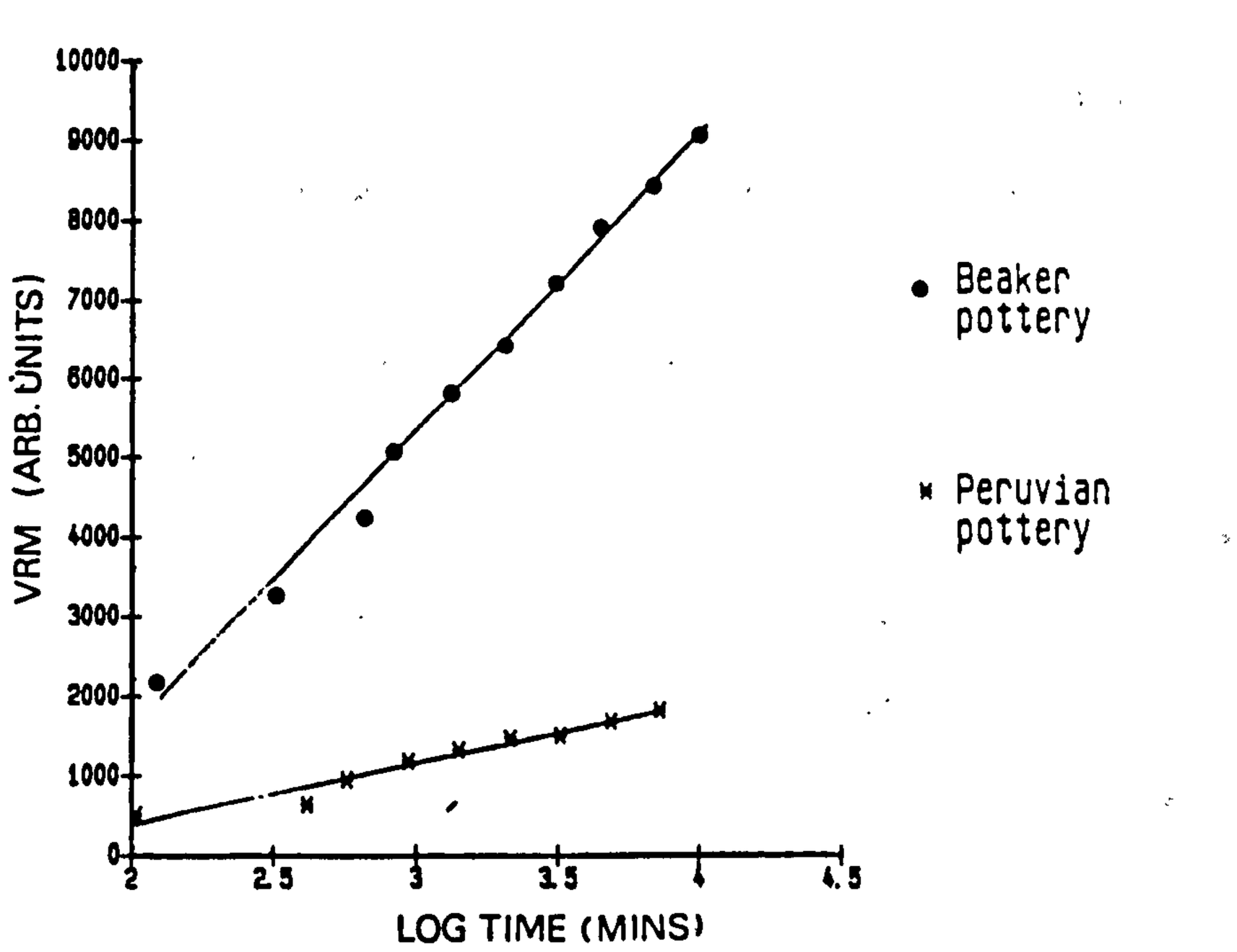

Figure 8.10. Two examples of the acquisition of viscous remanence of ancient ceramics measured using the system developed by Share (1986).

9 Archaeomagnetism of a Red Sandstone Kiln: a Case Study

9.1 Introduction

A magnetic investigation of samples from an ancient kiln was undertaken in order to determine the age of last firing by comparing the direction of remanence obtained from the kiln with an established reference curve of geomagnetic secular variation. The demagnetisation behaviour, magnetic mineralogy, magnetic fabric and the effect of refraction were investigated in order to determine the origin and fidelity of the remanence.

9.2 Sampling

The kiln investigated was discovered during excavation by archaeologists from the Grovesnor Museum, on a building site close to John Street in Chester, Cheshire. The site is very close to the wall of the Roman fortress in the centre of the city. The remains of the kiln consisted of a small curved wall, which was about 75 cm high, from what was considered to be the original floor level. The top of the wall, which was approximately horizontal, was constructed from roughly shaped red sandstone blocks of variable dimensions. Below these blocks the wall consisted of many small irregular pieces set within a very soft matrix. Evidence of firing was apparent from the blackened inner surface of the wall and the presence of ashes towards the base of the structure. The sandstone used to build the kiln is probably the local Triassic Red Sandstone which

has been used in many other constructions.

The large blocks on the top of the wall were oriented using a tripod mounted suncompass. The positions of the feet of the tripod were accurately marked on each block before they were removed intact. Four large blocks were taken for investigation. Attempts to orient some of the smaller blocks from lower in the wall were unsuccessful because they were easily disturbed on contact due to the weak cement.

No samples were taken from the kiln floor because of the lack of suitable sampling equipment for this type of material.

9.3 The direction of the remanent magnetisation

In the laboratory, cylindrical subsamples were obtained using a standard 25 mm diamond impregnated palaeomagnetic drill bit. The NRM and the remanence remaining after each step of incremental thermal demagnetisation was measured for each of the subsamples using a Molspin spinner magnetometer. The background noise level of the magnetometer was determined by repeating the measurement procedure without a sample, this indicated a noise level of about 10^{-7} Am^2kg^{-1}, for a sample mass of about that used in this study.

The unblocking spectrum obtained from each subsample within a block was plotted against the distance of the subsample from the heated surface of the block. This is shown for block 2 in figure 9.1. The temperature at which

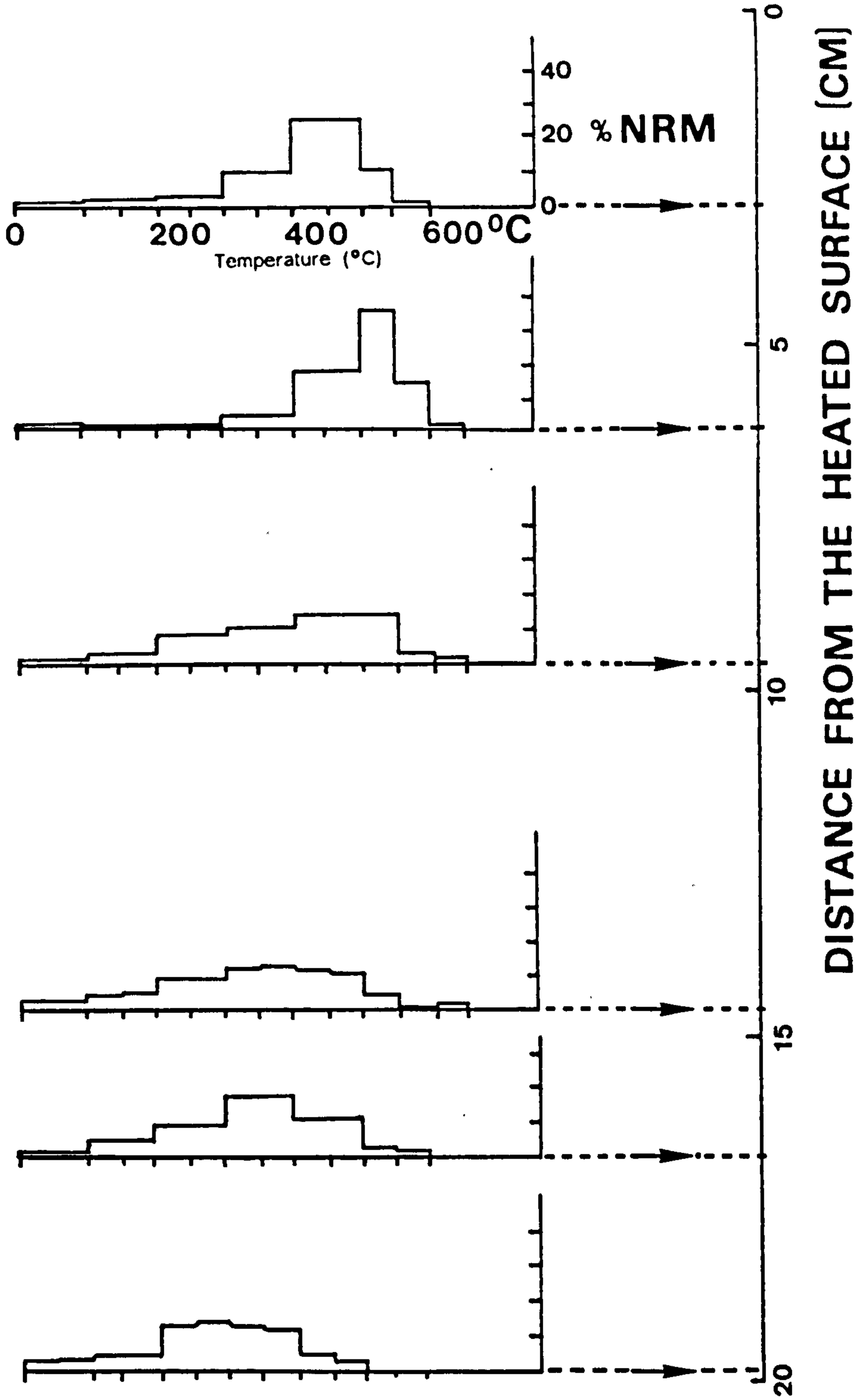

Figure 9.1. An example of the variation of the unblocking temperature spectra with distance away from the heated surface of a block. Data for block 2.

the largest fraction of the remanence is held increases slightly with distance then falls gradually with further increasing distance away from the heated surface. Also the unblocking spectra become broader with increasing distance from the surface. Similar behaviour is observed in the other blocks. The thermal demagnetisation results were analyzed using orthogonal vector plots. The direction of the components were determined from the best fitting straight line calculated using principal component analysis as described by Sherwood (1989). The orthogonal plots revealed that the vector composition of the NRM was dependent on the distance of a subsample from what would have been the inner (heated) surface of a block. A low intensity component was removed from all of the subsamples after heating to 200-300°C. The direction of this component is irregular, in particular at the lower temperatures, see figure 9.2a,b. The low unblocking temperature of this component suggests that it may be attributed to the effect of magnetic viscosity acting over time since the last firing, or to partial reheating in antiquity. In addition, all of the subsamples showed a relatively intense northerly/positive component of magnetisation of which 95% was removed by heating to between 470°C and 550°C. For the subsamples nearest to the heated surface this was the only other component, see figure 9.2a. In contrast, the subsamples taken furthest from the heated surface had an additional component which was observed at higher temperatures, up to 700°C, see

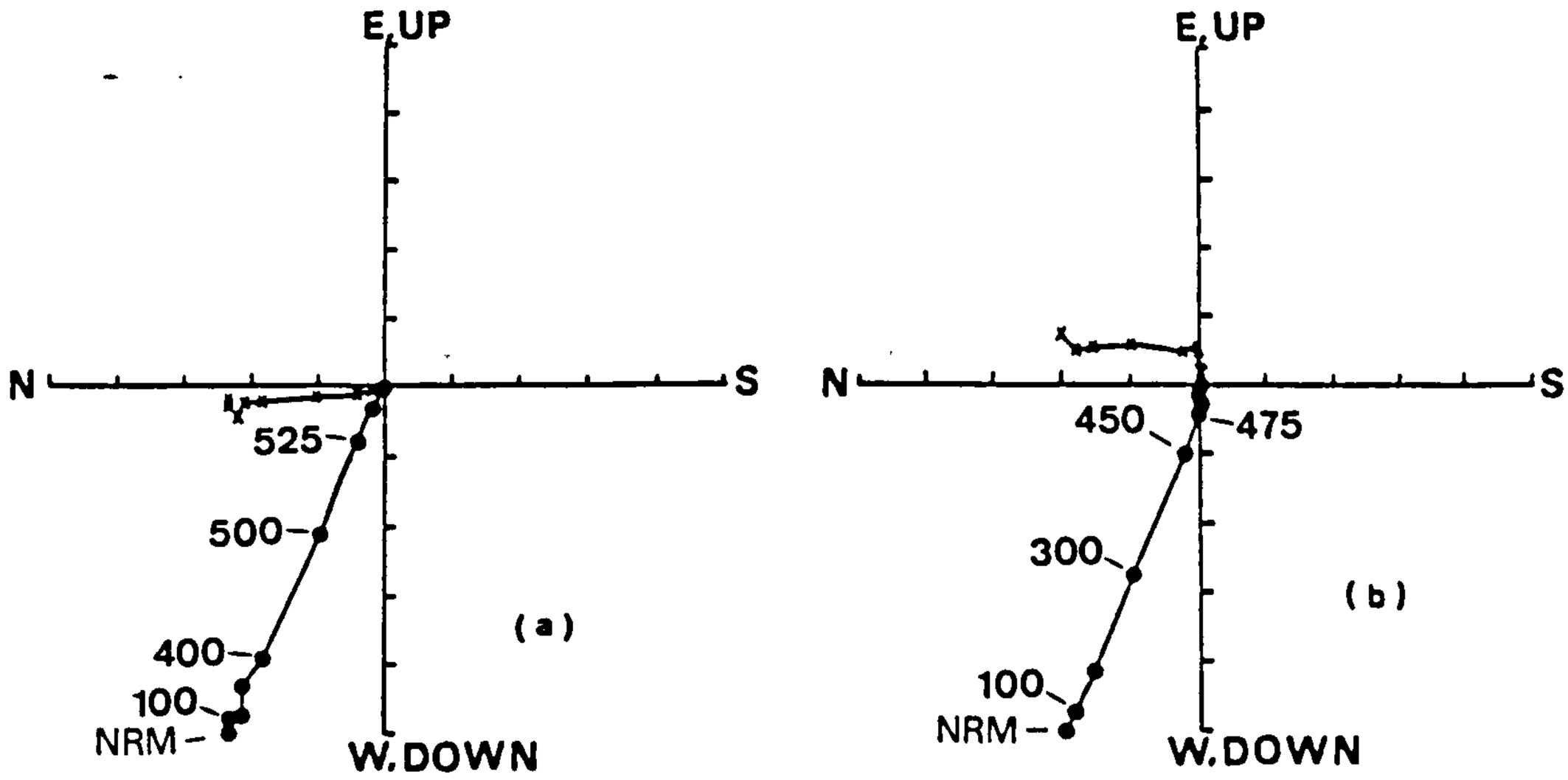

Figure 9.2. Orthogonal vector plots obtained by thermal demagnetisation of subsamples from (a) near the heated surface, B102, and (b) further from the heated surface, B104. The crosses indicate the horizontal projection and the circles the vertical projection. The numbers indicate the demagnetisation temperature.

figure 9.2b. This component was much weaker and its direction could not be precisely defined.

The high intensity and northerly/positive direction of the component of magnetisation that is unblocked between 470°-550°C was considered at this stage to represent the last firing of the kiln although additional measurements are needed to confirm this. The component is therefore referred to as the characteristic component. The mean direction of this component has been calculated for each of the four blocks, see table 9.1.

Table 9.1. Mean directions for the characteristic component in each block.

Block	Declination	Inclination	α_{95}	n
1	358.6°	66.4°	4.7°	5
2	7.7°	56.7°	1.3°	10
3	357.8°	65.0°	2.0°	7
4	350.0	65.8°	3.3°	4

Note: $_{95}$ is the half angle of the cone within which there is a 95% probability of finding the mean direction, according to the statistics of data on a sphere developed by Fisher (1953).

These directions and their associated errors are shown in figure 9.3. It can be seen that the direction of the characteristic component obtained from block 2 is not consistent with that from the other three blocks. It is possible that this may be the result of slight displacement of block 2 because it was situated on the end of the remains of the wall and was therefore more vulnerable to such disturbance. The data from block 2 was neglected in subsequent analysis.

A mean direction for the characteristic remanence direction of the kiln was calculated, from the direction cosines,to be;

Declination 355.4° Inclination 65.8° α_{95} 3.2.°

For dating purposes it must be shown that the characteristic remanence was induced by firing and subsequent cooling in antiquity and that its direction can be considered representative of the ambient magnetic field at that time.

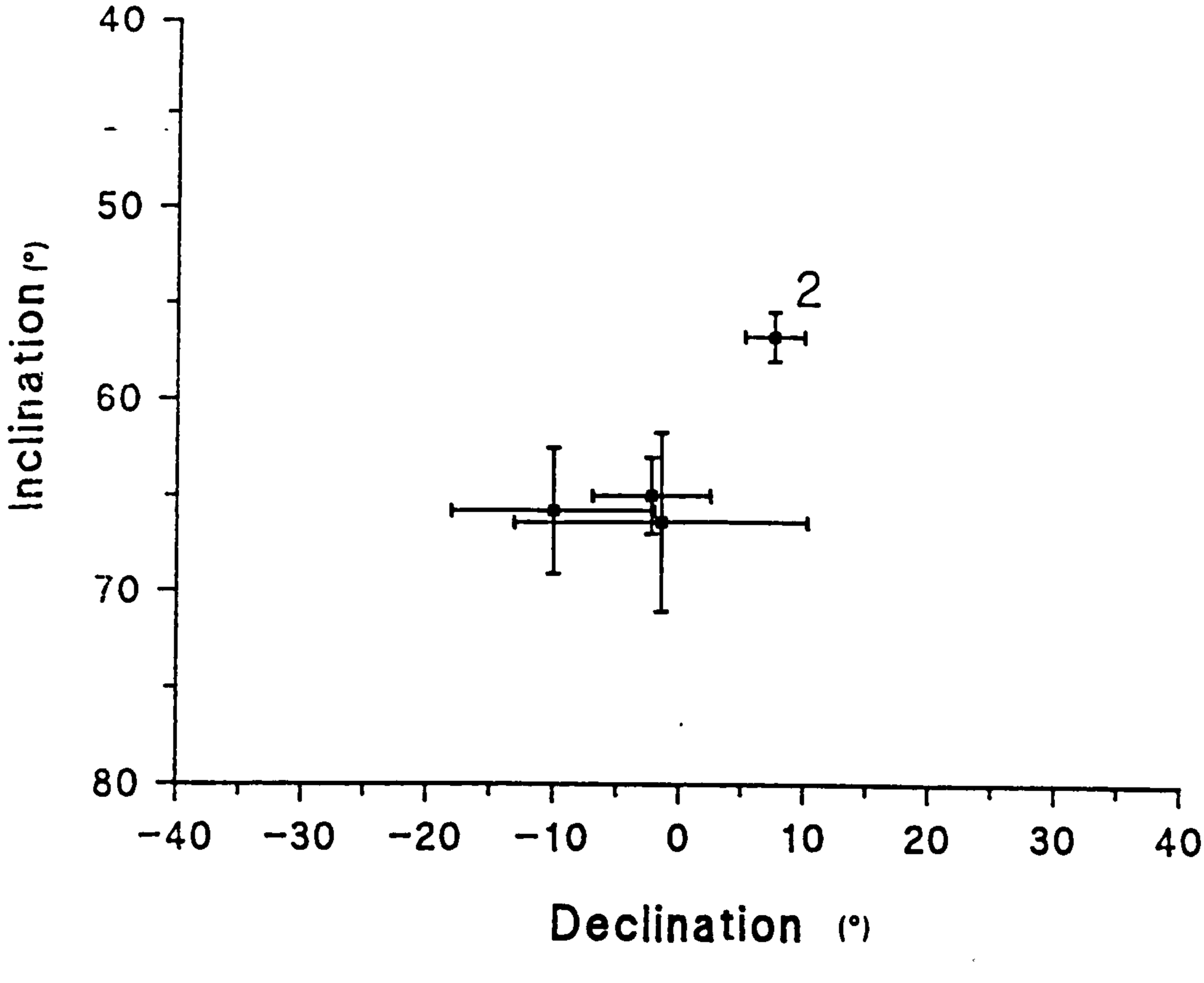

Figure 9.3. The mean remanence direction and 95% confidence limits, calculated from the α_{95}, for each of the blocks. The data for block 2 is indicated.

9.4 Magnetic mineralogy

In common with the unblocking spectra, the magnetic mineralogy is a function of the distance from the heated surface. The variation of the NRM and the bulk susceptibility, measured using a Bartington MS2 meter, are shown for block 2 in figure 9.4. The intensity of the NRM increases from around 100-200 x 10^{-5} Am^2kg^{-1} near the heated surface to a peak close to 800 x 10^{-5} Am^2kg^{-1} at approximately 5 cm from the surface. Further into the blocks the intensity falls rapidly further to a value of less than 0.5 x 10^{-5} Am^2kg^{-1} beyond about 10 cm. The trend

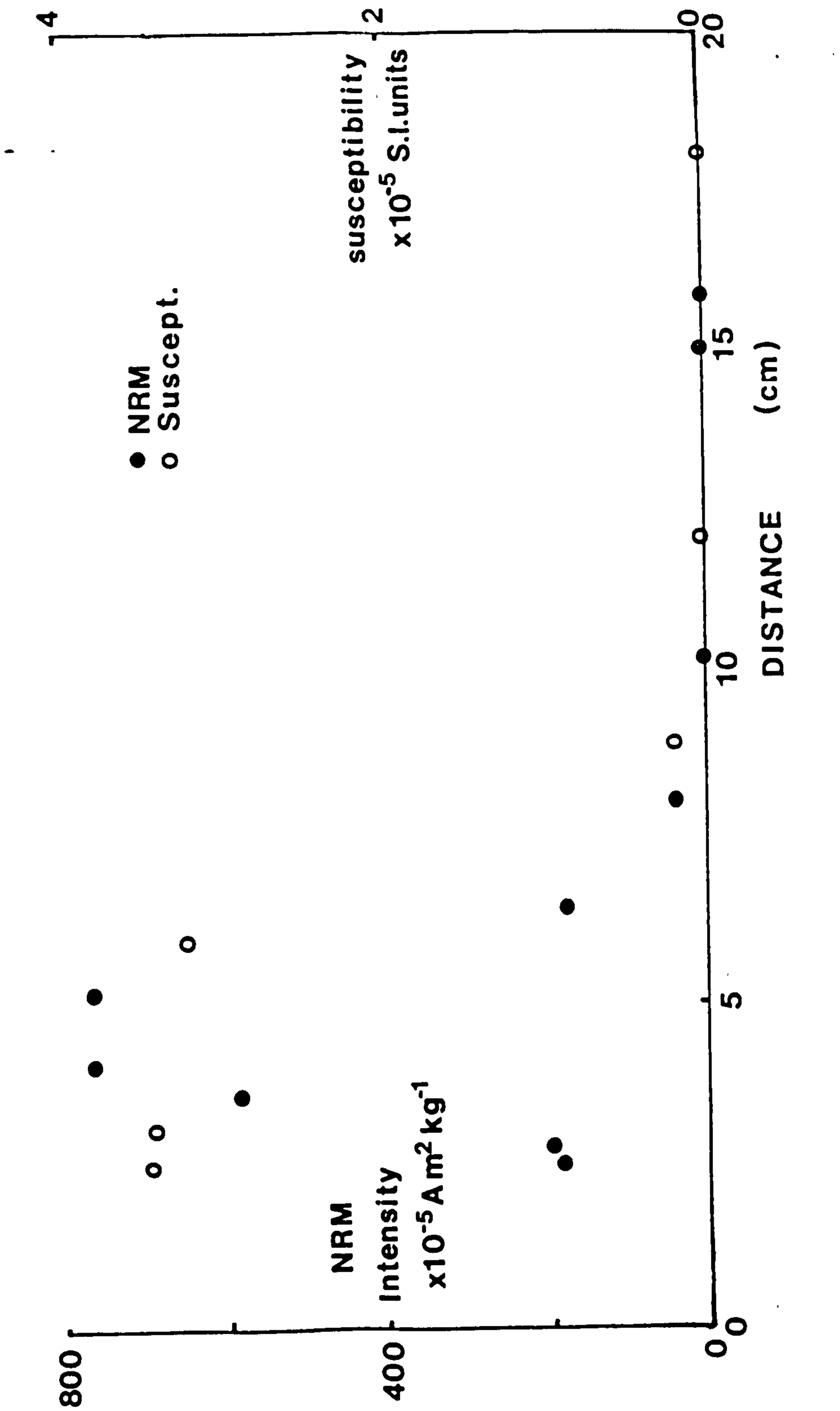

Figure 9.4. An example of the variation of the NRM intensities and the bulk susceptibility with distance from the heated surface. The errors in the remanence values are about +/- 0.01 Am^2kg^{-1} and the errors in the susceptibility are +/- 1x10-4 SI units.

of the susceptibility differs in that the susceptibility maintains a relatively high value of 3-4 x $10^{-5}m^3kg^{-1}$ within the first 5 cm from the heated surface, after which the susceptibility falls rapidly in a similar manner to that observed for the NRM, although the magnitude of the change is smaller.

Thermomagnetic analysis has been carried out on samples from the kiln wall and on samples from a block of similar, but unheated, red sandstone associated with the feature at the excavation site. The measurements were made using the Curie balance described in chapter 3. Figure 9.5 shows the variation of the thermomagnetic behaviour for three subsamples taken at increasing distances from the heated surface of block 3 and for a subsample from the unheated sediment. The behaviour of subsamples from the other blocks is similar. The samples closest to the heated surface are comparatively strongly magnetised and have a Curie point temperature of about 560°C, see figure 9.5a, suggesting magnetite or a slightly-titanium-substituted magnetite. Further from the heated surface, about 5-10 cm in block 3, the magnetisation becomes progressively weaker and the Curie point temperature shifts to higher temperatures of about 620°C, see figure 9.5b. This increase in the Curie point temperature is difficult to explain but may be due to the convoluted response of magnetite and haematite or alternatively it may be the result of oxidation of the magnetite to a cation deficient state. At even greater distances from the heated surface

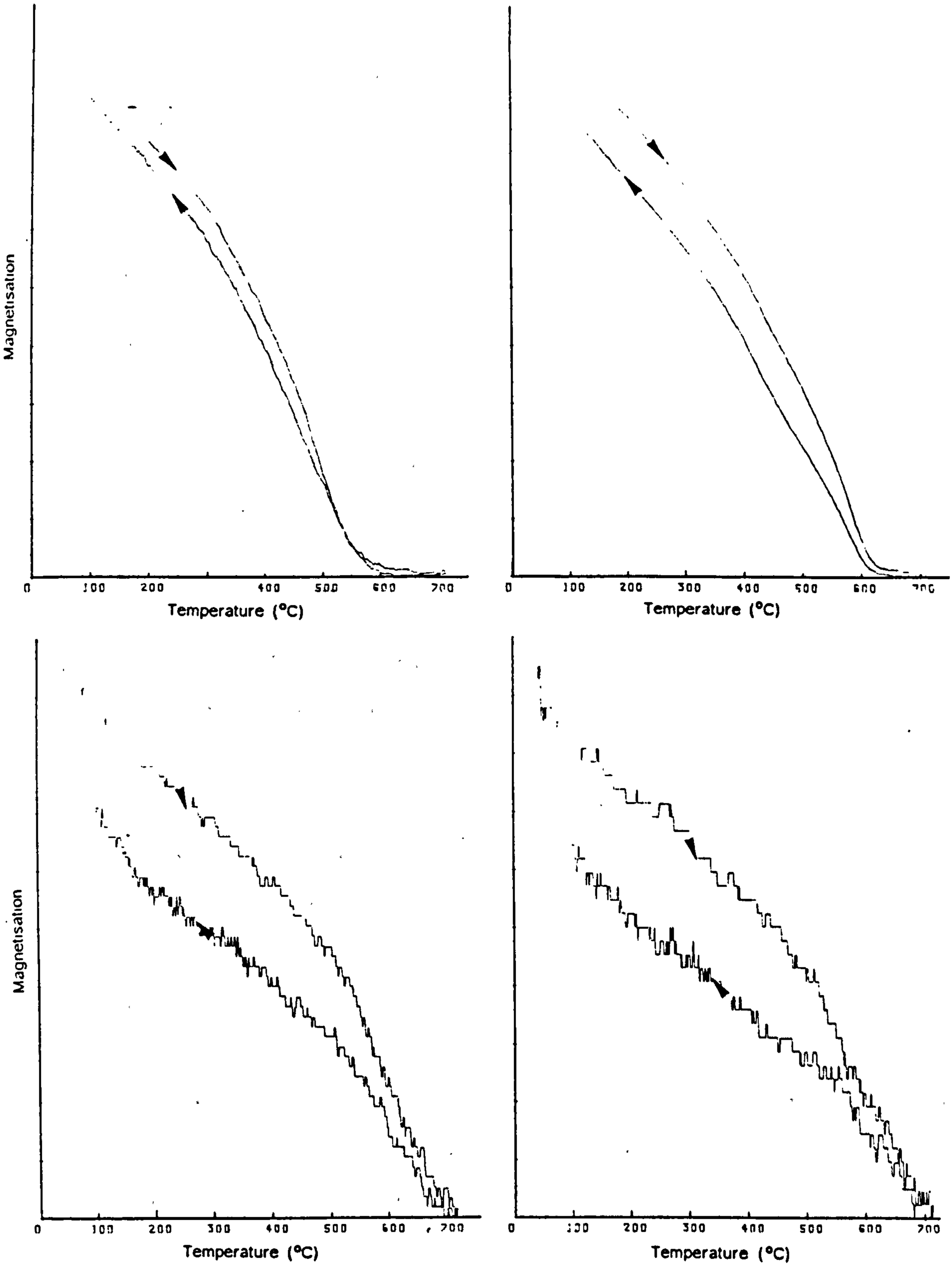

Figure 9.5. Thermomagnetic behaviour of subsamples from block 3 taken at (a) 1 cm, (b) 7 cm and (c) 12 cm from the heated surface and from the unheated sediment (d).

the magnetisation is much weaker. The curves of these samples are concave at lower temperatures indicating a paramagnetic component or possibly unblocking of haematite which is unlikely to have been saturated in the applied field of the Curie balance. The only clear Curie point at this distance is close to 700°C, this suggests the presence of haematite (see figure 9.5c). The thermomagnetic behaviour of the distal samples is similar to that of the unheated sediment, which is characterised by a haematite Curie point temperature, compare figures 9.5c and 9.5d.

The acquisition of isothermal remanence was also investigated as a function of distance from the heated surface and, following the work of Stephenson (1967) and Dunlop (1972), before and after laboratory heating. Isothermal remanence was induced using the two pulse magnetisers described in chapter 4, and the remanence was measured using a Molspin magnetometer, which was also described in chapter 4. Isothermal remanence acquisition was undertaken on some subsamples before and after laboratory heating at 600°C for 60 minutes. Figure 9.6 shows the isothermal remanence acquisition curves for subsamples close to and more distant from the heated surface of a block, and also the acquisition curves for the same subsamples after laboratory heating. The isothermal remanence acquisition characteristics of subsamples close to the heated surface are consistent with the presence of magnetite, but the lack of a high coercivity fraction suggests that no haematite is present. Further from the

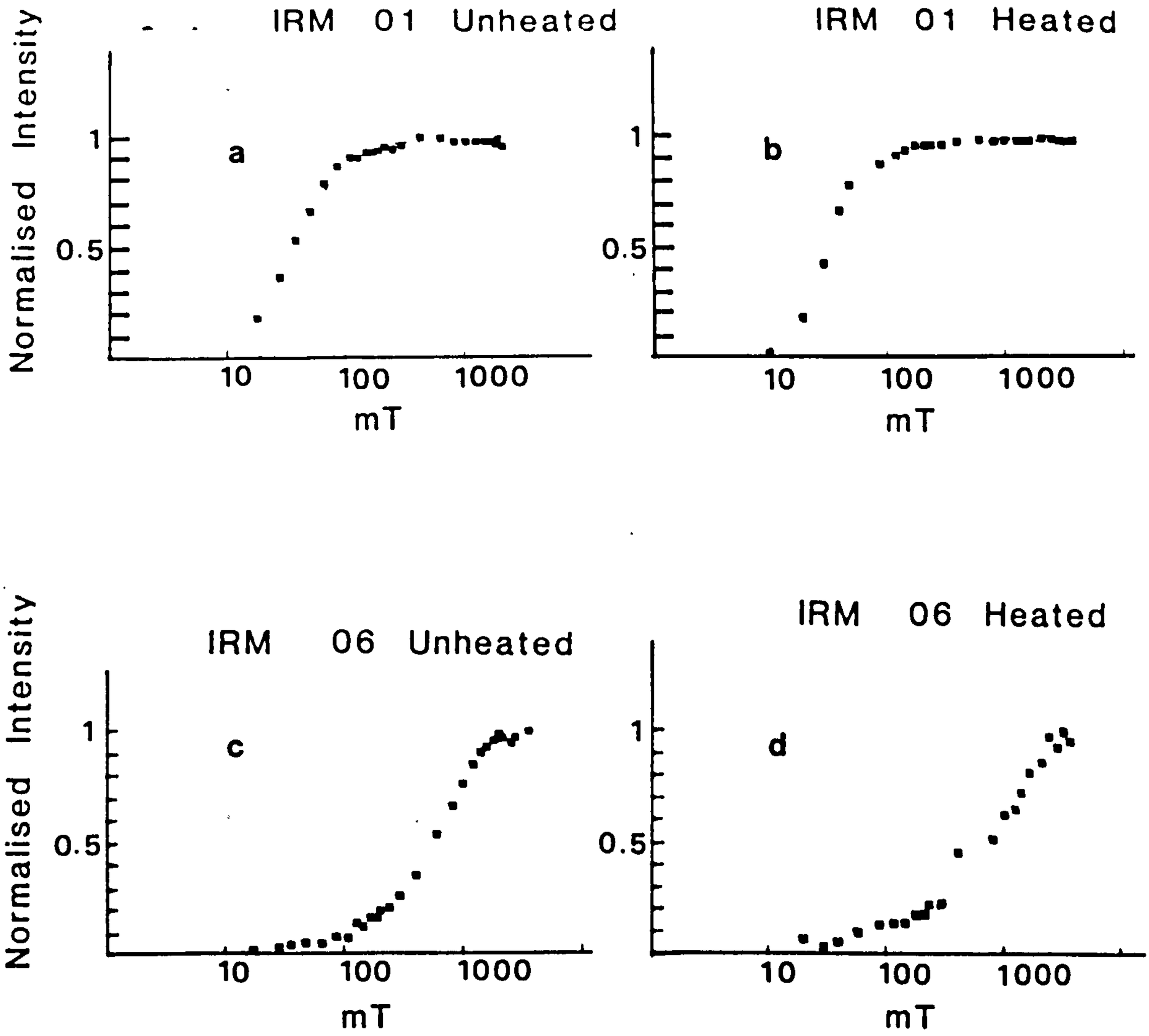

Figure 9.6. Isothermal remanence acquisition data for (a) a subsample close to the heated surface, (b) the same subsample after laboratory heating, (c) a subsample taken far from the heated surface and (d) the same subsample after laboratory heating.

surface the large fraction of the remanence held at higher coercivities indicates that the predominant magnetic mineral is haematite. Laboratory heating barely affects the IRM acquisition characteristics of the subsamples taken

from close to the surface, which show only a slight decrease in the saturation remanence after heating. In contrast, the coercivity spectra of the samples which contain predominantly haematite does alter as a result of heating. The saturation magnetisation increases and the remanence fraction acquired below 300 mT increases which suggests the production of magnetite.

Magnetic hysteresis measurements were undertaken using the Molspin VSM described in chapter 5, the maximum applied field was 1 T. The M_{rs}/M_s ratio was determined for samples for which the hysteresis loops were observed to saturate below 500 mT. The M_{rs}/M_s ratio for these samples was found to be between 0.29 and 0.31. Taking an average value of the M_{rs}/M_s ratio and combining this with the measured contribution of magnetite (low coercivity fraction) to the saturation remanence, as determined from the isothermal remanence acquisition experiments, the percentage, by mass, of magnetite in the bulk material was estimated with distance from the heated surface for block 1 (figure 9.7). The magnetite fraction is observed to fall, at first slowly, from about 0.1% and then more rapidly, between 9 cm and 11 cm from the surface to less than 0.002% of the total mass.

The variation of the demagnetisation behaviour and the magnetic mineralogy are consistent with the effect of firing.

The variation of the unblocking spectra and the vector composition of the natural remanent magnetisation with

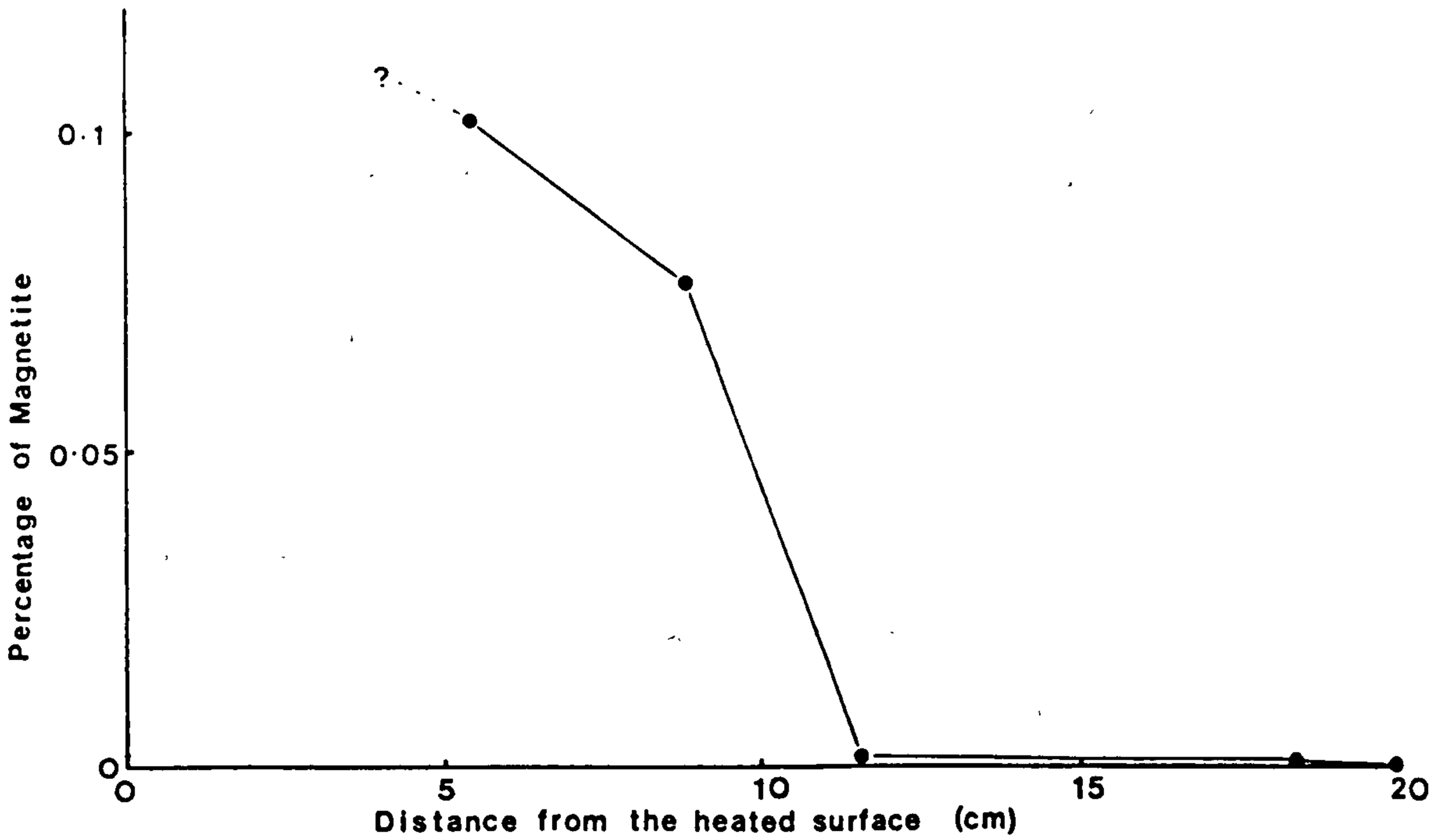

Figure 9.7. The variation of the mass fraction of magnetite with distance from the heated surface of block 1.

distance from the heated surface can be explained by considering the temperature through the wall during firing. The shift to lower temperatures of the peak in the unblocking spectra with increasing distance into the blocks is consistent with the temperature variation that would be expected if the inner side of the wall formed the inside of a kiln as supposed by the archaeologists. The vector composition of subsamples taken from close to the heated surface indicates the complete replacement of the original remanence with a new firing induced remanence. In the subsamples further from the heated inner surface the

presence of an additional component of magnetisation and the lower temperature required to remove the characteristic remanence indicates only partial replacement of the original remanence as a result of the lower temperature attained during firing. The higher temperature component in these subsamples is not consistent between the blocks, indicating that this remanence predates the construction of the structure; possibly representing the primary remanence of the sediment.

The study of the susceptibility, thermomagnetic behaviour and IRM acquisition indicate that the magnetic mineralogy has been greatly affected by firing. It is clear from figure 9.7 that firing has produced a relatively large amount of magnetite. The production of magnetite by laboratory heat treatment of red sandstone has been investigated by Stephenson (1967) and Dunlop (1972). Stephenson (1967) reports an increase in susceptibility after heating between 500°C and 700°C and above 850°C, which is attributed to the formation of magnetite. Dunlop (1972) draws a similar conclusion from analysis of the coercivity spectrum before and after heating suggesting that magnetite is formed by reduction of the primary haematite. Analysis of the coercivity spectra of the distal samples before and after laboratory heating at 600°C also reveals an increase in the low coercivity region indicating the production of magnetite. However, none of laboratory heat treatments of red sandstone reported here or previously, even after heating at 1000°C for 2 hours as

reported by Stephenson (1967), have produced the complete reduction of haematite to magnetite which appears to have occurred during firing in antiquity at the surface of the kiln wall, see figure 9.6a. This may be explained by considering the firing atmosphere which would have been enriched with carbon dioxide (CO_2) and carbon monoxide (CO), from the combustion of the fuel, both of which are strong reducing agents.

The production of magnetite can simply explain the increased susceptibility close to the heated surface. However, the variation of the NRM intensity requires a more complicated explanation. With increasing distance from the heated surface the NRM intensity rises to a peak and then falls with further distance, this may be explained in terms of the domain structure of the magnetite produced. The process of reduction is likely to have occurred from the surface of the original haematite particles towards their centre. The maximum size of the magnetite particles therefore depends on the size of the original haematite. If the production of magnetite is greatest at the heated surface, and assuming that the maximum magnetite size has not been reached, then the particles at the surface may have exceeded the single domain threshold size and hence display the reduced magnetisation associated with multidomain particles.

9.5 Deviation of the remanence

The effects of magnetic fabric anisotropy and refraction

upon the directional recording fidelity of the kiln samples has been investigated.

9.5.1 Anisotropy of magnetic susceptibility

If the easy axes of the magnetic particles in a material are randomly oriented, then the remanence acquired by the material will be in the direction of the inducing field. However, if there is some preferential alignment of the easy axes of the particles, for example due to the presence of a sedimentary fabric, the remanence acquired by the material will deviate from the direction of the inducing field. Such a material is referred as having a magnetic fabric. The magnetic fabric has been investigated by measuring the anisotropy of magnetic susceptibility (AMS) using a Molspin anisotropy delineator. The anisotropy delineator consists of two pairs of perpendicularly arranged coils which surround the sample. The sample is rotated about a vertical axis at about 7 Hz. One pair of coils carries an alternating current which provides an alternating field in the sample region of about 0.5 mT (Collinson, 1983). If the susceptibility of the sample is isotropic and the two sets of coils are exactly perpendicular, then no signal is picked up by the sensing coil. However, if the sample is anisotropic the presence of an applied field at some angle to the anisotropy axis will induce a magnetisation that will be detected in the sense coil. The alternating field leads to an alternating pick-up signal which is subjected to Fourier analysis to obtain a measurement of the susceptibility. A series of

six orthogonal measurements is used to determine the direction of anisotropy and to average out any inhomogeneity within the sample. The system was calibrated using the Molspin magnetic tape calibration sample provided.

The anisotropy of magnetic susceptibility was measured for subsamples taken from one of the blocks. The length to width ratio of the subsamples was 1.0 which is slightly greater than the optimum value of 0.9 calculated by Hounslow et al.(1988). A small anisotropy was observed, the direction of which was similar for the subsamples within the block. See figure 9.8. The mean value for the lineation, foliation and the percentage of anisotropy for the block are given in table 9.2.

The above measurements indicate the presence of a magnetic fabric, which will influence the direction of remanence recorded in a material. However, Hrouda (1982) has shown that the effect of magnetic fabric on the direction of remanence is negligible when the percentage anisotropy is less than 5%. In this study the mean percentage obtained from the block investigated is below 5%, although the range of percentages, represented by the standard deviation, shows that some samples have slightly larger than 5% anisotropy. It can be concluded that the effect of the magnetic fabric on the remanence direction will be very small or negligible.

9.5.2 Magnetic refraction

In addition to deviations of remanence which can result

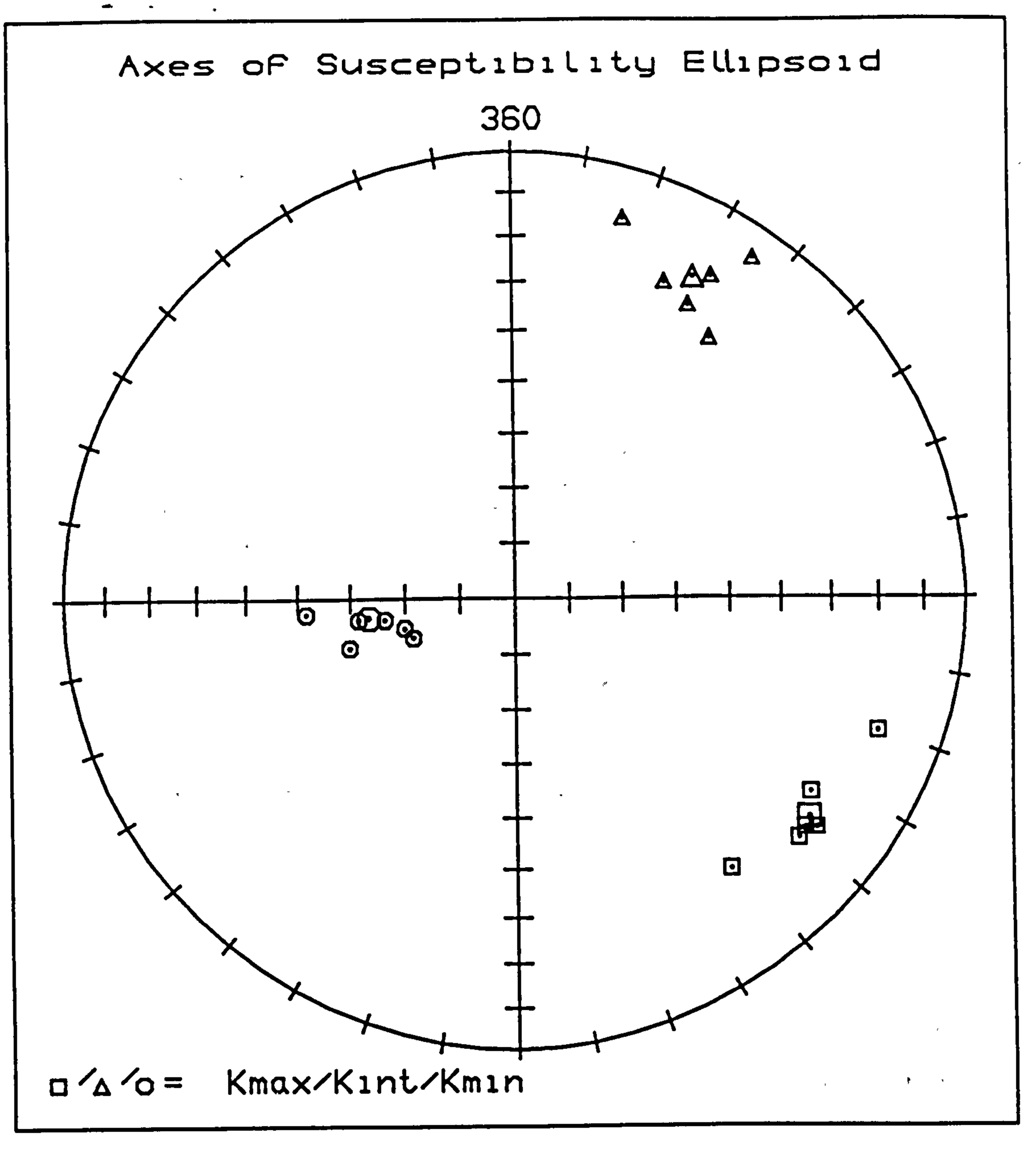

Figure 9.8. The direction of the maximum, minimum and intermediate axes of the susceptibility for block 1. The mean directions are shown as the larger symbols.

Table 9.2a. Parameters for the anisotropy of magnetic susceptibility

Block	Maximum			Minimum			Intermediate		
	Dec.	Inc.	α_{95}	Dec.	Inc.	α_{95}	Dec.	Inc.	α_{95}
1	124.6	18.3	8.9	29.8	15.8	9.6	261.5	66.5	7.8

Note: The direction and the 95% confidence limits for the maximum, minimum and intermediate susceptibility axes.

Table 9.2b

Block	P	E	Percentage
1	1.042 ± 0.011	1.025 ± 0.010	4.2 ± 1.1

Note: P is the ratio of the maximum to minimum susceptibility, E is the ratio of the intermediate to minimum susceptibility and the percentage is the ratio of maximum to minimum susceptibility multiplied by 100%. The errors are one standard deviation.

from an inherent alignment of the magnetic particles in a material, the direction of the magnetic remanence may be deflected from the true geomagnetic field direction if the local magnetic field is distorted. Such distortion can result from the presence of metallic objects or iron slag in the vicinity of a kiln (Aitken, 1990) or from the magnetic field associated with the stone or clay used to construct a kiln. The first of these causes of distortion is very difficult to assess, while the second may be estimated, although according to Aitken (1990) it remains poorly understood. Distortion due to the intrinsic magnetisation of a structure is termed magnetic refraction, analogous with the optical phenomena. Magnetic refraction is a magnetostatic effect, where the demagnetising field

associated with the magnetisation of a material acts to deflect the magnetisation itself. The demagnetising field depends on the intensity of the magnetisation and tends to drive the magnetisation of a material towards the position where the demagnetising field is smallest. In the case of a infinite sheetlike body, which has been commonly considered in theoretical treatments, the lowest demagnetising factor, and hence the smallest demagnetising field, is in the plane of the sheet, which therefore refracts the magnetisation of the body into the plane of the sheet. This causes a steepening and azimuthal deflection of remanence in vertical sheets and a shallowing of the remanence direction in horizontal sheets.

Magnetic refraction has been investigated by several workers including Aitken & Hawley (1971), Stacey & Banerjee (1974), Coe (1979), Abrahamsen (1986) and Evans & Hoye (1990). The studies by Stacey & Banerjee (1974), Coe (1979) and Abrahamsen (1986) are primarily concerned with the theoretical treatment of refraction while Aitken & Hawley (1971) and Evans & Hoye (1990) have investigated the occurrence of refraction in archaeological contexts.

The theoretical treatment of refraction by Stacey & Banerjee (1974) is the same as that of Abrahamsen (1986), which is followed here. In this treatment the degree of refraction is determined by considering an infinite sheet of magnetic material through which a magnetic field passes. The demagnetisation factor is zero in the plane of the sheet and is a maximum, 1.0 in SI and 4 in c.g.s. systems

respectively, perpendicular to it. The demagnetising field of a material acts in the opposite sense to the intrinsic magnetisation. The resultant field direction experienced by the material is the vector sum of the applied field and the demagnetising field, which leads to a reduction of the perpendicular component of the incident magnetic field in a sheet-like body. The degree of refraction depends on the intensity of the magnetisation of the material and the angle of incidence of the magnetic field. Abrahamsen (1986) obtained a relationship, for the c.g.s. system, between the angle of incidence and the angle of refraction of a magnetic field of the form;

$$\tan v_o = \frac{\tan v}{(1+4\ K_{app})} \qquad (9.1)$$

where v_o is the angle of incidence, measured from a perpendicular to the sheet, v is angle of the field in the material and K_{app} is the apparent susceptibility. The apparent susceptibility represents the combined effects of the remanence and the susceptibility at the blocking temperature. Rearranging equation 9.1 to determine the refraction error, $v-v_o$, leads to an expression of the form;

$$v\text{-}vo = v\text{-}\arctan\left(\frac{\tan v}{(1+4\ K_{app})}\right) \qquad (9.2)$$

The application of equation 9.2 requires some discussion. Firstly, the tan v dependence of the deviation leads to a maximum error when v is close to 45°. Secondly, a correct

estimate of K_{app} must be ascertained, in particular the value of K_{app} within the temperature interval in which the magnetisation blocks-in. In the simplest case of a sample which contains an assemblage of identical particles which are blocked-in at the same time, then the apparent susceptibility is simply the reversible susceptibility immediately prior to blocking-in. The apparent susceptibility in this case depends on the saturation magnetisation at the blocking temperature, which in turn depends on the size, domain configuration and concentration of magnetic particles in the sample. In a more typical sample, containing a distribution of blocking temperatures, the apparent susceptibility of the particles blocked-in just below the Curie point is the susceptibility measured at the blocking temperature. For particles blocked-in below this temperature interval, the apparent susceptibility includes both the reversible susceptibility at the lower blocking temperature and a contribution from the remanence blocked at higher temperature. Therefore, the assessment of the apparent susceptibility can be complex. Coe (1979) calculated the apparent susceptibility for basalts based on the temperature dependence of the remanence and susceptibility and suggested that the apparent susceptibility may be estimated empirically by 0.8k where k is the thermoremanent susceptibility. Evans & Hoye (1990) applied this method to data obtained from a collection of clay kiln samples and concluded that refraction greater than 4° is present in six samples from

five different kilns in a collection containing 287 samples from thirty kilns. The application of the method of Coe (1979) may not be appropriate to clay samples since the particle size distribution and unblocking spectra may be different from that of basalts.

The degree of magnetic refraction is calculated in this study by considering a block as a series of vertical sheets, which may be justified on the basis that the magnetic mineralogy and the intensity of remanence vary rapidly through the blocks. Since the most strongly magnetised region will show the largest refraction, then an upper limit on the refraction in the kiln can be obtained by calculating the amount of refraction in this region. The apparent susceptibility has been estimated by assuming that most of the remanence is blocked at the same temperature and with the apparent susceptibility being thus represented by the low field susceptibility at the blocking temperature. The temperature dependence of the low field susceptibility is shown for a subsample from the most strongly magnetised region of block 1 (see figure. 9.9). This was measured using a Bartington MS2 susceptibility meter with a water cooled sensor which surrounds an electrical furnace. The temperature dependence of the susceptibility reveals a relatively sharp peak suggesting a predominantly single domain particle size distribution (Dunlop, 1974) and which justifies, to some extent, the assumption of a single blocking temperature interval. The apparent susceptibility at the blocking temperature has

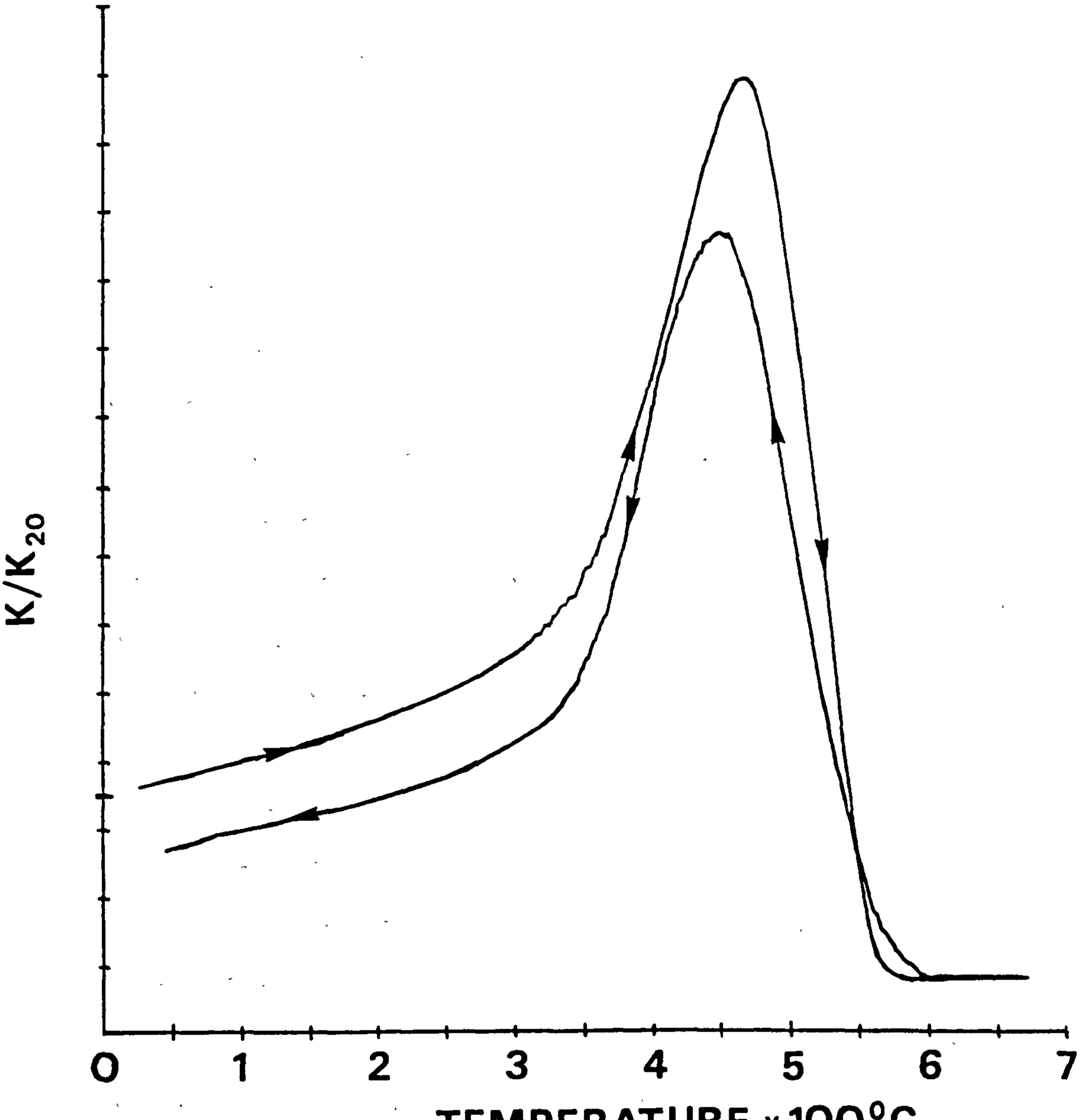

Figure 9.9. The variation of low field susceptibility with temperature for a subsample taken close to the heated surface.

been taken as the peak susceptibility measured at elevated temperature. The maximum K_{app} determined was 1.395 Am^{-1}, equivalent to the c.g.s. value of 1.395 x 10^{-3} emu cm^{-3}, which leads to a **maximum deviation** of 0.5° for v=45°. This deviation is the maximum based on the assumption of an infinite sheet of magnetic material and the estimated value of K_{app}. It is likely that the actual deviation will be less than this maximum, according to the analysis of Evans & Hoye (1990) who showed that the maximum deviation rarely occurs because the probability of v being close to 45° is small. The presence of systematic deviations of remanence in archaeological structures has been investigated by Aitken & Hawley (1971) and Schurr et al. (1984) by taking samples from several places around the walls of a structure. Unfortunately the remains of the kiln investigated in this study consisted of only a single wall from which the samples were taken in close proximity to each other and as such do not allow such a systematic study of the remanence deviation. However, the presence of refraction within a particular sample can be investigated by observing the direction of the characteristic remanence during demagnetisation. Considering the blocking of magnetisation during cooling, it is obvious that the apparent susceptibility will fall at higher temperatures and the degree of refraction will therefore be larger in the lower blocking temperature intervals than in the higher intervals. This will result in a systematic curvature of the direction of the characteristic remanence (e.g. Dunlop

& Zinn 1980). By inspection of the vector plots obtained in this study, for example see figure 9.2a, there is no evidence of systematic curvature and hence the earlier estimate of no significant refraction, is supported.

9.6 Archaeomagnetic dating

The investigation of the magnetic mineralogy and the deviation of the remanence suggests that the characteristic remanence is representative of the geomagnetic field at the time of last firing, although the possibility of subsequent physical disturbance cannot be discounted.

Archaeomagnetic dating is not an absolute dating method. In order to obtain a date for the last firing of a structure, the direction of remanence must be compared with a reference curve of past geomagnetic secular variation which has itself been constructed by dating using some other method, e.g. archaeological comparison, radiocarbon or dendrochronology. Archaeomagnetic reference curves of both direction and intensity have been compiled for several geographic regions (see Aitken, 1990). The necessity for more than one curve arises from the non-dipole contributions to the geomagnetic field and to its secular variation, which lead to regional differences that prevent the application of a reference curve from one region to the dating of a structure from another region. It has been suggested from observations of the present field configuration that no reference curve is applicable over a region with a radius greater than about 500 km (Clark et

al., 1988).

The most recent archaeomagnetic reference curve for Britain, representing over twenty years of work by various groups, has been compiled by Clark et al. (1988). The data for the reference curve has been obtained from various locations and as a consequence requires adjusting for the spatial variation of the geomagnetic field in order to make the individual data comparable. The method of correction assumes that over the geographical region to which the curve is applicable, the magnetic field can be represented by an inclined dipole. The declination and inclination of each data point is corrected to a standard location on the basis of this dipole assumption. The standard location to which British data are corrected is the town of Meriden (52.43°N, 1.62°W). To compare the results of this study to the reference curve, the declination and inclination must also be corrected to the appropriate standard location. After correction the declination and inclination of the characteristic remanence from Chester (53.20N, 2.90W) becomes;

Declination 355.9° Inclination 65.9°

A date for a structure can be simply obtained by plotting the data on the reference curve and observing where the error limits overlap with the curve. The application of this method to the kiln data is shown in figure 9.10, and gives dates for the last firing of ~50 BC, and ~100 to ~150 AD. However, this method may be regarded as unsatisfactory because it relies on the freehand best-

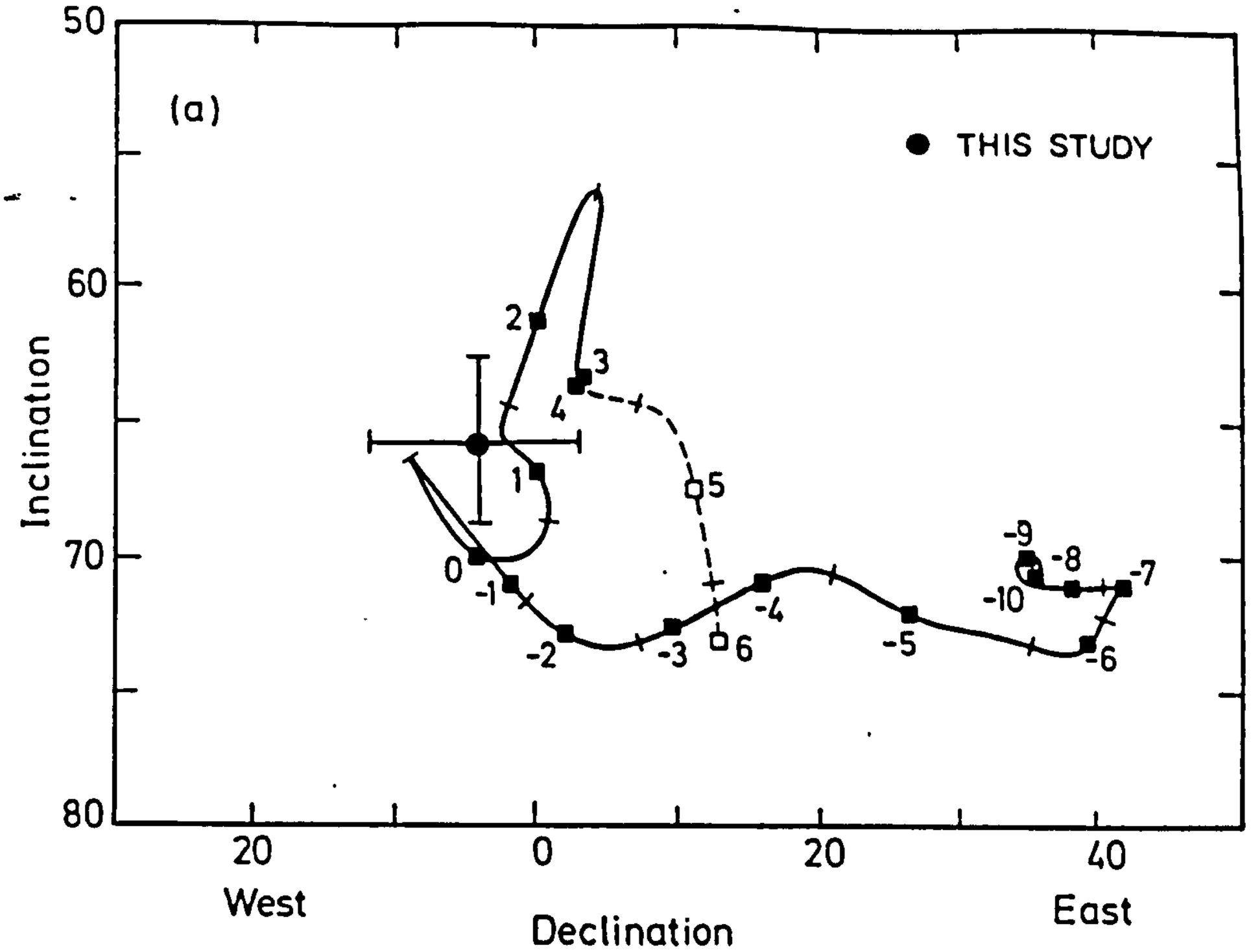

Figure 9.10. Direct comparison of the kiln direction with the archaeomagnetic reference curve of Clark et al. (1988). The numbers indicate the date in centuries, with -ve numbers representing dates BC, the tick marks on the curve indicate the midpoint of a century.

fit line drawn through the reference data and does not objectively involve the errors associated with the reference data. In order to improve the objectivity of the date assessment, the kiln data has been compared with the reference data and their associated 95% confidence limits, see figure. 9.11, from which a date range of 150 BC to 400 AD is obtained. It is apparent that this date range is larger than that obtained from the first method discussed. The most objective method of dating would be to statistically compare the kiln data with each of the reference data points in order to ascertain to within what confidence limit they both belong to the same population

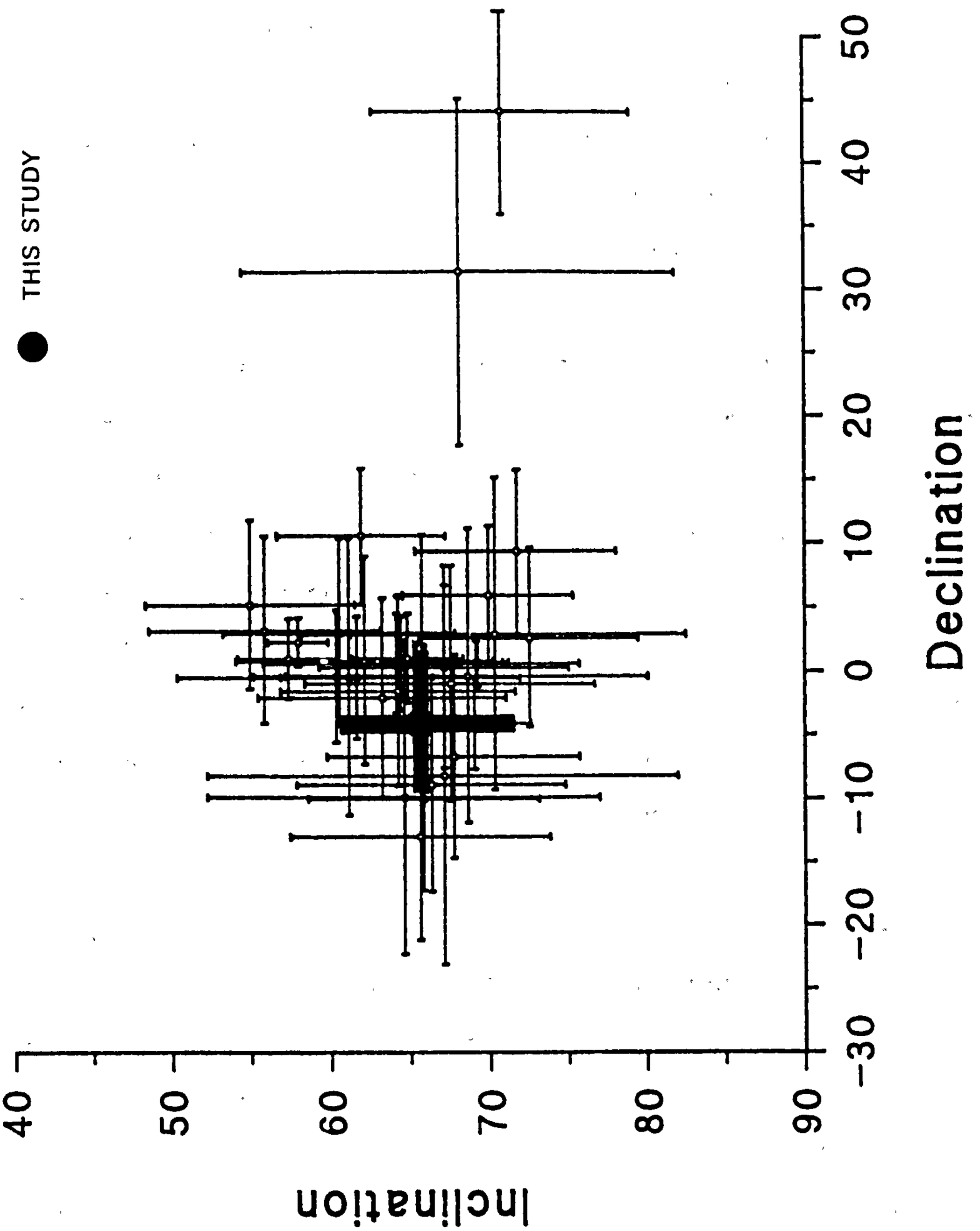

Figure 9.11. Comparison of the kiln direction with the reference data, including the errors associated with this data.

of directions. However, this analysis is not possible with the reference data presented by Clark et al. (1988) because the number of samples, N, from which the mean direction of each reference point was calculated, and which is required for the statistical comparison, is not given.

The archaeomagnetic dates obtained for the kiln coincide with the Roman period in England. This date conflicts with the archaeological evidence which indicates that the kiln post-dates the Roman activity and it has been suggested (D.J. Mason, pers. comm.) that the kiln was constructed in the Dark Ages (500-700 AD). The archaeomagnetic reference data for the Dark Ages has declinations greater than 10°E, well away from the kiln data, although the curve is poorly defined over this period (Clark et al., 1988).

Accepting the archaeological dates, the discrepancy between the archaeomagnetic and the archaeological dates might be explained by deviations of the remanence due to magnetic fabric or refraction, although the study of both of these aspects indicates they should have only a minor effect. An alternative explanation is that the whole kiln structure has subsided. Subsidence and slumping are problems that must be addressed in archaeomagnetic directional dating when a structure is not founded upon stable bedrock (Clark et al., 1988, Aitken, 1990). Aitken (1990) points out that structural movement is common in urban sites where previous ditch working and subsequent building lead to subsidence. An explanation for the discrepancy in terms of movement is therefore

reasonable and is supported by the archaeological excavation which revealed that part of the structure was built on sediment that infilled a ditch that was associated with the Roman wall (D. J. Mason, pers. comm.).

9.7 Conclusions

The magnetic remanence of samples obtained from an ancient red sandstone kiln have been investigated. Thermal demagnetisation and analysis of orthogonal vector plots have been used to investigate the vector composition of the natural remanent magnetisation and to identify the characteristic remanent magnetisation. The magnetic mineralogy has been investigated using thermomagnetic analysis, susceptibility measurements, isothermal remanence acquisition and hysteresis measurements to elucidate the origin of the characteristic remanence. In addition, the anisotropy of magnetic susceptibility and magnetic refraction have been investigated to determine the accuracy of the remanence direction.

Both the demagnetisation data and the magnetic mineralogy of a subsample are strongly dependent upon distance from the heated surface of the block. Close to the heated surface, the natural remanent magnetisation consists of a low temperature viscous component and the characteristic remanence at higher temperatures. The magnetic mineralogy of such subsamples is dominated by magnetite which accounts for up to about 0.1% of the mass of the material. Further from the heated surface the

natural remanent magnetisation has an additional component, the direction of which is poorly defined and is not consistent between the blocks. The magnetic mineralogy changes from magnetite-dominated to haematite-dominated at these distances. The variation of the magnetic mineralogy can be explained on the basis of the firing atmosphere which is likely to have been reducing and which lead to the conversion of the primary haematite to magnetite. The extent of this conversion will depend on the heating time, the temperature, the conductivity and the porosity and connectivity of the rock. The variation of the magnetic mineralogy and the natural remanent magnetisation indicates that the characteristic remanence can be attributed to the firing in antiquity. The accuracy of the recorded direction was investigated by considering the magnetic fabric and magnetic refraction, both were shown to have only a small effect. A comparison of the Meriden-adjusted direction of the characteristic remanence with the secular variation reference curve compiled by Clark et al. (1988) suggests that the kiln was lasted fired in the Roman period. This date does not agree with the archaeological information which suggests that the kiln dates from the Dark Ages, 500-700 AD. It is suggested, on the basis of the archaeological evidence that the disagreement arises as a result of subsidence of the kiln at some time after its last usage.

REFERENCES

Abrahamsen, N., 1973. Archaeomagnetic tilt correction on bricks. Archaeometry, 15, 267-274.

Abrahamsen, N., 1986. On Shape Anisotropy. In: Twenty-five years of geology in Aarhus, J.T. Muller (ed). GeoSkrifter, 24, pp 300.

Ade-Hall, J. M., Wilson, R. L. & Smith, P. J., 1965. The petrology, Curie points and natural magnetisations of basic lavas. Geophys. J. R. Astr. Soc., 9, 323-336.

Aitken, M.J., 1974. Physics and Archaeology (2nd edn), Clarendon Press, Oxford, pp 291.

Aitken, M.J., 1983. Basic techniques for archaeointensity determination. In: Geomagnetism of baked clays and sediments, K.M. Creer, P. Tucholka & C.E. Barton (eds), Elsevier, 76-87.

Aitken, M.J., 1990. Science-based dating in archaeology. Longman, London & New York, pp 274.

Aitken, M.J. & Hawley, H.N., 1971. Archaeomagnetism: evidence for magnetic refraction in kiln structures. Archaeometry, 5, 4-22.

Appel, E. & Soffel, H.C., 1985. Domain state of Ti-rich titanomagnetites deduced from domain structure observations and susceptibility measurements. J. Geophys., 56, 121-132.

Averyanov, V.S., 1967. Contribution to the theory of the thermally activated magnetic viscosity of multidomain particles of ferromagnetic materials. Izv. Earth Physics, 8, 74-82.

Barbetti, M., 1976. Archaeomagnetic analysis of six Glozelian ceramic artefacts. J. Arch. Sci., 3, 137-151.

Bate, G., 1980. Recording materials. In; Ferromagnetic Materials, E.P. Wohlfarth (ed), vol. 2. Elsevier, Amsterdam. pp 381-508.

Becker, R. & Döring, W., 1939. Ferromagnetismus. Verlag-Springer, Berlin. pp 440.

Bolshakov, V.A., 1975. On the mechanism of viscous magnetisation of rocks. Phys. Solid Earth (USSR), 251-255.

Boyd, J.R., Fuller, M. & Halgedahl, S., 1984. Domain wall nucleation as a controlling factor in the behaviour of fine magnetite particles in rocks. Geophys. Res. Letts., 11, 193-196.

Bozorth, R.M., 1951. Ferromagnetism. Van Nostrand, New York. pp 968.

Brooks P.J. & O'Reilly, W., 1970. Magnetic rotational hysteresis characteristics of red sandstones. Earth Planet. Sci. Letts., 9, 71-76.

Butler, R.F. & Banerjee, S.K., 1975. Theoretical single domain grain size range in magnetite and titanomagnetite. J. Geophys. Res., 80, 4049-4059.

Carmichael, C.M., 1967. An outline of the intensity of the palaeomagnetic field of the Earth. Earth Planet. Sci. Letts., 3, 351-354.

Chantrell, R.W., Hoon, S.R. & Tanner, B.K., 1983. Time dependent magnetisation in fine particle ferromagnetic systems. J. Magn. Magn. Mats., 38, 133-141.

Chevallier, R., Bolfa, J. & Mathieu, S., 1955. Titanomagnetites et ilmenites ferromagnetiques. Bull. Soc. Fr. Mineral. Cristallogr., 78, 307-346.

Clark, A.J., Tarling, D.H. & Noel, M., 1988. Developments in archaeomagnetic dating in Britain. J. Arch. Sci., 15, 645-688.

Coe, R.S., 1967. The determination of palaeo-intensities of the earth's magnetic field with emphasis on mechanisms which could cause non-ideal behaviour in Thellier's method. J. Geomag. Geoelec., 19, 157-179.

Coe, R.S., 1979. The effect of shape anisotropy on TRM direction. Geophys. J. Roy. Astron. Soc., 56, 369-384.

Coey, J.M.D., Bouchez, R. & Dang, N.V., 1979. Ancient Techniques. J. Appl. Phys., 50, 7772-7777.

Collinson, D. W., 1983. Methods in rock magnetism and palaeomagnetism. Chapman and Hall, London. pp 503.

Crangle, J., 1977. The magnetic properties of solids. Edward Arnold, London. pp 194.

Creer, K.M., 1957. Palaeomagnetic investigations in Great Britain. The remanent magnetization of unstable Keuper Marls. Phil. Trans. Roy. Soc. London, **A250**, 130-143.

Creer, K.M., Tucholka, P. & Barton, C.E., 1983. Geomagnetism of baked clays and sediments. Elsevier, Amsterdam, pp 324.

Dankers, P.H., 1978. Magnetic properties of dispersed natural iron oxides of known grain-size. PhD thesis, State University of Utrecht.

Davis, P.M. & Evans, M.E., 1976. Interacting single domain properties of magnetite intergrowths. J. Geophys. Res., 81, 989-994.

Day, R., Fuller, M. & Schmidt, V.A., 1977. Hysteresis properties of titanomagnetites: grain size and compositional dependence. Phys. Earth Planet. Interiors, 13, 260-267.

Deer, W.A., Howie, R.A. & Zussman, J., 1966. An introduction to the rock forming minerals. Longman, London. pp 528.

Dekkers, M.J., 1988. Some rockmagnetic parameters for natural goethite, pyrrhotite and fine grained haematite. PhD thesis; Geologica Ultraiectina, 51, pp 231.

Dodson, R.E. & McClelland-Brown, E., 1980. Magnetic blocking temperatures of single-domain grains during slow cooling. J. Geophys. Res., 85, 2625- .

Dunlop, D.J., 1971. Magnetic properties of fine grained haematite. Ann. Geophys., 27, 269-93.

Dunlop, D.J., 1972a. Magnetic mineralogy of unheated and heated red sediments by coercivity spectrum. Geophys. J. Roy. Astr. Soc., 27, 37-55.

Dunlop, D.J., 1972b. Magnetite: behaviour near the single domain threshold. Science, 176, 41-43.

Dunlop, D.J., 1973. Theory of magnetic viscosity in in lunar and terrestrial rocks. Rev. Geophys. Space Phys., 11, 855-901.

Dunlop, D. J., 1977. The hunting of the psark. J. Geomagn. Geoelectr., 29. 293-318.

Dunlop, D.J., 1981. The rock magnetism of fine particles. Phys. Earth Planet. Interiors, 26, 1-26.

Dunlop, D.J., 1983. Viscous magnetisation of 0.04-100 um magnetites. Geophys. J. Roy. Astron. Soc., 74, 667-687.

Dunlop, D.J. & Prevot, M., 1982. Magnetic properties and opaque mineralogy of drilled submarine intrusive rocks. Geophys. J., 16, 763-802.

Dunlop, D.J. & Zinn, M.B., 1980. Archaeomagnetism of a 19th century pottery kiln near Jordan, Ontario. Canadian J. Earth Sci., 17, 1275-1285.

Dzyaloshinsky, I., 1958 A thermodynamic theory of weak ferromagnetism of antiferromagnets. J. Phys. Chem. Solids, 4, 241-55.

Elder, T., 1965. Particle-size effects in oxidation of natural magnetite. J. Appl. Phys., 36, 1012-1013.

Enkin, R.J. & Dunlop, D.J., 1988. The demagnetisation temperature necessary to remove viscous remanent magnetisation. Geophys. Res. Letts., 15, 514-517.

Evans, M.E., 1987. New archaeomagnetic evidence for the persistence of the geomagnetic westward drift. J. Geomag. Geoelec., 39, 769-772.

Evans, M.E. & Hoye, G.S., 1990. Magnetic refraction and archaeomagnetic fidelity. Archaeometry '90. Birkhuser Verlag Basel, Basel.

Evans, M.E. & Mareschal, M., 1986. An archaeomagnetic example of polyphase magnetisation. J. Geomag. Geoelec., 38, 923-929.

Ewing, J.A., 1885. Experimental researches in magnetism. Proc. Res. Roy. Soc., A46, 269.

Fisher, R.A., 1953. Dispersion on a sphere. Proc. Roy. Soc., A217, 295-305.

Fox, J.M.W. & Aitken, M.J., 1980. Archaeomagnetism: cooling rate dependence of TRM. Nature, 283, p 462.

Franklin, U.M., & Vitali, V., 1989. The environmental stability of ancient ceramics. Archaeometry, 27, 1, 3-15.

Games, K., 1977. The magnitude of the Paleofield : a new non-thermal, non-detrital method using sun-dried bricks. PhD thesis. Liverpool University.

Gaunt, P.J., 1977. The frequency constant for thermal activation of a ferromagnetic domain wall. J. Appl. Phys., 48, 3470-3474.

Gorter, E. W., 1954. Saturation magnetisation and crystal chemistry of the ferrimagnetic oxides. Philips Res. Rep., 9, 403-443.

Gowlett, J.A.J., Harris, J.W.K., Walton,D. & Wood, B.A., 1981. Early archaeological sites, hominid remains and trace of fire from Chjesowanja, Kenya, Nature, 294, 125-129.

Grimes, N.W., 1972. Phil. Mag., 25, 67.

Grommé, C.S, Wright, T.L. & Peck, D.L., 1969. Magnetic properties and oxidation of iron-titanium oxide minerals in Alae and Makaopuki lava lakes. J.Geophys. Res., 74, 5277-5293.

Gubbins, D. & Roberts, N., 1983. Use of the frozen flux approximation in the interpretation of archaeomagnetic and palaeomagnetic data. Geophys. J. R. Astr. Soc., 73, 675-687.

Gunn, N., 1978. Archaeomagnetic field strengths from Peru. PhD thesis. Liverpool University.

Halgedahl, S.L. & Fuller, M., 1981. The dependence of magnetic domain structure on magnetisation state in polycrystalline pyrrhotite. Phys. Earth Planet. Interiors, 26, 93-97.

Hedley, I. G., 1971. The weak ferromagnetism of goethite (FeOOH). Z. Geophys., 37, 409-420.

Hedley, I.G. & Wagner, J.J., 1990. A magnetic investigation of Roman pottery. Archaeometry '90. Birkhauser Verlag Basel, Basel.

Heller, F. & Markert, H., 1973. The age of viscous remanent magnetization of Hadrian's Wall (Northern England). Geophys. J. Roy. Astron. Soc., 31, 395-406.

Höhne, R., Melzer, K., Hochschild, H., Libor, G., & Krause, R., 1975. Magnetic after-effects in titanium-doped magnetite. Phys. Stat. Sol., 27, 117-121.

Hounslow, W. M., Noel, M. & Bootes, P.A., 1988. Sensistivity and sample-shape related measuring effects on the MOLSPIN susceptibility anisotropy meter. Geophys. J., 93, 355-363.

Hoye, G.S., 1983. Magnetic properties of ancient coins. J. Arch. Sci., 10, 43-49.

Hrouda, F., 1982. Magnetic anisotropy of rocks and its application in geology and geophysics. Geophys. Rev. 5, 37-82.

Hsia, Y., Hu, Z., Liu, R., Zeng, Q., Yu, Z. & Zheng, Y., 1988. Fe-57 Mossbauer effect studies of some ancient Chinese pottery from Xudun. Hyperfine Interactions, 41, 803-806.

Ishikawa, Y., Akimoto, S. & Syono, Y., 1964. Neutron diffraction study of Fe_3O_4-Fe_2TiO_4 series. In: Annual progress report on rock magnetism in Japan. Tokyo University, Tokyo. pp 14-21.

Kittel, C., 1966. Introduction to solid state physics. 3rd edition. John Wiley, New York. pp 648.

Kono, M., 1978. Reliability of palaeointensity methods using alternating field demagnetization and anhysteretic remanence. Geophys. J.R. Astr. Soc., 54, 241-261.

Kovacheva, M., 1982. Archaeomagnetic investigations of geomagnetic secular variations. Phil. Trans. R. Soc. Lond., A 306, 79-86.

Kronmüller, R., Schützenauer & Walz, F., 1974. Magnetic after-effects in magnetite. Phys. Stat. Sol., 24, 487-

494.

Kropacek, V., 1974. Kinetics of oxidation processes in titanomagneites. J. Geophys., 40, 329-340.

Levi, S., 1977. The effect of magnetite particle size on palaeointensity determinations of the geomagnetic field. Phys. Earth Planet. Interiors., 13, 245-259.

McClelland-Brown, E., 1984. Experiments on TRM intensity dependence on cooling rate. Geophys. Res. Letts., 11, 205-208.

McDougall, I & Tarling D.H., 1983. The magnetic sourcing of obsidian samples from Mediterranean and Near Eastern sources. J. Arch. Sci., 10, 441-452.

McElhinny, M.W., 1973. Palaeomagnetism and plate tectonics. University Press, London. pp 358.

McNab, T.K., Fox, R.A. & Boyle, A.J.F., 1968. Some magnetic properties of magnetite microcrystals. J. Appl. Phys., 39, 5703.

Megaw, J.V.S. & Simpson, D.D.A., 1988. Introduction to British Prehistory. Leicester University Press, Leicester. pp 560.

Merrill, R.T. & McElhinny, M.W., 1983. The Earth's magnetic field: Its history, origin and planetary perspective. Academic Press, London. pp 401.

Middleton, M.F. & Schmidt, P.W., 1982. Palaeothermometry of the Sydney Basin. J. Geophys. Res., 87, 5351-5359.

Molyneux, L., 1971. A complete result magnetometer for measuring the remanent magnetisation of rocks. Geophys. J. R. Astr. Soc., 24, 429-433.

Moon, T. & Merrill, R.T., 1984. The magnetic moments of non-uniformly magnetised grains. Phys. Earth Planet. Interiors, 34, 186-194.

Moon, T. & Merrill, R.T., 1985. Nucleation theory and domain states in multidomain magnetic material. Phys. Earth Planet. Interiors, 37, 214-222.

Moskowitz, B.M., 1985. Magnetic viscosity, diffusion, after-effect, and disaccommodation in natural and synthetic samples. Geophys. J. Roy. Astron. Soc., 82,

143-161.

Nagata, T. & Akimoto, S., 1956.Magnetic properties of ferromagnetic ilmenites. Geofis. Pura e Appl., 34, 36-50.

Nakamura, A., Yamauchi, S., Fueki,K. & Mukaibo, T., 1978. Diffusion processes and magnetisation in magnetite. Phys. Chem. Solids, 39, 1203.

Néel, L., 1949. Théorie du trainage magnétique des ferromagnétique en grain fins avec application aux terres caites. Ann. Geophys., 5, 99-136.

Néel, L., 1950. Théorie du traînage magnétique des substances massives dans le domaine de Rayleigh. J. Phys. Radium, Paris, 11, 49-61.

Néel, L., 1955. Some theoretical aspects of rock magnetism. Advances in Physics, 4, 191-243.

O'Reilly, W., 1984. Rock and mineral magnetism. Blackie, Glasgow. pp 220.

Ozdemir, O., 1987. Inversion of titanomaghemites. Phys. Earth Planet. Interiors, 46, 184-196.

Ozdemir, O. & Banerjee, S.K., 1984. High temperature stability of maghemite (Fe_2O_3). Geophys. Res. Letts., 11, 3, 161-164.

Ozdemir, O & Dunlop, D.J., 1989. Chemico-viscous remanent magnetization in the Fe_3O_4- Fe_2O_3 system. Science, 243, 1043-1046.

Piper, J.D.A., Atkinson, D., Norris, S. & Thomas, S., 1991. Palaeomagnetic study of the Derbyshire lavas and intrusions, central England: Definition of Carboniferous apparent polar wander. Phys. Earth Planet. Ints., 69, 37-55.

Prévot, M., 1981. Some aspects of magnetic viscosity in subaerial and submarine volcanic rocks. Geophys. J. R. Astr. Soc., 66, 169-192.

Pullaiah, G., Irving, E., Buchan, K. L. & Dunlop, D.J., 1975. Magnetisation changes caused by burial and uplift. Earth Planet. Sci. Letts., 28, 133-143.

Radhakrishnamurty, C., 1985. Identification of

titanomagnetites by simple magnetic techniques and application to basalt studies. J. Geol. Soc. India, 26, 640-651.

Radhakrishnamurty, C., 1986. Selection of basalts for palaeointensity studies. J. Geomag. Geoelec., 38, 1365-1368.

Radhakrishnamurty, C., Likhite, S.D., Deutch, E.R., & Murthy, G.S., 1978. Nature of magnetic grains in basalt and implications for palaeomagnetism. Proc. Ind. acad. Sci. Sect., A87, 235-243.

Radhakrishnamurty, C. & Likhite, S.D., 1991. Low-temperature AC susceptibility studies of titanomagnetites with frequency. IUGG conference, Vienna 1991; IAGA, Program & Abstracts, p 139.

Readman P. W., & O'Reilly, W., 1970. The synthesis and inversion of non-stoichiometric titanomagnetites. Phys. Earth Planet. Interiors, 4, 121-128.

Readman, P. W. & O'Reilly, W., 1971. Oxidation processes in titanomagnetites. Z. Geophys., 37, 329-338.

Richter, G. 1937. ber die magnetiische nachwirkung am carbonyleisen. Ann. Phys., 29, 605.

Rigotti, P.A., 1978. The ARM correction method of palaeointensity determination. Earth Planet. Sci. Letts., 39, 417-426.

Roberts, N. & Piper, J. D. A., 1989. A description of the behaviour of the Earth's Magnetic Field. In: Geomagnetism, vol. 3, J.A. Jacobs (ed). Academic Press Ltd. pp 163-260.

Roberts, P.H. & Scott, S., 1965. On analysis of secular variation. I. A. hydromagnetic constraint theory. J. Geomag. Geoelec., 17, 137-151.

Robertson, D.J., 1990. Titanomagnetite granulometry and rock magnetism of some Plio-Pleistocene volcanic rocks. Geophys. Res. Letts., 17, 771-774.

Rogers, J., Fox, J.M.W. & Aitken, M.J., 1979. Magnetic anisotropy in ancient pottery. Nature, 277, 644-646.

Rolph, T.C. & Shaw, J., 1985. A new method of

palaeofield magnitude correction for thermally altered samples and its application to Lower Carboniferous lavas. Geophys. J. R. Astr. Soc., 80, 773-781.

Rolph, T.C., Shaw, J., Derbyshire, E. & Wang, J., 1989. A new basal age for the loess of Lanzhou, Northern China. Physics. Earth. Planet. Int., 56, 151-164.

Scherbakov, V. P. & Lamash, B. E., 1988. Metastability threshold sizes in single domain magneite particles. Geophys. Res. Letts., 15 (5), 526-529.

Schmidbauer, E. & Fassbinder, J., 1987. After effect of magnetic susceptibility in Fe-Ti spinels and cation diffusion. J. Mag. Mag. Mats., 68, 83-89.

Schurr, K., Becker, H. & Söffel, H.C., 1984. Archaeomagnetic study of medieval fireplaces at Mannheim-Wallstadt and ovens from Herrenchiemsee (southern Germany) and the problem of magnetic refraction. J Geophys., 56, 1-8.

Senanayake, W. E. & McElhinny, M. W., 1981. Hysteresis and susceptibility characteristics of magnetite and titanomagnetite: interpretations of results from basaltic rocks. Phys. Earth Planet. Interiors, 26, 47-55.

Share, J., 1986. A superconducting magnetomter for measuring magnetisation at high temperature. PhD thesis, Cardiff.

Shashkanov, V.A. & Metallova, V.V., 1970. Temperature dependence of the magnetic viscosity- coeffieint. Izv. Earth Physics, 7, 88.

Shaw, J., 1974. A new method of determining the magnitude of the palaeomagnetic field. Application to five historic lavas and five archaeological samples. Geophys. J. R. Astr. Soc., 39, 133-141.

Shaw, J., 1979. Rapid changes in the magnitude of the archaeomagnetic field. Geophys. J. R. Astr. Soc., 58, 107-116.

Shaw, J. Share, J.A. & Rogers, J., 1985. An automated superconducting magnetometer and demagnetisation system.

Geophys. J. R. Astr. Soc.,78, 209-217.

Sherwood, G.J., 1989. MATZIJ - a BASIC program to determine palaeomagnetic remanence directions using principal component analysis. Comput. Geosci., 15, 1173-1182.

Shimizu, Y., 1960. Magnetic viscosity of magnetite. J. Geomag. Geoelec., 11, 125-138.

Sholpo, L.Y., Afremov, L.M. & Pershin, V.L., 1972. Interpretation of the angular dependence of secondary magnetisation and demagnetisation of rocks. Phys. Solid Earth (USSR), 651-658.

Skovorodkin, O.Y., Tikhonov, L.V & Bezuglaya, L. S., 1975. Investigations of viscous magnetisation on monocrystals of natural magnetites. Izv. Earth Physics, 5, 56-61.

Smith, G.M. & Banerjee, S.K. 1987. The dependence of weak field susceptibility on applied magnetic field. Phys. Earth Planet. Interiors, 46, 71-76.

Soffel, H., 1971. The single domain-multidomain transition in natural intermediate titanomagnetites. Z. Geophys., 37, 451-470.

Sporer, H., 1984. On viscous remanent magnetisation of synthetic multidomain titanomagnetite. Geophys. Res. Letts., 11, 209-212.

Stacey, F.D., 1963. The physical theory of rock magnetism. Adv. Phys., 12, 45-133.

Stacey, F. D. & Banerjee, S. K., 1974. The physical principles of rock magnetism. Elsevier, Amsterdam. pp 195.

Stephenson, A., 1969. The temperature dependent cation distribution in titanomangetites. Geophys. J. R. Astr. Soc., 18, 199-210.

Stephenson, A., 1971. Single domain grain distributions. A method for the determination of single domain grain distributions. Phys. Earth Planet. Interiors, 4, 353-360.

Sternberg, R.S., 1989. Archaeomagnetic palaeointensity

in the American Southwest during the past 2000 years. Phys. Earth Planet. Interiors, 56, 1-17.

Stoner, E. C. & Wohlfarth, E. P., 1948. A mechanism of magnetic hysteresis in heterogenous alloys. Phil. Trans. R. Soc., A240, 599-642.

Street, R. & Wooley, J.C., 1949. A study of magnetic viscosity. Proc. Phys. Soc. London, A62, 562-572.

Tanguy, J.C., 1975. Intensity of the geomagnetic field from recent Italian lavas using a new palaeointensity method. Earth Planet. Sci. Letts., 27, 314-320.

Tarling, D.H., 1983. Palaeomagnetism. Chapman & Hall, London & New York, pp 379.

Taylor, J.J, Innes, J.B. & Jones, M.D.H., 1990. Integrating geophsical and palynological survey in wetlands. Archaeometry '90. Birkhauser Verlag Basel, Basel.

Thellier, E., 1937. Aimantation des terres cuites: application à la recherche de l'intensité du champ magnétique terrestre dans le passé. C. R. Acad. Sci. Paris, 204, 184-186.

Thellier, E., 1938. Sur l'aimantation de l'intensité du champ magnétique terrestre dans le passé. Ann. Inst. Phys. Globe, Paris, 15, 179-184.

Thellier, E. & Thellier, O., 1959. Sur l'intensité du champ magnétique terrestre dans le passe historique et geologique. Ann. Geophys., 15, 285-376.

Thomas, R.C., 1981. Archaeomagnetism of Greek pottery and cretan kilns. Unpublished PhD thesis, Univeristy of Edinburgh, pp 362.

Thomas, R. C., 1983. Mineralogical problems. In: Geomagnetism of baked clays and recent sediments. Creer, Tucholka & Barton (eds). Elsevier, Amsterdam. 98-103.

Thompson, R., 1986. Modelling magnetisation data using SIMPLEX. Phys. Earth Planet. Ints., 42, 113-127.

Thompson, R. & Oldfield, F., 1986. Environmental magnetism. Allen and Unwin, London.

Tite, M.S., 1991. The impact of electron microscopy on ceramic studies. In Press

Tivey, M. & Johnson, H.P., 1981. Characterisation of viscous remanent magnetisation in single- and multi-domain magnetite grains. Geophys. Res. Letts., 8, 217-220.

Tivey, M. & Johnson, H.P., 1984. The characterisation of viscous remanent magnetisation in large and small magnetite particles. J. Geophys. Res.

Tropin, Yu. D. & Vlasov, Ya. D., 1966. Some aspects of the theory of magnetic viscosity in multidomain rock grains. Izv. Akad. Nauk SSSR; Ser. Fiz. Zemli,5, 78.

Tucker, P. & Thomas R.C., 1983. Magnetisation processes in baked clays. In; Geomagnetism of baked clays and sediments. Creer, Tucholka & Barton (eds). Elsevier, Amsterdam. 2-9.

Turner, G.M. & Thompson, R., 1979. The behaviour of the Earth's magnetic field as recorded in the sediments of loch Lomond. Earth Planet. Sci. Letts., 42, 412-426.

Walton, D., 1980. Time-temperature relations in the magnetisation of assemblies of SD grains. Nature, 286, 245-294.

Walton, D., 1983a. The reliability of ancient intensities obtained by thermal demagnetization. In; Geomagnetism of baked clays and sediments, K.M. Creer, P. Tucholka & C.E. Barton (eds), 88-97.

Walton, D., 1983b. Viscous magnetization. Nature, 305, 616-619.

Walton, D., 1986. Rate of transition for single domain particles. J. Mag. Mag. Mats., 62, 392-396.

Walton, D., 1991. A new technique for determining palaeomagnetic intensities. In press.

White, D. & White, A., 1961. The firing of a pottery kiln of a Romano-British type at Boston, Lincs: Appendix II, gas analysis. Archaeometry, 4, 21-23.

Williams, W., 1986. The effect of time and temperature on magnetic remanence. PhD thesis, Cambridge.

Wilson, R.L. & Smith, P.J., 1968. The nature of secondary natural magnetization in some igneous and baked rocks. J. Geomag. Geoelec., 20, 367-380.

Worm, H.U. & Jackson, M., 1988. Theoretical time-temperature relationships of magnetisation for distributions of single domain magnetite grains. Geophys. Res. Letts., 15, 1093-1096.

Worm, H.U. & Markert, M., 1986. The preparation of dispersed titanomagnetite particles by the glass ceramic method. Phys. Earth Planet. Interiors, 46, 263-268.

Worm, H-U., Jackson, M, Schlinger, C.M. & Banerjee, S.K., 1991. Magnetic viscosity of single domain magnetite particles. J. Appl. Phys. (in press)

APPENDICES

1. Sample details
2. Thermomagnetic behaviour
3. Isothermal remanence acquisition
4. Magnetic hysteresis behaviour
5. Magnetic susceptibility behaviour
6. Low temperature susceptibility behaviour

APPENDIX 1.

Sample Details

French I

MC01. Six subsamples.

Source: J. Shaw, The Geomagnetism Laboratory, University of Liverpool. P.O. BOX 147, Liverpool, L69 3BX.

No additional information available.

British

MC02. Two samples.

Source: J. Shaw, The Geomagnetism Laboratory, University of Liverpool, P.O. BOX 147, Liverpool, L69 3BX.

Code	Original Code	Site	Long. °W	Lat. °N	Information	Age
0201	BO52	Fengate	0.15	52.35	Collared Urn	1460±120 BC
0202	BO51	" "	"	"		2445±50 BC

Peruvian

MC05. Five samples.

Source: N. Gunn (N. Gunn, 1978) c/o The Geomagnetism Laboratory, The University of Liverpool, P.O. BOX 147, Liverpool, L69 3BX.

Code	Original Code	Site	Long °W	Lat °S	Information	Age
0501	P13(X01)	Viru	78	8	Gallinazo fill	300-700 AD
0502	P13(J06)	"	"	"	Adobe/floor fill	300 BC
0503	P13(K05)	"	"	"	Sherds in brown soil	300-700BC (older than 0502)
0504	P13(L03)	"	"	"	" "	300-700BC (older than 0503)
0505	P13(M12)	"	"	"	cinder in brown soil	300-700 BC (oldest)

MC06. Two samples.

Source: N. Gunn, c/o The Geomagnetism Laboratory, The University of Liverpool, P.O. BOX 147, Liverpool, L69 3BX.

Code	Original code	Site	Long °W	Lat °S	Information	Age
0601	P23A02	Lambrayeque valley	79	6	Moche V period sherd from pot	1000AD
0602	P23C12	"	"	"	sherd from wall	"

MC07. Five samples.

Source: N. Gunn, c/o The Geomagnetism Laboratory, University of Liverpool, P.O. BOX 147, Liverpool, L69 3BX.

Code	Original code	Site	Long °W	Lat °S	Information	Age
0701	P37(I13)	Pachmachay Cave, Ondores	-	-	Sherd	Pre-ceramic 1400AD
0702	P37(S19)	"	"	"	"	"
0703	P37(H22)	"	"	"	"	"
0704	P37(P19)	"	"	"	"	"
0705	P37(P02)	"	"	"	"	"

MC08. Three samples.

Source: N. Gunn, c/o The Geomagnetism Laboraotory, University of Liverpool, P.O. BOX 147, Liverpool, L69 3BX.

Code	Original code	Site	Long °W	Lat °S	Information	Age
0801	P37(R06)	Pachamachay Cave, Ondores	-	-	Sherd	Pre-ceramic 1400AD
0802	P37(R09)	"	"	"	"	"
0803	P37(S06)	"	"	"	"	"

MC09. Six samples.

Source: N. Gunn, c/o The Geomagnetism Laboratory, University of Liverpool, P.O. BOX 147, Liverpool, L69 3BX.

Code	Original Code	Site	Long °W	Lat °S	Information	Age
0901	P02(I04)	Rimac Valley near Lima	77	12	sherd from cemetry	300-800 AD
0902	P02(J23)	"	"	"	sherd from ceremonial structure	300-800 BC
0903	P02(K43)	"	"	"	"	1000BC
0904	P02(K30)	"	"	"	"	"
0905	P02(Z01)	"	"	"		300-1000 BC
0906	P02(Z02)	"	"	"	"	"

MC10. Three samples.

Source: N. Gunn, c/o The Geomagnetism Laboratory, University of Liverpool, P.O. BOX 147, Liverpool, L69 3BX.

Code	Original Code	Site	Long °W	Lat °S	Information	Age
1001	P24	-	-	-	Reproduction	Modern
1002	P43(B02)	Ayacucho	74	13	Rooftile	1700-1750AD
1003	P43(C)	"	"	"	Rooftile	1600-1750AD

French II

MC11. Ten samples.

Source: Samples provided by J. Shaw, The Geomagnetism Laboratory, The University of Liverpool, P.O. BOX 147, Liverpool, L69 3BX.

Original source; P. Perin and the St. Germain Museum

Code	Original Code	Site	Long °E	Lat °N	Information	Age
1101	F01	Lezoux	3.5	45.8	Base of bowl	1st C AD
1102	F03	"	"	"	Bowl fragment	90-120 AD

1103	F09	Mont Avrollot à St Florentin	3.8	48.0	Sherds (Bilbracte type)	0-50BC
1104	FO12	Toulon-sur-Allier	4.0	46.4		150-200AD
1105	FO14	Moustferrand				1275-1300AD
1106	FO15	Clermont-Ferrand	3.1	45.5		1350-1400AD
1107	FO16	St-Victor de Massac	4.4	45.1		1500-1550AD
1108	FO18	Ardennes	4.5	49.5		600-700AD
1109	FO20	"	"	"		675-725AD
1110	FO19	"	"	"		600-700AD

MC13. Eleven samples

Source: samples from M.J. Aitken, Research Laboratory for Archaeology and History of Art, 6 Keble Road, Oxford University, Oxford.

Original source; P. Perin and the St. Germain museum.

Code	Original Site Code		Long °E	Lat °N	Information	Age
1301	FO9	Mont Avrollot à St Florentin	4.8	35.7	Sherd of Bilbracte type	0-50BC
1302	FO10	Lezoux	3.2	45.5		Upper Middle Ages
1303						
1304	FO07	"	"	"	fragment of bowl	150-200AD
1305	FO12	Toulon-sur Allier	4.1	46.4		150-200AD
1306						
1307	FO21	Ardennes	4.5	45.9		550-600AD
1308						
1309						
1310	FO13	Lezoux	3.2	45.5		1230-1250AD
1311						

Egyptian

MC12. Two samples.

Source: K. Games (K. Games, 1977), c/o The Geomagnetism Laboratory, The University of Liverpool, P.O. BOX 147, Liverpool, L69 3BX.

Code	Original Code	Site	Long °E	Lat °N	Information	Age
1201	E18 Ey	Saqqara	31.1	29.5	From adobe bricks	
1202	E20 Ey	Saqqara	31.1	29.5	"	

Greek

MC14. Three samples.

Source: M.J. Aitken, The Research Laboratory for Archaeology and History of Art, 6 Keble Road, Oxford University, Oxford.

Code	Original Code	Site	Long °E	Lat °N	Information	Age
1401	E20/S 223	Servia	22.0	40.1	Sherds from trench	Early bronze /Neolothic
1402	E20/S 224	"	"	"	"	"
1403	E20/S 225	"	"	"	"	"

MC15. Thirteen samples.

Source: M. J. Aitken, The Research Laboratory for Archaeology and History of Art, 6 Keble Road, Oxford University, Oxford.

Code	Original Code	Site	Long °E	Lat °N	Information	Age
1501	ExH20	Servia	22.0	40.1	Buff/greyware	Late Early-Bronze Age
1502		"	"	"	Roughened ware	"
1503		"	"	"	"	"
1504		"	"	"	"	"
1505		"	"	"	Tooled ware	"
1506		"	"	"	"	"
1507		"	"	"	Baking plate	"
1508		"	"	"	"	"

1509	"	"	"	"	"
1510	"	"	"	Scored-ware	"
1511	"	"	"	"	"
1512	"	"	"	"	"
1513	"	"	"	"	"

MC16. Five samples.

Source: M. J. Aitken, The Research Laboratory for Archaeology and History of Art, 6 Keble Road, Oxford University, Oxford.

Code	Original Code	Site	Long °E	Lat °N	Information	Age
1601	3633(12a)	Servia	22.0	40.1		Neolithic/ EBA
1602	3633(12b)	"	"	"	Geometrically painted	"
1603	3633(12c)	"	"	"	Coarseware with nailmarks	"
1604	3633(12d)	"	"	"		
1605	3633(12e)	"	"	"		"

South-Western USA

Source: R. S. Sternberg, Department of Geosciences, Franklin Marshall College, P.O. BOX 3003, Lancaster, Pennsylvania, USA.

Code	Original Code	Site	Long °E	Lat °N	Information	Age (archaeo logical)
1701	AH003A	Arroyo Hondo near Santa Fe	254.06	35.62	Tesuque corrugated	1355-1370 AD cross-dated to tree-rings
1702	AH006D	"			"	1410-1425 AD (cross date tree rings)
1703	AN001C	Antelope House Arizona	250.56	36.16	Lino Plain	700-750 AD

1704	AP001C	Green Bear Site, Arizona	251.00	35.33	Alma Plain	790-810 AD
1705	CC002	Chaco Canyon New Mexico	252.10	36.03	Lino Grey	600-650 AD
1706	CC003	Pueblo Alto New Mexico	252.04	36.07	Puerco Black-on-White	1045-1100 (cross-date tree rings)
1707	CC004	" "	252.04	36.07	Chaco McElmo	1050-1150 AD
1708	LA001C	Pueblo del Encierro New Mexico	253.67	35.64	roof material	1479-1520 AD (cross date with treerings)
1709	MV001	Long House Colorado	251.46	37.17	Mesa Verdi black-on-white	1280-1300 AD (cross date tree rings)
1710	PA002C	Papago Reserve, Arizona	249.98	32.30	Papago Red	1875-1910 AD
1711	UN003B	Unkar Delta, Arizona	247.91	36.06	Tusayan corrugated	1075-1100 AD (cross date tree rings)
1712	UN006	"	"	"	"	1100-1150 AD (" ")
1713	WA002E	Walpi Arizona	249.60	35.83	Orange Utility Ware	1700-1800 AD

Romano-British

MC18 (nine samples), MC19 (nine samples) , MC20 (twelve samples), MC21 (nine samples), MC22 (nine samples), MC23(six samples), MC24 (five samples)

Source: A. J. Clark, 19 The Crossways, Onslow Village, Guildford, Surrey, GU2 5QG.

Code	Original Code	Site	Long °E	Lat °N	Information	Age
MC18		Alice Holt Forest, Hampshire	0.45	51.13	mostly medium fine grey-ware	-
MC19		"	"	"	"	60-150AD
MC20		"	"	"	"	-
MC21		"	"	"	"	60-270AD (latter part)
MC22		"	"	"	"	60-270AD
MC23		"	"	"	"	60-270AD
MC24		"	"	"	"	60-150AD
MC25		"	"	"	"	150-200AD

Chinese I

MC26. Eight samples.

Source: Yang Shanlin, The Geomagnetism Laboratory, University of Liverpool, P.O. BOX 147, Liverpool, L69 3BX.

Code	Original Code	Site	Long °E	Lat °N	Age
2601	CNY-4	Qinan (Gansu)	105.7	35.0	5000-5400 BP
2602	CNY-7	Fangchen (JiangXi)	103.5	35.7	4500-5000 BP
2603	CNY-1	Donxiang (Gansu)	115.5	28.1	4500-5000 BP
2604	CNY-3	Yongden (Gansu)	103.2	36.8	4300-5000 BP
2605	CNY-5	YongQin (Gansu)	103.3	36.0	3400-3800 BP
2606	CNY-8	Zhenzhou (Henan)	113.2	34.7	2000-2300 BP
2607	CNY-6	Minyang (Henan)	113.7	34.7	3000 BP

2608	CNY-2	Zhenzhou (Henan)	113.2	34.7	2000-2300 BP

Chinese II

MC27. Thirteen samples.

Source: Yang Shanlin, The Geomagnetism Laboratory, University of Liverpool, P.O. BOX 147, Liverpool, L69 3BX.

Code	Original Code	Site	Long °E	Lat °N	Age
2701	FJ3	Fuzhou (Fujian)	119.2	26.1	420-589 AD
2702	FJ5	"	"	"	"
2703	FJ8	Huaian (Fujian)	117.5	25.1	420-589 AD
2704	FJ10	"	"	"	"
2705	FJ11	?			
2706	FJ13	Zhangpu (Fujian)	117.6	24.2	960-1368 AD
2707	FJ14	"	"	"	"
2708	FJ15	"	"	"	"
2709	FJ16	Donshan (Fujian)	117.5	23.6	960-1279 AD
2710	FJ20	Yunxiao (Fujian)	117.2	23.6	650-1000 AD
2711	FJ22	Donshan (Fujian)	117.5	23.6	960-1279 AD
2712	FJ25	Xiamen (Fujian)	118.1	24.5	618-907 AD
2713	FJ26	"	"	"	"

Indian

MC28. One sample

Source: I. C. Glover, Institute of Archaeology, London; c/o M. J. Aitken, Research Laboratory for Archaeology and the History of Art, 6 Keble Rd, Oxford University, Oxford.

Code	Site	Description
2801	Shringawpar, Ramchansa Road Station Northern India	Black fine-ware

No additional information available.

APPENDIX 2.

Thermomagnetic Behaviour

Note: This table contains Curie point and inflexion temperatures estimated from the heating (HT) and cooling (CL) curves. Alteration resulting from the thermal cycle is indicated by the ratio of the final to initial magnetisation (M_f and M_i) at 99°C, which is expressed as a percentage.

Code	T_C, inflex. (°C) HT	T_C, inflex. (°C) CL	M_f/M_i (%)	Comments
0101	557	523	84	
0102	570	537	78	
	575	545	92	
0103	580	543	73	
	560	540	76	
0104	595	550	84	
	565	557	85	
0105	588	565	93	1 piece
0106	565	540	101	
	565	538	105	
0201	580,370	575	104	
0202	580,120,335	580	121	
0501	598,320	585	93	
0502	580,340	580	88	
0503	587,345	570	88	
0504	585,350	580	80	
0505	588	578	75	
0601	563	555	95	
0602	563	543	97	
0701	585,425	583	112	
0702	575	560	86	
0703	585	582	107	
0704	583	558	96	
0801	620,305	570	91	
0802	595,385	560	100	
	580	553	90	
0803	–	–	84	Paramagnetic
0901	585	585	90	
0902	590	583	81	
	590	580	72	
0903	600	590	55	
	600	590	60	
	595	585	53	
0904	588	580	91	
0905	590	583	87	
0906	585	583	92	

Thermomagnetic behaviour continued...

Code	T_c,inflex. (°C) HT	T_c,inflex. (°C) CL	M_f/M_i (%)	Comments
1001	573	545	85	
1002	570,250	545,225	90	
	588,260	568,233	78	
1003	595	565	126	
	578,215	560,210	119	
1101	–	–	100	Weak/paramagnetic
1102	–	–	98	Weak/paramagnetic
1103	578	575	123	
1104	–	–	100	Weak/paramagnetic
1105	580	565	91	
1106	540	515	91	
1108	613	583	116	
1110	585	540	110	
1201	575	553	85	
1202	570	560	82	Haematite?
1301	583	578	92	
	580	580	104	
1302	–	–	–	Very weak/paramagnetic
1303	605,350	580	91	
1304	–	–	98	Weak/paramagnetic
1305	–	–	70	paramagnetic
1306	590,320	595	103	
1307	570,310	–	105	
1308	590,320	595	91	
1309	590,295	580	105	
	588,295	590	108	
1310	590	570	120	Weak
1311	540	535	98	Poorly defined
	558	555	93	
1401	605	588	83	
	608	600	88	
1402	600	595	81	
	605	600	81	
	605	598	87	
1403	605	598	86	
	610	600	86	
	608	590	91	
1501	583	578	78	
1502	610	598	74	orange (outer)
	608	573	92	black (inner)
1503	600,420	585	56	
	595,410	587	52	
1504	600	590	95	
1505	605	590	87	
1506	–	–	–	Weak/paramagnetic
1507	603,320	590	85	

Thermomagnetic behaviour continued...

Code	T_C,inflex. (°C) HT	T_C,inflex. (°C) CL	M_f/M_i (%)	Comments
1508	608	600	85	
1509	605	595	92	Poorly defined
1510	595	593	82	
	600	605	85	
1511	595	568	98	
1512	625	615	75	
	603	598	71	
1513	590	580	89	
1601	603	560	87	
	600	568	76	
1602	593	568	105	
	590	573	94	
1603	595	578	85	
	588	538	78	
1604	600,325	580	92	
	600,325	570	91	
1605	588	570	92	
1701	588	595	90	
	583	603	99	
1702	588	613	98	
1703	575	575	89	Poorly defined
	570	754	90	" "
1704	625	613	86	
1705	570	590	76	
1706	615	593	77	
1707	575,320	558	98	
1708	555	545	75	
1709	595	585	75	
1710	620	620	85	
1711	585	568	82	
1712	585	578	86	
1713	595,370	570,365	97	haematite?
1801	528	523	97	
	510	520	97	
1802	553	530	99	
1803	585	535	95	
1804	593,270	588	116	
	600,218	580	110	
1805	568	560	87	
	578	558	87	
1806	550	555	100	
1807	478	495	108	
1808	495	510	106	
1809	575	565	86	
1901	573	550	100	grey (inner)
	590,230	570,210	94	orange (outer)
1902	580	570	93	

Thermomagnetic behaviour continued...

Code	T_c,inflex. (°C) HT	T_c,inflex. (°C) CL	M_f/M_i (%)	Comments
1903	565	590	98	
1904	573	565	88	grey (inner)
	575,180	563,190	85	orange (outer)
1905	563	558	90	
1906	552	545	99	grey (inner)
	550	548	96	orange (outer)
1907	-	-	112	Paramagnetic
1908	568	550	83	
1909	570	560	91	
2001	513	513	100	
2002	553	540	89	
2003	525	540	110	Poorly defined
2004	573	580	111	grey (inner)
	563	558	110	orange (outer)
2005	583	565	94	
2006	578	575	-	Overload on feedback
2007	530	535	98	
2008	555,300	558	105	
2009	578	538	91	
2010	585	575	92	
2011	580,245	580	115	
2101	550	570	114	
2102	515	523	102	
2103	555	545	85	orange (outer)
2104	575	575	89	
2105	565	555	109	
2106	533	555	119	
2107	580,315	590	126	
2108	563,330	560	127	
2109	580	590	94	
2201	570	570	97	
2202	560	545	93	
2203	598,220	575,205	68	
2204	560	-	83	
2205	580	570	98	
2206	600	590	99	
2207	580	570	90	
2208	590,270	580	127	
2209	575	540	89	
2301	565,345	580	100	
2302	560,265	570	120	
2303	615	580	86	
2304	583	570	82	grey (inner)
	575	555	81	orange (outer)
2305	585	575	77	
2306	605	578	85	

Thermomagnetic behaviour continued...

Code	T_C,inflex. (°C) HT	T_C,inflex. (°C) CL	M_f/M_i (%)	Comments
2401	553	543	100	
	568	563	93	
2402	590,280	580,225	90	
2403	578	573	81	
2404	-	-	109	Paramagnetic?
2501	575,440	560	74	
2502	580	530	97	
	550	513	92	
2503	570	-	-	experimental problem
2504	585	545	97	
2505	488	515	113	
2601	580	575	85	
	563	555	88	
2602	608	608	90	
	615	575	88	
2603	585	565	100	
	585	560	100	
2604	592	588	90	
	595	583	87	
2605	552	542	95	
	558	546	93	
2606	565	560	98	
	555	550	93	
2607	590	560	102	
	608	555	98	
2608	595	575	93	
	595	570	97	
2701	615	573	93	
2705	-	-	100	Very weak/paramagnetic
2706	-	-	100	" " "
2707	-	-	100	Weak/paramagnetic
2708	545,175	483,138	89	
2709	-	-	80	Weak
2710	-	-	100	Paramagnetic
2711	-	-	78	Weak/paramagnetic
2712	-	-	97	Weak/paramagnetic
2713	520	480	97	Weak/poorly defined
2801	-	-	88	Paramagnetic

APPENDIX 3.

Isothermal remanence acquisition

Note: This table summarises the parameters of the two gaussian (on log scale) distributions which provide the 'best fit' curve to the normalised experimental IRM data plotted against the logarithm of applied field in mT. These distributions have means of x_1 and x_2 and standard deviations of SD_1 and SD_2. Mean coercivities (in mT) can be obtained for each distribution by calculating 10^x and approximate maximum coercivities are obtained from 10^{x+2SD}.

Where two or more subsamples from the same sherd have been measured this is denoted by A, B, C, etc. after the sample code. When these subsamples are from the inner or outer part of a sherd a comment to this effect is given.

CODE	1st Mineral			2nd Mineral			Comments
	%SIRM	x_1	SD_1	%SIRM	x_2	SD_2	
0201	100	1.48	0.19	-	-	-	
1002	69	1.68	0.36	31	3.10	0.24	
1003	16	1.80	0.36	84	2.83	0.27	
1103	98	1.66	0.29	2	3.00	0.30	
1106	98	1.75	0.31	2	3.00	0.25	
1107	92	1.58	0.32	8	3.00	0.30	
1109	100	1.58	0.26	-	-	-	
1110	100	1.57	0.30	-	-	-	
1201A	98	1.75	0.37	2	3.0	0.30	Inner
1201B	92	1.72	0.32	8	3.1	0.28	Outer
1202	97	1.34	0.34	3	3.1	0.30	Bulk
1401A	100	1.66	0.32	-	-	-	
1402A	100	1.66	0.34	-	-	-	Inner
1402B	98	1.52	0.34	2	3.00	0.35	Outer
1402C	100	1.64	0.34	-	-	-	Inner
1402D	97	1.47	0.34	3	3.00	0.26	Outer
1402E	100	1.64	0.35	-	-	-	Inner
1402F	96	1.58	0.38	4	3.00	0.30	Outer
1403A	100	1.65	0.40	-	-	-	Bulk
1403B	100	1.58	0.40	-	-	-	Bulk
1501A	100	1.75	0.27	-	-	-	Inner
1501B	96	1.76	0.24	4	3.05	0.26	Outer
1502A	100	1.67	0.32	-	-	-	Inner
1502B	100	1.56	0.36	-	-	-	Outer
1502C	100	1.68	0.32	-	-	-	Inner
1502D	95	1.64	0.30	5	3.10	0.25	Outer
1503A	100	1.76	0.33	-	-	-	Inner
1503B	100	1.72	0.32	-	-	-	Outer
1503C	100	1.73	0.36	-	-	-	Inner
1503D	100	1.66	0.38	-	-	-	Outer
1504A	100	1.77	0.31	-	-	-	

Isothermal remanence acquisition continued ...

CODE	1st Mineral			2nd Mineral			Comments
	%SIRM	x_1	SD_1	%SIRM	x_2	SD_2	
1505A	98	1.44	0.37	2	3.00	0.30	
1505B	100	1.43	0.37	-	-	-	
1506A	100	1.50	0.33	-	-	-	Inner
1506B	80	1.70	0.36	20	2.50	0.50	Outer
1506C	100	1.55	0.35	-	-	-	Inner
1506D	95	1.75	0.32	5	2.80	0.50	Outer
1507A	96	1.52	0.31	4	2.80	0.40	Bulk
1508A	92	1.39	0.37	8	2.75	0.40	Bulk
1508B	90	1.52	0.39	10	2.90	0.37	Bulk
1509A	95	1.61	0.40	5	2.80	0.35	Bulk
1509B	95	1.57	0.43	5	2.80	0.30	Bulk
1511A	100	1.66	0.35	-	-	-	Inner
1511B	96	1.37	0.36	4	3.00	0.35	Outer
1512A	100	1.55	0.39	-	-	-	Inner
1512B	89	1.64	0.37	11	2.85	0.30	Outer
1513A	100	1.54	0.36	-	-	-	Bulk
1513B	100	1.58	0.34	-	-	-	Bulk
1601A	100	1.54	0.36	-	-	-	Inner
1601B	100	1.76	0.35	-	-	-	Outer
1602A	100	1.43	0.375	-	-	-	Inner
1602B	100	1.39	0.36	-	-	-	Outer
1603	100	1.59	0.39	-	-	-	
1701	92	1.67	0.27	8	2.50	0.60	
1702	94	1.76	0.37	6	2.90	0.25	
1704	90	1.55	0.31	10	2.55	0.35	
1705	91	1.71	0.32	9	2.85	0.30	
1706	100	1.82	0.29	-	-	-	
1707	98	1.68	0.35	2	2.80	0.30	
1708	96	1.63	0.34	4	2.90	0.30	
1709	100	1.72	0.31	-	-	-	
1710	100	1.66	0.31	-	-	-	
1711	100	1.88	0.32	-	-	-	
1713	91	1.735	0.39	9	2.75	0.3	
1801	100	1.78	0.30	-	-	-	
1802	100	1.83	0.31	-	-	-	
1803	100	1.89	0.30	-	-	-	
1804	96	1.64	0.24	4	2.70	0.30	
1805	100	1.78	0.32	-	-	-	
1806	98	1.78	0.28	2	2.75	0.30	
1807	98	1.93	0.29	2	2.80	0.30	
1808	100	1.76	0.29	-	-	-	
1809	100	1.76	0.35	-	-	-	
1901A	94	1.69	0.34	6	2.90	0.35	Inner
1901B	50	1.74	0.32	50	3.01	0.26	Outer
1902	83	1.67	0.25	17	2.95	0.24	
1903	83	1.35	0.27	17	3.05	0.27	

1904A	79	1.85	0.31	21	3.05	0.23	Inner
1904B	79	1.72	0.31	21	2.93	0.25	Outer
1905A	96	1.81	0.28	4	2.90	0.30	Inner
1905B	98	1.79	0.28	2	3.00	0.30	Outer
1906	91	1.80	0.32	9	2.90	0.32	
1907	96	1.86	0.34	4	2.50	0.39	
1908	97	1.74	0.34	3	2.85	0.30	
1909	98	1.86	0.24	2	3.00	0.30	
2001	100	1.91	0.29	-	-	-	
2002	100	1.87	0.29	-	-	-	
2003	100	1.76	0.30	-	-	-	
2004A	100	1.85	0.31	-	-	-	Inner
2004B	100	1.89	0.27	-	-	-	Outer
2005	99	1.86	0.24	1	2.90	0.30	
2006	99	1.75	0.29	1	2.90	0.30	
2007	99	1.81	0.33	1	3.00	0.30	
2008	96	1.85	0.29	4	3.00	0.30	
2009	99	1.83	0.27	1	2.80	0.30	
2010	100	1.78	0.32	-	-	-	
2011	100	1.69	0.27	-	-	-	
2101	100	1.95	0.25	-	-	-	
2102	100	1.88	0.26	-	-	-	
2103A	97	1.87	0.30	3	2.90	0.30	Inner
2103B	99	1.80	0.30	1	2.90	0.30	Outer
2104	99	1.80	0.30	1	2.80	0.30	
2105	100	1.90	0.30	-	-	-	
2106	100	1.76	0.34	-	-	-	
2107	100	1.75	0.35	-	-	-	
2108	100	1.73	0.29	-	-	-	
2109	79	1.75	0.28	21	3.15	0.20	
2201A	99	1.66	0.30	1	2.85	0.30	Inner
2201B	82	1.36	0.30	18	2.80	0.34	Outer
2202	100	1.89	0.29	-	-	-	
2203	71	1.85	0.28	29	2.87	0.20	
2204A	100	1.78	0.24	-	-	-	Inner
2204B	99	1.81	0.26	1	2.80	0.30	Outer
2205A	82	1.66	0.33	18	2.79	0.30	Inner
2205B	99	1.78	0.30	1	3.00	0.30	Outer
2206	100	1.46	0.26	-	-	-	
2207A	94	1.73	0.27	6	2.80	0.30	Inner
2207B	97	1.73	0.26	3	2.80	0.30	Outer
2208	100	1.75	0.25	-	-	-	
2209	99	1.90	0.26	1	2.90	0.30	
2301	56	1.52	0.30	44	3.00	0.28	
2302	100	1.80	0.30	-	-	-	
2303	100	1.84	0.34	-	-	-	
2304	95	1.89	0.35	5	3.00	0.25	
2401	100	1.82	0.29	-	-	-	
2402	72	1.74	0.33	28	3.00	0.25	
2403	100	1.80	0.28	-	-	-	
2404	100	1.76	0.28	-	-	-	

Isothermal remanence acquisition continued ...

CODE	1st Mineral			2nd Mineral			Comments
	%SIRM	x_1	SD_1	%SIRM	x_2	SD_2	
2405	93	1.73	0.34	7	3.10	0.26	
2501	100	1.83	0.32	-	-	-	
2502	96	1.91	0.30	4	3.00	0.29	
2503	100	1.79	0.27	-	-	-	
2504	100	1.79	0.26	-	-	-	
2505A	100	1.86	0.26	-	-	-	Inner
2505B	100	1.90	0.28	-	-	-	Outer
2602	76	1.16	0.29	24	2.40	0.30	
2604	100	1.50	0.28	-	-	-	
2606	90	1.66	0.39	-	-	-	
2701	98	1.58	0.24	2	2.80	0.35	
2708	58	1.81	0.32	42	2.95	0.17	
2709	84	1.76	0.38	16	3.10	0.14	
2801	96	1.68	0.39	4	2.90	0.30	

APPENDIX 4.

Magnetic hysteresis behaviour

Note: Samples codes followed by two sets of data indicates that the same sample has been measured twice. Where consecutive sample codes are A, B etc. this indicates that two or more subsamples from the same sherd have been measured. Where these subsamples are visually disctinct a comment to this effect is given, and where they are not distinct no comment is given. Addition comments in the table indicate when hysteresis curves are not saturated or are constricted. See text for further details.

CODE	M_s (Am_2Kg^{-1})	M_{rs} (Am^2Kg^{-1})	M_{rs}/M_s	COMMENTS
0101A	0.147	0.042	0.288	
0101B	0.167	0.047	0.279	
0102A	0.257	0.045	0.176	
0102B	0.475	0.074	0.157	
0103A	0.249	0.062	0.250	
0103B	0.206	0.052	0.252	
0104A	0.712	0.166	0.233	
0104B	0.676	0.135	0.199	
0105A	0.748	0.085	0.114	
0105B	1.320	0.150	0.114	
0106A	0.247	0.066	0.268	
0201A	1.760	0.308	0.175	
0202A	1.860	0.347	0.187	
0501A	0.424	0.104	0.245	
0501B	0.527	0.116	0.220	
0502A	0.479	0.063	0.133	
0502B	0.581	0.071	0.122	
0503A	0.378	0.091	0.240	
0503B	0.381	0.097	0.236	
0504A	0.638	0.110	0.172	
0504B	0.586	0.097	0.165	
0601A	0.199	0.040	0.203	
	0.199	0.043	0.217	
0601B	0.194	0.042	0.214	
0602A	0.367	0.123	0.336	Open at 600mT?
	0.353	0.115	0.326	" "

Magnetic hysteresis behaviour continued...

CODE	M_s (Am_2Kg^{-1})	M_{rs} (Am^2Kg^{-1})	M_{rs}/M_s	COMMENTS
0702A	1.110	0.283	0.253	
0703A	0.195	0.023	0.117	
0801A	0.039	0.006(3)	0.161	
0803A	0.124	0.013	0.101	
0901A	0.636	0.097	0.152	
0902A	1.280	0.231	0.180	
0902B	1.870	0.338	0.181	
0903A	0.349	0.108	0.305	
0903B	0.387	0.115	0.298	
0904A	0.297	0.017	0.059	
0904B	0.247	0.017	0.068	
0905A	0.395	0.057	0.145	
0905B	0.171	0.025	0.147	
0906A	0.461	0.027	0.059	
1001A	-	-	-	Constricted
1002A	-	-	-	Open up to 1T
1002B	-	-	-	" "
1003A	-	-	-	Constricted
1003B	-	-	-	Constricted
1101A	-	-	-	Constricted
1102A	-	-	-	Constricted
1102B	-	-	-	Constricted
1103A	0.135	0.022(5)	0.168	
1104A	-	-	-	Constricted
1105A	0.082	0.025	0.307	
1106A	0.065	0.014	0.208	
1107A	0.455	0.103	0.227	Closed??
1108A	0.085	0.022	0.258	
1109A	0.114	0.022	0.198	
1110A	0.500	0.099	0.198	
1201A	0.176	0.059	0.336	
1201B	0.404	0.110	0.272	
1202A	0.051	0.007(6)	0.148	Open at 600 mT?

Magnetic hysteresis behaviour continued...

CODE	M_s (Am_2Kg^{-1})	M_{rs} (Am^2Kg^{-1})	M_{rs}/M_s	COMMENTS
1301A	19.10	2.450	0.124	
1302A	0.001(4)	0.000(3)	0.019	
1303A	–	–	–	Constricted
1304A	–	–	–	Constricted
1305A	0.035	0.001(3)	0.057	
1307A	0.273	0.062	0.227	
1309A	–	–	–	Constricted
1310A	0.0034	0.000(1)	0.042	Grey (inner)
1310B	0.0154	0.002(0)	0.131	(outer)
1311A	0.0403	0.013	0.320	
1401A	0.230	0.046	0.196	
1401B	0.207	0.040	0.193	
1402A	0.263	0.047	0.178	Black (inner)
1402B	0.216	0.042	0.193	" "
1402C	0.151	0.025	0.163	Orange (outer)
1403A	0.247	0.033	0.135	
1403B	0.159	0.026	0.165	
1501A	0.053	0.011	0.209	
1502A	0.164	0.030	0.182	Grey (inner)
1502B	0.129	0.018	0.143	Orange (outer)
1503A	0.247	0.043	0.175	Outer
1504A	0.068	0.016	0.235	Black (inner)
	0.065	0.016	0.241	" "
1504B	0.153	0.034	0.224	Orange (outer)
	0.154	0.039	0.253	" "
1505A	0.189	0.027	0.141	
1506A	0.004	0.000(6)	0.164	Black (inner)
	0.005	0.000(1)	0.018	" "
1506B	0.007	0.001(4)	0.201	Orange (outer)
	0.007	0.001(9)	0.250	" "
1507A	0.143	0.026	0.178	Black
	0.140	0.026	0.184	" "
1507B	0.205	0.034	0.167	Orange (outer)
	0.199	0.034	0.169	" "
1508A	0.045	0.004(3)	0.095	
	0.045	0.002(3)	0.051	

Magnetic hysteresis behaviour continued...

CODE	M_s (Am_2Kg^{-1})	M_{rs} (Am^2Kg^{-1})	M_{rs}/M_s	COMMENTS
1509A	0.006(7)	0.000(7)	0.106	
	0.007(1)	0.000(9)	0.122	
1510A	0.060	0.005(3)	0.089	Black (inner)
	0.059	0.004(6)	0.078	" "
1510B	0.052	0.005(5)	0.107	Orange (outer)
	0.051	0.001(9)	0.038	" "
1511A	0.067	0.001(2)	0.180	
	0.066	0.001(1)	0.170	
1512A	0.030	0.003(8)	0.128	
	0.030	0.003(7)	0.126	
1513A	0.222	0.058	0.261	
	0.219	0.056	0.256	
1601A	0.081	0.015	0.182	
	0.078	0.015	0.195	
1602A	0.309	0.049	0.158	
	0.306	0.048	0.157	
1602B	0.423	0.081	0.199	
1603A	0.150	0.031	0.203	
	0.135	0.029	0.209	
1603B	0.098	0.021	0.216	
1604A	0.073	0.014	0.185	
	0.087	0.016	0.179	
1604B	0.086	0.014	0.185	
1605A	0.056	0.014	0.249	Grey (inner)
1605B	0.075	0.018	0.232	" "
1605C	0.237	0.055	0.231	Orange (outer)
	0.235	0.058	0.249	" "
1701A	0.162	0.038	0.235	
1701B	0.194	0.048	0.248	
1702A	0.052	0.015	0.282	
	0.051	0.014	0.281	
1702B	0.061	0.018	0.293	
1703A	0.012	0.003(1)	0.260	
	0.007(2)	0.002(8)	0.400	
1704A	0.089	0.034	0.377	
	0.074	0.027	0.367	

Magnetic hysteresis behaviour continued...

CODE	M_s (Am_2Kg^{-1})	M_{rs} (Am^2Kg^{-1})	M_{rs}/M_s	COMMENTS
1704B	0.090	0.030	0.339	
1705A	0.010	0.001(9)	0.190	
1705B	0.013	0.002(6)	0.197	
1706A	0.041	0.012	0.284	
	0.038	0.009(6)	0.251	
1706B	0.023	0.007(2)	0.319	
1707A	0.228	0.040	0.177	
	0.222	0.026	0.119	
1707B	0.179	0.027	0.151	
1708A	0.514	0.100	0.202	
1708B	0.538	0.102	0.190	
1709A	0.123	0.017	0.134	
	0.111	0.016	0.144	
1709B	0.137	0.023	0.170	
1710A	0.791	0.120	0.152	
1710B	0.692	0.108	0.154	
	0.672	0.107	0.160	
1710C	0.769	0.129	0.162	
1711A	0.008(7)	0.003(5)	0.403	
	0.010	0.003(9)	0.381	
1712A	0.019	0.006(1)	0.326	
	0.018	0.005(6)	0.308	
1713A	–	–	–	Open at 600 mT
1801A	0.562	0.127	0.224	
1801B	0.616	0.134	0.217	
1802A	0.045	0.014	0.316	
1802B	0.052	0.016	0.303	
1803A	0.086	0.028	0.327	
	0.086	0.027	0.319	
1803B	0.107	0.038	0.354	
1803C	0.081	0.025	0.316	
1804A	0.174	0.029	0.165	
	0.176	0.028	0.156	
1804B	0.208	0.039	0.189	
1805B	0.137	0.045	0.333	
1805C	0.099	0.030	0.298	
1806A	0.022	0.005(6)	0.258	

Magnetic hysteresis behaviour continued...

CODE	M_s (Am_2Kg^{-1})	M_{rs} (Am^2Kg^{-1})	M_{rs}/M_s	COMMENTS
	0.021	0.004(6)	0.222	
1806B	0.023	0.004(3)	0.188	
1807A	0.348	0.157	0.451	
	0.346	0.157	0.454	
1807B	0.382	0.172	0.450	
1808A	0.232	0.086	0.370	
	0.226	0.083	0.368	
1808B	0.205	0.070	0.341	
1809A	0.245	0.087	0.353	
	0.251	0.087	0.348	
1809B	0.252	0.089	0.353	
1901A	0.049	0.012	0.249	Inner
	0.049	0.012	0.249	" "
1901B	0.042	0.011	0.266	Inner
1901C	-	-	-	Outer/Constricted
1902A	0.185	0.054	0.292	
	0.208	0.059	0.285	
1902B	0.444	0.120	0.270	
1903A	0.228	0.070	0.306	
1903B	-	-	-	Open at 600mT
1904A	0.082	0.028	0.337	Inner
	0.094	0.030	0.316	
1904B	-	-	-	Inner/Open at 600mT
1904C	0.205	0.068	0.333	Outer
	0.207	0.068	0.330	
1904D	-	-	-	Outer/Open at 600mT
1905A	0.176	0.056	0.316	Inner
	0.179	0.054	0.299	" "
1905B	0.210	0.068	0.323	Inner
1905C	0.237	0.076	0.321	Inner+outer
1906A	0.266	0.097	0.366	Inner
	0.266	0.092	0.343	" "
1906B	0.387	0.149	0.386	Outer
	0.386	0.150	0.388	" "
1907A	0.031	0.009(4)	0.300	
	0.033	0.009(7)	0.292	
1908A	0.081	0.024	0.292	

Magnetic hysteresis behaviour continued...

CODE	M_s (Am_2Kg^{-1})	M_{rs} (Am^2Kg^{-1})	M_{rs}/M_s	COMMENTS
	0.081	0.024	0.293	
1908B	0.117	0.034	0.287	
1909A	0.249	0.092	0.372	
	0.249	0.093	0.374	
1909B	0.585	0.230	0.394	
2001A	0.259	0.115	0.444	
	0.268	0.118	0.440	
2002A	0.159	0.057	0.357	
	0.162	0.058	0.357	
2003A	0.028	0.080	0.289	
2004A	0.132	0.051	0.387	Inner
	0.134	0.051	0.378	" "
2004B	0.227	0.088	0.388	Outer
	0.235	0.093	0.394	" "
2005A	0.640	0.241	0.377	
	0.651	0.249	0.382	
2006A	1.110	0.543	0.487	
2007A	0.131	0.048	0.370	
	0.130	0.048	0.366	
2008A	0.451	0.118	0.262	
	0.448	0.118	0.263	
2009A	0.062	0.018	0.296	
	0.064	0.019	0.296	
2010A	0.220	0.064	0.290	
	0.200	0.058	0.290	
2011A	0.341	0.076	0.224	
	0.345	0.074	0.215	
2101A	0.274	0.102	0.371	
	0.271	0.102	0.376	
2102A	0.147	0.056	0.380	
	0.158	0.060	0.379	
2103A	0.268	0.104	0.390	
2103B	0.272	0.118	0.435	
2104A	0.231	0.075	0.323	
2104B	0.244	0.078	0.318	
2105A	0.256	0.097	0.376	

Magnetic hysteresis behaviour continued...

CODE	M_s (Am_2Kg^{-1})	M_{rs} (Am^2Kg^{-1})	M_{rs}/M_s	COMMENTS
2105B	0.249	0.093	0.375	
2106A	0.039	0.010	0.271	
2107A	0.255	0.062	0.244	
2107B	0.221	0.060	0.270	
2108A	0.060	0.014	0.227	
2108B	0.058	0.013	0.223	
	0.045	0.010	0.229	
2109A	0.140	0.033	0.236	
	0.156	0.035	0.227	
2201A	0.419	0.117	0.279	
	0.422	0.110	0.260	
2202A	0.189	0.070	0.372	
	0.184	0.068	0.369	
2203A	0.194	0.088	0.454	
	0.181	0.090	0.497	
2204A	0.163	0.063	0.386	
	0.177	0.069	0.389	
2205A	0.330	0.100	0.303	
	0.337	0.102	0.302	
2206A	0.738	0.148	0.193	
2206B	0.702	0.144	0.205	
2207A	0.485	0.155	0.320	
2207B	0.509	0.165	0.324	
2208A	0.167	0.046	0.274	
2208B	0.136	0.039	0.288	
	0.115	0.032	0.276	
2209A	0.885	0.478	0.540	
2209B	1.310	0.520	0.395	
2301A	0.209	0.052	0.247	
2301B	0.214	0.052	0.244	
2302A	0.654	0.194	0.296	
2302B	0.643	0.188	0.292	
2303A	0.071	0.023	0.328	
2303B	0.070	0.022	0.317	
2304A	0.081	0.025	0.311	Inner

Magnetic hysteresis behaviour continued...

CODE	M_s (Am_2Kg^{-1})	M_{rs} (Am^2Kg^{-1})	M_{rs}/M_s	COMMENTS
2304B	0.069	0.026	0.373	" "
2304C	0.353	0.124	0.350	Outer
2304D	0.349	0.123	0.352	" "
2305A	-	-	-	Constricted
2306A	0.055	0.018	0.332	
2306B	0.054	0.017	0.309	
2401A	0.145	0.045	0.308	
2401B	0.142	0.048	0.336	
2402A	0.136	0.045	0.333	
2402B	0.132	0.046	0.350	
2403A	0.375	0.131	0.350	
2403B	0.367	0.128	0.347	
2404A	0.050	0.017	0.344	
2404B	0.051	0.017	0.342	
2405A	0.614	0.180	0.292	
2405B	0.562	0.168	0.299	
2501A	0.373	0.132	0.353	
2501B	0.359	0.129	0.361	
2502A	0.276	0.092	0.365	
2503A	0.075	0.027	0.365	
2503B	0.076	0.027	0.359	
2504A	0.058	0.014	0.247	
2504B	0.057	0.017	0.293	
2505A	0.253	0.087	0.344	
2601A	0.180	0.037	0.203	
	0.178	0.035	0.199	
2601B	0.192	0.043	0.226	
	0.187	0.041	0.219	
2602A	0.028	0.004(6)	0.161	
	0.029	0.004(8)	0.166	
2602B	0.030	0.005(3)	0.178	
2603A	0.282	0.090	0.316	
	0.291	0.095	0.326	
2603B	0.282	0.087	0.309	
	0.281	0.093	0.331	

Magnetic hysteresis behaviour continued...

CODE	M_s (Am_2Kg^{-1})	M_{rs} (Am^2Kg^{-1})	M_{rs}/M_s	COMMENTS
2604A	0.248	0.054	0.218	
	0.251	0.057	0.227	
2604B	0.284	0.063	0.222	
	0.299	0.071	0.238	
2605A	0.116	0.028	0.240	
	0.111	0.029	0.263	
2605B	0.098	0.023	0.235	
	0.098	0.023	0.235	
2606A	0.125	0.028	0.224	
	0.130	0.031	0.234	
2606B	0.168	0.031	0.185	
	0.173	0.033	0.193	
2607A	0.133	0.045	0.336	
	0.136	0.044	0.327	
2607B	0.124	0.042	0.342	
	0.122	0.042	0.340	
2608A	0.128	0.036	0.278	
	0.129	0.036	0.277	
2701A	0.327	0.090	0.276	
2702A	–	–	–	Open up to 1 T
2703A	–	–	–	Open at 600 mT?
2704A	–	–	–	Open up to 1 T
2705A	–	–	–	
2706A	–	–	–	Very weak/paramag
2707A	–	–	–	Constricted/open
2708A	–	–	–	Constricted/open
2709A	0.005(3)	0.001(5)	0.288	
2710A				
2711A				
2712A				
2713A	–	–	–	Open up to 1 T
2801A	0.037	0.008(4)	0.225	

APPENDIX 5.

Magnetic susceptibility behaviour

Note: K_{total} is the total mass specific susceptibility of the sample, K_{para} is the mass specific paramagnetic susceptibility obtained from magnetic hysteresis. K_{ferri} is the mass specific susceptibility of the ferrimagnetic minerals in the sample, i.e. $K_{total}-K_{para}$. The frequency dependence of the susceptibility is obtained by dividing the difference between low and high frequency susceptibilities by the low frequency susceptibility of a sample.

CODE	K_{total}	K_{para}	K_{ferri}	Frequency dependence
	($x10^{-8}m^3Kg^{-1}$)	" "	" "	
0501	504.65	10.00	494.65	0.0330
0502	473.33	11.10	463.23	0.0201
0503	526.47	9.47	517.00	0.0426
0504	468.28	13.60	453.68	0.0289
0601	391.50	6.00	385.51	0.0706
0602	839.30	0.00	839.31	0.0983
0702	1455.44	6.60	1448.84	0.0638
0703	495.27	1.40	493.87	0.1053
0801	102.94	7.00	95.94	0.1204
0802	500.00	10.90	489.10	0.0904
0901	1093.20	14.50	1078.70	0.0876
0902	1314.75	15.10	1299.65	0.0265
0903	252.73	13.70	239.03	0.0304
0904	194.88	12.20	182.68	0.0250
0905	259.35	13.90	245.45	0.0662
1002	240.03	8.20	231.83	0.1003
1003	56.62	8.60	48.02	0.0996
1101	122.74	6.00	116.74	0.1551
1102	43.26	5.70	37.56	0.1355

Magnetic susceptibility behaviour continued...

CODE	K_{total} ($x10^{-8}m^3Kg^{-1}$)	K_{para} " "	K_{ferri} " "	Frequency dependence
1103	235.94	9.60	226.34	0.0828
1104	49.58	4.90	44.68	0.1460
1107	554.57	19.10	535.47	0.0592
1301A	9763.70	10.00	9753.7	0.0056
1301B	12652.2	10.00	12642.2	0.0080
1302A	2.32	-	-	Below noise level
1303A	114.69	9.30	105.39	0.0664
1304A	36.20	6.00	30.20	0.1635
1305A	65.27	5.60	59.67	0.0438
1306A	242.16	7.20	234.96	0.0371
1307A	328.60	7.40	321.20	0.0884
1310A	2.67	1.00	1.67	Below noise level
1310B	39.64	5.00	34.64	0.1477
1311A	68.22	6.30	61.92	0.0876
1401A	301.83	9.80	292.03	0.072
1402A	312.15	12.80	299.35	0.081
1402B	191.21	10.00	181.21	0.074
1402D	195.83	10.00	185.83	0.043
1402E	358.80	12.80	346.00	0.084
1402F	153.83	10.00	143.85	0.101
1403A	320.14	11.90	308.24	0.087
1403B	308.54	11.90	296.64	0.082
1501A	116.02	10.00	106.02	0.052
1501B	74.53	10.00	64.50	0.096
1502A	355.29	12.70	342.54	0.093
1502B	330.84	12.70	318.15	0.070
1502C	348.16	12.70	335.46	0.096
1502D	251.70	12.70	239.00	0.057
1502E	346.35	12.70	333.65	0.091
1502F	313.95	12.70	301.25	0.077
1503A	397.13	11.50	385.63	0.039
1503B	429.35	11.50	417.85	0.065
1503C	375.00	11.50	363.50	0.044
1503D	413.58	11.50	402.08	0.061
1504A	58.04	6.34	51.70	0.000

Magnetic susceptibility behaviour continued...

CODE	K_{total} ($x10^{-8}m^3Kg^{-1}$)	K_{para} " "	K_{ferri} " "	Frequency dependence
1504B	211.73	7.80	203.93	0.090
1504C	152.78	6.34	146.45	0.082
1504D	115.38	7.80	107.58	0.101
1505A	364.62	6.80	357.82	0.085
1505B	380.50	6.80	373.70	0.08
1506A	24.23	7.00	17.23	0.06
1507A	242.89	7.80	235.09	0.07
1508A	135.15	9.95	125.20	0.10
1508B	155.04	9.95	145.09	0.11
1509A	15.15	7.95	7.20	0.35
1509B	14.88	7.95	6.93	0.43
1509C	17.41	7.95	9.46	0.26
1511A	110.22	8.70	101.52	0.08
1511B	115.87	8.70	107.17	0.13
1512A	109.65	8.35	101.30	0.09
1512B	18.15	8.35	9.80	0.34
1513A	210.27	10.85	199.42	0.06
1513B	356.04	10.85	345.19	0.08
1701A	304.97	9.40	295.57	0.07
1702A	80.35	4.60	75.75	0.07
1704A	137.59	4.15	133.44	0.05
1705A	25.28	3.30	21.98	0.03
1706A	36.18	4.30	31.88	0.02
1707A	196.95	8.50	188.45	0.01
1708A	416.55	8.20	408.35	0.02
1709A	82.61	3.70	78.91	0.01
1710A	714.08	10.80	703.28	0.04
1802A	44.75	8.90	35.85	0.035
1803A	85.22	7.10	78.12	0.065
1805A	125.54	5.60	119.94	0.060
1806A	28.17	8.40	19.77	0.047
1807A	200.91	10.10	190.81	0.028
1808A	165.79	8.90	156.89	0.053
1809A	313.21	7.00	306.21	0.070

Magnetic susceptibility behaviour continued...

CODE	K_{total} ($\times 10^{-8} m^3 Kg^{-1}$)	K_{para} " "	K_{ferri} " "	Frequency dependence
1901A	63.38	7.40	55.94	0.054
1901B	260.71	9.70	251.01	0.092
1902A	134.68	7.00	127.68	0.073
1903A	634.19	6.80	627.39	0.062
1904A	128.57	8.40	120.17	0.088
1904B	268.31	9.10	259.21	0.089
1905A	241.18	9.30	231.88	0.076
1905B	210.59	9.30	201.29	0.076
1906A	536.23	9.45	526.78	0.083
1908A	227.01	6.50	220.51	0.126
1909A	538.01	9.30	528.71	0.056
2104A	260.51	8.40	252.10	0.061
2105A	208.93	8.60	200.33	0.065
2106A	18.28	6.40	11.88	0.000
2107A	564.62	14.80	549.82	0.064
2108A	111.68	6.15	105.53	0.060
2108B	168.75	6.15	162.60	0.038
2109A	179.19	8.95	170.24	0.078
2201A	733.62	10.10	723.52	0.082
2201B	1127.36	10.10	1117.27	0.068
2202A	149.47	12.70	136.77	0.058
2204A	54.16	7.85	46.32	0.090
2204B	566.92	7.85	559.08	0.060
2205A	289.56	8.50	281.06	0.060
2205B	1139.59	8.50	1131.10	0.065
2206A	1169.73	13.50	1156.24	0.083
2207A	113.88	10.50	103.39	0.081
2207B	676.28	10.50	665.78	0.029
2208A	273.07	11.50	261.58	0.044
2209A	1081.88	20.00	1061.90	0.030
2301A	312.16	9.00	303.17	0.071
2302A	404.47	16.00	388.47	0.050
2303A	55.45	9.00	46.45	0.078
2303B	758.82	9.00	749.82	0.051

Magnetic susceptibility behaviour continued...

CODE	K_{total} ($x10^{-8}m^3Kg^{-1}$)	K_{para} " "	K_{ferri} " "	Frequency dependence
2304A	116.43	8.90	107.54	0.123
2401A	91.16	9.70	81.47	0.087
2401B	93.59	9.70	83.90	0.088
2402A	276.59	9.90	266.70	0.086
2403A	489.74	10.00	479.74	0.062
2404A	37.93	7.20	30.73	0.112
2405A	1811.11	9.00	1802.10	0.117
2501A	264.43	11.60	252.84	0.036
2501B	71.42	10.30	61.13	0.000
2502A	97.42	10.40	87.03	0.042
2503A	44.11	7.90	36.22	0.058
2503B	161.53	7.90	153.64	0.025
2504A	46.63	6.50	40.13	0.000
2504B	41.48	6.50	34.98	0.062
2505A	76.47	8.00	68.47	0.000
2505B	95.94	8.00	87.94	0.021

APPENDIX 6.

Low Temperature Susceptibility

Note: The RS value is defined as the ratio of the susceptibility at -196°C to the susceptibility at room temperature. The definitions and interpretation of the group numbers are given in chapter 6. Where a group number is listed as e.g. 1/3 this indicates that the curve appears as a combination of group 1 and group 3 behaviour.

Code	RS	Group
0101	0.77	1
0102	0.75	1/3
0103	0.74	1
0104	0.68	1/3
0105	0.52	1
0106	0.71	1
0201	0.61	1
0202	0.71	1
0501	0.80	1/3
0502	0.67	3
0503	0.82	1/3
0504	0.80	3/1
0601	0.66	1/3
0602	0.61	1/3
0701	0.84	1/3
0702	0.56	1
0703	0.57	1
0704	0.57	1
0801	0.90	1/2
0802	0.61	1
0901	0.51	1/3
0902	0.74	3/1
0903	0.78	1/3
0904	0.76	3

Low temperature susceptibility behaviour continued...

Code	RS	Group
0905	0.70	1/3
1001	0.54	1/3
1002	0.83	1/2
1003	0.95	1/2
1201	0.91	1
1202	0.73	1
1101	0.55	1
1103	0.79	1
1104	0.97	1/3
1106	0.68	1/2
1107	0.61	1
1109	0.84	1
1110	0.65	1
1301	0.54	3
1302	1.52	2
1303	0.66	1
1304	0.98	1
1305	2.91	2
1306	0.73	1
1307	0.56	1
1310	1.18	1/2
1311	0.90	1
1401	0.75	1/3
1402	0.72	1/3
1403	0.73	1/3
1501	0.71	1
1502	0.65	1/3
1503	0.76	3
1505	0.64	1
1506	1.61	2

Low temperature susceptibility behaviour continued...

Code	RS	Group
1507	0.66	1
1508	0.78	1
1509	1.40	2
1511	0.61	1
1512	1.14	2
1601	0.66	1
1602	0.41	1
1603	0.71	1
1604	0.82	1
1605	0.63	1
1701	0.67	1/3
1704	0.59	1
1705	1.35	2
1706	0.94	1
1707	0.50	1/3
1708	1.10	2
1709	0.90	3
1710	0.73	1/3
1712	1.14	1/2
1713	0.69	1
1801	0.90	1
1802	1.1	1/2
1803	0.88	1
1804	0.59	1
1805	0.64	1
1806	1.48	2
1807	0.63	1
1808	0.62	1
1809	0.56	1
1901	0.72	1
1902	0.82	1
1903	0.50	1

Low temperature susceptibility behaviour continued...

Code	RS	Group
1904	0.67	1
1905	0.62	1
1906	0.61	1/3
1907	0.99	1
1908	0.58	1/3
1909	0.77	1
2001	0.66	1
2002	0.75	1
2003	1.67	2
2004	0.74	1
2005	0.56	1/3
2006	0.61	1/3
2007	0.55	1
2008	0.80	1/3
2009	1.06	1/2
2010	0.73	1
2011	0.51	1
2101	0.64	1
2102	0.67	1
2103	0.71	1/3
2104	0.60	1
2105	0.56	1
2106	1.33	1/2
2107	0.64	1
2108	0.65	1
2109	0.95	1
2201	0.52	1
2202	0.71	1/3
2203	0.62	1
2204	0.64	1/3
2205	0.74	1
2206	0.46	1
2207	0.84	1/3

Low temperature susceptibility behaviour continued...

Code	RS	Group
2208	0.64	1
2209	0.65	1/3
2301	0.64	1
2302	0.62	1
2303	0.73	1
2304	0.63	1/3
2305	0.62	1
2306	0.66	1
2401	0.61	1
2402	0.71	1
2403	0.69	1
2404	0.91	1
2405	0.46	1
2501	0.69	1
2502	0.90	1
2503	0.95	1
2504	1.00	1
2505	0.91	1
2601	0.64	1/3
2602	0.59	1
2603	0.70	1
2604	0.75	1
2605	0.69	1
2606	0.62	1
2607	0.81	1/2
2608	0.69	1/2

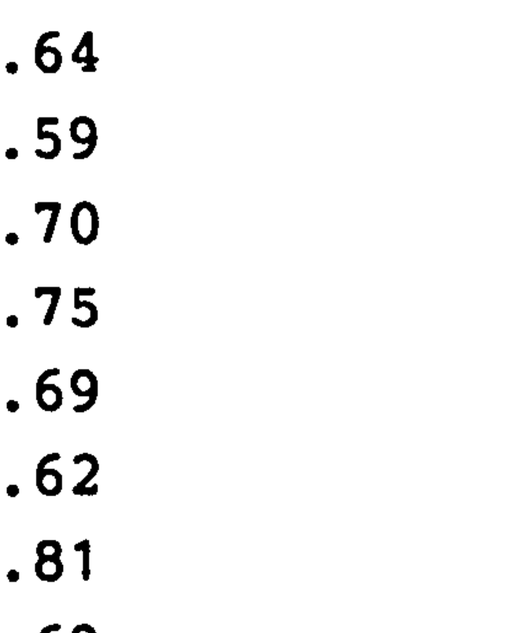

RED FIRED SANDSTONE: A GOOD RECORDER OF ANCIENT GEOMAGNETIC FIELD?

D. Atkinson & J. Shaw

Geomagnetism Laboratory, Institute of Prehistoric Sciences and Archaeology, Oliver Lodge, University of Liverpool, P.O. Box 147, L69 3BX.

Abstract

The magnetic properties of samples from an ancient red sandstone kiln have been investigated to determine their possible archaeological applications. The magnetic mineralogy and domain states have been defined. Also the problem of magnetic refraction or the presence of a magnetic fabric have been investigated. The results suggest that fired sandstone is useful for archaeomagnetic directional dating, but the determination of firing temperature or the intensity of the ambient magnetic field at the time of firing are unobtainable due to the thermochemical nature of the sandstone's magnetisation.

Introduction

Continued developments in archaeomagnetism have led to the assembly of a reference curve of geomagnetic directional secular variation for Britain extending back to 1000 BC (Clark *et al.*, 1988). The curve is now routinely used to date fired archaeological artefacts that are in situ. It also provides information about the geomagnetic field (Tarling, 1989). Most of the data for the curve are derived from baked clays; other materials such as burnt soil and brick have been utilised to a limited extent. It is the aim of this study to investigate the magnetic properties of baked red sandstone, collected from a hearth in Chester, to determine its value to archaeomagnetism.

Sampling

The sandstone samples investigated came from a single site in Chester. The sandstone is probably the local Triassic sandstone which is predominantly composed of quartz grains with a haematite cement. Samples were removed from a small curved wall considered by the site archaeologists to be part of a kiln or hearth. The wall was constructed from large, roughly worked blocks of sandstone with soft cement between them. The inner side of the wall was blackened with ashes. Blocks from the top of the wall were oriented using a suncompass, mounted on a small tripod, and a theodolite.

In the laboratory the blocks were reoriented in the horizontal plane and set with plaster of paris for subsampling. Four blocks were subsampled using a standard 25 mm diameter palaeomagnetic drill. The distribution of subsamples in individual blocks allowed the correlation of magnetic properties with distance from the inside of the kiln (ie the heat source).

Thermal demagnetisation behaviour

Incremental thermal demagnetisation was undertaken on between four and ten samples from each of the blocks using a Magnetic Measurements thermal demagnetiser. The direction and intensity of remanence was measured after each heating stage using a Molspin spinner magnetometer.

The demagnetisation behaviour of subsamples was similar between blocks and showed systematic variations of blocking temperature spectra and magnetic vector components when plotted against distance from the heated surface of the blocks.

The variation of blocking temperature spectra against distance is illustrated by subsamples from block 2 (Figure 1). The temperature of the spectra peaks is seen to reduce and the peaks broaden with increasing distance from the heated face.

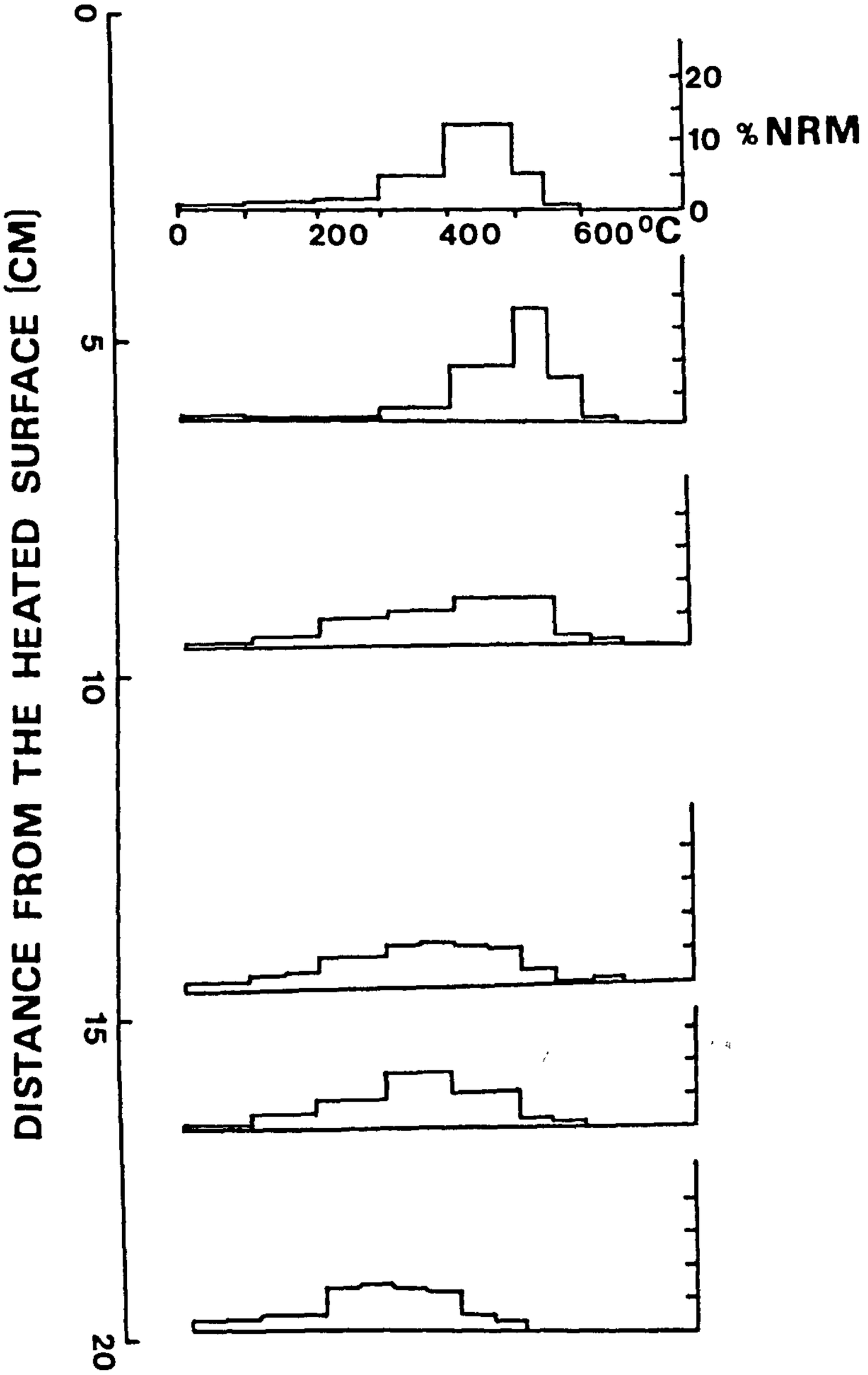

Figure 1. Variation of the blocking temperature spectra with distance from the heated surface, obtained from incremental thermal demagnetisation.

The vector composition of the natural remanent magnetisations (NRMs) is dependent on the distance from the heated surface. A low intensity component was removed from all subsamples after heating to 200-300°C. All subsamples showed an intense northerly/positive component of which 95% was removed by heating to 470-550°C. For subsamples nearest to the heated surface this was the only definable component (Figure 2). For the subsamples taken furthest from the heated surface a second higher temperature component was also observed. The very low intensity of this component did not allow an accurate determination of its direction.

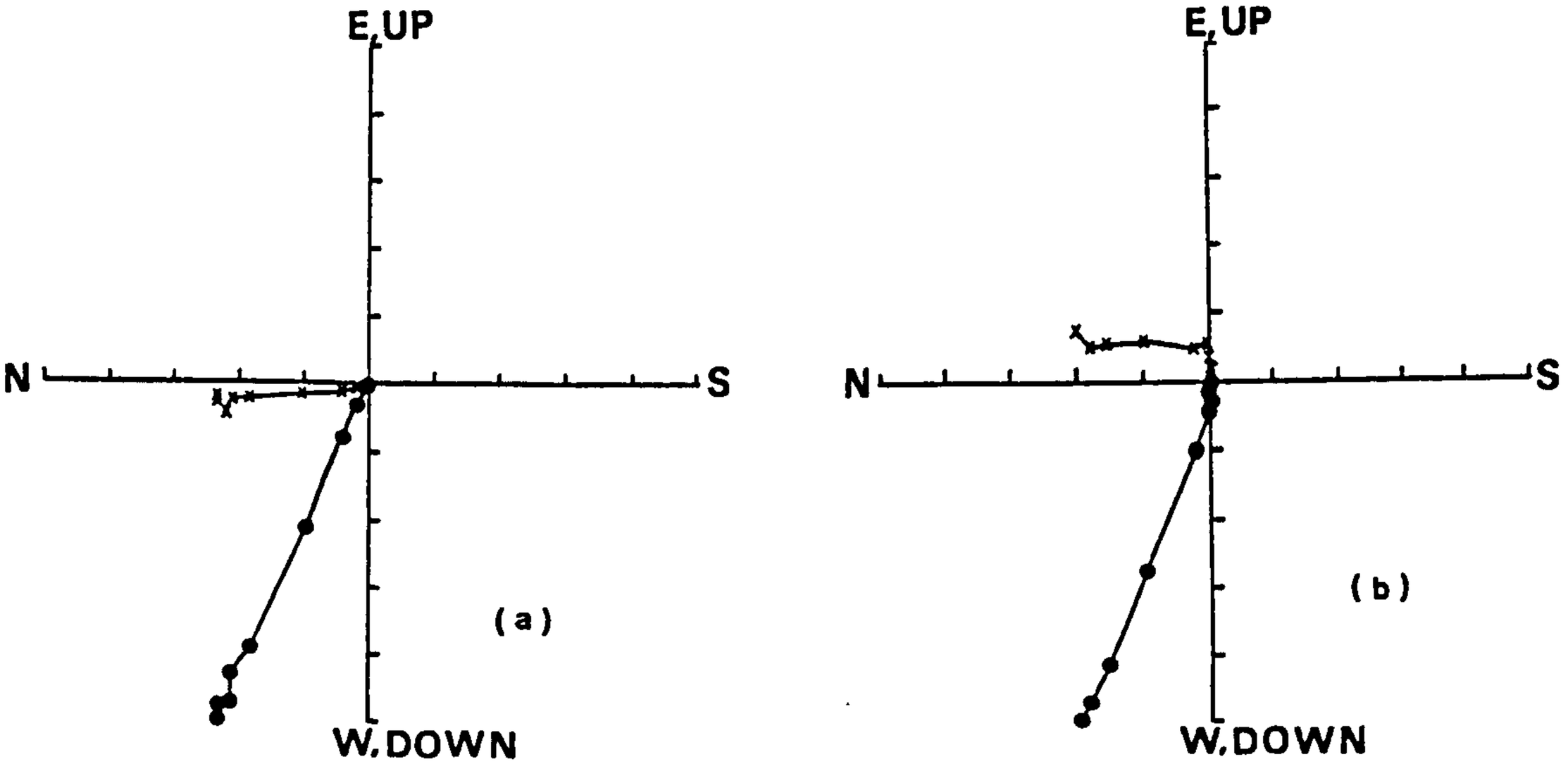

Figure 2. Orthogonal vector plots of the NRMs of subsamples (a) nearest to the heated surface and (b) furthest from the heated surface. Crosses indicate the horizontal projection and circles the vertical projection.

Rock magnetic properties

In common with the demagnetisation behaviour, the magnetic mineralogy is a function of distance from the heated surface. The variation of NRM intensity and bulk susceptibility against distance are shown in Figure 3. Isothermal remanence acquisition (IRM) curves with a maximum applied field of 3.6 T indicate a rapid change in mineralogy. Subsamples closest to the heated surface show simple behaviour saturating at 250-300 mT. With increasing distance from the heated surface this component is very much reduced in intensity and a much higher coercivity component is observed to saturate toward 4 T (Figure 4). Uncalibrated hysteresis measurements in a maximum field of 1 T show similar characteristics, with only samples closest to the heated surface being saturated. The ratio of saturation remanence to saturation magnetisation (Mrs/Ms) obtained from saturated loops fall between 0.29 and 0.31.

Thermomagnetic behaviour of subsamples obtained from heating in air is of two types. Those subsamples closest to the heated surface have single Curie temperatures around 580°C and those further than 7 or 8 cm from the heated surface have Curie temperatures in the region of 650-720°C.

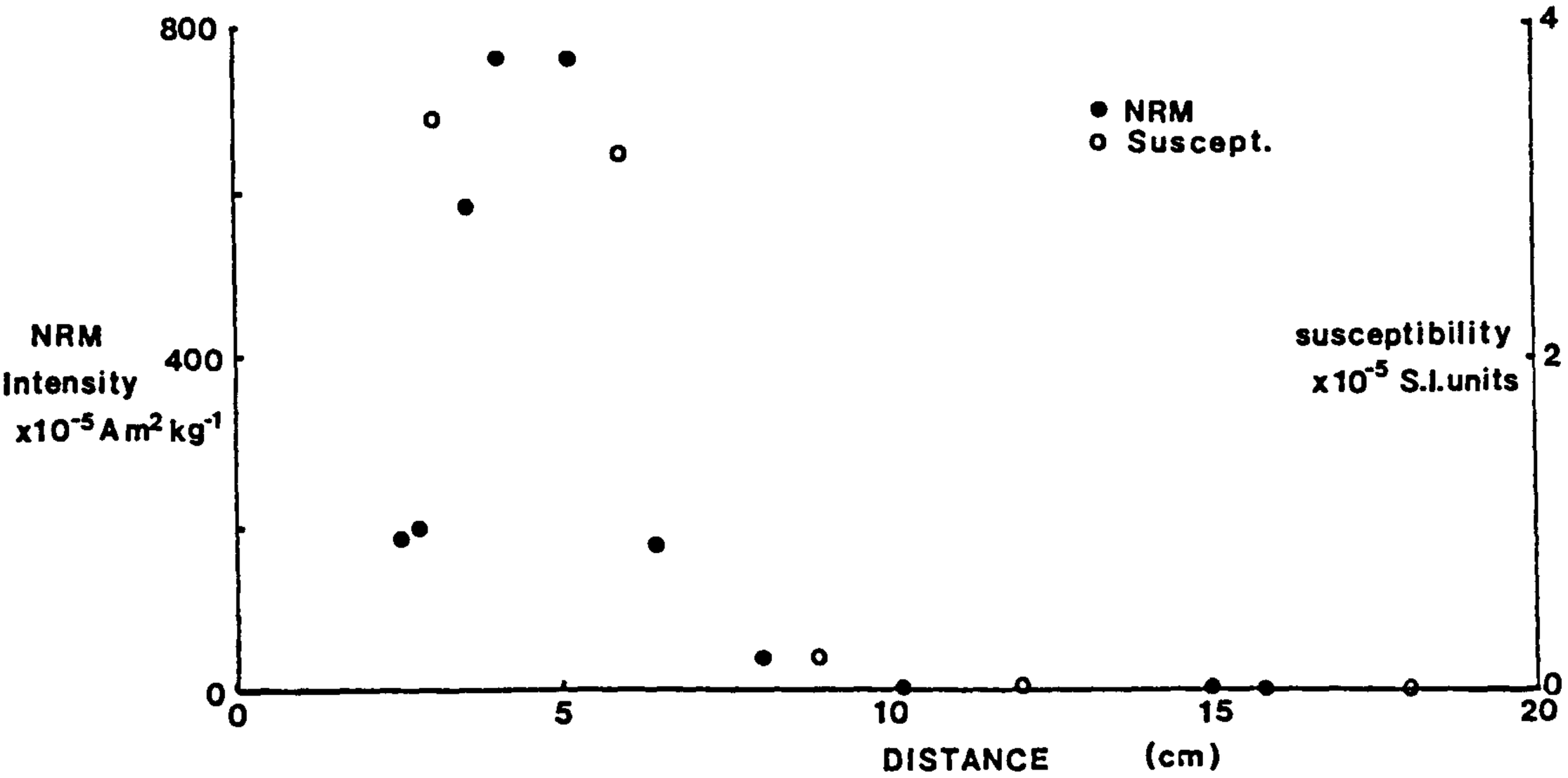

Figure 3. Variation of the NRM intensities and room temperature susceptibilities with distance from the heated surface.

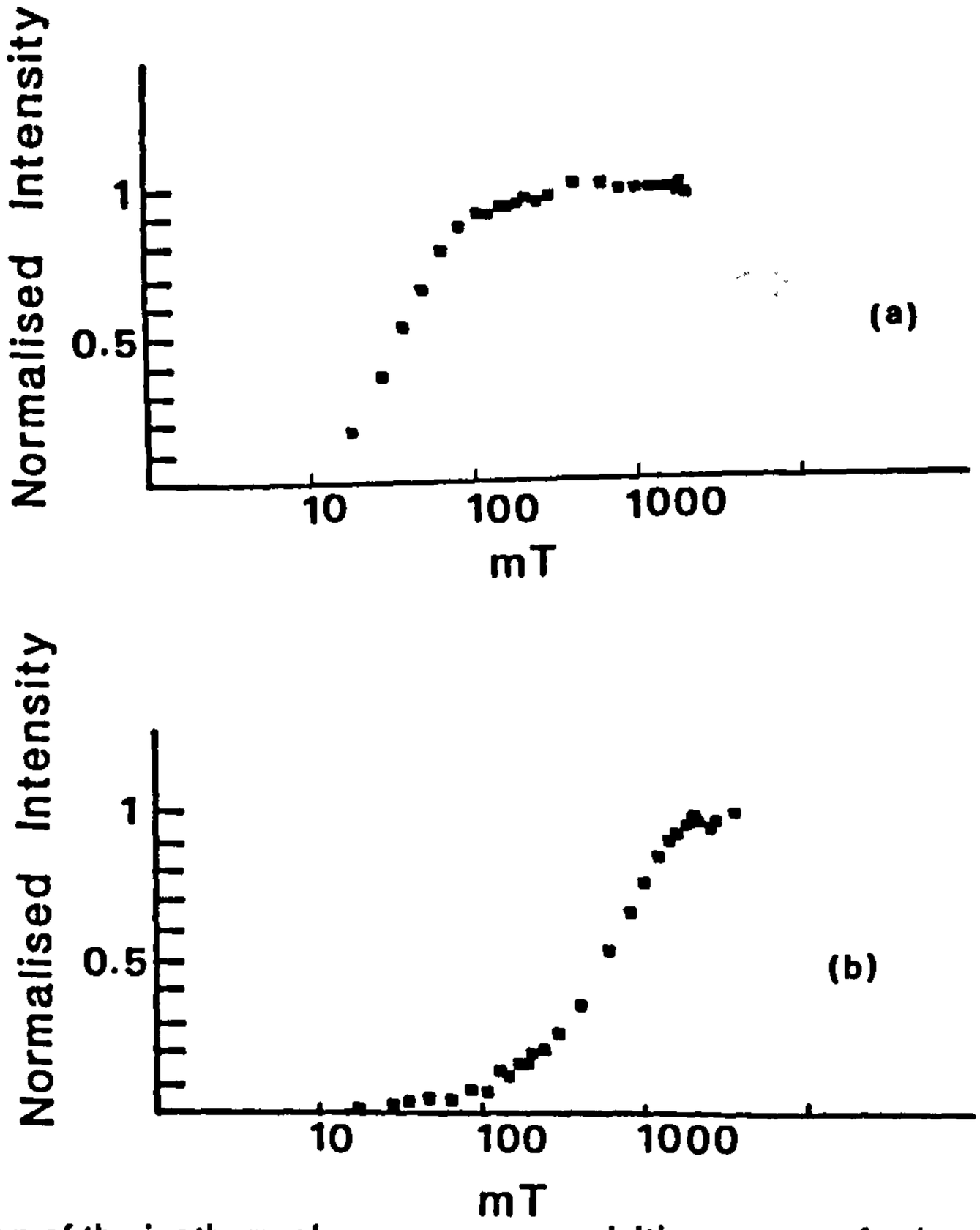

Figure 4. Comparison of the isothermal remanence acquisition curves of subsamples (a) closest and (b) furthest from the heated surface of the blocks.

High temperature susceptibility measurements were undertaken using a Bartington MS2 bridge. The temperature variation of susceptibility of subsamples up to about 9 cm from the heated surface of the blocks was similar (Figure 5). The Curie temperatures determined from the descending arms of the peaks of the curves are between 500 and 560°C. The temperature variation of susceptibility of subsamples from further than 9 cm from the heated surface of the blocks was not distinguishable from the noise level of the bridge. Anisotropy of magnetic susceptibility (AMS) measurements, using a Molspin minisep anisotropy delineator, indicate that the blocks have a magnetic fabric. The ratio of maximum to minimum susceptibility being similar within and between blocks. The ratio varies between 1.014 and 1.065. These values are slightly larger than the actual ratios because the length to width ratio of the subsamples was 1, not the ideal value of 0.9 calculated by Hounslow *et al.* (1988). The direction of the maximum and minimum axes are the same within blocks but vary between blocks. These AMS measurements indicate a very small degree of alignment of the magnetic grains.

Discussion of magnetic properties

The most striking feature of the magnetic properties is their dependence upon distance from the inner side of the wall. This distance dependence, which is consistent between blocks, strongly suggests that the magnetic properties are the result of firing the structure.

Assessing the reliability and applicability of the magnetic record obtained from fired red sandstone, both specific to this study and for the general case, requires an understanding of demagnetisation behaviour, magnetic mineralogy, domain states, and possible refraction effects.

The variation of the magnetic vector components of subsamples can be explained by the variation of temperature within blocks. Before heating the sandstone blocks would have held a remanence arising from the growth of haematite when cementation occurred. With heating or firing, the magnetic minerals may alter and their magnetisations will be partially or completely reset toward the ambient field direction depending on

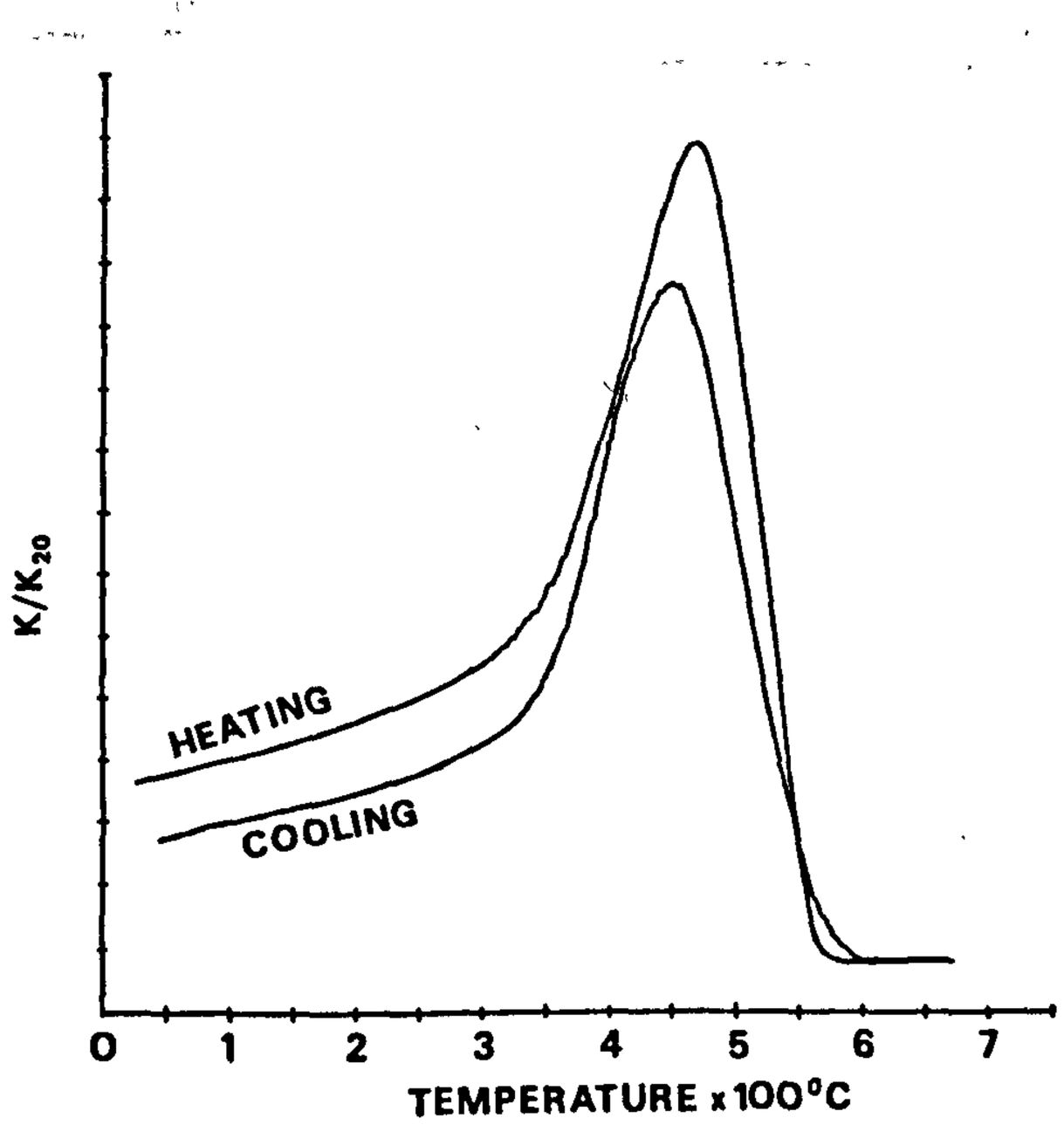

Figure 5. High temperature susceptibility measurements showing an increase in susceptibility up to the Hopkinson peak.

whether the temperature of heating exceeds the maximum blocking temperature of the minerals. Subsamples closest to the heated surface have only a low temperature viscous component, and a steep northerly component, whereas samples further from the heated surface have an additional component at higher unblocking temperatures.

Firing has had a major effect on the rock magnetic character of the sandstone. Subsamples nearest to the heated surface have high susceptibilities and NRM intensities. These subsamples are saturated by 250-300 mT during IRM acquisition, and have Curie temperatures in the range 500-580°C. This is indicative of a single phase of titanium poor magnetite. Mrs/Ms ratios obtained from hysteresis loops suggest grain sizes predominantly in the single domain region (Thompson & Oldfield, 1986).

Subsamples taken furthest from the heated surface have very low susceptibility and remanent intensity and are not quite saturated by 3.6 T. Curie temperatures for these samples are in the range 650-700°C. The rock magnetic parameters for these samples suggest that the predominant magnetic mineral is haematite.

The mineralogy of intermediate samples shows a rapid gradation from the magnetite rich surface to the haematite rich distal zone. This gradation was only observable in IRM acquisition, the haematite signal being swamped by magnetite in other analyses. The mean ratio of Mrs/Ms was taken as representative of the magnetite in the blocks. It was used with the SIRM intensities of he magnetite component observed during IRM acquisition, and the saturation magnetisation value for magnetite (92 Am^2kg^{-1}, O'Reilly,1984) to calculate the magnetite content present at increasing distance from the heated surface (see Figure 6).

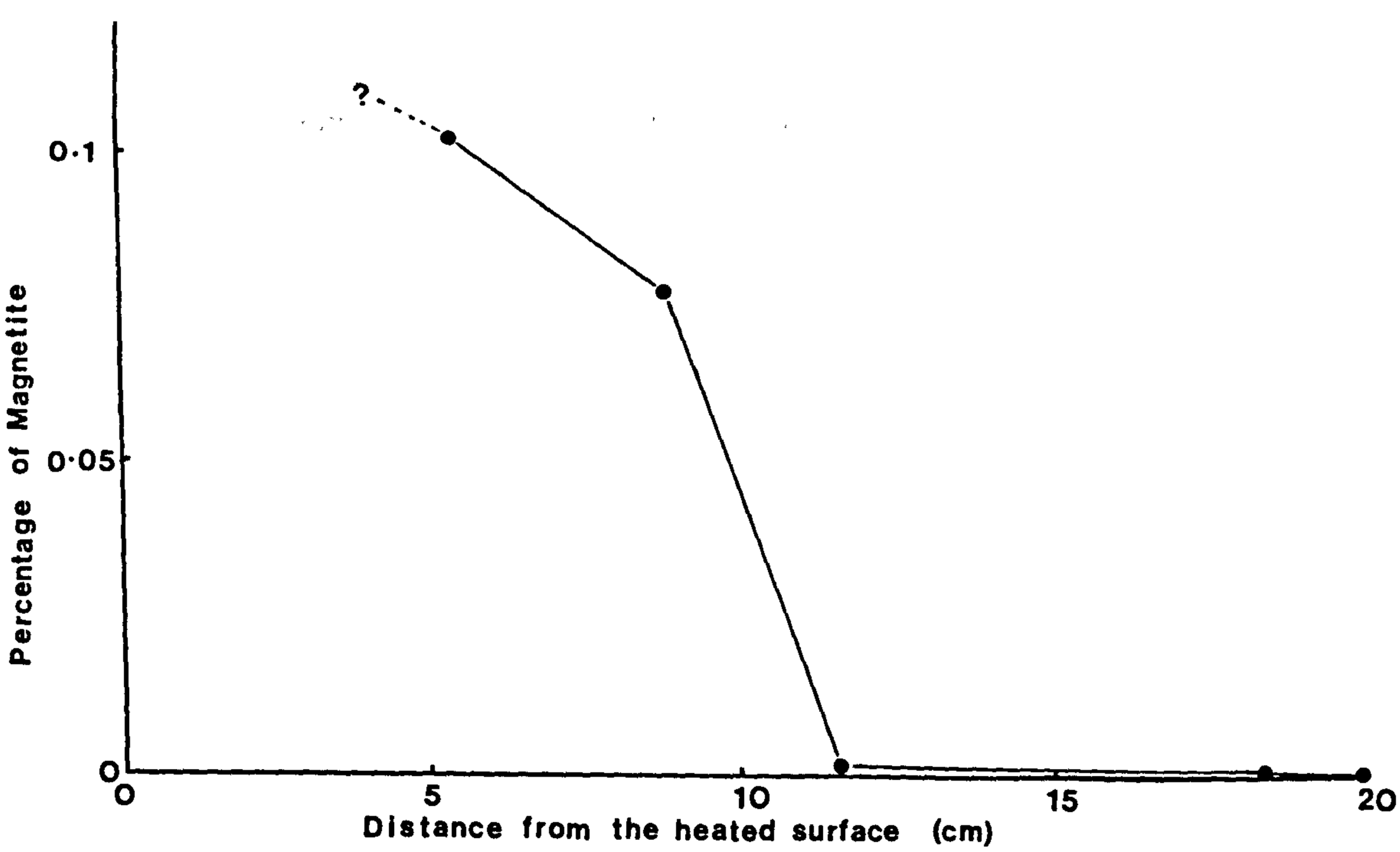

Figure 6. Variation of the magnetite content of the rock with distance from the heated surface (shown as the percentage by mass of magnetite).

The primary nature of haematite in red sandstone and the concentration of magnetite at the heated surface suggest that magnetite is the result of heating or firing. The magnetite is probably derived from reduction of haematite in a hot carbon monoxide atmosphere produced by fuel, the ashes of which are preserved on the kiln wall. The rapid reduction of magnetite with distance may be due to a combination of duration and temperature of heating and the porosity of the rock.

With an understanding of the mineralogy it is clear that remanence is not a simple thermoremanent magnetisation (TRM). The growth of magnetite particles, by the reduction of the primary haematite, combined with the temperature and duration of firing, results in a more complex thermochemical remanence (TCRM). Because of this complexity a description of the variation in the blocking temperature spectra cannot be based solely on thermal activation theory and hence no temperature information can be easily obtained.

Deflection of the direction of remanence from that of the ambient field can arise from shape anisotropy (refraction) or the presence of a magnetic fabric. Both aspects have been investigated.

The problem of shape anisotropy leading to magnetic refraction has been investigated by several workers (eg Aitken & Hawley, 1971; Stacey and Banerjee, 1974; Abrahamsen, 1986). The approach followed in this study is that of Abrahamsen (1986) which is essentially the same as that of Stacey and Banerjee, (1974). The angular deviation from the ambient field direction for an elongated body is derived in the general form:

$$Deviation = v - \arctan\left(\frac{\tan v}{1+K_a}\right) \quad (1)$$

where v is the angle of the magnetisation to a perpendicular to the surface of the body and Ka is the apparent susceptibility in S.I. units ie. the magnetisation at the blocking temperature. The maximum deviation occurs where the angle of magnetisation is in the range $45 < v > 52$ (Abrahamsen, 1986). Values for the maximum apparent susceptibilities of the red sandstone have been obtained from the Hopkinson peaks observed during high temperature susceptibility measurements. The maximum angular deviation of the magnetisation has been calculated by considering a block as a series of vertical slices and then using equation (1) as an approximation. The maximum deviation occurs close to the heated surface but is only 0.54 degrees.

The presence of a weak magnetic fabric in the sandstone is indicated by AMS measurements. The average percentage anisotropy of subsamples (the percentage difference between the maximum and minimum susceptibilities) is 3.8%. The presence of a magnetic fabric will influence the accurate recording of the ambient field, but the deflection of magnetisation has been shown to be negligible when the AMS is less than 5% (Hrouda, 1982).

Conclusions

Usually archaeomagnetic work is undertaken to determine the age of last firing of an in situ artefact using geomagnetic directional secular variation. Also information about the intensity of the geomagnetic field at the time of firing and the firing temperature can be obtained.

Firing red sandstone in a reducing environment clearly alters its magnetic signature. This has both advantages and disadvantages in terms of the information that can be retrieved. The NRM intensity of the original haematite bearing rock is very low, making the precise definition of the direction of magnetisation difficult. The conversion of haematite to magnetite close to the heated surface increases the NRM intensity by several orders of magnitude greatly improving the precision of the determination of the direction of magnetisation. The increases NRM intensity coupled with negligible deflection

effect (almost no refraction or magnetic fabric) suggests that fired red sandstone is useful for dating *In situ* artefacts using the directional secular variation method. The determination of geomagnetic field intensities usually requires the magnetisation of samples to have only a thermal origin, ie a TRM, this is also necessary for the determination of the temperature of firing. The growth of magnetite during firing may preclude the formation of a simple TRM and therefore care must be exercised when using fired red sandstone for field intensity and temperature determinations.

Acknowledgements

The authors would like to thank Jennifer King, Drs T.C. Rolph and D.J. Robertson for guidance and assistance during sampling and for discussions. We would also like to thank Chester City Council for permission to take samples.

References

Abrahamsen, N. (1986). On shape anisotropy. In: *Twenty-five Years of Geology in Aarhus*, ed. J.T. Moller, pp.11-21. Geoskrifter, 24.

Aitken, M.J. & Hawley, H.N. (1971). Archaeomagnetism: Evidence for magnetic refraction in kiln structures. *Archaeometry* 13, 83-85.

Clark, A.J., Tarling, D.H. & Noel, M. (1988). Developments in archaeomagnetic dating in Britain. *Journal of Archaeological Sciences* 15, 645-667.

Hounslow, M.W., Noel, M. & Bootes, P.A. (1988). Sensitivity and sample-shape related measuring effects on the MOLSPIN Susceptibility Anisotropy Meter. *Geophysical Journal* 94, 355-363.

Hrouda, F. (1982). Magnetic anisotropy of rocks and its application in Geology and Geophysics. *Geophysical Reviews* 5, 37-82.

O'Reilly, W. (1984). *Rock and Mineral magnetism*. Blackie, Glasgow.

Stacey, F.D. & Banerjee, S.K. (1974). *The Physical Principles of Rock Magnetism*. Elsevier, Amsterdam.

Tarling, D.H. (1989). Secular variation during the last 2000 years. In: *Geomagnetism and Palaeomagnetism. NATO Advanced Study Institute on Geomagnetism and Palaeomagnetism*, Newcastle upon Tyne, 1988, ed. F.J. Lowes. Kluwer Academic, Dordrecht, 1989.

Thompson, R. & Oldfield, F. (1986). *Environmental Magnetism*. Allen & Unwin, London.

Archaeometry '90

MAGNETIC VISCOSITY DATING

D. Atkinson and J. Shaw

Geomagnetism Laboratory, Institute of Prehistoric Sciences and Archaeology, University of Liverpool, PO Box 147, Liverpool L69 3BX, UK.

SUMMARY: The present work is a discussicn of the theoretical and experimental observations pertinent to the application of magnetic viscosity to the dating of fired artefacts such as pottery and brick. A thermal method for obtaining dates, based on the treatment of viscosity as an activation process is under development.

INTRODUCTION

The possibility of retrieving age information using magnetic viscosity (the time variation of the magnetisation of a magnetic body in a weak magnetic field) has been explored by Heller and Markert (1973). They investigated some samples of igneous rock used in the construction of part of Hadrian's Wall (Northern England). Their application of an alternating magnetic field demagnetisation method based on the multidomain viscosity model of Neel (1950) gave results in reasonable agreement with the archaeological age.

Since this work, no further investigations using magnetic viscosity as a dating tool have been reported. This is surprising since the observation of magnetic viscosity is common in palaeo- and rock magnetism, although some discrepancies are recognised

between the theoretical work and experimental observations. In the following examination of viscosity, examples of experimental observations are drawn mainly from work on a variety of rocks and their synthetic analogues. These are considered pertinent to fired materials because the magnetic properties of rocks show similarities with those of some fired materials, as witnessed by the application of standard palaeomagnetic analysis to fired archaeological materials (see for example Aitken, 1974). The similarity arises because both rocks and pottery contain small percentages of magnetic iron oxides dispersed in a non-magnetic matrix.

THEORY AND OBSERVATION

Experimental observations of the time varying magnetisation of a variety of rocks and synthetics have been obtained by several workers (reviewed by Dunlop, 1973). Most are in agreement about the nature of the time dependence of the acquisition of viscous magnetisation which is logarithmic within experimental limits (eg. Shimizu, 1960, fig. 1a). From these early observations the common notation used for describing the acquisition of viscous magnetisation has been:

$$J(t)=S_a(\ln(t)) \qquad (1)$$

where J(t) is the viscous magnetisation acquired in the presence of a weak magnetic field over time t since the orientation of the material, relative to the field, was last disturbed. S_a is termed the viscosity coefficient.

The limited experimental work of the present study indicates that some pottery exhibits viscous behaviour and that the time dependence is approximately logarithmic over the experimental timescale (fig. 1b). Dunlop (1973) also summarizes work on several rock types which indicate a non-linear dependence on the logarithm of time for the acquisition of viscous magnetisation. More recently, work on well characterised synthetic magnetite

(eg. Dunlop, 1983, Tivey & Johnson, 1981, 1984) suggests that the log time dependence is not a fundamental feature of the process but is a function of the particle size distribution and the domain states of the particles.

Theoretical models of viscosity behaviour have been developed around a thermal activation energy approach in which a system of magnetic particles "decays" toward a lower energy state imposed by the application of a weak magnetic field. The magnetic moments of individual particles are considered to align toward the applied field direction with time.

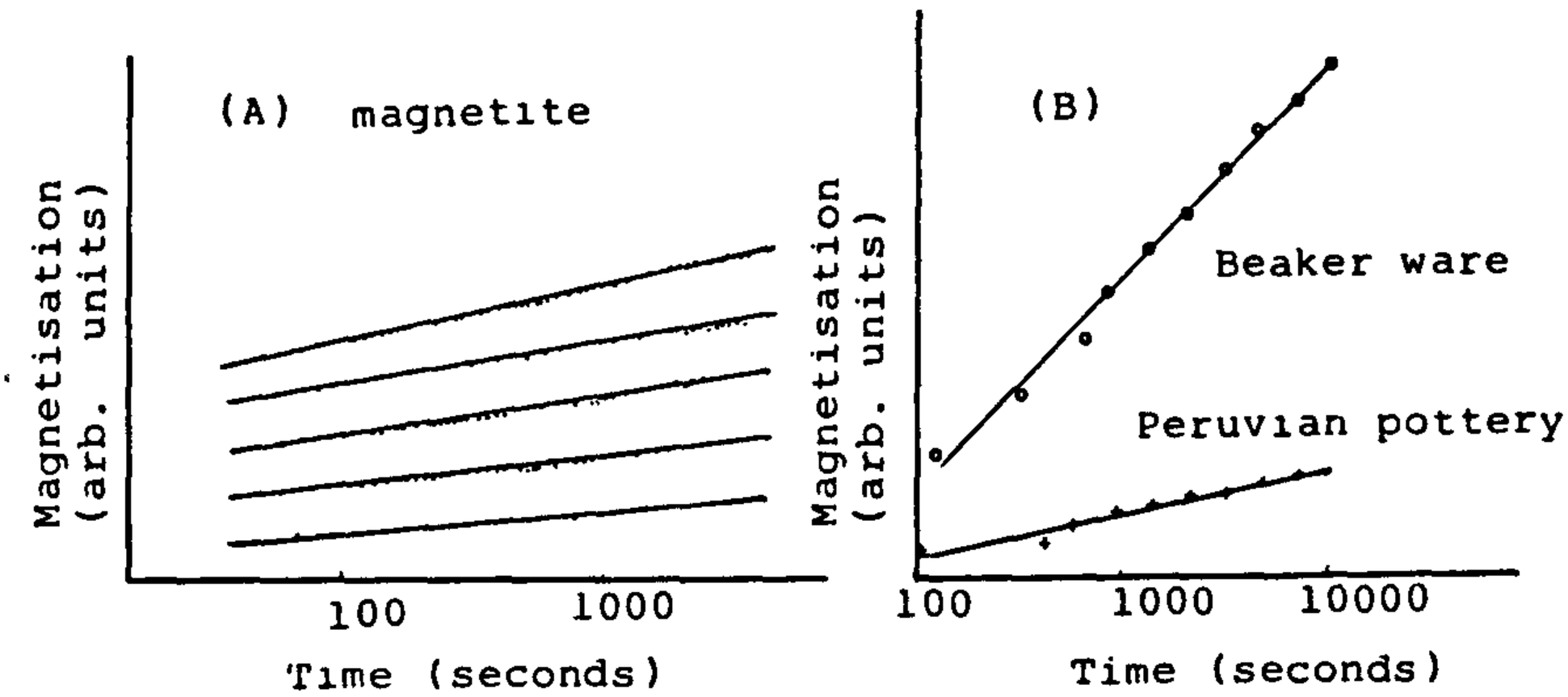

Fig. 1. Logarithmic time dependence of viscosity

The early activation model developed by Street and Woolley (1949) was successful in producing the logarithmic time dependence of viscosity which fitted their observations. This model was considered applicable to both the mechanisms of moment rotation in single domain particles and the change of magnetisation by domain wall reordering in multidomain particles. The more recent work of Walton (1980), restricted to single domain particles, states explicitly that the particle size distribution affects the time dependence of viscous acquisition.

These activation energy models have been shown to fit well with the experimental observations of single domain particles (Walton, 1983, Williams, 1986). However the recent experimental work

referred to earlier, has shown that simple thermal activation is inconsistent with the viscous behaviour of multidomain grains. In particular thermal activation models predict no dependence on the previous magnetic history of a sample. This is contrary to experimental work which has shown the effect of different magnetic histories (eg. Tivey & Johnson, 1984). The suggested explanation for the observed multidomain behaviour includes the effect of the diffusion of defects and impurities within particles as well as thermal activation. The diffusion of impurities and defects across domain walls with time can alter the position of internal energy minima. This may lead to the change of a particle's magnetisation because the domain structure may be reordered to achieve a new energy minimum. An associated effect termed susceptibility disaccommodation leads to a local redistribution of vacancies or cations in the magnetic particles which can stabilise the new energy minimum (Moskowitz, 1985).

A further aspect of viscosity which is of primary interest to the present study is the temperature dependence of this phenomenon. The thermal activation models predict a dependence of the viscosity coefficient of the form:

$$S_a \propto T/J_s(T) \qquad (2)$$

where T is the absolute temperature of the magnetic body and $J_s(T)$ is the saturation magnetisation of the body at that temperature. This leads approximately to a variation of S_a with T except near the Curie temperature where $J_s(T)$ falls rapidly. However, experimental observations have shown the relationship can be more complicated (eg. Dunlop, 1983) fig. 2).

The basis of the thermal activation models appear to be correct suggesting that the proportionality of S_a to T is also correct. Experimental observations are complicated by the size distribution of the magnetic particles in experimental samples.

IMPLICATIONS FOR DATING

Despite the brevity of the theoretical and experimental review

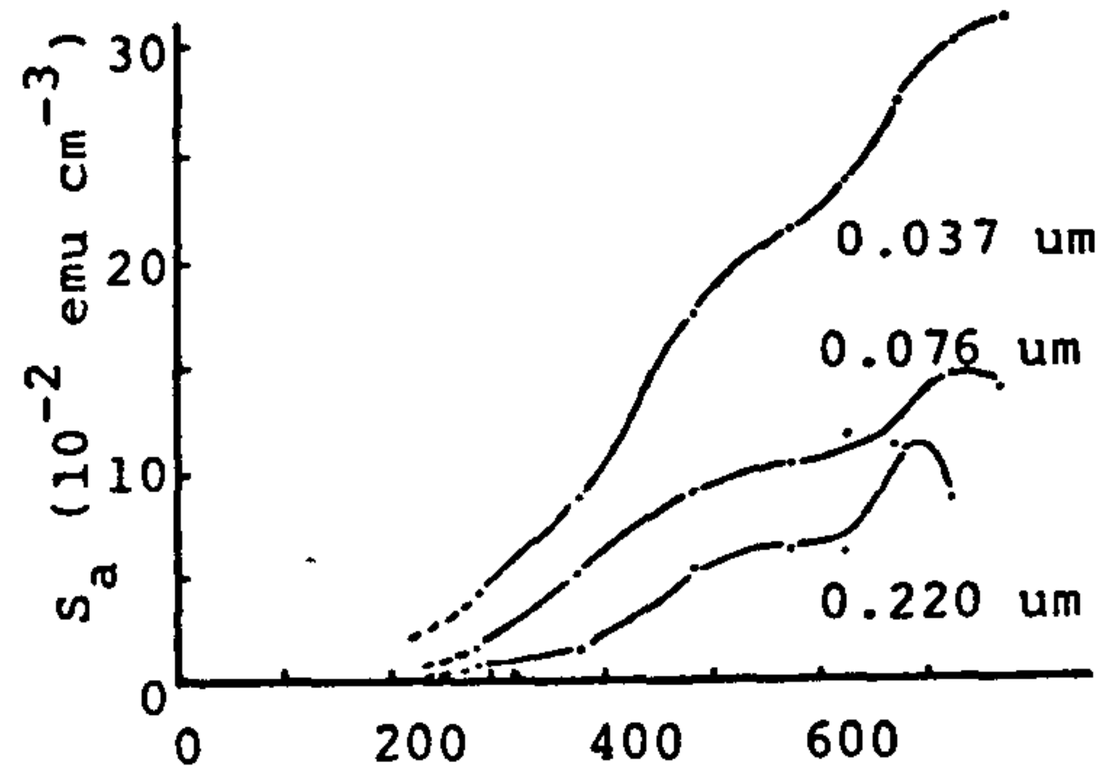

Fig. 2. Temperature dependence of S_a (after Dunlop, 1983)

several implications can be drawn which are relevant to the development of a dating technique based on viscosity. The first implication concerns the approximately logarithmic time dependence of the magnetisation process. It is apparent that a rapid loss in the resolution of the acquisition time will occur with increasing acquisition time. Further implications can be taken from the work on the effects of domain state and particle size distribution on the acquisition of viscous magnetisation. Experimental work on multidomain samples suggest that the energy barriers within the particles which are overcome during viscous activation can change with time. This change is the result of diffusion processes. Since the energy barriers are changing with time the particles are, in terms of their internal energy, different from when the acquisition of viscous magnetisation commenced. Hence information about the original rate of acquisition of magnetisation is lost, thus implying that unless the effects of diffusion are negligible or can be assessed, then multidomain materials should be avoided.

The dependence of viscosity on the magnetic particle size distribution is predicted from theoretical modelling and is evident from observations. This dependence imposes restrictions on the design of a dating method.

Any experimental approach must determine the time dependence of the acquisition of viscous magnetisation. More precisely, the time dependence of the thermal activation of those particles which

contribute to the viscous magnetisation of a material must be determined. In more simple terms, all of the particles that were activated in a sample since it was last disturbed must be reactivated in the laboratory if the age of last disturbance is to be determined. For archaeological samples the temperature of the laboratory reactivation must be increased because reactivation at ambient temperatures would require the same length of time as did the original activation. Because the particle size distribution of real samples is unknown the temperature dependence of the viscosity process must also be determined. With knowledge of the temperature dependence the viscous acquisition rate at high temperatures can be related to the ambient temperatures of the original viscous acquisition over archaeological time. From this, the age of last disturbance of an artefact can be obtained.

MAGNETIC MINERALOGY

An investigation of the magnetic mineralogy of an expanding collection of potteries, from several regions and spanning a broad time period, is in progress. This investigation aims to gain an insight into the magnetic properties of relevance to the application of viscosity dating.

The magnetic domain states have been determined from hysteresis measurements on powdered samples. The results are presented as a plot of the ratio of saturation remanent magnetisation to saturation magnetisation against the ratio of initial susceptibility to saturation magnetisation. The theoretical divisions of domain state are also plotted (fig. 3). The results suggest that the domain states of different materials are variable but a grouping between the boundaries of pure multidomain and pure single domain is apparent. This grouping is considered to represent various compositions of single and multidomain particles.

The temperature dependence of viscosity becomes more complex

close to the Curie temperature of the magnetic minerals making an understanding of the Curie temperature necessary. Curie temperatures have been determined using a Curie balance. Most of the samples investigated have a single Curie temperature around 550-600°C with exceptions having two Curie temperatures or Curie temperatures around 700°C. These results indicate that experimental reactivation up to 300-400°C will not be complicated by significant variations of $J_s(T)$.

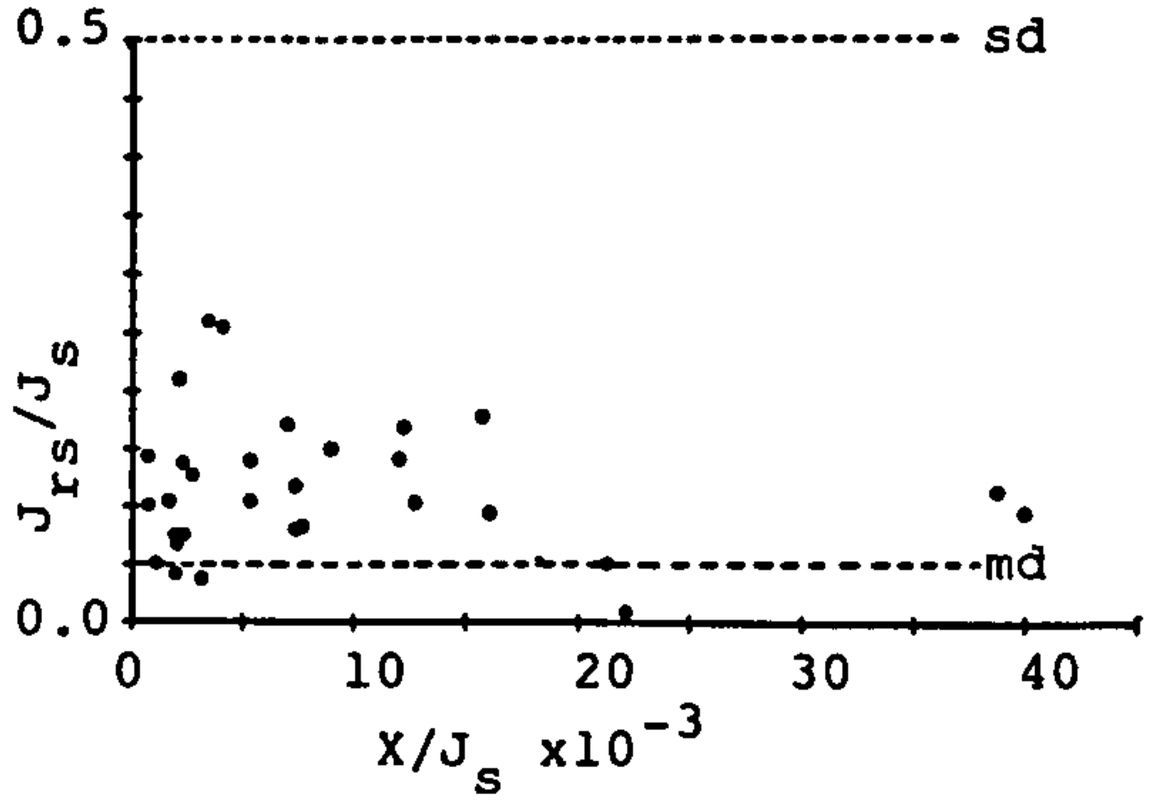

Fig. 3. Domain states of several pottery types

An important point not yet considered is the possible alteration of the magnetic mineralogy by laboratory heating. Any significant thermal alteration of the mineralogy induced in the laboratory will affect the determination of the rate of acquisition of viscous magnetisation. By comparing hysteresis measurements before and after heating any alteration should be apparent. Preliminary results from this analysis indicate that the degree of alteration is variable.

INTERIM CONCLUSIONS

The experimental observations and theoretical developments of a number of workers suggest that the viscous magnetisation of a material may retain information about the age of this magnetisation. Several problems have been highlighted and, where

appropriate, possible solutions have been suggested. The magnetic mineralogy study indicates the application of a thermal method for retrieving time information from the viscous magnetisation record of certain predominantly single domain pottery types may be possible but the difficulties arising from the domain states of the magnetic constituents and the effects of thermal alteration must be investigated in depth.

ACKNOWLEDGEMENTS: Del Atkinson acknowledges the receipt of a SERC studentship.

REFERENCES

Aitken, M.J. (1974). Physics and archaeology. Second edition. Clarendon Press, Oxford, pp.291.

Dunlop, D.J. (1973). Theory of the magnetic viscosity of Lunar and Terrestrial rocks. Rev. Geop. Space. Phys., vol.11, no.4, 855-901.

Dunlop, D.J. (1983). Viscous magnetisation of 0.04-100 m magnetites. Geophys. J.R. Astr. Soc., vol.74, 667-687.

Heller, F. & Markert, H. (1973). The age of viscous remanent magnetisation of Hadrian's Wall (Northern England). Geophys. J.R. Astr. Soc., vol.31, 395-406.

Moskowitz, B.M. (1985). Magnetic viscosity, diffusion aftereffect and disaccommodation in natural and synthetic samples. Geophys. J.R. Astr. Soc., vol.82, 143-161.

Neel, L. (1950). Theorie du trainage magnetique des substances massive dans le domaine de Rayleigh. J. Phys. Rad. Paris, vol.11, 49-61.

Shimizu, Y. (1960). Magnetic viscosity of magnetite. J.Geomag. Geoelect., vol.11, 125-138.

Street, R. & Wooley, J.C. (1949). A study of magnetic viscosity. Proc. Phys. Soc. Lond., vol.A62, 562-572.

Tivey, M. & Johnson, H.P. (1984). The characterisation of viscous remanent magnetisation in large and small magnetite particles. J. Geop. Res., vol.89, 543-552.

Walton, D. (1980). Time-temperature relations in the magnetisation of assemblies of single domain grains. Nature, vol.286, 245-247.

Walton, D. (1983). Viscous magnetisation. Nature, vol.305, 616-619.

Williams, W. (1986). The effect of time and temperature on magnetic remanence. Unpublished Ph.D. thesis, Darwin College, Cambridge University.